How do Eclogites Deform in Subduction and Collision Zones? – An Alpine Study

UNIVERSITY OF LIVERPOOL

Thesis submitted in accordance with the requirements of the University of Liverpool for the degree of Doctor of Philosophy

By

David Daniel McNamara

April 2009

Abstract

Eclogites are high pressure, moderate to high temperature rocks that are found in some of the Earth's most geologically dynamic environments such as collision and subduction zones. As such it is thought that the rheology of these areas is strongly controlled by the properties of eclogite rocks. Microstructures found in eclogite mineralogy, namely omphacite and garnet, contain key information to determining the state of stress in subduction and collision zones.

Omphacite LPO is a common microstructure found in deformed eclogites but one that can form through a variety of mechanisms. S-type lattice preferred orientation patterns in Zermatt-Saas omphacite is created by a combination of diffusion and dislocation creep whereas omphacite in the streaked eclogite of the Sesia-Lanzo Zone is due to dislocation creep and significant anisotropic grain growth during deformation. Lattice preferred orientation patterns in omphacite are thought to relate to the strain regime eclogite is deformed under. S-type lattice preferred orientation patterns in the Zermatt-Saas infer deformation in a flattening strain regime. Garnet deformation shows variable deformation features within different eclogite facies rocks. In the Zermatt-Saas garnet contributes little to eclogite deformation though in the Sesia-Lanzo Zone streaked eclogites containing garnet layers show evidence for dislocation creep, suggesting arrangement of garnet in eclogite rocks may affect how they contribute to the rocks deformation.

Mimetic processes are active in eclogite facies rocks in various ways. Retrogression of the Zermatt-Saas Unit in the Punta Telcio area shows part of the exhumation was static rather than dynamic due to the identification of amphibole mimetic lattice preferred orientation patterns. Interphase misorientation is a key tool in exploring these types of microstructural controls. The location fabric of the streaked eclogite of Colle della Barme d'Oropa also displays evidence in the eclogite facies microstructures and in structural observations that eclogite facies location fabrics may be inherited from those formed in the Sesia-Lanzo Zone's prior deformation history.

Acknowledgements

First and foremost I would like to thank my supervisor, Professor John Wheeler, for his support, insight, understanding and patience throughout the course of this PhD. I also thank him for his patience with my eccentricities and common 'blonde moments'. Thanks goes to Professor David Prior and Dr. Elisabetta Mariani for their help with SEM and EBSD work. I am forever grateful to Professor Wolfgang Müller for doing some TEM work for me. Also a huge thank you to Mark Pearce for helping me to understand the basics of MATLAB code. I would also like to thank Craig Barrie, Dan Tatham and Dan Faulkner and the Microstuff gang for always being on hand to help explain sciencey stuff and the support staff of the University of Liverpool. I also thank NERC for funding this work.

I am indebted to those field assistants who braved the Alpine hikes and crazy Italian drivers with me; Frances McGilloway, my sister Louise McNamara and Andy Alvey. Speeding fines and missing pieces of the car aside you all did an excellent job.

A massive, squishy thank you goes to my topsie, Ciara, for being pretty much amazing in every way all the time. Craig thanks for being an inspiration to actually do this work and for being a great friend, housemate and officemate this last few years. To all my now former housemates, Rob, Eleanor and Andy, thanks for some really memorable house parties. I want to give a massive shout to my best mate Roger for making me love Liverpool and for all the crazy, amazing adventures we had, Kate for being such a caring and supportive friend, Mark for his frank opinions and advice, Rich for telling Mark to be quiet, Tom for his relentless energy, Pete for being a great drinking buddy, Mary for so many things I can't even start to list them, Naomi for her constant good humour, Pilky for being one of the most fun people I have ever met, Matt for a being a fellow unicorn, Eddie and Gemma for helping represent the Irish, Vijay for all his help when I first moved to Liverpool, Ceri for being my little Welsh care bear, Natalie who I owe most of my first year fun to, Kimbo for loving some pretty bad dance music with me, Sarah for being a supportive and fantastic friend (bring on New Zealand), John and Val for being my Liverpool surrogate parents, Goz, Rhodri, John, Emma, Phil, Katie, Gaby, Sarah, Cathal, Krystal, Lisa, Nikki, Liz, Mike Lee, Mike King, Leanne, Gwilym, Steph and all my other friends I have made in the department and Herdman Society and my friends

from Trinity College Dublin and from back home for their continued support and love.

I want to acknowledge the University of Liverpool Skydivers; I never thought I would meet such an amazing bunch of people who would get me involved in one of the craziest and fun experiences of my life. Jumping out of planes and all the amazing weekends away and nights out have been a major part of my PhD life in Liverpool. Thanks Ade, Steve, Joe, Heather, Carys, Helen, Lynda, Mark, Kieran, Becki, Matt and everyone else in the club. I also want to thank the staff at the Northwest Parachute Centre for providing the opportunity, training and encouragement to get involved in the best de-stressing exercise ever.

Lastly and certainly not least, I want to thank my parents, Danny and Noreen McNamara and the rest of my family, who have always been there to support and encourage me throughout this PhD and everything else I have done and will do with my life.

Table of Contents

1 Chapter 1: Introduction

1.1 Eclogites and Eclogite Facies Rocks

In 1822 René-Just Haüy coined the name 'eclogite' meaning *select* or *chosen rock.* The term refers to a high pressure, moderate to high temperature metamorphic rock. Over the last two centuries this rock type has contributed to the birth of several major concepts in metamorphism, including the 'volume law' and the role of pressure, the existence of metamorphic rocks derived from igneous rocks and the widely used concept of metamorphic facies (Godard, 2001). The rock type has also been involved in the development of ideas on a number of geodynamic processes. Until the late twentieth century a hypothetical 'eclogite layer' was thought to have existed underneath the Earth's crust. After the advent of plate tectonics in the 1960s most eclogites came to be considered as a result of subducting oceanic crust. Finally in the last few decades the discovery of ultrahigh-pressure coesite-bearing rocks has drastically changed geologist's ideas concerning the upper limits of eclogite facies metamorphism (Godard, 2001).

Eclogites are important with respect to understanding the processes that occur in the deep crust and upper mantle due to their high abundance there. In fact subduction and exhumation geodynamic models often rely on the rheological aspects of these rocks. For example the flow strength of eclogite is inferred to impose an upper bound to shear stress across the plate boundary in the deeper levels of a subduction zone (Piepenbreier and Stöckhert, 2001). Eclogitisation of mafic lower crust and the associated increase in density is thought to be responsible for recycling of mafic material into the mantle as well as for promoting plate convergence (Doin and Henry, 2001).

Microstructures found in eclogites have the potential to provide important information on the mechanical state of a subducting plate at depth, on deformation mechanisms occurring within constituent minerals, and provide an insight into the state of stress in subduction zones. The main constituent minerals of eclogite and eclogite facies rock can help provide constraints on pressure and temperature regimes of a metamorphic terrain, recording essential information on the metamorphic

evolution of geological units and mountain belts. All of these factors together make eclogites an important and geologically useful resource.

The mineral assemblage of eclogite is thermodynamically stable at high pressures and moderate to high temperatures, restricting their occurence to a few geological environments, such as kimberlitic pipes and more importantly subduction and collision zones. Based upon the geological environment they form within, eclogites can be divided into three separate groups (Coleman et al., 1965). Group A are eclogites found as inclusions within kimberlites and basalts and as layers within ultramafic rocks. Group B are those eclogites that occur as bands or lenses within migmatites and gneissic terrains and are associated with amphibolite facies rocks. Group C eclogites are those associated with alpine-type metamorphic rocks and blueschist facies rocks and minerals.

1.2 Objectives of the Study

The aim of this thesis is to investigate the microstructures and microchemistry of the main mineral constituents of eclogite and eclogite facies rocks from both metamorphosed oceanic and continental tectonic slabs (eclogite group C). This is done with the purpose of improving the understanding of the way eclogite rocks behave during burial and exhumation. In addition the microstructure and chemistry of minerals overprinting eclogite facies ones are studied to analyse the effect of inheritance of pre-existing microstructures. To this end the northwest Italian Alps are selected as a case study as they contain excellent examples of both eclogitised oceanic and continental material that has undergone various amounts of retrogression.

Such a study is of interest because understanding the mechanisms operating in the deformation of eclogite facies minerals allows an insight into the rheology of the rock and its possible influence on the dynamics of subduction and collision zones. Also the study of how microstructure develops in retrogressive phases has the potential to reveal information on the exhumation pathways of these units. On a more regional scale the results of this study will allow a deeper understanding of the burial and exhumation pathways of the Alpine tectonic units concerned.

The major aims of the thesis are:

1. To understand the deformation mechanisms responsible for LPO development in omphacite in both monometamorphic and polymetamorphic terrains, using electron backscatter diffraction data (EBSD) and chemical data.
2. To understand the role of garnet, if any, in the deformation of eclogite rocks in monometamorphic and polymetamorphic rocks, using EBSD and chemical data.
3. To examine the effect of pre-existing microstructure on later forming mineral phases.
4. To link microstructural findings to the overall regional evolution of eclogite facies tectonic units.

1.3 Deformation Mechanisms, Microstructures and Rheology

Microstructures in a rock and the phases that make up that rock can develop through a variety of processes. Rocks are fundamentally amalgams of individual crystal grains which are discontinuous at grain boundaries. Various processes deform these grains allowing solid rocks to 'flow'. These processes are known as deformation mechanisms and certain mechanisms operate in specific conditions, the constraints of which are determined by the phase experiencing deformation. Different types of microstructures in a rock, from the microscopic scale and up, can reflect which of these processes may have been active, allowing observations to be made about the deformation conditions and rheology of the rock.

What follows here is a general explanation of the various deformation mechanisms that contribute to the development of microstructure in the minerals of a rock. Emphasis is placed on lattice preferred orientation (LPO), the term used to refer to alignment of the crystal lattice of all grains of a phase in a rock. It is a common example of a microscopic microstructure that can be produced by various processes in different minerals. For the mineral phases this study is concerned with, a more detailed review of how they deform, LPO types and what processes create them can be found later in this chapter.

1.3.1 Brittle Deformation Mechanisms

Brittle deformation mechanisms are not large contributors to the formation of LPO in a phase. However processes such as cataclastic flow are noted as causing LPO development in some phases (Berger and Stünitz, 1996, Díaz Aspiroz et al., 2007). Fracturing and mechanical twinning are also noted in some phases as potential mechanisms (Trepmann and Stöckhert, 2001, Brenker et al., 2002).

1.3.2 Plastic Deformation Mechanisms

Ductile deformation mechanisms are thought to be the main causes of LPO in most mineral phases. As such a description of these mechanisms is included here to aid understanding of the processes and microstructures discussed for the minerals this study is concerned with.

1.3.2.1 Diffusive Mass Transfer

The mechanisms included within this group all operate through movement of mass by diffusion. Diffusion creep is any deformation that takes place by actual transfer of material from areas of high compressive stress to areas of low compressive stress. It may result from the diffusion of point defects through a crystal lattice or by movement of atoms or ions along grain boundaries. Point defects include such things as interstitials, extra atoms placed between lattice sites, and vacancies, unoccupied lattice sites. The lattice around these is deformed by expanding or collapsing respectively. As an interstitial is a higher energy defect than a vacancy the concentration of vacancies increases with temperature. Therefore vacancies are more integral to ductile flow and more common.

Diffusion creep can be divided into two different types, Nabarro-Herring Creep and Coble Creep. Applying a differential stress to a grain causes vacancies to be created at the surface of least compressive stress, and destroys them at surfaces of high compressive stress. Thus the crystal changes shape by atoms moving through the lattice from high stress surfaces and accumulating at low stress surfaces. In Nabarro-Herring Creep the motion of vacancies occurs through the crystal lattice. Coble creep involves the movement of vacancies or interstitials along grain boundaries rather than internally through the crystal.

Pressure solution/dissolution involves the dissolution of material at grain to grain contacts into a pore fluid. It is then transported from areas of relatively high stress to areas of relatively low stress, where it is then deposited.

Diffusive mass transfer processes can create LPO in a phase through the preferential dissolution of some grains and the growth of others. Depending on the phase certain crystallographic directions will grow/dissolve faster than others. Those grains within a rock whose fast dissolution directions are aligned with the direction of maximum stress will eventually become eradicated from the rock leaving behind those grains whose fast dissolution rate directions are aligned parallel to the minimum stress direction. Thus the rock evolves to contain grains all with a certain preferred orientation giving that phase a lattice preferred orientation.

1.3.2.2 Dislocation Creep

Dislocation creep is concerned with the movement of crystal defects known as dislocations throughout the lattice of a mineral. As a dislocation moves through the crystal lattice part of the lattice is moved one lattice point along a plane relative to the rest of it, causing deformation. The plane that this occurs in is referred to as a glide plane. Movement involves breaking lattice atomic bonds in a step by step process as breaking them all at once requires unrealistic amounts of energy. Instead as old bonds are broken, new ones are immediately created.

Two types of dislocations exist, edge and screw types. They both form a dislocation line, a linear defect, through the crystal lattice. Edge dislocations form the edge of an extra layer of atoms within the crystal lattice and move perpendicular to the dislocation line (Fig. 1.1A). Screw dislocations form a line along which the crystal lattice jumps one lattice point and moves parallel to the dislocation line (Fig. 1.1B). A dislocation will not always be a straight line and thus will be able to move along more than one glide plane. Where the orientation of a dislocation line changes, a screw dislocation may become an edge dislocation and vice versa. The length of the displacement of the crystal lattice caused by the dislocation movement is called the Burgers vector, which is equal to the distance between two atoms in the lattice.

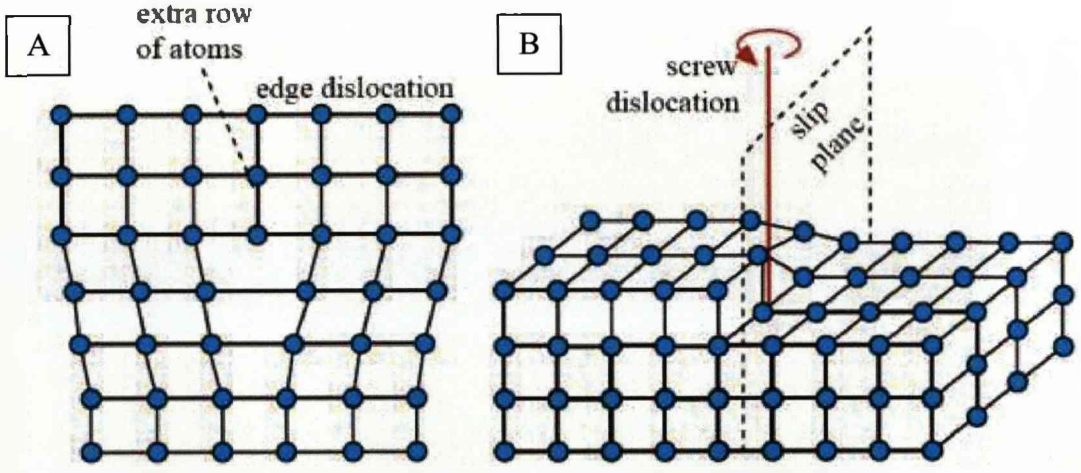

Fig. 1.1 Schematic diagrams of A) an edge and B) screw dislocation in an atomic lattice.

The crystal system of a mineral determines how many glide planes are possible for and in which orientations. Chemistry and close packing of atomic planes also determine the 'easy' glide planes. The orientation of differential stress will then

determine which of these are active during deformation. A fundamental constraint on dislocation creep in a crystal lattice is set out by the Von Mises criterion. This states that to deform a mineral by dislocation creep movement along at least five different glide planes in required (Von Mises, 1928).

The formation of LPO in a mineral phase by dislocation creep requires a mechanism by which crystals rotate towards a preferred orientation as a result of slip on slip systems associated with that phase. Two models offer an explanation for this process. The Taylor-Bishop-Hill theory requires crystals to rotate by enough to equal the imposed large scale homogeneous deformation. This model assumes that the Von Mises criterion is met. Another model, referred to as the misfit minimisation model, determines the rotations necessary to minimise the geometric misfit in an aggregate of crystals that can deform on a limited number of slip systems. Both models predict observed aspects of LPOs but actual LPO creation likely involves both (Twiss and Moore, 1992).

Dislocation however cannot operate efficiently as a deformation mechanism due to strain hardening. This is a result of increasing amounts of dislocations propagating and accumulating within a crystal lattice and interacting with each other forming tangles. These impedes dislocation glide along a glide plane. This increases the stored strain energy within a grain. Dislocation creep is aided by dislocation climb which allows dislocations to move up or down into another glide plane allowing them to move past one another and other obstacles in the crystal lattice (impurities) so dislocation creep can continue.

1.3.2.3 Recovery, Dynamic Recrystallisation and Grain Growth

Strain hardening in a phase of a rock is overcome by what are known as recovery processes. These reduce stored strain energy within a grain and remove or rearrange dislocations within a grain. These processes include grain boundary migration (GBM) and subgrain rotation recrystallisation, both known as dynamic recrystallisation. Dynamic recrystallisation differs from static recrystallisation of a rock in that it occurs in tandem with deformation rather than being a static overprint of a rock's mineralogy.

Grain boundary migration is a recovery process that allows atoms along a grain boundary of a highly strained crystal to jump across the grain boundary to the lattice of a neighbouring, lower-energy crystal. By doing this the grain boundary of the lower strain crystal is swept into and through the high energy crystal, releasing strain energy stored in dislocations and reorienting the lattice as it does so (Passchier and Trouw, 1998).

A second recovery process, known as subgrain rotation recrystallisation, involves the rotation of subgrain (low angle) boundaries within a grain so that they become high angle enough to be considered separate grains. In this study subgrain boundaries are considered to be those where the crystal lattice is only at an angle of less than ten degrees relative to the rest of the grain, anything over that is considered a separate, individual grain (Twiss and Moores, 1992).

1.3.2.4 Grain Boundary Sliding

Grain boundary sliding is a process in which grains slide past each other along, or in a zone immediately adjacent to, their common boundary (Langdon and Vastava, 1982). It must act in conjunction with other mechanisms (usually diffusive mass transfer) so that voids are not created between the sliding grains.

1.4 Omphacite: A Review

Omphacite is one of the main constituents of eclogites and usually forms the framework supporting or bulk mineral phase with other phases scattered throughout the rock. It is well documented that garnet usually acts as a rigid body in the deformation of eclogites and that the omphacite deforms plastically, accommodating any strain on the rock. Understanding the mechanisms that control omphacite plastic deformation (such as intracrystalline defect structures, shape fabrics and lattice preferred orientations) is therefore essential to furthering our understanding of models involving high pressure and ultra-high pressure lithologies.

1.4.1 Omphacite Chemistry in Eclogites

Omphacite is a high pressure, moderate to high temperature, clinopyroxene. It usually displays a green colour of varying shade dependent on its composition, with lighter shades having a higher sodic component and darker ones having a higher calcic component. Chemically omphacite forms a solid solution between end members jadeite ($NaAlSi_2O_6$), aegirine ($NaFe^{3+}Si_2O_6$), diopside ($CaMgSi_2O_6$), hedenbergite ($CaFe^{2+}Si_2O_6$), Ca-Tschermak ($CaAlAlSiO_6$) and Ca-Eskola pyroxene ($Ca_{0.5}AlSi_2O_6$). The last four can be grouped together to represent augite ($Ca(Mg,Fe,Al)Si_2O_6$) and thus omphacite chemistry can be displayed on triangular composition diagrams (Fig. 1.2).

Changes in the jadeite component of omphacite can shed light on the temperature-pressure pathway of eclogites. As the Na content decreases the eclogite is likely to be on an exhumation pathway and thus experiencing decreasing temperature and pressure conditions (Kurz et al., 2003). It is also shown that the jadeitic component of omphacite changes with a change in eclogite type. Jadeite content increases from group A to group B whereas the diopside content decreases (Coleman et al., 1965).

Calcium self-diffusion in diopside may also hold significance for omphacite as diopside is often used as a proxy for certain properties of omphacite, as explained later. Ca self-diffusion appears to be a function of temperature, pressure, crystallographic orientation and iron content. In omphacite, of all the elements (bar silicon) the diffusion coefficient of Ca is the lowest and thus may be a kinetically limiting species for diffusion controlled processes (Dimanov et al., 1996).

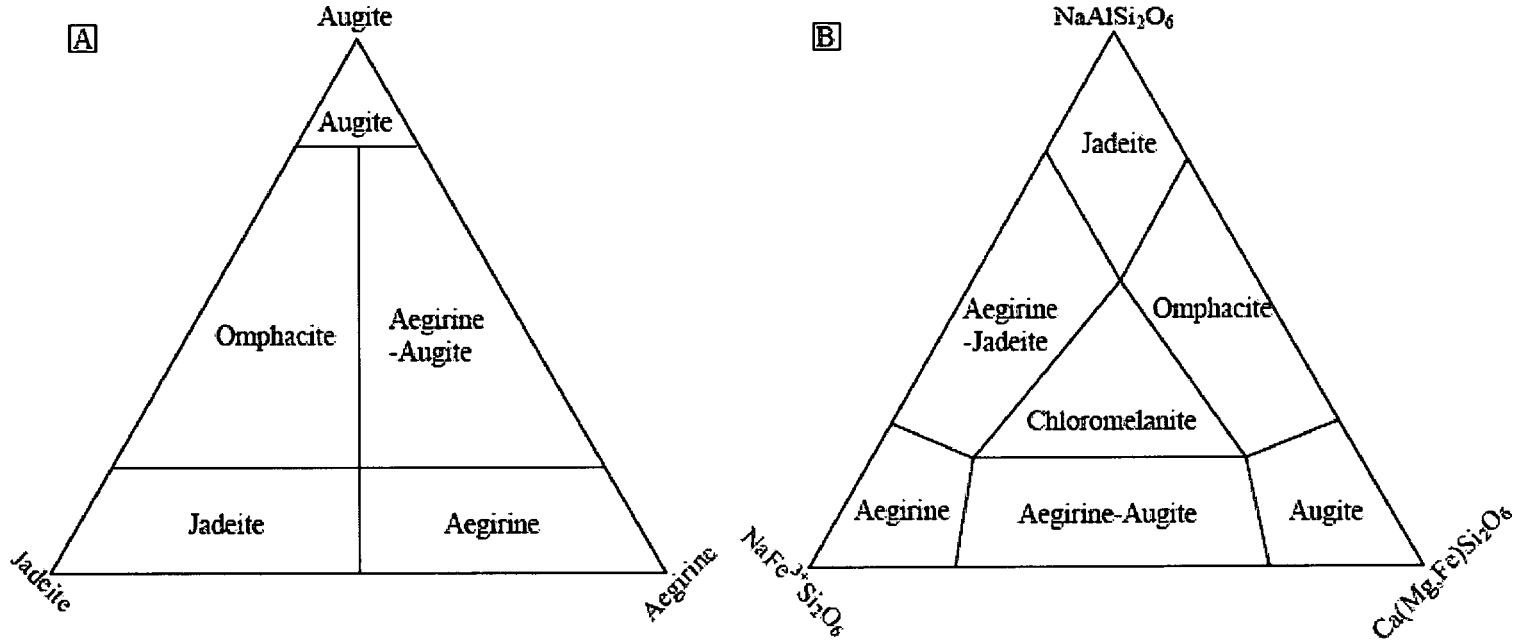

Fig. 1.2 End member compositions of clinopyroxene A - the Essene and Fyfe (1967) scheme and B - the Clark and Papike (1968) scheme

1.4.2 Crystal Structure of Omphacite

Omphacite is of the monoclinic crystal system such that **a** ≠ **b** ≠ **c** (where **a** = 9.45-9.68 Å, **b** = 8.57-8.9 Å, **c** = 5.23-5.28 Å). Angles between the axes follow the monoclinic rule with $\alpha = \gamma \neq \beta$, where $\alpha = \gamma = 90°$ and $\beta = 105\text{-}108°$. The <100> and <001> axes intersect their respective planes obliquely whereas the <010> axes intersects the (010) plane perpendicularly (Fig. 1.3) (Deer et al., 1992).

With point group 2/m symmetry (prismatic monoclinic), omphacite exists in either the disordered, C2/c space group or the ordered, P2/n space group. Ordered omphacite means the ions in omphacite chemistry are arranged in an ordered, regular pattern. Chemically, omphacite end members diopside and jadeite are of the C2/c structure and intermediate omphacite compositions are of the P2/n structure (Clarke and Papike, 1968, Carpenter, 1978).

C2/c omphacite has the structural formula M2M1T2O6. M2 eight co-ordinated sites contain Ca, Na, and (Fe, Mg), M1 octahedral sites contain Mg, Fe^{2+}, Fe^{3+}, Al and Cr, and T (tetrahedral) sites contain Si and Al. At high temperatures all the M1 sites in the crystal structure are the same but as temperature decreases Al and Mg arrange themselves in an alternating sequence. Due to this, Ca and Na are also arranged in a similar way to maintain local charge balance. This creates the ordered P2/n space group structure in omphacite which leads to a loss of symmetry. In this space group there are two distinct octahedral sites, one being Mg rich (M1) and the other Al rich (M11). There are also two different eight coordinated sites, the Na rich M2 site and the Ca rich M21 site (Fig. 1.4) (Clarke and Papike, 1978, Deer et al., 1992).

Whether omphacite has a C2/c (disordered) or P2/n (ordered) structure is dependent on temperature and as previously stated chemistry. Exsolution lamellae and antiphase domains are common microstructures observed in omphacite crystals. These microstructures are interpreted in terms of a combined system in which a field of ordered omphacite at intermediate compositions is superimposed onto an immiscibility gap between disordered omphacite end members giving broad two-phase fields between impure jadeite and omphacite and between omphacite and sodic-augite (Fig. 1.5) (Carpenter, 1980).

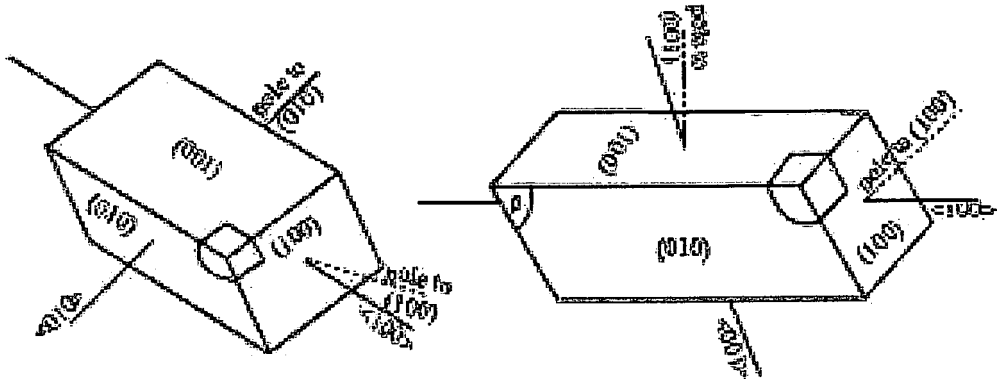

Fig. 1.3 Diagrams showing the monoclinic crystal structure of omphacite

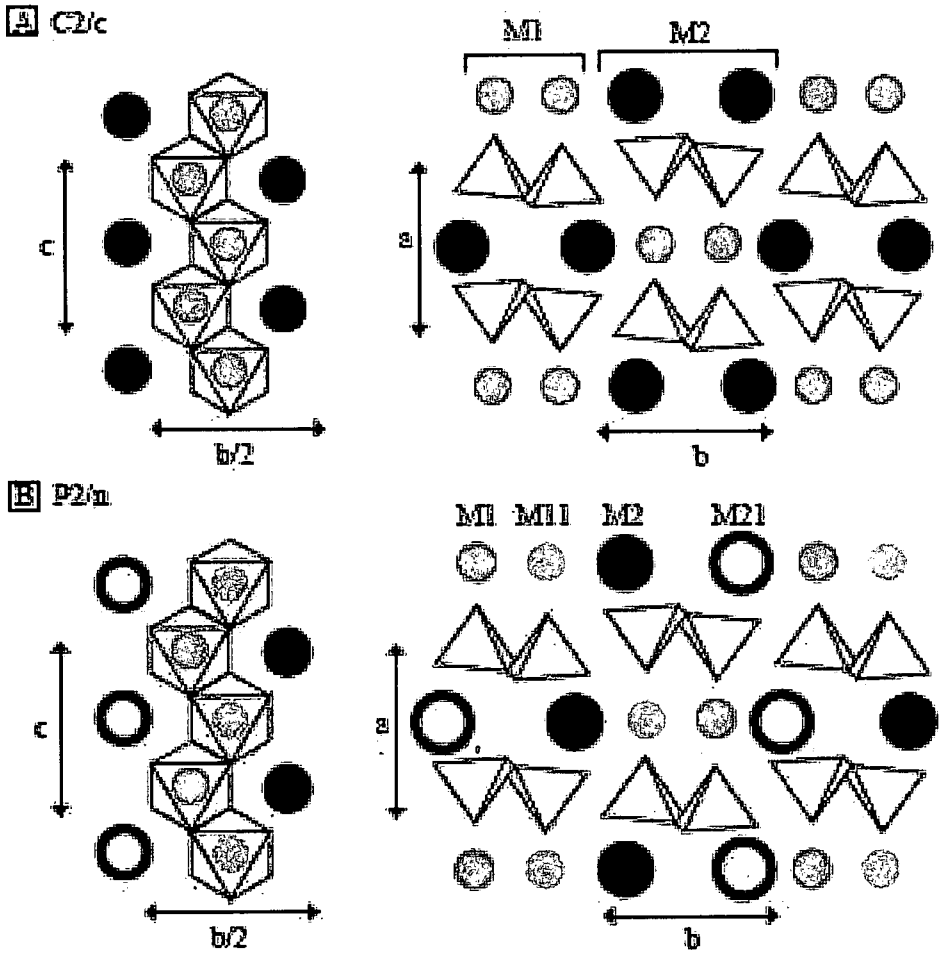

Fig. 1.4 Diagrammatical representation of A - the disordered (C2/c) and B - the ordered (P2/n) space group structures of omphacite

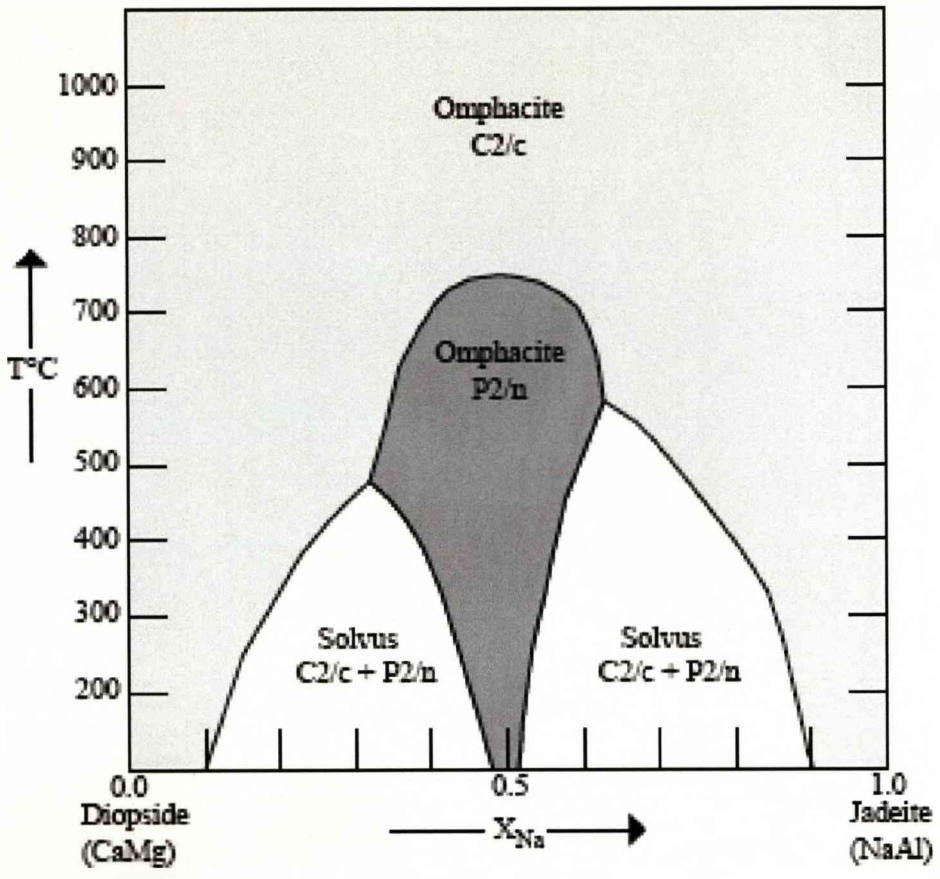

Fig. 1.5 Equilibrium phase diagram of space groups and solvi in the Di-Jd system at pressure exceeding the stability of jadeite (from Carpenter, 1980a)

1.4.3 Common Omphacite Microstructures

Omphacite is often found defining a foliation within deformed eclogites. The foliation is often a shape fabric with omphacite typically having a shape preferred orientation (SPO). In other eclogites it also known for omphacite to form part of a location fabric, concentrated into bands with garnet and quartz forming other bands. It is also found forming mineral and aggregate lineations within eclogites.

Common intracrystalline defects of omphacite include undulose extinction, deformation twinning, sub-grains and exsolution lamellae, (Boland and Tullis 1986, Buatier et al. 1991, Philippot and Van Roermund, 1992, Godard and Van Roermund, 1995, Abalos, 1997, Mauler et al. 2001, Piepenbreier and Stöckhert, 2001, Bascou et al. 2001, Brenker et al., 2002, Kurz et al., 2004, Foreman, 2004). Added to this there are many recorded occurrences of chemical zoning in omphacites (Carpenter, 1981, Piepenbreier and Stöckhert, 2001, Kurz et al., 2004).

Transmission electron microscopy (TEM) of omphacite often shows the mineral contains microstructures such as isolated, curved-free dislocations, isolated, long-straight dislocations, isolated loops, isolated nodal points, tilt walls, complex dislocation networks, (100) microtwins, (010) planar faults, chain multiplicity faults and antiphase domains (Phakey and Ghose, 1973, Carpenter 1981, Van Roermund and Boland, 1981, Buatier et al. 1991, Philippot and Van Roermund, 1992, Godard and van Roermund, 1995, Barnert et al. 2001, Han et al. 2001, Brenker et al. 2002, Müller et al. 2004, Müller et al. 2007, Müller and Franz, 2008).

1.4.4 Description of Omphacite Fabrics

Investigation of lattice preferred orientations (LPO) of omphacite started with Helmstaedt et al. (1972) which resulted in a classification scheme defining two end type fabrics. These are referred to as the L-type and S-type LPOs (Fig. 1.6).

The L-type LPO is characterised by a point maximum of <001> poles parallel to the lineation of a deformed eclogite and the <010> poles forming a girdle perpendicular to the foliation. Poles cluster in a girdle like fashion in (110) and seem to have very little pattern (i.e. random) in (100).

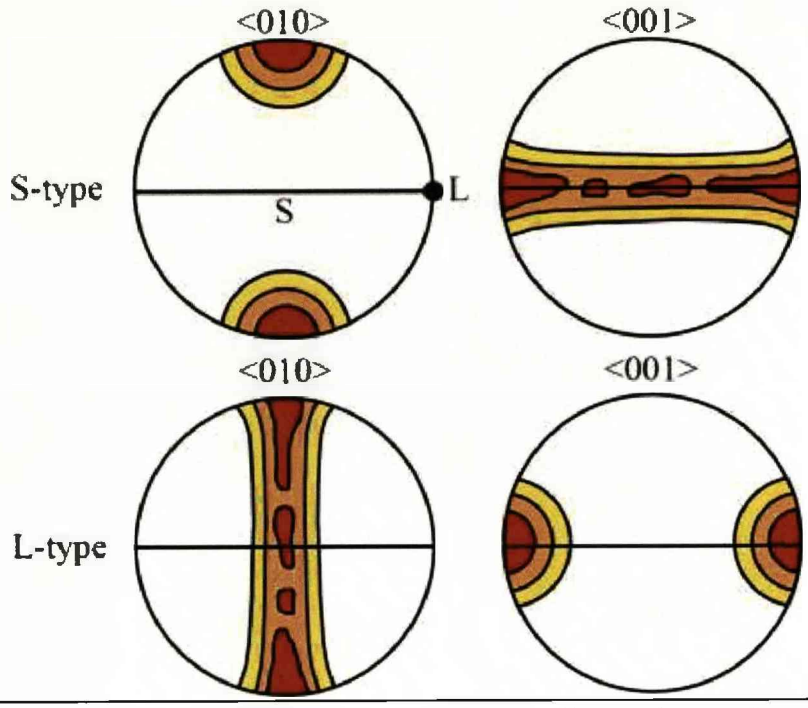

Fig. 1.6 Representative pole figures displaying the end member patterns of omphacite LPO. S marks the foliation plane and L marks lineation.

The S-type LPO shows a point maximum of <010> poles normal to the foliation and the <001> poles are dispersed in a girdle pattern within the foliation plane. Also poles to (100) have a random distribution and the poles to (110) occasionally describe small circle distributions around the foliation normal at an angle of about 45° (the angle between (110) and (010)).

An extensive investigation into omphacite LPOs by Godard and Van Roermund (1995) showed both of the Helmstaedt classifications but also transitional variations between the two end member types. These are known as LS or SL types depending on the predominance of one over the other.

A numerical qualification scheme exists to determine how much an intermediate omphacite fabric is of the L type and S type end members. Previously, authors have tried to give more precise descriptions of this by using eigenvalue classification. The magnitude of three eigenvalues ($\lambda_1 \geq \lambda_2 \geq \lambda_3$ with the normalisation $\lambda_1+\lambda_2+\lambda_3=1$) can be used to define the three fabric indices; point maximum ($P=\lambda_1-\lambda_2$; P has a high value when $\lambda_1>\lambda_2\approx\lambda_3$), girdle ($G=2(\lambda_2-\lambda_3)$; G has a high value when $\lambda_1\approx\lambda_2>\lambda_3$) and random ($R=3\lambda_3$; R has a high value when $\lambda_1\approx\lambda_2\approx\lambda_3$).

Plotting on triangle diagrams using the above eigenvalue calculations (Vollmer, 1990) shows that S-type fabrics are characterised by a strong point component for the <010> direction and a strong girdle component for the <001> direction. In L-S fabrics eigenvalues <010> still have an important point component and <001> still has an important girdle component. L fabrics [010] have an important girdle component and <001> has a strong point component (Mauler et al., 2001).

An equation composed by Ulrich and Mainprice (2004) allows a quantitative analysis of how L or S type an intermediate L-S LPO type is. Where the eigenvalue analysis only looks at one pole figure this method combines the eigenvalue analysis of the <010> and <001> pole figures. They introduce the LS index which has a value of 1 for the end member L type LPO and 0 for the end member S type LPO. It is defined by,

$$LS_{index} = \frac{1}{2}\left[2 - \left(\frac{P_{010}}{G_{010} + P_{0101}}\right) - \left(\frac{G_{001}}{G_{001} + G_{001}}\right)\right]$$

where P and G indices refer to the pole figures (010) or [001]. For real data, the random index R is never zero, hence the P_{010} and G_{001} values are normalized by the sum of G_{010}+P_{010} and G_{001}+P_{001}, respectively, to give the desired range of 0–1 for any value of R.

Qualification and description of omphacite LPO type is important as it can be used to make certain assumptions about eclogite facies rocks. These may include things such as strain regime the omphacite was deformed in, or assumptions on what space group the crystal structure of the omphacite is. This is discussed in detail later in the chapter.

1.4.5 Omphacite Deformation Mechanisms and LPO Development

There are a variety of mechanisms proposed for being responsible for the development of LPO in omphacite. Among the main arguments on omphacite deformation is whether LPO patterns are a result of dislocation creep (Buatier et al., 1991, Philippot and van Roermund, 1992, Brenker, 1998, Brenker et al., 1999, Bascou et al., 2000) or whether other mechanisms such as diffusion creep and preferred crystal growth (Helmstaedt et al., 1972, Godard, 1988, Godard and van Roermund, 1995) are responsible. Generic descriptions of the brittle and plastic deformation mechanisms have already been provided earlier in this chapter and what follows is a discussion of those associated with omphacite LPO formation and the evidence for the action of these mechanisms.

1.4.5.1 Twinning

Twinning is one such mechanism. Limited deformation twinning, parallel to (100) [001] has been observed (Trepmann and Stöckhert 2001, Brenker et al. 2002) but it is thought that significant contribution of this process to deformation of omphacite only occurs at low temperatures and very high strain rates.

1.4.5.2 Dislocation Creep

Commonly observed microstructures in deformed omphacite such as sutured high angle grain boundaries, subgrain development and undulose extinction have contributed to the assumption that dislocation creep is the dominant deformation mechanism in omphacite. Sutured high angle grain boundaries can be a result of heterogeneous dislocation density in a grain causing areas of it to bulge and curve creating high angled boundaries with other grains (grain boundary migration). Subgrain development is the result of mobile dislocations within an omphacite grain gathering in walls effectively creating an area of the grain that is misoriented slightly from the rest of it. Undulose extinction can be due to dislocations throughout a single omphacite grain that alter the lattice orientation across the grain but without forming distinct walls, yet provide a significant cumulative misorientation across the grain, thus giving the sweeping extinction effect under crossed polars.

Many studies have, through the use of microscopy techniques such as EBSD and TEM, revealed direct evidence for the action of dislocation creep in omphacite. These include isolated dislocations and well ordered dislocation walls. The most common slip systems in omphacite include [001] (100), [001] {110} and ½<110> {110} (van Roermund and Boland, 1981, van Roermund, 1983, van Roermund, 1984, Godard and Van Roermund, 1995). At lower temperatures [100] (010) is also observed (Philippot and van Roermund, 1992) although this particular system has apparently not been found in further studies (Müller and Franz, 2008). It is shown in Raterron et al. (1994) that at high temperatures (>1000°C) the dominant slip system in diopside is ½<110> {110} whereas at intermediate temperatures (<1000°C) the dominant slip system in diopside is [001] (100), with ½<110> {110} supplying minor strains. The same may apply to omphacite of which diopside is a proxy.

Recent work displays abundant occurrences of chain multiplicity faults (CMFs) parallel to (010) in omphacite from eclogites of the Tauern Window, Italy. These CMFs may have important implications for omphacite deformation (Müller et al. 2004, Müller and Franz, 2008). CMFs are intercalations of atomic layers which have different atomic structures, for instance a single chain silicate intercalated with a double chain silicate. CMFs in omphacite from this area show the pyroxene matrix of single chains is interrupted by intercalations of one or two unit cell layers of double chains of the amphibole structure. The omphacite CMFs formed by a single double chain layer are stretched between two partial dislocations with Burgers vector ½<011>. These have been shown to act as slip planes as they displace small angle grain boundaries across them. The frequent occurrence of these in the omphacite of Tauern Window eclogites suggests that ½[011] (010) may be an important slip system in omphacite in addition to those previously mentioned (Müller and Franz, 2008).

While creep data for eclogite is now available (Jin et al, 2001, Orzol et al., 2006), and includes omphacite data, lack of accompanying microstructural data means that diopside experimental data (Avé Lallement, 1978, Boland and Tullis, 1986, Bystricky and Mackwell, 2001) still remains the most applicable for studying dislocation creep mechanisms in all omphacite compositions. However this may not be ideal as extrapolating the flow law of diopside for temperatures below 700°C

creates unreasonably high stresses or low strain rates in order for strain to be accommodated meaning diopside could not flow (Godard and van Roermund, 1995, Mauler, 2001, Abalos, 1996, Piepenbreier and Stöckhert, 2001, Orzol et al., 2006).

The answer to this problem may lie in the differences in chemistry between diopside and more sodic omphacite (jadeite). This difference may create variable defect behaviour between the two minerals, thus making diopside creep laws poor analogues for sodic omphacite. Significant differences in the homologous temperatures (actual temperature of a material expressed as a fraction of its melting temperature (°K)) of diopside and sodic omphacite add to this argument. Creep resistance and thus creep laws are sensitive to melting temperature. However what qualifies as a high temperature for different crystalline materials varies, which is where the homologous temperature concept is useful.

Melting temperatures of sodic omphacite are significantly lower than diopside (~200°C, though varies with pressure) and thus the true creep law for these compositions must be shifted toward lower temperatures in comparison to that for diopside (Yoder, 1952, Bell and Davis, 1969, Williams and Kennedy, 1970, Litvin and Gasparik, 1993, Godard and van Roermund, 1995). This implies that sodic omphacite has a significantly higher homologous temperature than diopside. It is this that leads to the suggestion that dislocation creep microstructures in moderate to low temperature eclogite omphacite (as low as 450°C) may be due to lower creep resistance of sodic omphacite, in accordance with the homologous temperature concept (Piepenbreier and Stöckhert, 2001, Godard and Van Roermund, 1995, Buatier et al., 1991). This is supported by data from experiments on synthetic jadeite which displays low flow strength (Stöckhert and Renner, 1998, Zhang et al., 2006, Zhang and Green, 2007).

Experiments carried out by Jin et al. (2001) on the rheology of synthetic eclogites found an extrapolated flow law for slow geological strain rates that gives flow strengths between that of pre-existing ones for diopside. This refutes the idea that sodic pyroxene has a lower flow strength than that of diopside. However these experiments were carried out where the eclogitic garnet is extremely strong and as such provide more of an upper bound for eclogite rheology (Ji et al., 2002).

Further differences between jadeite and diopside arise from low to moderate temperature micro-indentation tests carried out by Dorner and Stöckhert (2004). These reveal that the strength of jadeite is significantly higher than diopside in the dislocation glide (low temperature plasticity) regime with intermediate compositions having intermediate strengths between the two end members. This is the reverse of what is seen in the dislocation creep regime as described above. This serves to further highlight that although both end member omphacite compositions are isomechanical their rheological behaviour is significantly different.

The presence of water has also been shown to have a significant effect on experimentally deformed eclogites (Zhang and Green, 2007), such as providing a significant decrease in creep strength and a change in deformation microstructures. Natural sodic clinopyroxene normally contains hundreds to thousands of ppm hydroxyl in their structures while other pyroxene (diopside and enstatite) typically contain much less. This property may also contribute toward lower flow strength for jadeite.

While there is plenty of evidence that dislocation creep is active in omphacite, problems with it being the sole, responsible mechanism exist. Models for the formation of LPO by dislocation creep fall between two end-member classifications, (Wenk and Christie, 1991).

The first end member model is known as the single slip model or 'lower bound' critical resolved shear stress (CRSS) model and is based on the stress equilibrium condition where only the easiest activated slip system is active. It particularly applies to materials with low symmetry. The model involves the creation of a heterogeneous stress distribution around or within individual grains. As material coherency must be maintained the model puts limits on the differential stress levels that can be produced in the deforming material. Thus the boundary condition is stress equilibrium. An LPO is generated by lattice rotations accompanied by mechanical grain rotation in order to maintain stress equilibrium.

The second end member model is the multiple slip system model or 'upper bound' CRSS model. This model assumes strain compatibility achievable by the operation of five independent slip systems and is often invoked for materials with high symmetry.

This model involves homogeneous deformation at all scales in which each individual grain is accommodating the strain. The boundary conditions set by strain compatibility imply there are no mechanical grain rotations and that crystal lattice rotations occur solely by dislocation glide and climb.

Previously, due to the low crystal symmetry, the single slip model has been applied to dislocation creep in clinopyroxene (Mainprice and Nicolas, 1989). This requires the slip systems [001] (100) and [001] (010) (the 'easiest' slip systems in clinopyroxene), to be dominant. While the [001] (100) slip system occurs in omphacite the [001] (010) slip system is rarely recorded (Godard and van Roermund, 1995), suggesting that the single slip model is unlikely to be the case for LPO development in omphacite.

Applying a multiple slip model to omphacite also raises its own problems. Only three commonly observed active slip systems are noted in naturally and experimentally deformed omphacite. This fails to meet the von Mises criterion of five independent slip systems. This is related to the fact that none of the three slip systems intersect the tetrahedron chains and thus for some crystallographic orientations deformation cannot be accommodated by slip and another process must be in operation (Godard and van Roermund, 1995). In addition a multiple slip model assumes homogeneous deformation and garnet in eclogites is commonly noted for acting as a rigid body, though evidence exists to suggest otherwise (see later in this chapter for a full discussion on this).

Despite these problems the use of viscoplastic self consistent (VPSC) models suggest that omphacite LPO can be formed purely from dislocation creep. These models have two assumptions; that the crystals forming the aggregate material deform uniquely by homogeneous intracrystalline slip on selected crystallographic planes and that the aggregate behaviour is calculated as an average of the crystals behaviour (Bascou et al., 2002). Two main studies using this method (Bascou et al., 2002, Ulrich and Mainprice, 2005) involve the consideration of only those slip systems, associated stress exponents and CRSSs that are found in naturally and experimentally deformed eclogites and deformation experiments on single crystal diopside. These studies show that the VPSC model reproduces the typical omphacite LPOs of naturally deformed eclogites. The model results also show that the patterns developed can be directly

produced by dislocation creep occurring mainly on the 1/2 <110> {110}, [001]{110} and [001] (100) systems, with other systems contributing to a lesser extent.

In light of this it is undeniable that dislocation creep plays a significant role in omphacite LPO development but there also exists evidence for an important contribution by other processes, especially diffusive mass transfer mechanisms.

1.4.5.3 Diffusive Mass Transfer, Grain Boundary Mobility and Crystal Growth Mechanisms

Given the inherent problems involved with creating an omphacite LPO by dislocation creep alone it is thought that it likely works in tandem with other mechanisms, such as diffusive mass transfer (DMT), grain boundary mobility and preferential crystal growth (Helmstaedt et al., 1972, Godard and van Roermund 1995, Mauler et al., 2001). What follows here is a summary of said mechanisms and the evidence for their operation in omphacite.

Crystal growth during deformation is noted as active in omphacite (Godard and van Roermund, 1995, Mauler et al., 2001), evidenced by differences in size and shape of different omphacite populations; deformed matrix omphacite is larger than that found sheltered in hollow garnet grains.

Deformation induced grain growth can be achieved through two mechanisms; mass transfer or GBM. In the case of the first, atoms for growth are sourced from far off dissolution and for the latter mechanism from neighbouring crystals with dislocation density as the driving force (as discussed earlier in the chapter). In either case crystals dissolve at faces under compression and grow at faces under tension. Where evidence for deformation induced clinopyroxene is observed authors tend toward a GBM mechanism (Boland and Tullis, 1986 and Buatier et al., 1991). There is however significant evidence in the literature to suggest diffusive mass transfer mechanisms are important in eclogites. This includes omphacite growth in garnet cracks (Erambert and Austrheim, 1993), overgrowth of strained omphacite crystals (Godard and van Roermund, 1995) and syntectonic omphacite vein growth (Essene and Fyfe, 1967, Carpenter, 1980, Philippot, 1987, Philippot and van Roermund, 1992). In addition omphacite foliations wrapping garnet and subsequent omphacite

pressure shadows indicate omphacite growth is sensitive to local changes in stress orientation, which can be explained by mass transfer but not by GBM (Godard and van Roermund, 1995, Mauler et al., 2001).

Grain growth, by whatever mechanism, alters the shape of the grains but not the crystal orientation. Rather it affects and creates LPO in a mineral by the selective growth of some grains and the elimination of others. Strain induced GBM rates will vary depending on the relative orientations of the two grains involved and in this way may have an effect on LPO (Poirier and Guillopé, 1979, Godard and van Roermund, 1995). Anisotropic growth and dissolution rates of diffusive mass transfer processes will have an effect on LPO. In clinopyroxene attachment energies and face growth and dissolution rates are minimum for <010>, intermediate for <100> and maximum for <001> (Van Panhius-Sigler and Hartman, 1981). Therefore grains with <001> parallel to the tensional direction will grow faster than other grains and those with <010> parallel to the compressional direction will dissolve slower, favouring the crystal orientations compatible with omphacite LPO patterns observed in deformed eclogite (Godard and van Roermund, 1995) (Fig. 1.7). Similar studies of preferential c-axis growth in quartz veins show LPO formation by this mechanism (Cox and Etheridge, 1983, Shelley, 1983).

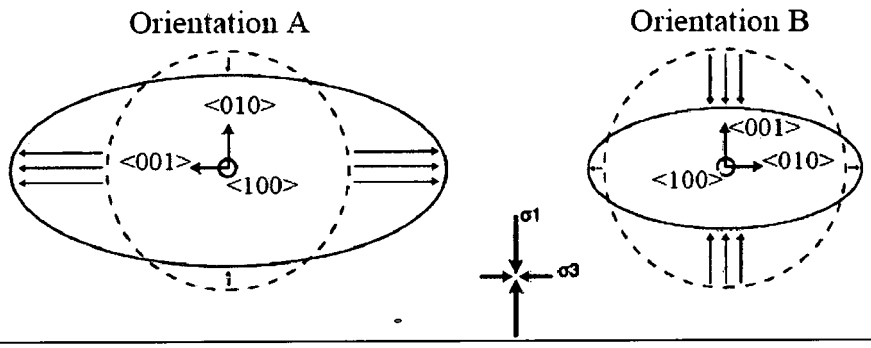

Fig. 1.7 From Mauler et al. (2001). Schematic diagram of anisotropic grain dissolution and growth in omphacite and its effect on LPO. This process will favour preservation of grains in orientation A and those in orientation B will ultimately vanish.

Mauler et al. (2001) suggest that a DMT mechanism is dominant in LPO formation and is the rate controlling one as opposed to dislocation creep. Their evidence is similar to that described above. Diffusion creep is grain size sensitive; with increasing grain size the length of diffusion pathways increase and potential dissolution and precipitation sites decrease, thus flux decreases. However eclogites

examined in this study show that omphacite reaches grain sizes of over 7mm but still show evidence for diffusion creep. They suggest that in the Earth the domain of geological conditions in which diffusion processes are active is wider than expected.

1.4.5.4 Recrystallisation Mechanisms

Deformed omphacite in some low temperature eclogites ($\leq$600°C) contains microstructures that suggest subgrain rotation recrystallisation (progressive rotation of subgrains into independent grains) is active in omphacite (van Roermund, 1984, Buatier et al., 1991, Philippot and van Roermund, 1992). Studies of low strain omphacite (Buatier et al., 1991) show that large omphacite parent grains recrystallise into smaller ones with daughter grains having the same geometric and crystallographic characteristics of the parent. New grain boundaries are thought to have developed from {110} tilt walls which accommodated lattice bending produced by slip on the ½<110>{110} system. Relevant to LPO formation, Buatier et al. (1991) and Philippot and van Roermund (1992) show that LPO in newly formed grains is similar to that of strained, parent omphacite although weaker. Therefore this process does not create strong LPO in omphacite.

From the literature it is obvious that both dislocation creep and diffusion creep play a significant role in the formation of the LPO patterns observed in omphacite. It also seems unlikely that either mechanism operates independently of the other, and that both work in tandem. Twinning and dynamic recrystallisation are shown to be lesser mechanisms associated with LPO development.

What needs further clarification is what deformation mechanism, dislocation creep or diffusive mass transfer and crystal growth, contributes more to LPO development, and under what conditions are they dominant. An investigation of omphacite microstructures and chemistry in eclogites from the Internal Zones of the Alps is carried out here in an attempt to shed light on these questions.

1.4.6 Interpreting Omphacite LPO – The Debate

As mentioned earlier the formation of L/S type fabrics in deformed omphacite can tell us about certain properties of the eclogite rock. Whether or not an L or an S type LPO develops has two possible causes; the strain regime the eclogite rock was deformed under, or the transition between space groups of omphacite in response to temperature changes and chemistry changes.

The latter is investigated in Brenker et al. (2002) where a suite of eclogites from variable temperatures is studied. LPOs from the samples is collected and correlated to the C2/c and P2/n omphacite phase diagram using deformation temperatures and omphacite chemical compositions (Fig 1.8). The results show a strong correlation between the temperature of deformation and the resulting LPO. They also display a pattern such that S-type LPOs fall within the C2/c field whereas the L-type LPO mainly falls within the P2/n field. The authors then go on to suggest that this apparent correlation means it is the space group of omphacite that controls the mechanisms by which it deforms and through these the type of LPO that is generated.

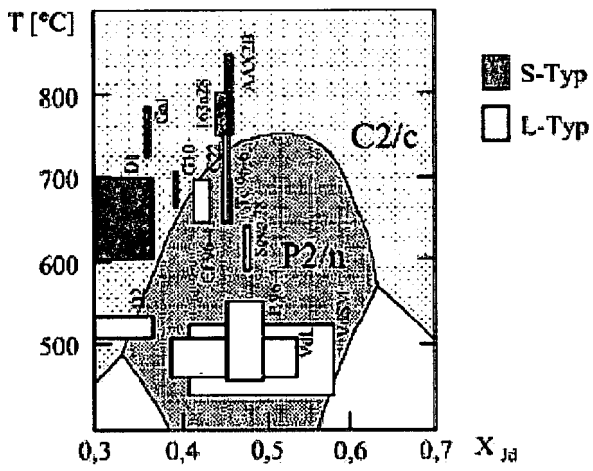

Fig. 1.8 From Brenker et al. (2002). Omphacite phase diagram showing omphacite samples with jadeite component plotted against deformation temperature. A strong correlation can be seen between space group and omphacite LPO type.

The main argument supporting this theory rises from slip system investigation in both ordered and disordered omphacite. The **b** = ½<110> dislocation is a perfect dislocation in the C2/c space group. Cation ordering in the P2/n space group produces a doubling of the length of the burgers vector for a perfect dislocation to **b** =<-110> (Fig. 1.9). For energy reasons this will then split into two partial dislocations <-110>=½<-110> + ½<-110> and a stacking fault forms between them. Compared to the C2/c structure the length of the burgers vector remains the same but extra energy is required by the formation of stacking faults. Thus b=½<-110> dislocations will be less mobile in P2/n omphacite than in C2/c omphacite.

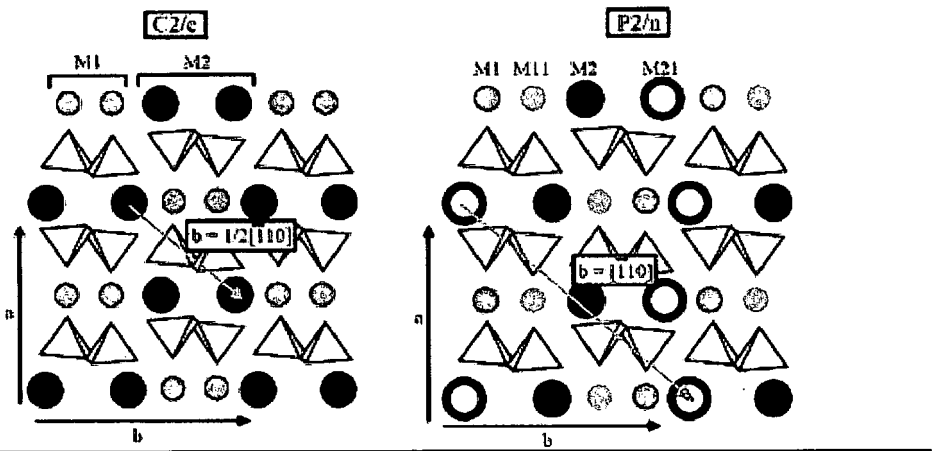

Fig. 1.9 Schematic diagram of the omphacite structure viewed parallel to the c direction. In C2/c omphacite space group the grey arrow indicates the perfect dislocation b=1/2<-110>. In P2/n omphacite space group the grey arrow shows the doubled length of the perfect dislocation to b=<-110>.

From this it is inferred that the deformation behaviour of P2/n omphacite will be significantly different from C2/c omphacite. As the partial dislocation in P2/n require more energy due to stacking faults they are more likely to be pinned by obstacles in the crystal lattice. This suggests that the slip system b=½<-110> will contribute less to deformation than other slip systems in P2/n omphacite (Brenker et al., 2002). This study further suggests that this difference in operating slip systems is enough alone to create different LPO patterns in the two space groups of omphacite.

Most P-T-t pathways of eclogite pass through both stability fields allowing deformation in both. Thus all P2/n are thought to have first crystallised with C2/c structure. If deformation corresponds to early stages of omphacite crystallisation even if it is within the P2/n field it will probably show characteristics of the C2/c structure. This is because large strains are necessary to overprint pre-existing lattice

orientations and cause significant recrystallisation in a sample. Deformation in both diffusion and dislocation creep fields will not rapidly alter the initial LPO (Mauler, 2001).

The second theory for omphacite LPO pattern development, as mentioned, is that LPO type in omphacite is dependent on the strain regime in which the eclogite deforms. The theory states that S-type LPO relates to deformation geometry within the flattening field and that L and LS-types relate to a more constrictional deformation geometry. There are a few studies that support this hypothesis and that directly contradict the previous space group control theory.

One of the strongest arguments for this theory is the use of viscoplastic self consistent (VPSC) models to simulate omphacite LPO development in response to deformation solely by dislocation glide. The model has two assumptions; that the crystals that form the aggregate deform uniquely by homogeneous intracrystalline slip on selected crystallographic planes and that the aggregate behaviour may be calculated as an average of the crystals behaviour (Bascou et al., 2002). Two main studies using this method (Bascou et al., 2002, Ulrich and Mainprice, 2005) involve using only those slip systems, associated stress exponents and critical resolved shear stresses (CRSS) that are found in naturally and experimentally deformed eclogites and from deformation experiments on single crystal diopside. This includes those commonly noted in previous studies; ½<110> {-110}, [001] {110} and [001] (100) as well as other less common slip system, e.g. [100] (010) and [001] (010).

The study carried out by Bascou et al. (2002) show that the VPSC model reproduces the typical omphacite LPOs of naturally deformed eclogites. The model results also show that the patterns developed can be directly produced by slip occurring mainly on the 1/2 <110> {110}, [001] {110} and [001] (100) systems. They also suggest that the variable patterns developed in the model (L and S types) are a result of differing strain regimes, with simple shear experiments displaying a more LS type fabric, transpression tests give strong S types, transtension gives strong L types and axial compression and pure shear provide strong S-types and LS types respectively. They also suggest that the asymmetry of some of the LPOs may indicate non-coaxial strain during deformation. A study done by Ulrich and Mainprice (2005) emulates these results, with extension tests producing strong L-type fabrics, compression tests

giving strong S-type fabrics and pure shear and simple shear experiments giving LS types (Fig. 1.10). They explain how, by increasing the CRSS by one order of magnitude for the ½<110> {110} system, there is a significant reduction in its activity but this does not produce a change in the LPO of omphacite from S to L-type. This suggests that the activity of this slip system does not have a significant effect on LPO development in omphacite.

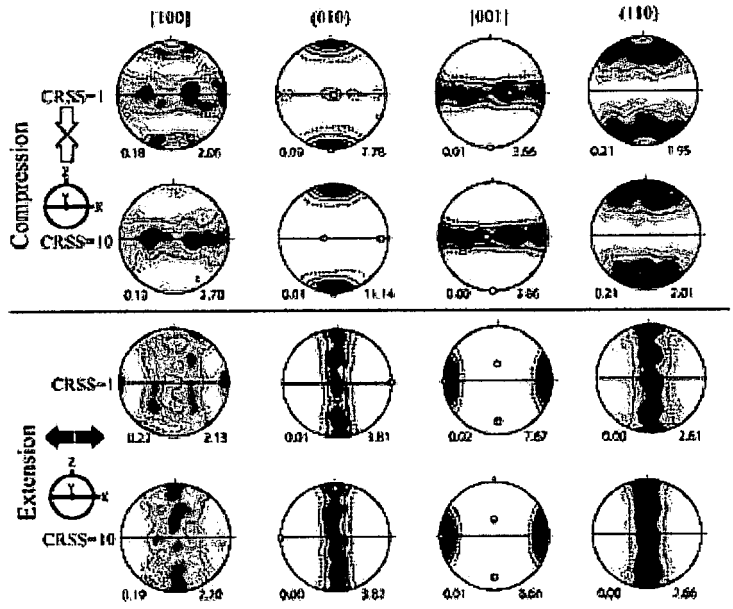

Fig. 1.10 From Ulrich and Mainprice (2005). Omphacite LPO patterns generated from compression and extension VPSC models. XY plane is horizontal, compression is parallel to Z and extension is parallel to X. Minimum and maximum densities are marked on the bottom left and bottom right of each pole figure respectively.

There is evidence in other forms that support the theory that LPO is dependent on strain regime and not cation ordering changes. Examples exist where similar omphacite textures were found in eclogites of contrasting pressure-temperature conditions. Conversely contrasting LPO types are known to exist in small sample areas which have similar if not identical pressure-temperature conditions and have the same omphacite chemical compositions (Kurz et al., 2003, Mauler et al., 2001). These cases thus contradict the idea that space group theory is the cause of differing LPO patterns in omphacite. These authors suggest that differing types are thus interpreted in terms of regional variations in the strain geometry of the eclogite body.

It has also been noted in some studies that a relationship exists between the shape fabric of omphacite and its LPO (Helmstaedt et al., 1972, Godard et al., 1995, Abalos, 1997, Mauler et al., 2001). Godard et al. (1995) stated that as the SPO of

omphacite changes from oblate to prolate a corresponding change occurs in the LPO going from an S-type to an L-type. Similar results are shown in omphacite in the Cabo Ortegal eclogite (NW Spain) (Abalos, 1997). This idea is also supported by Mauler et al. (2001) who explain L and S-type fabrics in terms of anisotropic growth and dissolution although it is now known thanks to VPSC modelling that these patterns can be produced solely by dislocation creep. In other words a combination effect of dislocation and diffusion creep forms LPO in omphacite although which one is that rate controlling factor is debatable.

Taking into account the information and data presented for each theory it seems more likely that strain regime controls the omphacite LPO pattern in eclogites rather than the space group of the mineral. In this thesis it is hoped to be able to add to the body of evidence for this debate, and to determine what control on omphacite LPO pattern is present in the eclogite facies units of the Internal Zones on the Western Alps.

1.5 Garnet: A Review

The garnet group, though a relatively minor component of the Earth's crust and upper mantle, is an important group of minerals. It is a key constituent of eclogite and eclogite facies rocks at the base of thickened continental crust as well as in subducted slabs and is also present in upper mantle peridotites and Mantle Transition Zone (400-650km) as majoritic garnet. Its prominent occurrence in said areas suggests that garnet should have some control of their rheology. Garnet is also a vitally important mineral in many metamorphic rocks especially for pressure-temperature estimations and geochronology.

1.5.1 Garnet Chemistry in Eclogites

Garnet has the general chemical structure $X_3Y_2(SiO_4)_3$, where X sites can be filled by Mn, Mg, Fe^{2+} and Ca and Y sites can be filled by Al, Cr, Mn^{3+} and Fe^{3+}. It is rare though for a garnet to be a pure end member composition and it is usually named for its most dominant component. The mineral group can be divided into two series; the pyralspites (pyrope, almandine, and spessartine) and the ugrandites (uvarovite, grossular, and andradite). Complete and continuous variation occurs easily within the groups but is difficult between them. Depending on its variable chemistry garnet can display a range of colours (Table 1.1).

Name	Chemistry	Colour
Pyrope	$Mg_3Al_2(SiO_4)_3$	Crimson-purple
Almandine	$Fe_3Al_2(SiO_4)_3$	Dark red
Spessartine	$Mn_3Al_2(SiO_4)_3$	Red
Grossular	$Ca_3Al_2(SiO_4)_3$	Clear-pink
Andradite	$Ca_3(Fe/Ti)_2(SiO_4)_3$	Yellow-dark brown
Uvarovite	$Ca_3Cr_2(SiO_4)_3$	Green

Table 1.1 Common varieties of garnet, their chemistry and colour

Three main garnet types are found within eclogite facies rocks; pyrope, almandine and grossular. Pyrope is typical of high-grade metamorphic terrains usually containing between 40-70% of the pyrope molecule with the rest being predominantly almandine and grossular. Pyrope content can be used to distinguish between the three different eclogite groups; A, B and C as defined by Coleman et al.

1965 (Fig. 1.11). Group A has greater than 55% pyrope, group B has 30-55% and group C has less than 30% pyrope.

Almandine is the most common garnet species and generally contains large amounts of both the pyrope and spessartine molecule and may also have significant grossular components. Grossular incorporates a significant amount of the andradite molecule with which it can form a continuous series. Also despite a grossular-hydrogrossular series there is no evidence that it is typical of thermal metamorphism as it contains significant amounts of water (Deer et al. 1992).

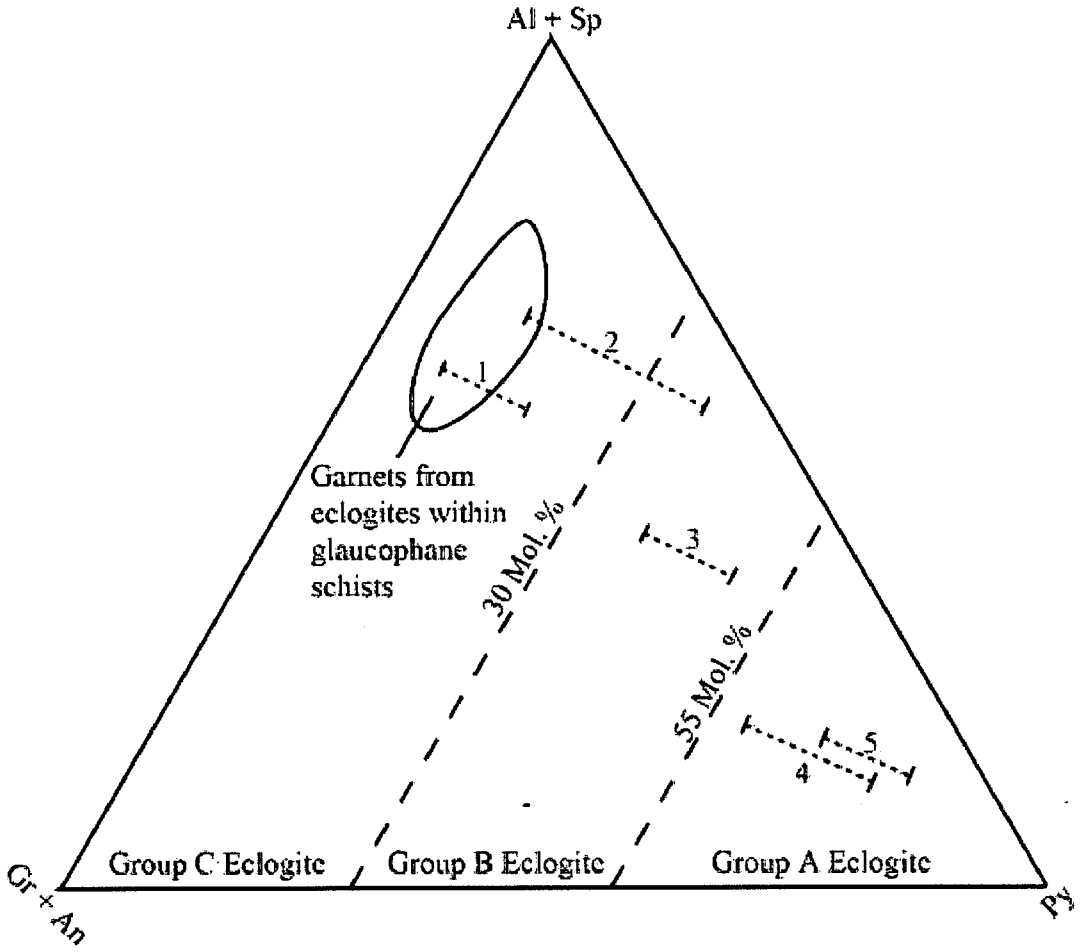

Fig. 1.11 Relative proportions of end-member garnet molecules for garnet in eclogites and related rock types. Dotted lines show average garnet compositions in; 1 - amphibolites, 2 - charnockites and granulites, 3 - eclogites in gneisses or migmatitic terrain, 4 - eclogites associated with kimberlite pipes, 5 - eclogites within ultramafic rocks.

Garnet is commonly used for elucidating the metamorphic pathway taken by a rock due to the chemical composition of the mineral being sensitive to pressure and temperature, and also because cation diffusion rates in garnet are low, increasing the potential for preservation of a longer metamorphic history. Most high pressure and ultrahigh pressure eclogites contain garnet with growth zonation patterns in major and trace elements.

Typically, with increasing temperature, increasing Fe and Mg and decreasing Mn and Ca zonation patterns, from core to rim can be found (Vance and O'Nions, 1990). Manganese zonation is thought to be an excellent chemical marker in eclogitic garnet especially in the initial stages of garnet growth as Mn strongly fractionates into growing garnet grains. A commonly observed Mn zoning pattern in almandine garnet, developing through prograde metamorphism, is of high core Mn and low rim Mn. Fe on the other hand tends to show an opposite pattern to this (Freer, 1979). The usefulness of Mn as a marker decreases as the garnet continues to grow because Mn sources become depleted around growing garnets. Even then decreasing Mn values when used in ratio with other major garnet elements (Ca, Fe, Mg) remain useful for examining timing of growth stages in prograde growth of eclogite garnet (Săbău et al., 2006).

As mentioned, cation diffusion is slow in garnet, though some cations diffuse slower than others. Calcium diffusion within garnet is orders of magnitude lower than that of magnesium, thought to be due to the large ionic size of calcium (Schwandt et al., 1996). Other diffusion studies (Loomis et al., 1985, Chakraborty and Ganguly., 1992) have shown that diffusion coefficients for Mn are higher than those for Fe and Mg, which are approximately the same.

It must be kept in mind that with respect to eclogitic garnet, diffusion rates are thought to be faster than lower grade garnet explaining the often less well defined zonation patterns observed in higher grade rocks (Freer, 1979).

1.5.2 Crystal Structure of Garnet

All garnet is of the cubic crystal system (Fig. 1.12A), with axes lengths; $\mathbf{a} = \mathbf{b} = \mathbf{c}$ and angles between axes; $\alpha = \beta = \gamma = 90°$. Garnet also has a body centred cubic lattice arrangement (space group Ia3d). The unit cell of garnet contains eight

$X_3Y_2(SiO_4)_3$ formula units (Fig. 1.12B). The structure has alternating SiO_4 tetrahedra and YO_6 octahedra which share corners to form a 3D network. Within these exist 'cavities' which contain the X ions. Garnets are most often found in the dodecahedral habit but also commonly form a deltoidal icositetrahedon. It is important to keep in mind that all garnet species are isomechanical, meaning that all species behave the same way mechanically (Karato et al., 1995).

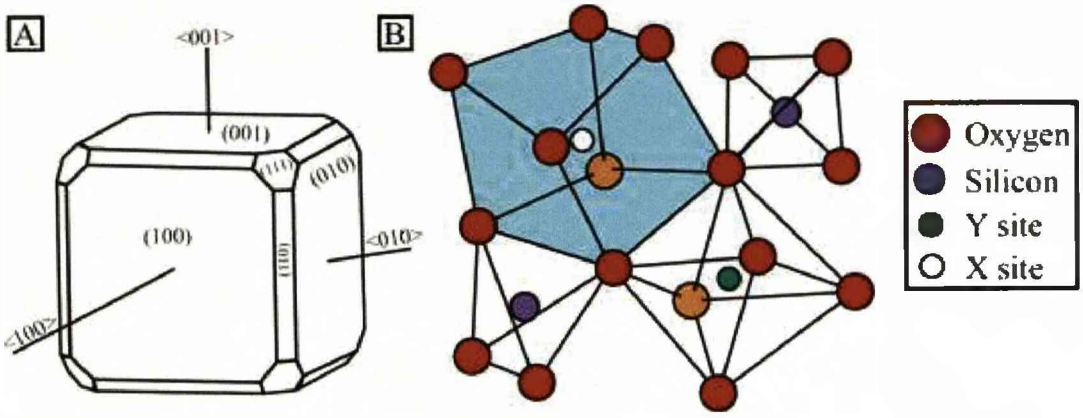

Fig. 1.12 A – Diagram of the cubic crystal system garnet belongs to, B – diagrammatical structure of garnet showing the distorted 'cubes' of oxygen atoms that form around the X sites

1.5.3 Garnet Deformation

As mentioned many previous studies of eclogite deformation consider garnet to act as a rigid body, with omphacite accommodating strain (Godard and Van Roermund, 1995, Voegelé et al., 1998, Brenker et al., 2003, Kurz et al., 2003, Mauler et al., 2001, Jin et al., 2001, Piepenbreier and Stöckhert, 2001). However with developments in scanning electron microscopy (SEM) and electron backscatter diffraction (EBSD) (for full descriptions of equipment and technique see Chapter 3) detailed analysis of eclogite facies garnet crystal lattice is possible. Since then many cases have been made for crystal plastic deformation in garnet. Evidence for various brittle and plastic deformation mechanisms in garnet is laid out here, with a focus on those mechanisms noted in eclogite facies rocks.

1.5.3.1 Brittle Deformation

Brittle deformation such as fracturing is well documented in garnets from all rock types it occurs in. The cause and meaning of such fracturing however can be varied and only when the microstructure of garnet is thoroughly investigated can it be said what brittle deformation in garnets may tell us.

Fractures can develop from differential expansion of inclusions within the garnet during isothermal decompression (Whitney, 1996), for example radial fractures developing around quartz inclusions which were once coesite at ultrahigh-pressure conditions. Internal conditions are not the only way of forming fracturing in garnets, external forces such as hydrofracturing (Whitney, 1996), when fluid pressure exceeds the minimum principal stress, deformation and subcritical processes, such as dissolution at stressed crack tips and reprecipitation as the tip propagates (Prior, 1993), are also involved in brittle deformation. There is evidence that fracturing in garnet may have a strong control on certain chemical heterogeneities within the mineral (Matthews et al., 1992, Prior, 1993) and that fracturing can be related to seismic activity (Trepmann and Stöckhert, 2002).

Careful consideration and examination of garnet fracture patterns is essential to understand various properties of garnets as well as revealing certain aspects of deformation and metamorphic history of the tectonic unit the garnet occurs in.

1.5.3.2 Plastic Deformation

Plastic deformation of garnet is presently poorly understood although plenty of studies have attempted to rectify this.

Karato et al. (1995) tested oxide and silicate garnets to explore their plastic properties. Using high temperature compression tests on single crystal garnet in the <100> and <110> orientation they showed that the <110> orientation was ~10% greater in creep strength than the <100> orientation. Using TEM to determine Burgers vectors and slip plane traces the <111> {1-10} slip systems seemed to be dominant in their experimental range. They explain that in comparison with other minerals garnet is shown to have significantly higher creep strength.

Karato et al. (1995) also carry out hardness tests on the (100) garnet surface resulting in plastic deformation involving dislocation glide with minor cracking. They suggest from this that the strength of garnet is very high. Further mechanical data (Zhang et al., 2007) confirm the high strength of garnet, stating that it is at least four to six times as strong as omphacite and twice as strong as harzburgite i.e. olivine. Using the hardness test results (Karato et al., 1995) a Peierls stress (a fundamental quantity characterising the difficulty of dislocation glide) is estimated for garnet giving values of ~0.17. Compared with other minerals this is significantly higher indicating that garnet has a higher resistance to dislocation glide (Karato et al., 1995, Voegelé et al. 1998).

The same study uses a stress-dip test to attempt to determine the importance of dislocation climb versus dislocation glide in garnet. In the stress dip test the response of sample strain is measured after a sudden reduction in stress. When deformation rate is dominated by dislocation climb the applied stress from steady state deformation is almost balanced by internal stresses due to dislocation interactions. As a result a sudden decrease in stress will halt deformation as the internal stress of interacting dislocations will exceed the applied stress. In contrast when resistance to dislocation creep itself controls the rate of deformation (creep) then a decrease in applied stress will only result in a finite decrease in deformation.

Karato et al. (1995) propose that if the observed high creep strength of garnet is due to slow dislocation climb then cation diffusion rates in garnet should be lower than that of other minerals. However compared to minerals like olivine, diffusion rates are not dissimilar suggesting that climb is not the rate controlling factor, rather dislocation glide is. This is consistent with the high hardness of garnet and makes sense when considering the crystal structure of garnet. A large unit cell gives garnet long Burgers vectors and dislocation dissociation in the bcc structure is also a contributing factor to the high creep strength of garnets. The authors urge caution though when translating the results of these single crystal deformation results to naturally deformed garnet. Observation of subgrain boundaries in naturally deformed garnet (Ando et al., 1993) suggest significant amounts of dislocation climb occurs in garnet. That these are not seen in experimentally deformed garnet may be due to the effect of static annealing in naturally deformed garnet and that subgrain formation

may form at higher strains than those reached in experiments. In addition diffusion coefficients for garnet may not be low enough to significantly retard climb. Also these experiments were primarily concerned with the **b** = ½<111> partial dislocation rather than the other common type of **b** = <100>.

Further investigation into garnet plastic deformation is carried out in a pair of papers by Voegelé et al. (1998). They performed a series of tests on both garnet single crystals and naturally deformed samples. High pressure experiments on garnet single crystals in a range of 700-1440 °C revealed that below 1000 °C the specimens show only evidence of micro-plasticity associated with micro-cracking. The dislocations present were characterised by Large Angle Convergent Beam Electron Diffraction (LACBED) and for the low temperature experiments were predominantly of the ½<111> type with some <100>. Above 1000 °C garnet becomes more ductile and the microstructure becomes more characteristic of dislocation creep accompanied by recovery. Subgrain boundaries are evident and the dominant dislocations found are of the ½<111> and <100> types. The predominance of the ½<111> dislocation may be due to the fact that in bcc garnet this dislocation corresponds to the shortest lattice vector and glide direction depends on the Bravais lattice. The glide plane however is more variable as shown by characterising simultaneously the Burgers vector and the line direction.

Naturally deformed samples were taken from a spectrum of localities so that group A, B and C eclogite garnets could be investigated. The group C eclogites from the Sesia-Lanzo in the Italian Alps displayed little plastic deformation with most of it being restricted to micro-plasticity related to micro-fracturing, such that dislocation nucleation is assisted by stress concentration at the crack tips. These dislocations however do not propagate far from the cracks due to a very strong lattice friction. The most common dislocation recorded was the ½<111> type with some <100> type and a few <110>. These operated within a variety of glide planes. Group B eclogites from Bragança, Portugal had homogeneous deformation microstructures with lots of free dislocations mainly organised into subgrain boundaries. Again the dislocations were determined with ½<111> and <100> being predominant. A selection of group A eclogites studied in this investigation showed subgrain boundaries were present and the dislocations were mostly of the ½<111> type.

Voegelé et al. (1998) conclude from their experiments that a brittle-ductile transition exists between eclogites of groups C and B. Below 600 °C (group C eclogites) garnets are mainly brittle and plasticity occurs only near micro-fractures. Above this temperature dislocations appear to become mobile and garnet can be plastically deformed with dislocation glide and climb being important mechanisms. Scanning Electron Microscope (SEM) orientation images have shown that in naturally deformed garnets recovery is also an important deformation mechanism (Prior et al., 2000). However it is important to remember that temperature is not the only control on garnet deformation; other factors such as strain rate, pressure and crystal orientation are also viable variables.

The dominant Burgers vector in deformed garnets is ½<111> (a partial dislocation) and based on dislocation line directions these glide in three types of planes; {110}, {11-2} and {12-3}, with {110} being the most commonly found. Other slip systems noted are <100> {010} and <100> {011} (Voegelé et al., 1998).

As mentioned technological development of SEM systems allowed the collection of orientation contrast (OC) images in polyphase specimens (Prior et al., 1996). This allowed imaging of lattice distortions and misorientations on micron to millimetre scale which in turn allows more complete studies of garnet deformation. The first evidence of crystal plasticity in garnet on a scale larger than 30 μm is documented in Prior et al. (2000). Domains of varying crystallographic orientation (<3°) are present and the boundaries of these comprise arrays of two partial dislocations possibly with <110> vectors. These microstructures contradict experimental data and previous observations of natural garnet which suggest that garnet deforms by glide alone (Karato et al., 1995), although this was already suggested as a possibility in such studies. These SEM observations of natural garnets indicate that recovery and therefore climb are indeed important mechanisms in garnet deformation as well.

It is also suggested that microstructure and chemistry of garnets display a correlation, suggesting diffusion is affected by microstructure (Prior et al., 2000, Cuthbert and Buckman, 2005). Whether the variations are fixed during deformation or by post deformational diffusion controlled by the microstructure, is unknown.

Again technological advances in electron backscatter diffraction (EBSD) provided a unique method for collecting statistically significant misorientation data sets quickly and easily (Prior et al., 2002) (For a full description of this technique see Chapter 3). Application of this to optically isotropic garnet enables observation of crystal structures and helps to constrain processes that were otherwise unknown before these technological developments.

Prior et al. (2002) studied garnets from Glenelg, Scotland and from the Alps using EBSD. Orientation maps reveal that garnets can have either a domainal structure or simply have regular orientation with little internal distortion. Misorientation angle distribution analyses (see Chapter 3) shows that neighbour pair angles are biased to low misorientations, unlike random pair angles. Existence of such microstructures suggests a more complicated story to garnet histories, and in conjunction with other more traditional methods allow a more insightful interpretation of the processes responsible, be they related to plastic deformation or other common mechanisms such as fracturing, multiple nucleation and growth processes.

Eclogites within the Haram Gabbro, Haramsøya, Norway contain evidence of grain boundary sliding as a significant deformation mechanism in garnet (Terry and Heidelbach, 2004). They infer that shape preferred orientation (SPO) in fine grained garnet layers are similar to those formed in low strained metal alloys deforming by grain boundary sliding. Diamond shaped garnet grains noted are also similar to those formed by grain boundary sliding in synthetic olivine. This combined with a lack of LPO is taken as indirect evidence for grain boundary sliding. The paper shows that initial fine grained garnet, due to its formation being concurrent with deformation, deformed by grain boundary sliding. In addition, curved garnet grain boundaries, grain boundary bulging and new grains associated with bulging or possible strain induced growth suggest grain boundary migration is acting during deformation. Whereas most studies previously have been performed on larger garnets in a matrix of other smaller minerals, here the garnets are small and in layers, helping to define foliations and lineations as polycrystalline layers.

This work leads to the suggestion that here the garnet has a small strength contrast to the surrounding minerals. As previously mentioned, where other studies maintain that garnet is much stronger than most other rock forming minerals (Karato et al.,

1995, Voegelé et al. 1998, Zhang et al., 2007), here and in experimental work done on synthetic fine grained garnetites (Wang and Ji, 2000), it is thought that the difference is reduced in the diffusion-creep regime. Work on similar garnetite layers within eclogites in the Sulu Region, China (Ji et al., 2003), comes to more or less the same conclusion and suggests that garnet strength compared to that of omphacite is lower than previously expected.

In a further study of Glenelg garnets by Storey and Prior (2005), further microstructures are explored and interpreted as a function of strain. This includes low strain garnets with subgrains with low angle misorientations which are dispersed around rational crystallographic axes across their boundaries. Towards higher strains misorientations increase and become less controlled by crystallography showing more random patterns. In high strain areas garnets have a polygonal microstructure and their orientations are dispersed around the original single crystal orientation. A suggested evolution starts with dislocation creep and recovery in low strains to dynamic recrystallisation by subgrain rotation at higher strains and finally to deforming by diffusion creep assisted grain boundary sliding and associated rotations at high strain.

Numerical simulations of garnet LPO development in garnets using VPSC models (Mainprice et al. 2004) and slip systems determined by TEM from experimentally and naturally deformed samples have been carried out (Fig. 1.13). The ½<111>{110}, ½<111>{112}, ½<111>{123}, [110]{001}, [100]{010} and [100]{011} provide a possible sixty-six slip systems for plastic deformation of garnet, therefore meeting the Von Mises criterion for strain compatibility at large strains. The ½<111> {110} slip systems provides more than 86% of the total strain. Pole figures from VPSC models of axial compression, pure shear and simple shear, show weak patterns, with <100> poles aligned with the main shortening direction. Comparison to natural LPOs shows little similarity however as natural garnet studies show random LPO patterns. This may be due to natural samples having a lower proportion of garnet, preventing it from becoming highly strained and developing LPO.

Although flattened garnet is recorded in eclogites (Storey and Prior, 2005, Zhang and Green, 2006) there seems to be a disconnect between strong SPO and the random

LPO observed. Experimental work on wet and dry eclogite shows that structurally bonded hydroxyl in garnet has a significant effect on its mechanical properties, such that its strength is reduced (Zhang at al., 2007). As dislocation creep is ruled out as the cause of elongate garnet formation other mechanisms are invoked, such as grain boundary sliding mechanisms assisted by subgrain formation and rotation. Microstructural observations made in experiments on 'wet' and 'dry' eclogite by Zhang et al. (2007) suggest this mechanism is a likely cause for garnet flattening in eclogites.

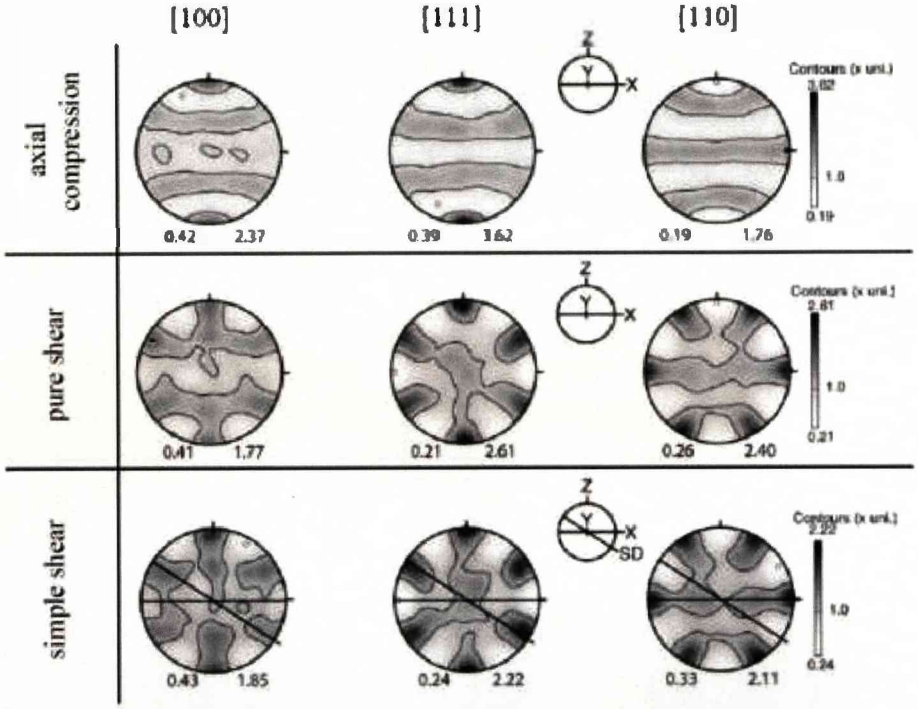

Fig. 1.13 From Mainprice et al. (2004). Examples of LPO patterns in garnet pole figures for VPSC models of axial compression, pure and simple shear. For axial compression model compression axis is vertical (Z). For pure shear compression axis is vertical (Z) and extension axis is horizontal (X). For simple shear model X and Y axes are finite strain axes with the X and Z axes being the maximum and minimum extension directions respectively and a horizontal line marks the XY finite strain plane.

1.6 Hornblende: A Review

A brief review of the properties of the hornblende family is included here as it constitutes one of the main mineralogical phase associated with the retrogressive event that overprints the Zermatt-Saas and Sesia-Lanzo Zone. As such the formation, microstructure and chemistry of this mineral is important when considering the dynamics of the exhumation of these eclogitic units.

1.6.1 Hornblende Chemistry

The mineral group of hornblende has the chemical composition range, $(Na,K)_{0-1}Ca_2(Mg,Fe^{2+},Fe^{3+},Al)_5Si_{6-7.5}Al_{2-0.5}O_{22}(OH)_2$. Resulting colours are black to green. The term hornblende is used sensu stricto for the end member chemistry $Ca_2(Mg,Fe)_4AlSi_7AlO_{22}(OH)_2$ (magnesio-hornblende and ferro-hornblende), for amphiboles near this composition and for all calcic amphiboles with significant aluminium content. Hornblende occurs, in both iron and magnesium rich forms, as part of various solid solution series involving other amphiboles; tremolite, actinolite, edenite, tschermakite, pargasite and hastingsite through various chemical substitutions.

Amphibole nomenclature based on chemistry, as laid out in Leake (1978), divides amphiboles into iron-magnesium-manganese amphiboles, calcic amphiboles, sodic-calcic amphiboles and the alkali amphibole group. Most hornblende falls into the calcic amphiboles although more sodic hornblende (barroisite) is found at higher temperatures and falls into the sodic-calcic grouping.

1.6.2 Crystal Structure of Hornblende

Hornblendes have a monoclinic crystal structure such that $\mathbf{a} \neq \mathbf{b} \neq \mathbf{c}$ (where $\mathbf{a}$ = ~9.9Å, $\mathbf{b}$ = ~18.0Å, $\mathbf{c}$ = ~5.3Å). Angles between the axes follow the monoclinic rule, $\alpha = \gamma \neq \beta$, with $\alpha = \gamma = 90°$ and $\beta = 105.5°$. They have the space group C2/m (C-centred with a mirror plane). The **a** and **c** axes intersect their respective planes obliquely whereas the **b** axes intersects the (010) plane perpendicularly in the same fashion as omphacite (Fig. 1.3). Good cleavage in the {110} is common in hornblendes producing 56° and 124° angles and the phase generally has a hexagonal or granular habit.

1.6.3 Hornblende Deformation

There is a general consensus that in greenschist facies conditions hornblende deforms by brittle processes often in combination with metamorphic breakdown reactions (Berger and Stünitz, 1996). In conditions above that of the greenschist facies, hornblende deformation becomes more complex, involving varying contributions from fracturing, intracrystalline plasticity and dissolution/precipitation.

Brittle deformation is well documented in amphibole deformed in higher grade conditions (Brodie and Rutter, 1985, Babaie and La Tour, 1994) including glide along fractures and microfracturing associated with mass transfer. Twinning is a common deformation mechanism in hornblende and has been noted in a wide range of conditions in experimental work (Rooney et al., 1975, Dollinger and Blacic, 1975) with the dominant twin being (-101). Twinning in naturally deformed samples is also noted however with the dominant twin plane being (100) with some (-101) twins occurring (Biermann, 1981, Hacker and Christie, 1990).

Crystal plasticity is also documented in deformed hornblende, although it has been noted that amphiboles are relatively resistant to crystal plastic deformation even at high metamorphic grades (Brodie and Rutter, 1985). In deformation experiments from 650 to 950°C hornblende in natural amphibolite displayed dislocation glide and dynamic recrystallisation accompanying fracturing (Hacker and Christie, 1990). Dislocation glide and subgrain formation are noted in amphibole (Biermann and Van Roermund, 1983) and dislocation creep documented by dynamic recrystallisation has also been recorded by Skrotzki (1992).

1.6.4 Lattice Preferred Orientation in Hornblende

It is true for amphiboles that few fabrics have been reported. Strong concentrations of <001> parallel to lineation are noted (Schwerdtner, 1964, Gapais and Brun, 1981, Rousell, 1981) as is a concentration of <001> within the foliation plane with a concentration of (110) planes parallel to lineation (Kern and Fakhimi, 1975, Gapais and Brun, 1981). Fabrics with concentrations of <100> perpendicular to the foliation and <001> parallel to lineation are also documented (Mainprice and Nicolas, 1989, Siegesmund et al., 1994, Baratoux at al., 2005, Díaz Aspiroz et al., 2007, Tatham et al., 2007).

It was originally suggested by Schwerdtner (1964) that amphibole fabrics developed as a result of non-hydrostatic stress through the thermodynamic method outlined by Kamb (1959). This however was refuted by the existence of similar fabrics found in other minerals with different elastic properties which contradict the predictions made in the non-hydrostatic theory.

A common cause of LPO in many mineral phases is plastic deformation. The amphibole structure leads to the idea that easy glide would occur on the (100) [001] system as no strong Si-O bonds need be broken along it. Evidence for such slip has been experimentally produced (Rooney et al., 1975), has been inferred from optical measurements (Dollinger and Blacic, 1975), from naturally deformed hornblende (Skrotzki, 1992) and from TEM investigations (Biermann and Van Roermund, 1983).

Hornblende fabrics in the Bergell tonalite, Central Alps, show that those formed in solid-state deformation are identical to those that formed by rotation and alignment of hornblende as elongate, rigid particles in magmatic flow (Berger and Stünitz, 1996). The LPO consists of <100> pole perpendicular to the foliation plane and concentrations of <001> poles parallel to lineation. This suggests that as the hornblende transitioned from the magmatic flow regime to the solid state diffusion regime it behaved in a similar manner, that of rigid particles in a viscous material. Lack of intracrystalline defects and the fact that quartz apparently accommodates most of the strain, though plastic deformation, further proves this theory. Thus commonly observed hornblende LPO patterns can potentially be reached through alignment and pressure solution processes. Rigid body rotation of hornblende and amphibole as a cause of LPO development is also noted as a possibility in metagabbros and ultramylonites from the European Variscides (Baratoux et al., 2005) and in rock containing clino-amphibole prisms in a plagioclase matrix and from the Aracena metamorphic belt, SE Spain (Díaz Aspiroz et al., 2007).

2 Chapter 2: The Geology of the Internal Western Alps

The Geology of the Western Alps is split into two broad divisions, the Internal and External Zones. The Internal Zone contains relics of oceanic crust, obducted during the Alpine Orogeny as well as slices of continental basement, all of which are metamorphosed at high to ultra-high pressures and moderate to high temperatures. The External Zones consist of those areas of the Western Alps that contain weak or unmetamorphosed Mesozoic-Cenozoic sediments and their associated basement rocks.

The Internal Zones are bound to the southeast by the Quaternary deposits of the Po Plain and the Canavese Tectonic Line and to the northwest by the Penninic Thrust Front (Fig. 2.1). The zone records the closure of the Piemontese (Tethyan) ocean and the subsequent collision of the Adriatic plate in the south with the European continent in the north.

Included within the Internal Zones are a variety of lithological units that display, in part, high to ultrahigh pressure metamorphism. These units can be separated into three different groupings (Fig. 2.1). The Austroalpine units include the Sesia-Lanzo Zone (SL) and the Dent Blanche nappe system (DB). The Internal Crystalline Massifs include the Monte Rosa (MR), Gran Paradiso (GP), Dora-Maira (DM) and the Briançonnais Zone (BZ) units. Finally, the ophiolitic units derived from the Mesozoic Tethys Ocean, make up the Piemonte Zone. This includes the Zermatt-Saas units (ZS) and the Combin Zone units (C).

During the Alpine Orogeny the Internal Crystalline Massifs and the Piemonte Zone oceanic units were subducted southwards underneath the Austroalpine units. Together all three units locally developed high pressure metamorphic mineral assemblages (ultra-high in some cases), with the Sesia-Lanzo Zone showing the oldest example of eclogite facies metamorphism. This study deals with two units in particular, from two of the three main divisions of the Internal Zones, the Zermatt-Saas Unit and the Sesia-Lanzo Zone.

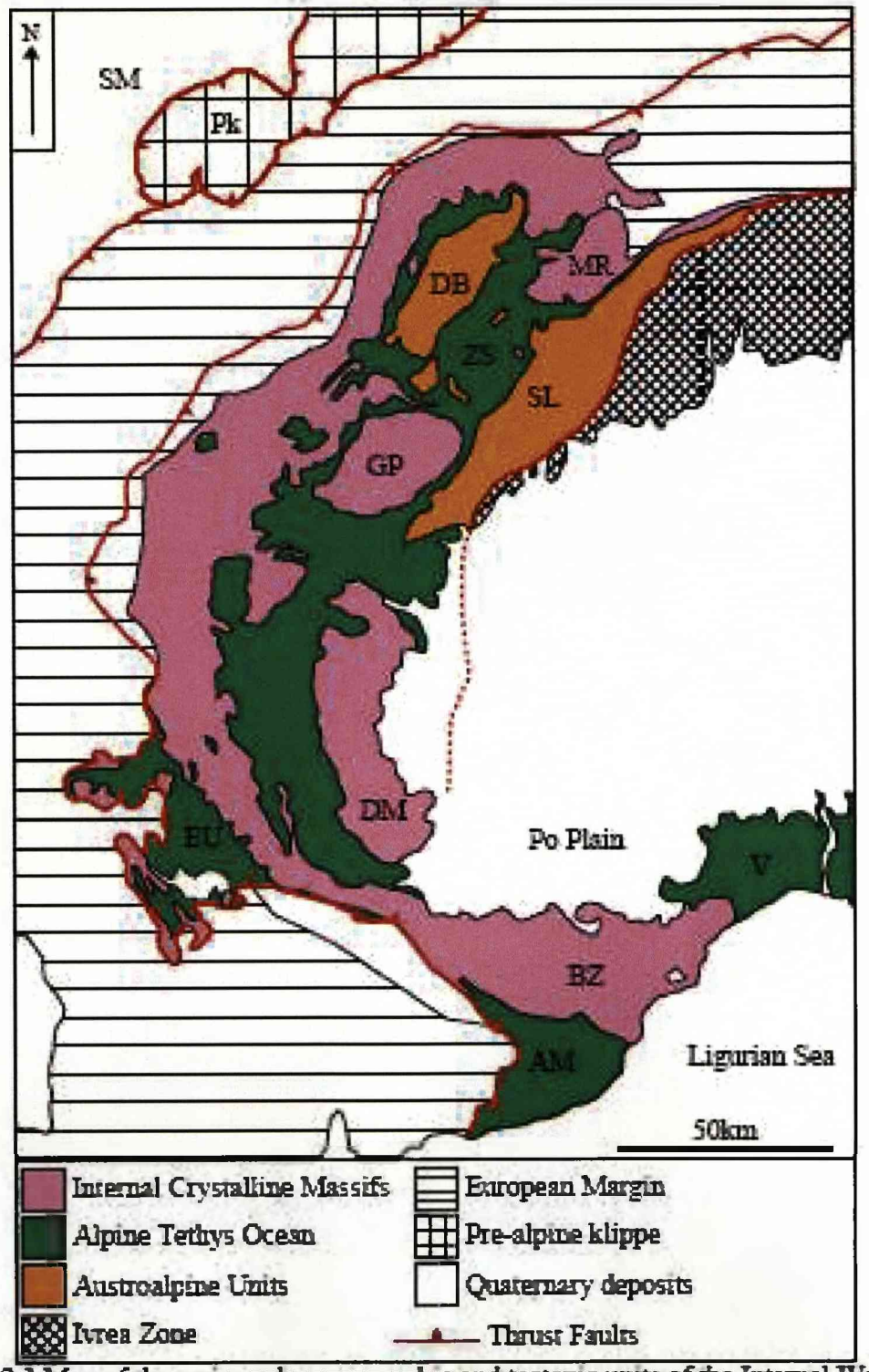

Fig. 2.1 Map of the major palaeogeographic and tectonic units of the Internal Western Alps. Austroalpine units: the Sesia-Lanzo (SL) and the Dent Blanche nappe (DB). Alpine Tethys Ocean Units of the Piemonte Zone: Zermatt-Saas and Combin units (ZS) and the Volri Massif (V) and the Helminthoid Flysch nappes: Embrunais Ubaye (EU) and Alpes Maritimes (AM). The Internal Crystalline Massifs: Monte Rosa (MR), Gran Paradiso (GP), Dora Maira (DM) and the Briançonnais Zone. The External Zone includes the Po Plain, the Ivrea Zone, the European Margin units, the Pre-alpine klippe (Pk) and the Swiss Molasse (SM)

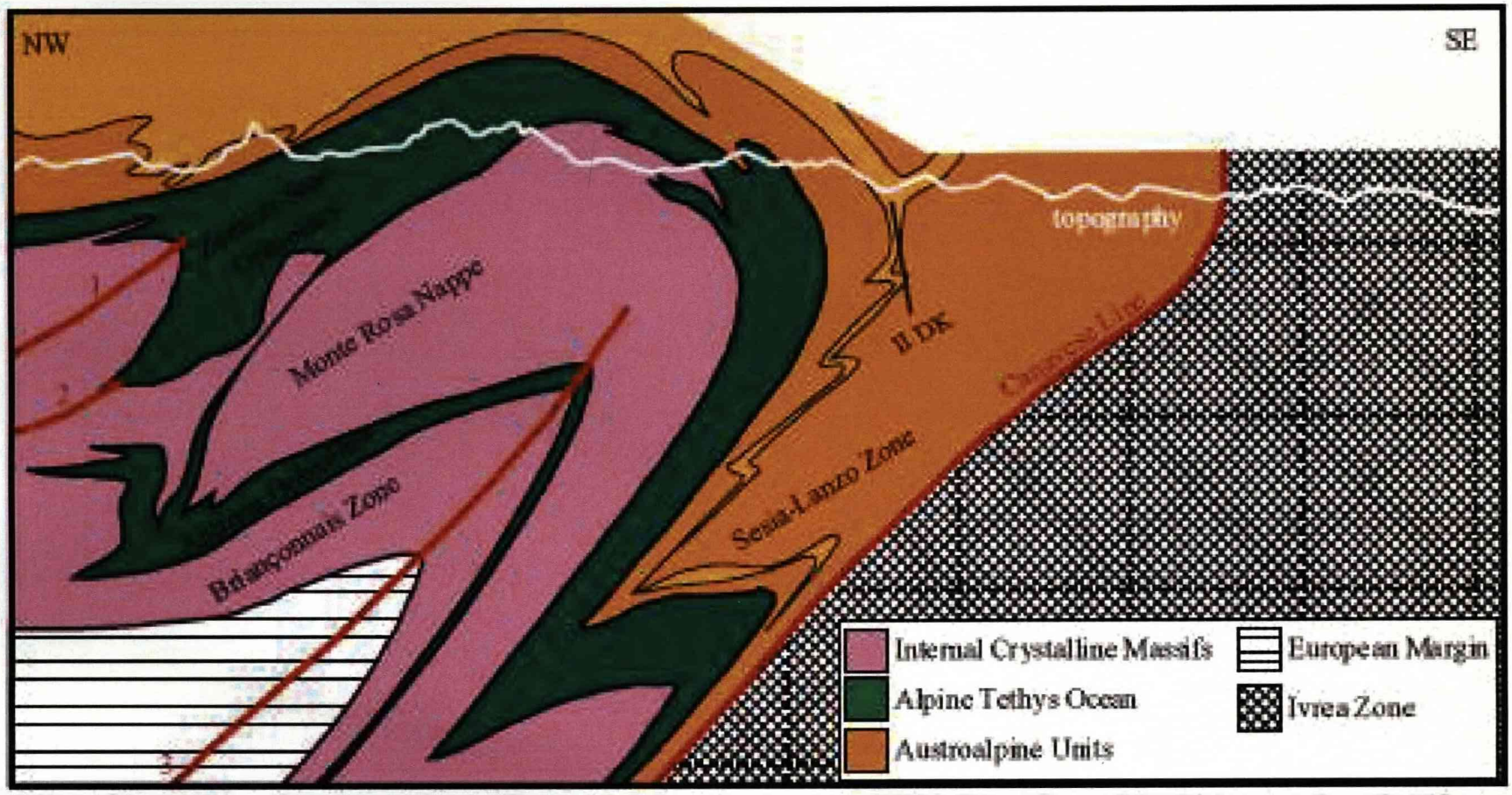

Fig. 2.2 Modified cross section of the Internal Western Alps from Escher et al. (1997). The units are folded into a number of antiforms and synforms, 1 - Mischabel antiform, 2 - Mittaghorn synform, 3 - Vanzone antiform

These two geological units are in structural contact with each other in Val Gressoney, NW Italy and were thrust upon one another during the Alpine Orogeny which began in the Western Alps in the Late Cretaceous. The subduction of Piemonte oceanic lithosphere below the Adriatic plate margin (Sesia-Lanzo) eventually led to the Eocene collision between Europe and Adria. Following this was the syn-collisional subduction of the Monte Rosa unit beneath the Adriatic plate (Dal Piaz et al., 2003). This resulted in the following structural layering. Starting with the structurally lowest unit; the Monte Rosa is overlain by the Zermatt-Saas which in turn is overlain by the Sesia-Lanzo unit, the structurally topmost geological unit (Fig. 2.2). Evidence exists for pre-Alpine metamorphism in the Sesia-Lanzo which is discussed later. As all these units were subducted during the Alpine Orogeny all have locally developed eclogite facies rocks and, in the Lago di Cignana area of the Zermatt-Saas, ultra high pressure rocks.

An exception to this is the Combin zone of the Piemonte ophiolitic material which lies structurally above the Zermatt-Saas unit and below the Sesia-Lanzo unit. Here a significant metamorphic break exists. Although the Zermatt-Saas and Sesia-Lanzo have been significantly retrogressed, they still contain relics of an eclogite facies event. The Combin Zone contains no such evidence suggesting it has never been to eclogite conditions. This is explored later in the chapter.

What follows now is a detailed literature review of the structural and metamorphic evolution of the Zermatt-Saas Unit and Sesia-Lanzo Zone beginning with the structurally lowest tectonic unit first.

2.1 The Zermatt-Saas Unit

The Zermatt-Saas together with the associated Combin zone forms the northern portion of the Piemonte Nappe. The unit itself overlies the Internal Crystalline Massifs which include the Monte Rosa, Gran Paradiso and Dora Maira. It is then overlain by Austroalpine rocks including the Sesia zone and the Dente Blanche klippe (Fig. 2.2).

2.1.1 Structure and Tectonic History

During the Alpine Orogeny the Zermatt-Saas unit and continental units of the European and African continental crust were subducted. The latter units have participated in one or more pre-Alpine orogenic events whilst the Zermatt-Saas has only been involved in one.

The Zermatt-Saas originated as Late Jurassic oceanic lithosphere which was the crust of the Piemontese (Tethyan) ocean that originally separated the older continental crust of the European continent and the African margin (Amato et al., 1999). A Late Jurassic age is constrained by U-Pb zircon dating (Rubatto et al., 1998). Nowhere is undisturbed ophiolite material preserved; rather it is evidenced by serpentinised ultrabasic lithologies, layered and isotropic metagabbros, sheeted dykes, pillow lavas and cherty metasediments (some manganiferous), all of which are present, each within separate thrust slices (Barnicoat and Fry, 1986), and commonly pervasively deformed.

A reversal of plate motion took place in the Mid-Cretaceous and the oceanic crust of the Zermatt-Saas started to subduct under the African margin, in what was once referred to as the Eoalpine event (first compression) (Dal Piaz and Ernst, 1978). While shortening occurred throughout the Tertiary, a major second compressional stage called the Lepontine event is prominent. It occurred during the Eocene to Late Oligocene and resulted in widespread compressional, ductile deformation and renewed metamorphism. This event created more crustal shortening through structures such as recumbent folds, back-folds, and thrusting.

The ophiolitic rocks of the Zermatt-Saas unit appear to have been emplaced upon the Monte Rosa at an early stage of the Alpine Orogeny and subsequently deformed by

the same back-folding and back-thrusting which can be seen in that unit. It has in some areas caused the unit to become overturned. At the Monte Rosa/Zermatt-Saas contact, where Zermatt-Saas metabasites are heavily retrogressed, retrogressive fabrics in Zermatt-Saas and Monte Rosa are sub-parallel, suggesting that the two units were juxtaposed post eclogite facies metamorphism (Reddy et al., 1999).

Internally the unit is composed of a series of thrust slices up to 1km thick (Barnicoat and Fry, 1986, Reddy et al., 1999).

2.1.2 Metamorphic History

The ultra high pressure eclogites exist only in one locality of the Zermatt-Saas Unit, at Lago di Cignana and are evidenced by the occurrence of coesite in the assemblage. A detailed P-T-t gives peak pressures of 2.7-2.9 GPa and temperatures of 600-630°C (based on garnet-clinopyroxene pairs and garnet-dolomite-aragonite assemblages) (van der Klauw et al, 1997; Reinecke, 1998). The exhumation has a three step pathway with the first part consisting of an early high pressure segment with ~100°C cooling to ~525°C at 2.0 GPa during decompression. The second step involves near-isothermal decompression from ~2 to ~1 GPa and the final, third stage involves further decompression during which the ultra-high pressure rocks reach their current tectonic position.

A Sm-Nd isochron age from garnet in eclogites found at Lago di Cignana show they are ~40.6 ± 2.6 Ma old. Rb-Sr whole rock-phengite isochrons date the greenschist facies conditions of the Zermatt-Saas at around 38±2 Ma. This combined with P-T data provide an estimate for the initial exhumation rate of this area (10-26 km/m.y.) followed by slow exhumation (0.3 km/m.y.) from 34-14 Ma (Amato et al., 1999).

A more recent Lu-Hf, garnet-omphacite-whole-rock isochron age of 48.8 ± 2.1 Ma for the ultra-high pressure rocks is reported by Lapen et al. 2003. Burial rates (Lapen et al., 2003), calculated from a garnet growth interval (50-38 Ma) and an assumed average crustal density of ~2.8-3.2 g/cc, give a range of 0.47 ± 0.03 cm/yr (garnet growth starting at 1.0 GPa) and 0.23 ± 0.02 cm/yr (garnet growth starting at 1.8 GPa). This is however older than the ages reported in Amato et al. (1999). The range of ages ~50-38Ma are interpreted as the duration of prograde metamorphism and possibly as the duration of garnet growth too. The difference in measured Sm-Nd and

Lu-Hf ages can be explained by expected core and rim variation in Lu, Hf, Sm and Nd. Lu is highest in garnet core and lowest in the rim generally following a Rayleigh fractionation profile. Higher core concentrations of Lu produce older Lu-Hf ages in these areas compared to those found in the rim. Sm-Nd dates indicate later garnet growth as predicted by Rayleigh fractionation of Sm and Nd. The difference between the two ages can be taken as a minimum estimate for the duration of garnet growth and prograde metamorphism given that Sm-Nd and Lu-Hf blocking temperatures are not exceeded for a long period of time (Lapen et al., 2003)

Putting the ultra-high pressure rocks aside, pressure and temperature estimates for the Zermatt-Saas are estimated at ~1.75-2.0 GPa and 550-600°C (Barnicoat and Fry, 1986). This metamorphism was once dated at 80-100 Ma (Hunziker, 1974) and at 70-100Ma (Bocquet et al., 1974) using K-Ar isochrons of alkali amphiboles. However, since then the timing of eclogite-facies metamorphism has been better constrained, with the Zermatt-Saas giving Tertiary metamorphic ages (50-40Ma) using Lu-Hf dating of garnets (Duchêne et al., 1997), and U-Pb dating on zircons (Rubatto et al., 1998).

For certain areas of the Zermatt-Saas, detailed P-T pathways have been given for the metamorphic history. Fry and Barnicoat (1987) describe one such pathway. The earliest assemblage recorded in the Zermatt-Saas is from garnet core inclusions; glaucophane, clinozoisite, quartz and rutile (Fig. 2.3 Stage 1). Transformation of this assemblage to an eclogite can be seen by the appearance of omphacite and the disappearance of glaucophane inclusions in the rims of these garnets. The peak assemblage (Fig. 2.3 Stage 2) of omphacite, garnet, clinozoisite, kyanite, talc, quartz and rutile is preserved in eclogites with the P-T constrained at 1.75-2.0 GPa and 550-600°C (Barnicoat and Fry, 1986).

The presence of high pressure and ultra high pressure metamorphism of the Zermatt-Saas protolith indicates that the unit may not be one continuous unit. Rather it may be made up of various tectonic slices some of which may have different prograde pathways from others, which then became juxtaposed upon each other later.

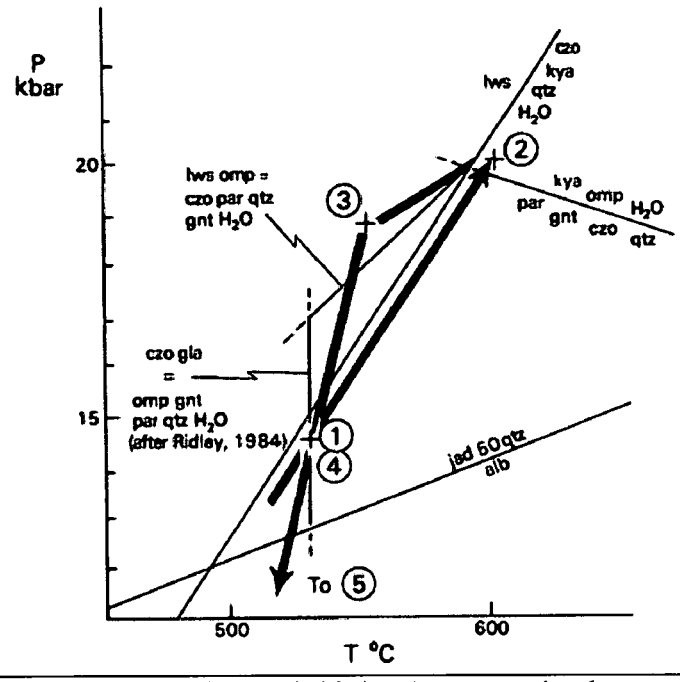

Fig. 2.3 From Fry and Barnicoat (1987). A constrained pressure-temperature pathway for the metamorphic evolution of the Zermatt-Saas Unit. Stages are shown by numbers in circles and explained within the text.

2.1.3 Exhumation and Retrogression

Eclogites of both high and ultra high pressure Zermatt-Saas have experienced significant amounts of retrogression. There are two main retrogressive events noted in the Zermatt-Saas Unit although Fry and Barnicoat (1987) report an initial stage of retrogression involving the development of lawsonite eclogites as temperature decreases toward glaucophane conditions (Fig. 2.3 Stage 3). The first is a blueschist facies overprint (Fig. 2.3 Stage 4) at pressures and temperatures of 1.2-1.5 GPa and $\leq$500°C and the second event is an amphibolite/greenschist event (Fig. 2.3 Stage 5) at pressures <1.0 GPa and temperatures < 550-500°C (Fry and Barnicoat, 1987, van der Klauw et al., 1997, Reinecke, 1998). The amphibolite/greenschist retrogression developed more uniformly and is better preserved than the blueschist one. The overprint of both retrogressive events is however incomplete and pre-existing higher pressure assemblages are still preserved in much of the unit.

As retrogression is tied to exhumation of a unit it is important to understand a unit's retrograde pathway. One described for the Zermatt-Saas, by Fry and Barnicoat (1987), involves a stepped or smooth pathway consisting of cooling into the lawsonite-eclogite field, followed by unloading to conditions of paragonite eclogites,

followed by more cooling causing regrowth of glaucophane and finally unloading allowing greenschist facies assemblages to form. The tectonic setting for such a path needs repeated thrust steps (for a stepped pathway) or continual thrusting (for a smooth pathway), emplacing cool continental crust beneath the ophiolites. This would have the effect of rapid cooling followed by isostatic uplift and pressure decreases attributed to the buoyancy effect of underlying continental crust combined with unroofing either by erosion or extensional tectonics.

Evidence for the latter can be witnessed in the extensional shear zone (Gressoney Shear Zone - GSZ) located in the top 10km or so of the Combin Zone (Reddy et al., 2003, Reddy at al., 1999). This structure is partly responsible for the exhumation of the Zermatt-Saas. The contact between the Zermatt-Saas and the overlying Combin Zone represents a significant metamorphic break, between eclogite and greenschist facies respectively. The GSZ has a geometry and kinematic framework consistent with SE directed extensional reactivation of convergent structures (Reddy et al., 1999). Rb/Sr dating of synkinematic, recrystallised white mica from the shear zone shows that extension continued from 44 Ma - 36 Ma, unroofing the Zermatt-Saas footwall from 18 kbar to 9 kbar (Reddy et al., 1999). Their dates overlap with those of peak high-pressure metamorphism, indicating that extension commenced before high pressure metamorphism in this area had ceased. $^{40}Ar/^{39}Ar$ dates of white mica from the shear zone indicate cooling after juxtaposition of the different tectonic units and are consistent with Rb/Sr ages (Reddy et al., 2003).

Extensional shear zones displaying SE directed transport are noted in the Täschalp area (Cartwright and Barnicoat, 2002). Rb-Sr data show these shear zones formed at 42-37Ma with the age of shearing becoming younger away from the Zermatt-Saas zone and into the overlying Grand St. Bernhard Nappe. Pressure and temperature estimates record conditions of 400-475°C and 400-500 MPa down to 300-350°C and 300-350 MPa. These shear zones thus formed during greenschist conditions and the timing of deformation (42-37Ma) is similar to that of the GSZ, suggesting they were involved in unroofing of the Zermatt-Saas.

Subsequent unroofing of the Zermatt-Saas since ~36Ma appears to be a result of erosion following uplift caused by further shortening (Reddy et al., 1999), and no younger extensional structures exist to suggest otherwise.

2.2 The Sesia-Lanzo Zone

The Sesia-Lanzo Zone is an elongate body of continental crust trending SW-NE and marks the SE limit of the Internal Zones. Part of the Austroalpine continental crust is thrust over the ophiolitic rocks of the Piemonte Zone and is in contact with the Zermatt-Saas unit and the Combin Zone at various points. It forms the southern margin of the Western Internal Alps and is separated from the Ivrea Zone by the Canavese Line an extension of the major fault zone, the Insubric Line. It is a polymetamorphic terrain recording events both before and contemporaneous with the Alpine Orogeny.

2.2.1 Structure and Tectonic History

Originally the Sesia-Lanzo Zone along with the Ivrea Zone was part of a sub-plate of the leading edge of Africa. In the Late Hercynian granite was intruded into the Sesia-Lanzo Zone as is evident at Monte Mucrone. This intrusion is dated around 286Ma using U-Pb zircon techniques (Paquette et al., 1989). During the Alpine Orogeny it split apart from the African block and Ivrea Zone and took part in Alpine tectonics and metamorphism (Desmons and Ghent, 1977).

The Sesia-Lanzo Zone is mainly composed of metamorphic, basic and pelitic rock, a smaller amount of carbonates and siliceous rocks, and granitoid bodies. It was originally divided into three main tectonic units based on lithology, metamorphism, deformation and tectonic contacts (Compagnoni et al., 1977 and references within). These are the "Eclogitic Micaschist Complex (EMC)", "Gneiss Minuti Complex (GMC)" and the "Zona Seconda Diorito-kinzigitica (IIDK)". These are grouped into the Upper Element (IIDK) and the Lower Element (EMC and GMC).

The EMC consists of mainly paraschists and orthogneisses with some undeformed metagranite bodies, metabasites and marbles. The IIDK forms the structurally highest unit and mainly contains paraschists and paragneisses, amphibolites and marbles. Little Alpine deformation seems to have affected the IIDK and evidence for such is only developed locally. This may suggest that the IIDK acted as a rigid body while the EMC and GMC were undergoing ductile deformation (Rubie and Danthine, 1982).

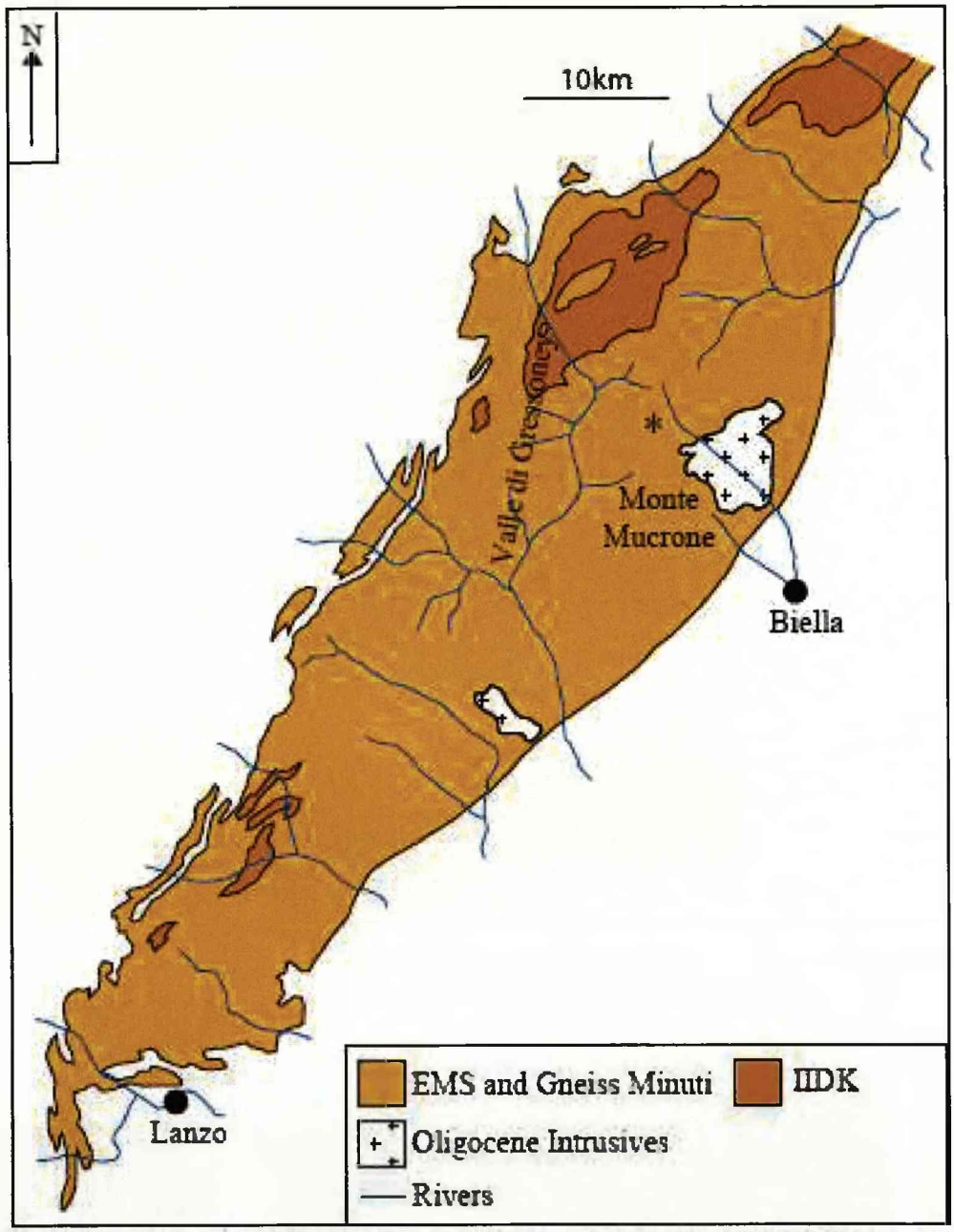

Fig. 2.4 Map of the Sesia-Lanzo Zone and the tectonic units within. The asterisk marks the location of studied eclogite facies rocks from the Colle della Barme d'Oropa

How the EMC and IIDK became juxtaposed is controversial. One hypothesis states that it was achieved by thrusting during the Alpine Orogeny (Dal Piaz et al., 1971, Gosso et al., 1979, Passchier et al., 1981, Rubie and Danthine, 1982, Williams and Compagnoni, 1983). Sheared amphibolites at the contact between the IIDK and the EMC contain glaucophane, garnet and zoisite indicating that the units were emplaced in their current positions during high-pressure/low-temperature conditions (Rubie and Danthine, 1982). A second theory implies the units were already in their present day positions before the Alpine Orogeny and that the variable metamorphism is a result of kinetic restrictions on the attainment of metamorphic equilibrium (Ridley, 1989, Stünitz, 1989).

A period of igneous activity (28-33Ma) emplaced andesitic dykes into the Sesia-Lanzo Zone. The Biella and Travesella intrusions are emplaced near the south of the zone at around 30Ma too and andesitic volcanics are found along the southern margin. These intrusions postdate the Alpine deformation of the unit.

Early Alpine deformation is thought to have occurred while the Sesia-Lanzo Zone formed a ductile shear zone between the subducting oceanic lithosphere and overlying continental crust of the Ivrea Zone (Rubie and Danthine, 1982). This deformation produced transposed lithological layering, isoclinal folds and layer parallel schistosity. Retrogression of the eclogite assemblage is accompanied by small and large scale folding and in areas where the deformation was intense a new schistosity (Pognante et al., 1980, Rubie and Danthine, 1982).

2.2.2 Metamorphic History

Both the Sesia-Lanzo Zone and the Ivrea Zone were affected by amphibolite to granulite facies metamorphism before the Alpine Orogeny (Desmons and Ghent, 1977, Rubie and Danthine, 1982). The main evidence for this in the Sesia-Lanzo Zone can be found within the IIDK which is markedly similar to granulite facies rocks in the Ivrea Zone (Hunziker, 1974, Beccaluva et al., 1978). Here assemblages containing garnet, biotite, quartz, sillimanite, K-feldspar and plagioclase are common (Rubie and Danthine, 1982). Conditions for granulite metamorphism have been estimated at 700-800°C and 0.5-1.0 GPa (Vuichard and Ballèvre, 1988, Lardeaux and Spalla, 1991, Rebay and Spalla, 2001). Evidence of this Pre-Alpine

metamorphism is also found in the EMC (Williams and Compagnoni, 1983). Here large lenses of amphibolite contain hornblende aggregates which are overprinted by eclogite and greenschist facies assemblages.

Granulite rocks from the Ivrea have Rb-Sr dates of 478 Ma (Hunziker and Zingg, 1980). Due to similarity between the IIDK, pre-Alpine assemblages in the EMC and rocks of the Ivrea Zone, metamorphism is thought to be of a similar age in all. In contrast to this Rb-Sr dates from a structural equivalent to the IIDK in the Dent Blanche klippe yielded pre-Alpine biotite ages of 180-200Ma, also similar to ages garnered from Ivrea Zone rocks (Hunziker, 1974). An $^{40}Ar/^{39}Ar$ study of biotite in IIDK rocks give a Permian to Late Cretaceous age range dependent on grain size, with smaller grains giving younger ages (Reddy et al., 1996). The study also states biotite underwent argon loss due to an Alpine heating event in the IIDK (that did not reach temperatures hotter than 300°C) which happened no later than 70Ma. In a study by Pickles et al. (1997), $^{40}Ar/^{39}Ar$ ages were determined across large biotite grains in IIDK samples. Ages ranged between 514 and 161 Ma within individual grains. Older ages occurred at the edges of grains and vice versa. This phenomenon cannot be explained by chemical alteration; rather it is caused by diffusion of excess argon into grains.

The Sesia-Lanzo Zone, like the Monte Rosa Nappe and the Zermatt-Saas Unit, underwent high pressure - moderate temperature metamorphism. This event is well documented in the EMC by petrological studies (Dal Piaz et al., 1972, Compagnoni and Maffeo, 1973, Compagnoni et al., 1977, Pognante et al., 1980, Vuichard and Ballèvre, 1988). Various eclogite mineral assemblages are formed dependent on bulk composition of a variable protolith. Common throughout are coexisting omphacite, garnet, glaucophane, quartz, zoisite, chloritoid, kyanite and white mica and in the more granitic areas of the zone, jadeite is common in the assemblage.

Williams and Compagnoni (1983) divide this high pressure event into four different stages based on observation in the Bard area. The first stage is represented by formation of glaucophane, white mica, clinozoisite, sphene and rutile. This assemblage forms a foliation that is preserved in garnet, omphacite/jadeite and zoisite that developed in the second stage. This second stage also saw the formation of rutile and chloritoid. A third stage is characterized by a similar assemblage to the

first stage which is difficult to separate from relics of the first stage. A final stage is described by albite pseudomorphs of jadeite and the development of acmite-rich pyroxene and crossitic blue-amphibole. This last stage is ascribed to the lower pressure limit of blueschist metamorphism.

Based on mineral assemblages, chemistry, phase relations and equilibria, temperatures and pressures reached during this high pressure metamorphism were around 500-600°C and 1.3-1.5 GPa (Dal Piaz et al., 1972, Compagnoni and Maffeo, 1973, Compganoni et al., 1977, Oberhänsli et al., 1985, Koons, 1986, Vuichard and Ballèvre, 1988, Lardeaux and Spalla, 1991, Tropper et al., 1999). Distribution coefficient values of Fe^{2+}/Mg in garnet and Na-pyroxene have also been used to provide a temperature for the eclogite facies event of around 525-550°C with pressures greater than 1.2GPa (Desmons and Ghent, 1977, Reinsch, 1979). Temperatures calculated from oxygen isotope fractionations between minerals (quartz/rutile and quartz/phengite) provide an average temperature of 540°C (Desmons and O'Niel, 1978).

The high pressure-low temperature eclogite facies event has been dated as Early Cretaceous (Oberhänsli et al,. 1985) and as Late Cretaceous (Dal Piaz et al., 1972, Hunziker, 1974, Compagnoni, 1977, Ramsbotham et al., 1994). The Late Cretaceous age for this metamorphic event is more likely. An $^{40}Ar/^{39}Ar$ study of phengite in EMC rocks shows heterogeneously distributed excess argon in the grains. This throws doubt on previous argon data from the EMC that produced ages older than 60Ma and thus negates an early Cretaceous age for eclogite facies metamorphism in the EMC (Reddy et al., 1996). Rb-Sr white mica ages and U-Pb sphene data dates the eclogite facies metamorphism at ~60-70Ma (Inger et al., 1996). Similar U-Pb dates of ~65 Ma from zircon rims crystallized during eclogite facies metamorphism are noted from Sesia-Lanzo rocks (Rubatto et al., 1999).

Retrogression of the Sesia-Lanzo Zone to greenschist facies is thought to have occurred at 40Ma (Compagnoni et al., 1977). This overprint is more extensive in the GMC where evidence for an earlier high pressure event is rare. Common assemblages include albite, epidote, actinolite, chlorite, sphene and biotite (Williams and Compagnoni, 1983). The greenschist facies event conditions are thought to be <500°C and 0.25-0.35 GPa in metagabbros in the unit (Rebay and Spalla, 2001).

2.3 Relevance to the Aims of the Project

As stated in Chapter 1 the main goals of this project are to investigate the microstructures and microchemistry of the main mineral phases of eclogite and eclogite facies rocks, with the purpose of improving the understanding of the way eclogite rocks behave during burial and exhumation. An additional aim is to comprehend how the microstructure and chemistry of retrogressive minerals overprinting eclogite facies may be affected by possible inheritance of pre-existing microstructures.

The Zermatt-Saas provides expansive exposure of eclogite facies rocks that have reached eclogite facies without experiencing any previous metamorphic events. Good preservation of the high pressure mineral assemblage provides excellent samples for testing omphacite and garnet to see what microstructures may have formed during the eclogite facies conditions and what processes may have created them. Understanding this may shed light on how the tectonic unit behaved during subduction. The retrogression of the eclogite facies rocks to greenschist facies conditions also allows a direct look at the possible effect any eclogite facies mineral microstructures may have had on microstructures formed in the greenschist mineralogy. Having a full suite of eclogite rocks, partially retrogressed and fully retrogressed eclogites allows a unique opportunity to investigate microstructural development through the various retrogressive stages. Also as retrogression is intrinsically linked to exhumation, study of retrogressive microstructures and the processes that created them may allow us to understand the dynamics of the exhumation of the Zermatt-Saas unit better.

The Sesia-Lanzo unit being a slice on continental crust that experienced eclogite facies conditions allows similar opportunities that the Zermatt-Saas Unit does but with some significant differences. Where the Zermatt-Saas Unit had never experienced a metamorphic event prior to eclogite facies conditions the same is not true of the Sesia-Lanzo Zone, as discussed. This may allow for an investigation of what affect previous microstructures may have had on the development of eclogite facies microstructures. In addition the eclogite facies rocks are likely to take various forms depending on the parent rock they formed in. It is entirely possible that different rock types deformed variably during deformation and this may be

represented in the microstructures recorded in eclogite facies minerals. Also knowing the eclogite facies mineral microstructures and what possible deformation mechanisms may have formed them will provide insight into the behaviour of the Sesia-Lanzo, or areas within the unit, during subduction. Retrogressive minerals of the unit, like those in the Zermatt-Saas, also provide another avenue to investigate the effect of pre-existing microstructures (eclogite facies) on newly forming minerals (greenschist facies).

3 Chapter 3: Methodology

3.1 Field Mapping and Sampling

3.1.1 Field Mapping

Fieldwork was carried out over a period of approximately nine weeks, spaced over three separate field excursions. Eclogite facies rocks from the EMC unit of the Sesia-Lanzo Zone, metabasics of the Zermatt-Saas Unit and paragneisses of the Monte Rosa nappe were selected for this study. Val de Gressoney in NW Italy was selected as the locale. It is a north-south trending valley starting at Pont St. Martin in the south where it joins the larger Valle d'Aosta and terminating at Staffal in the north. The valley offers access to excellent exposure of all geological units the study is concerned with.

Field mapping was carried out in the Zermatt-Saas Unit. A *'Garmin etrex'* GPS using 'UTM/UPS' position format and 'European 1950' map datum aided location on the maps. Foliations are recorded in the order of strike, dip and dip direction e.g. 120/34S. Lineations and fold axes are recorded in the order of plunge and azimuth e.g. 23→238. Plunge and azimuth of many folds are calculated using stereonets of poles to foliation measured around the fold.

For the Zermatt-Saas Unit the mountain known as Punta Telcio (2833m) was selected for investigation, in particular the area around Lago Blu, which contains large amounts of exposure of the lithologies associated with the unit. The area has a significant amount of preserved eclogite facies rock, only partially altered by the retrogressive event common across this unit which are essential to this project.

The area of Lago Blu (2600m) was mapped on a scale of 1:1250 using a scaled enlargement of 1:25000 maps from the Instituto Geographico Centrale (1999). An area of approximately 430m x 210m was mapped here with Lago Blu located at the north end of the map and extending south to a large serpentinite body. Though the field map (Fig. 4.2) shows defined boundaries between the four mapped lithologies these are not observed as so in the field. Exposure in the area while very good is not complete and lithological boundaries on the map are inferred within the accuracy of tens of metres. In addition boundaries between the fresh eclogite and amphibolite

lithologies of the Punta Telcio area are not abrupt and are gradational from one to the other.

3.1.2 Sample Collection

All samples were collected from the field as oriented samples following the methodology of Prior et al. 1987. Each sample is given an orientation mark before it is removed from the outcrop. The foliation and lineation (where measurable) are recorded for each sample and it is then photographed, sketched and placed in a labelled sample bag. Sample numbering is based on chronology of field season and order they are collected in. For example, S6.8 is collected in the 2006 field season, and was the eighth sample collected that season.

Zermatt-Saas Unit samples are collected from the Lago Blu area of Punta Telcio in four 'batches' and a few are collected on a larger reconnaissance of the Punta Telcio area. Each 'batch' is collected from four separate areas of the mapped area and includes four samples each; three samples of fresh to partially retrogressed eclogite and one amphibolite (retrogressed eclogite). Altogether there are twenty-six samples collected from the area fourteen eclogite samples, one serpentinite sample, three garnet mica schist samples and six amphibolite samples.

Sesia-Lanzo Zone samples are gathered from Colle della Barme d'Oropa and represent the variable lithologies of the EMC unit. They include samples of aplites and the eclogite micaschist they are intruded into, a lithology referred to as 'streaked eclogite', and eclogite micaschist collected from the limbs and hinges of folds found in the area. In total twenty-six samples were collected from the area; six 'streaked eclogite' samples, one eclogite pod sample, fourteen eclogite micaschist samples and five aplite samples.

In addition to the samples collected in the field two samples held on record at the University of Liverpool were used, an eclogite sample from the Punta Telcio region of the Zermatt-Saas and a paragneiss samples from the Stolemberg area of the Monte Rosa Nappe.

3.2 Sample Preparation

Oriented rock samples are collected from the three tectonic units concerned with this study. The foliation, lineation and surface orientation are all recorded for each sample. They are then re-oriented in the laboratory and marked for cutting following the methodology of Prior at al. (1987). Each cut is made perpendicular to the foliation and parallel to the lineation of each sample. A thin section sized area of the cut surface (~ 1.5 x 3 cm) is then selected and isolated from the rest of the rock, leaving small squares. These rock squares are then polished on a lapmaster until the saw marks have been removed from the desired thin section surface. Cut samples are then sent to Birmingham University or Trinity College Dublin where they are made into 30μm thick, uncovered thin sections. A total of fifty-seven thin sections were prepared in this manner.

Specimens intended for back scatter electron (BSE) analysis have most of their topography removed prior, so as to maximise imaging and data collection (Fynn and Powell, 1979, Lloyd, 1987, Prior et al, 1999). To this end thin sections are polished on a polyurethane lap for 2.5-3 hours using a suspension of 0.05μm colloidal silicon (SYTON^{TM}) which etches the surface introducing an amorphous layer which is then removed through mechanical polishing making the crystalline structure available for high quality electron backscatter diffraction (EBSD) analysis. This is a chemical-mechanical polishing technique and holds various benefits over conventional, mechanical and other chemical or electrochemical polishing techniques (Fynn and Powell, 1979, Lloyd, 1987).

The sample is placed face down on the polishing surface, inside a circular holder ring. This is then slid in between two rollers attached to a sweeping arm set so that the sample in the holder will move between the centre and the edge of the polyurethane lap while rotating slowly. The sample is held under slight vertical pressure by a metal block that fits into the top of the circular holder. As the sample is swept across the polishing surface Syton fluid is circulated by a rotary pump. After polishing the sample is removed from the holder and rinsed in cold, running water, then in ethanol to prevent drying stains and finally the ethanol is evaporated off using a hairdryer.

The samples were given a very thin carbon coat in order to minimise charging effects and maximise the crystallographic signal (Llyod, 1987, Prior et al, 1996).

3.3 Light Microscopy

A Vickers optical microscope (Fig. 3.1) is used to investigate thin sections for simple petrographical descriptions and locating areas intended for further investigation using other techniques. A Nikon coolpix 4500 camera is attached in order to digitally capture photomicrographs of the thin sections in both plane polarised light (PPL) and crossed polarised light (XP).

Fig. 3.1 Photograph of the Vickers optical microscope

3.4 Scanning Electron Microscope (SEM) Techniques

3.4.1 SEM Systems

All electron backscatter diffraction (EBSD) and energy dispersive X-ray (EDX) data presented throughout this thesis were collected at Liverpool University using two separate SEM systems.

The Philips XL30 utilises a tungsten filament electron gun and a Nordlys HKL CCD electron backscatter camera and detector. It is also equipped with an Oxford Instruments INCA EDX system with a $10mm^2$ detection area, lithium drifted silicon (LiSi) detector for chemical mapping and quantitative microgeochemical analysis. The other SEM system used is a CamScan X500 Crystal Probe fitted with a thermionic field emission gun, a Hamamatsu CCD electron backscatter camera and detector and a FASTRACK stage. The FASTRACK stage allows automated EBSD mapping by moving the sample by predetermined increments while the electron beam remains stationary. The CamScan X500 is also equipped with an Oxford Instruments, INCAx-sight EDX system with a $10mm^2$ detection area, LiSi detector. The EDX detectors in both systems are cooled using liquid nitrogen.

The CamScan SEM is unique in terms of the geometry of the equipment (Prior et al., 1996, Seward et al., 2002). The electron gun is tilted 70° from vertical so that the specimens loaded into the SEM chamber remain flat (Fig. 3.2 and Fig. 3.3). This allows greater freedom of stage movement, which is limited by the classic SEM setup of the Philips SEM. In the Philips SEM the stage itself must be rotated so that it is at an angle of 70° to the vertical electron beam (Fig. 3.2 and Fig. 3.3).

While the CamScan SEM allows certain advantages for EBSD, certain restrictions to EDX are present in the equipment. The EDX system on the CamScan SEM cannot measure elements below the atomic number of sodium as the EDX detector is protected by a beryllium window. A beryllium window absorbs the X-rays produced by lighter elements and is included in the CamScan for its higher heat resistance, needed to protect the EDX detector from the high temperature EBSD experiments carried out in this machine. Thus most EDX work presented here was carried out in the Philips SEM, where the EDX detector is windowless, which allows elements with as low atomic numbers as 4 (beryllium).

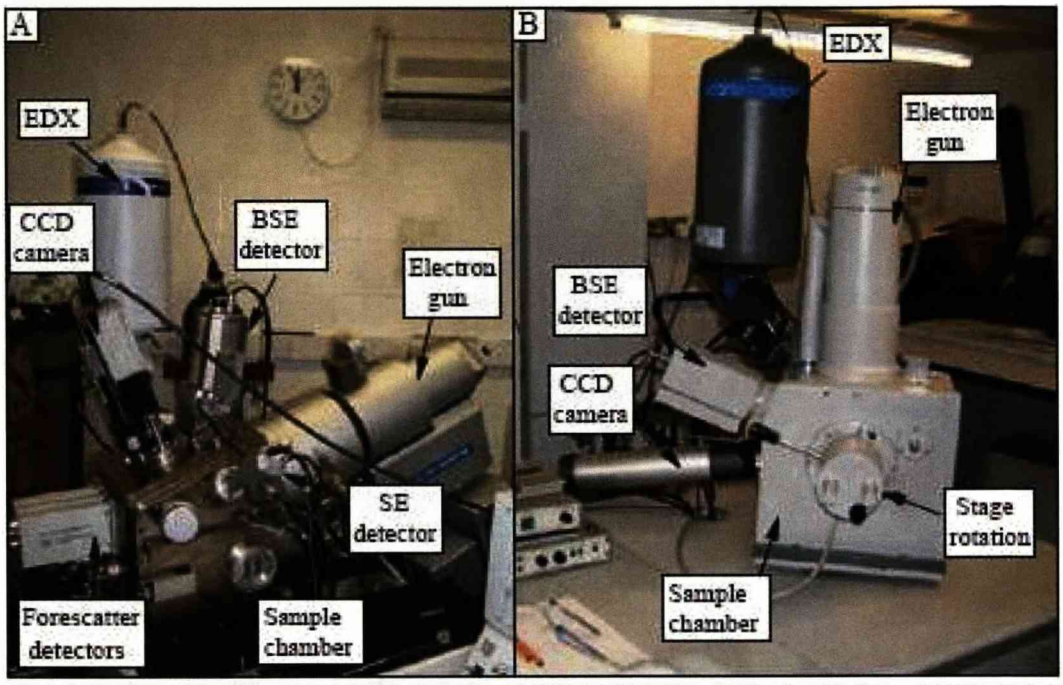

Fig. 3.2 Photographs of A) The CamScan X500 SEM and B) the Philips XL30 SEM used to gather EBSD and EDX data presented in this thesis

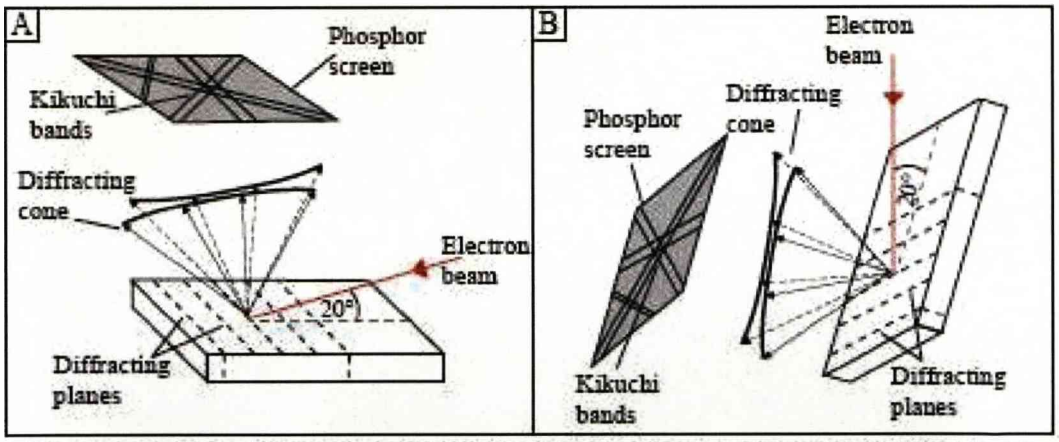

Fig. 3.3 Schematic illustration of EBSP production in A) a CamScan X500 where the sample is horizontal and the electron beam is fired at 70° from vertical and B) a Philips XL30 where the sample is tilted at 20° from the vertical electron beam

3.4.2 Electron Backscatter Diffraction (EBSD)

Electron backscatter diffraction (EBSD) is a Scanning Electron Microscope (SEM) technique for examining the orientation of crystalline materials. EBSD has been studied and discussed in literature since the 1960's and only a brief outline of the basic principles will be laid out here (Alam et al., 1954, Venables and Harland, 1973, Venables and Bin-jaya, 1977, Dingley, 1984, Llyod, 1987, Dingley and Randle, 1992, Prior at al., 1996, Prior et al., 1999, Trimby and Prior, 1999, Prior et al., 2002, Seward et al., 2002).

A focused beam of high energy electrons is accelerated toward a sample surface in a vacuum. The beam interacts with the surface at a high angle (~20° from horizontal). The electrons penetrate into the sample where they undergo elastic scattering and impinge upon crystal planes. These scattered electrons act as the source for electron backscatter patterns (EBSP) in the SEM. The generation of EBSPs is dependent on the trajectories of the scattered electrons that satisfy the Bragg condition, defined by the Bragg equation

$$n\lambda = 2d_{hkl} \sin\theta$$

where θ is the diffraction angle, n is the order of diffraction, λ is the wavelength of the electron beam energy (correspondent to accelerating voltage) and d_{hkl} is the hkl crystal lattice spacing.

The back-scattered electrons (BSE) that satisfy the Bragg equation generate, in 3D, Kikuchi cones, two for every crystal plane, one form the upper side of the plane and the other from the lower side. The cones approximate planes due to the small Bragg angle (~0.5°) of electrons accelerated through a few tens or hundreds of KeV. The cones are thus imaged on a phosphor screen as a series of Kikuchi bands each one corresponding to a discrete hkl crystal plane. These bands from EBSPs which are recorded 'live' by a low light, charge-couple device (CCD) camera, mounted behind the phosphor screen (Fig. 3.3).

Table 3.1 Summary table of the general operating conditions on the CamScan X500 and the Philips XL30 SEMs used to gather EBSD data in this research

Operating Conditions	
Voltage (Kv)	20
Beam Current (nA)	30 (XL30) -60(X500)
Working Distance (mm)	25
Hough Resolution	100 - 120
No. Of Detected Bands	6 – 9
Time/ frame (secs)	40-50
Background Frame	64
Noise Reduction Frames	5

EBSPs captured by the CCD camera are then sent to the on-line computer where they are processed using the imaging software CHANNEL + v5 (*Oxford Instruments Ltd.*), in particular the program known as 'Flamenco'. This software compares the EBSP to theoretical patterns of phases predetermined by the user and produces the crystallographic orientation represented by the EBSP.

3.4.3 Energy Dispersive X-Ray Spectroscopy (EDX)

Energy dispersive X-ray spectroscopy (EDX) is an analytical technique used to characterise the chemistry of a sample. Interactions between electromagnetic radiation and the sample and the analysis of the X-rays emitted by the sample in response to being hit by charged particles form the basis of investigation by this technique. Chemical characterisation capabilities are reliant on the fundamental principle that each element has a unique atomic structure. Thus X-rays produced by the bombardment of the sample by electrons will be characteristic and uniquely identifiable from each other.

To stimulate X-ray emission from a sample an electron beam is focused onto a desired area of study. The incident beam may excite an electron in an inner shell of

the atomic structure of an element, ejecting it from its shell creating an electron hole. An electron from an outer shell of higher energy will then move in to fill this hole and the difference in energy between the shells may be released as X-rays. The number and energy of X-rays emitted from a sample is then measured by an energy dispersive spectrometer. The energy of X-rays is characteristic of the element from which they are emitted and of the atomic structure of the element thus allowing the elemental composition of a sample to be measured.

Both the CamScan and the Philips SEMs utilise a $10mm^2$ detection area, LiSi EDX detector. When an X-ray strikes this detector it generates a photoelectron within the body of the silicon. As the photoelectron travels through the silicon it generates electron hole pairs. The electrons and holes are attracted to opposite ends of the detector with the aid of a strong electric field. The size of the current pulse thus generated depends on the number of electron hole pairs created which in turn depends on the energy of the incoming X-ray.

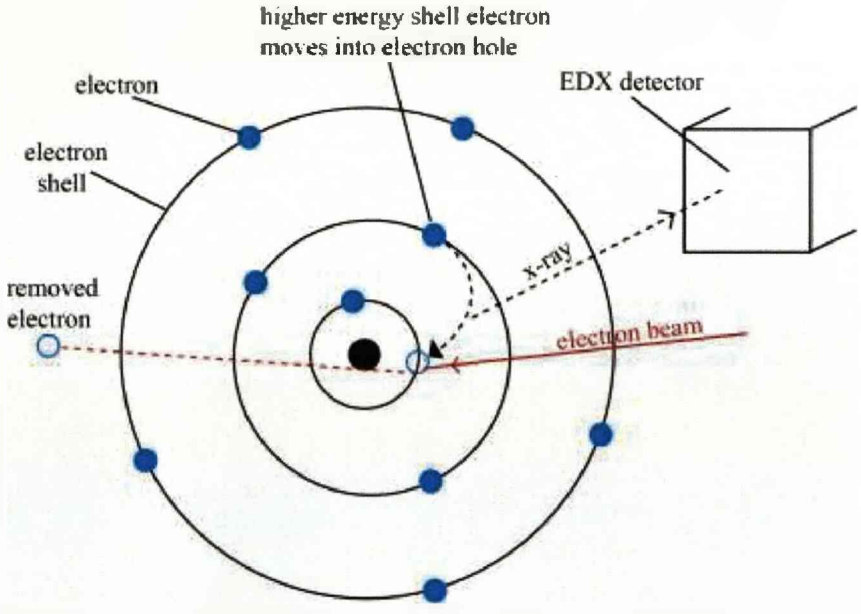

Fig. 3.4 Diagrammatic representation of X-ray production by an SEM-EDX system

Some of the chemical data in this study is collected using the EDX systems on the previously mentioned SEM systems in the University of Liverpool. Other data is collected on the Cameca SX-100 electron microprobe in the University of Manchester. In contrast to the Liverpool University machines the Cameca SX-100 uses wavelength dispersive spectrometry.

3.4.3.1 Wavelength Dispersive Spectroscopy (WDS)

Wavelength dispersive spectroscopy (WDS) is a method used to count the number of X-rays of a specific wavelength diffracted by a crystal. The wavelength of an impinging X-ray and the crystal's lattice spacing are related by Bragg's law and produce constructive interference if they fit the criteria of Bragg's law. WDS counts the X-rays of only a single wavelength rather than producing a broad spectrum of wavelengths or energies as with EDS. This means that the element of interest to a study must be defined to find a crystal capable of diffracting it properly.

X-rays emitted by a sample are collimated by parallel copper blades (called collimator or Soller slits), and irradiate a known single crystal at a precise angle. The single crystal diffracts the photons which are collected by a detector, usually a scintillation counter or a proportional counter. The single crystal, the specimen, and the detector are mounted precisely on a goniometer with the distance from the source of X-rays (the specimen) and the crystal equal to the distance from the crystal to the detector. It is usually operated under vacuum to reduce the absorption of low-energy photons. Modern systems contain a small number of crystals of known but differing properties, with automated changing of the crystal depending on the energy being analysed, enabling elements from the entire periodic table (excepting the very light elements) to be analyzed.

The Cameca SX-100 at the University of Manchester is fitted with a standard tungsten electron emitter and five wavelength dispersive detectors each of which can be fitted with a choice of diffracting crystals.

3.4.4 Combined EBSD and EDX

The CamScan X500 SEM allows for the combined collection of crystal orientation data and EDX chemical counts. The resultant data is collected in a map or grid format where each pixel contains both the EBSD orientation data and element amounts. This information can then be manipulated as described later in this chapter.

3.4.5 Transmission Electron Microscopy (TEM)

Transmission electron microscopy (TEM) is a technique by which a beam of electrons is transmitted through a thin sample, interacting with it as it does so. An image is formed from the electrons transmitted through the sample, magnified and focused by an objective lens and detected by a fluorescent screen, photographic film or a CCD camera.

Electrons are generated by either thermionic emission (using a tungsten filament) or by field emission in a vacuum and accelerated toward the sample under investigation. The electron beam may then be manipulated by the user by two physical effects. Electromagnets can be used to generate magnetic fields to manipulate the electron beam. This allows formation of a magnetic lens of variable focusing power with lens shape originating due to the distribution of magnetic flux. The second method of beam manipulation is by using electrostatic fields which can cause the electrons to be deflected through a constant angle. Combining two deflections allows for the formation of a shift in the beam path.

The lenses of a TEM allow beam convergence to happen, the angle of which can be varied. This allows the magnification to be changed simply by changing the current that flows through the lenses. In a typical TEM there are three stages of lenses, with many possible configurations. These are known as the condenser lenses, objective lenses and projector lenses. The condenser lenses are responsible for primary beam formation, the objective lenses for focusing the beam on the sample and the projector lenses to expand the beam onto the phosphor screen. The magnification of the TEM is due to the ratio of the distances between the sample and the objective lens' image plane.

TEM work presented in this thesis was carried out by Prof. Wolfgang F. Müller at the Institute of Applied Geosciences at Technische Universität Darmstadt. The work is carried out on a Philips CM 12 transmission electron microscope operated at 120 kV acceleration voltage. It is equipped with a system for energy dispersive X-ray microanalysis of the type EDAX Genesis 2000.

The investigated petrographic thin sections (35 μm thick), are prepared from the sample 6.4 in the usual way, however using CRYSTALBOND as glue. Specimens with a diameter of 3 mm are drilled from the uncovered thin section by an ultrasonic driller. These specimens are then glued on Mo grids in order to provide mechanical stability. Three specimens suitably thin for TEM are obtained by Ar+ ion milling using a GATAN Duo Mill.

3.5 EBSD Data and Processing

3.5.1 Misorientation

The crystal lattice of a grain of a phase can be mapped or translated onto the crystal lattice of another grain of the same or different phase via a rotation axis and rotation angle. These are referred to as the misorientation axis and the misorientation angle. The axis is a vector but not directional as the rotation that maps point A to B has the opposite sense to that which maps B to A, yet there is no geometric significance to which grain is taken first in the calculation. The misorientation angle is always positive and the maximum angle it can be is 180° as any greater angle is equivalent to a smaller angle in the opposite sense. This rotation is only unique if the crystal system being dealt with has no symmetry (triclinic) but when dealing with symmetry things become more complicated. In highly symmetric crystals there may be several options of axis and angle. The automatic indexing uses the disorientation convention in this case to select the solution with the lowest misorientation angle.

3.5.2 Noise Reduction

EBSPs are indexed and processed using the software package CHANNEL+ v5 from *Oxford Instruments Ltd.* (Prior et al., 1999). Initial processing on beam mapped grains and 'stage' mapped grains (with small spacing between points ($\leq$10μm)) involves the removal of isolated points that have been incorrectly indexed (often referred to as wild spikes). What then follows is the processing procedure laid out in Prior et al. (2009) which involves manipulating the band contrast (BC) of the scanned area. Band contrast is an EBSP quality number, the higher the value the better the EBSP quality. Low BC values are usually found in deformed regions and grain boundaries.

A subset of the band contrast is created that excludes those values measured in the grain boundaries of the scanned area. This subset is then subjected to successive levels of noise reduction, which involves non indexed points, being replaced using copied information of neighbouring correctly indexed points. As grain boundaries are not included in the BC subset, noise reduction does not spill over into other grains. This reduces the amount of artefact creation and consequent incorrect microstructure interpretation which can arise from noise reduction. Most of the EBSD maps

presented in this thesis have noise reduction carried out for non indexed points that have at least five neighbouring indexed points.

3.5.3 EBSD in Eclogites

As omphacite and garnet are the two main constituents of eclogite and thus the focus of this thesis, it is important to understand how they are indexed by the EBSD procedure. Other minerals investigated in this thesis also present further difficulties during EBSD data collection and are discussed here also.

The influence of composition variations between end members of omphacite chemistry and space groups on EBSP was investigated by Mauler et al. (1998). Due to the low symmetry crystal structure of omphacite, EBSPs show a high number of different Kikuchi bands. Forty reflection families were identified for both C2/c and P2/n space groups of omphacite. Change in omphacite composition occurs mainly with cation substitution. Replacement of Mg or Fe^{2+} by Fe^{3+} and Na by Ca does not produce significant changes in the unit cell due to similar ionic radii. Substitution of Mg or Fe^{2+} by Al, which has a larger ionic radius, results in the atomic ordering of the P2/n space group. As both space groups have many identical reflection families, with only a few rare C2/c ones not found in P2/n, it can be said that neither space group nor chemical composition has a strong impact on indexing omphacite.

Cubic minerals, due to high symmetry, are often subject to systematic misindexing in EBSD. Garnet is noted to have a few possible systematic errors in indexing (Prior et al. 2002). These include a 27° rotation from the true orientation around one of three axes; <001>, <112> and <142> and a 60° rotation around the <111> axes. Where signals of this misindexing were found in the datasets presented in this thesis, they were manually removed by erasing the data points contributing to them based on the microstructures they appeared to form. From combined EBSD and EDX maps on garnet with variable chemistry, garnet composition seems to have no effect on measurement of the crystal orientation.

This thesis is also concerned with minerals found in retrogressed eclogite, namely the amphiboles glaucophane and hornblende. Collecting orientation data via EBSD for these minerals presents its own issues which are discussed here. The hornblende present in retrogressed areas of the study often occurs as a multi stage phase, with

different hornblende populations of variable chemistry. There exists no study aimed directly at understanding how EBSPs may be affected by hornblende chemistry, but from the data presented in this thesis, it appears that there is no effect.

Due to the similar crystallography of hornblende and glaucophane the EBSPs for both are virtually indistinguishable. This results in the automatic indexing software often indexing one phase as the other. While the indexing may result in the wrong mineral being assigned to the EBSP, this phenomenon has no effect on the crystallographic orientation measurements (Fig. 3.5). This is confirmed by comparing the mean angular deviation (MAD) values that accompany each solution. When an EBSP index solution is produced an MAD value accompanies it. This value measures the goodness of fit of the EBSP solution, the smaller the number, the better the solution. For an EBSP for either barroisite or glaucophane the software will usually offer both hornblende and glaucophane solutions. The MAD value for each is approximately the same. The fact that this indexing problem has no effect on the crystal orientation measurements is further proven by the near identical Euler angles that each solution provides within a 1.5° error bar.

To overcome incorrect indexing of barroisite and glaucophane, EBSD scans (including all three types of scanning methods used here) are performed alongside an energy dispersive X-ray (EDX) scan. This provides each point with not only orientation data and a phase diagnosis based on the EBSP but also element abundances as well. For each sample the chemical maps show a strong difference between the calcium content for barroisite and glaucophane. This forms a reliable way of distinguishing the two phases. The data is exported and run through a MATLAB program that changes the phase identification number based on the upper and lower limits imposed on the calcium counts. The resulting output is then imported back into CHANNEL + v5 with the barroisite and glaucophane points now correctly distinguished. Once this is done the EBSD data is then put through the same processing procedures described above. Before and after images and a Ca map for one data set are shown in Figure 3.6.

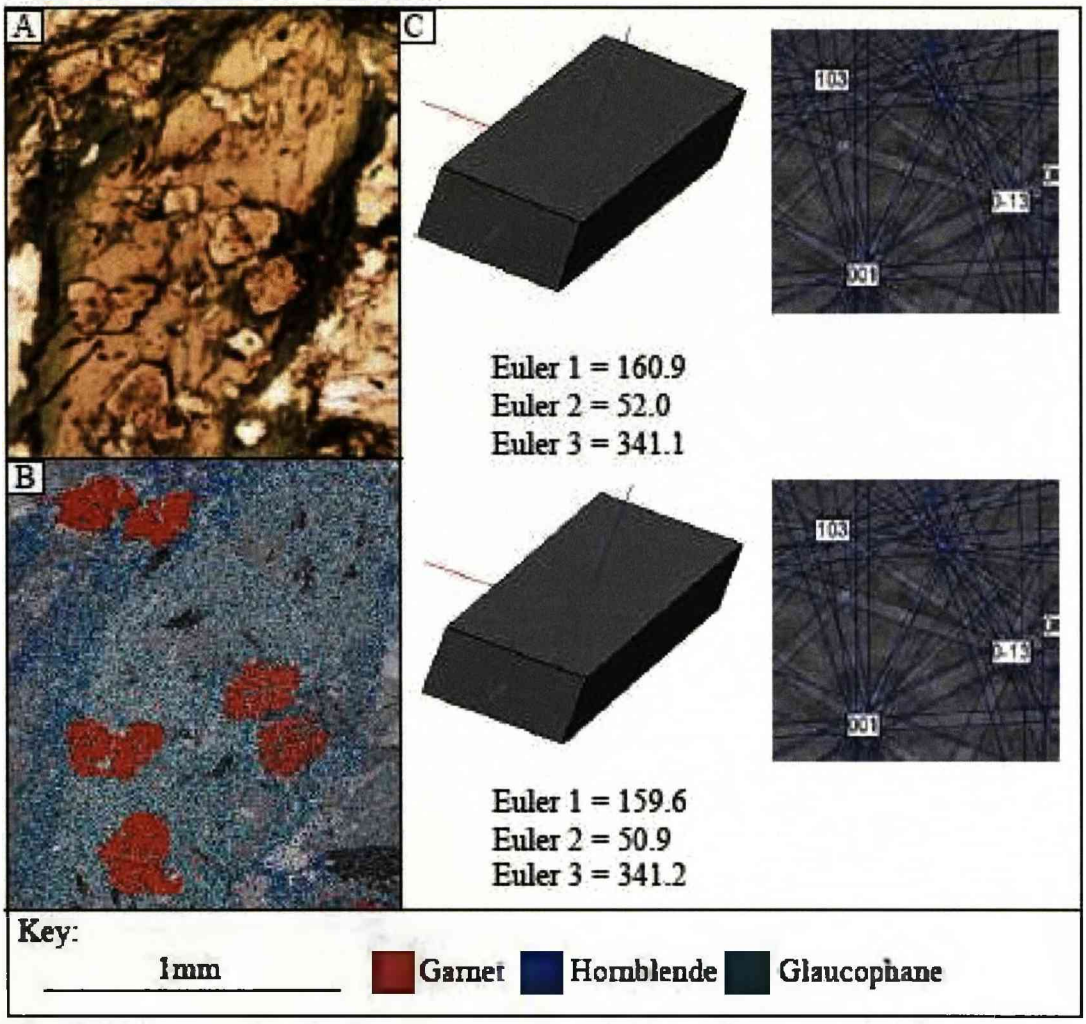

Fig. 3.5 Diagrams showing how hornblende and glaucophane can mis-index as each other due to crystallographic similarities. A - Photomicrograph of a porphryoblast of glaucophane with some hornblende overprint and overgrowth, B - Phase identification map showing the glaucophane area is occasionally indexed as hornblende, C - Euler angles from two neighbouring pixels one of glaucophane and the other of misindexed glaucophane (hornblende), the 3D crystal orientation of those pixels and the indexing patterns of both the pixels.

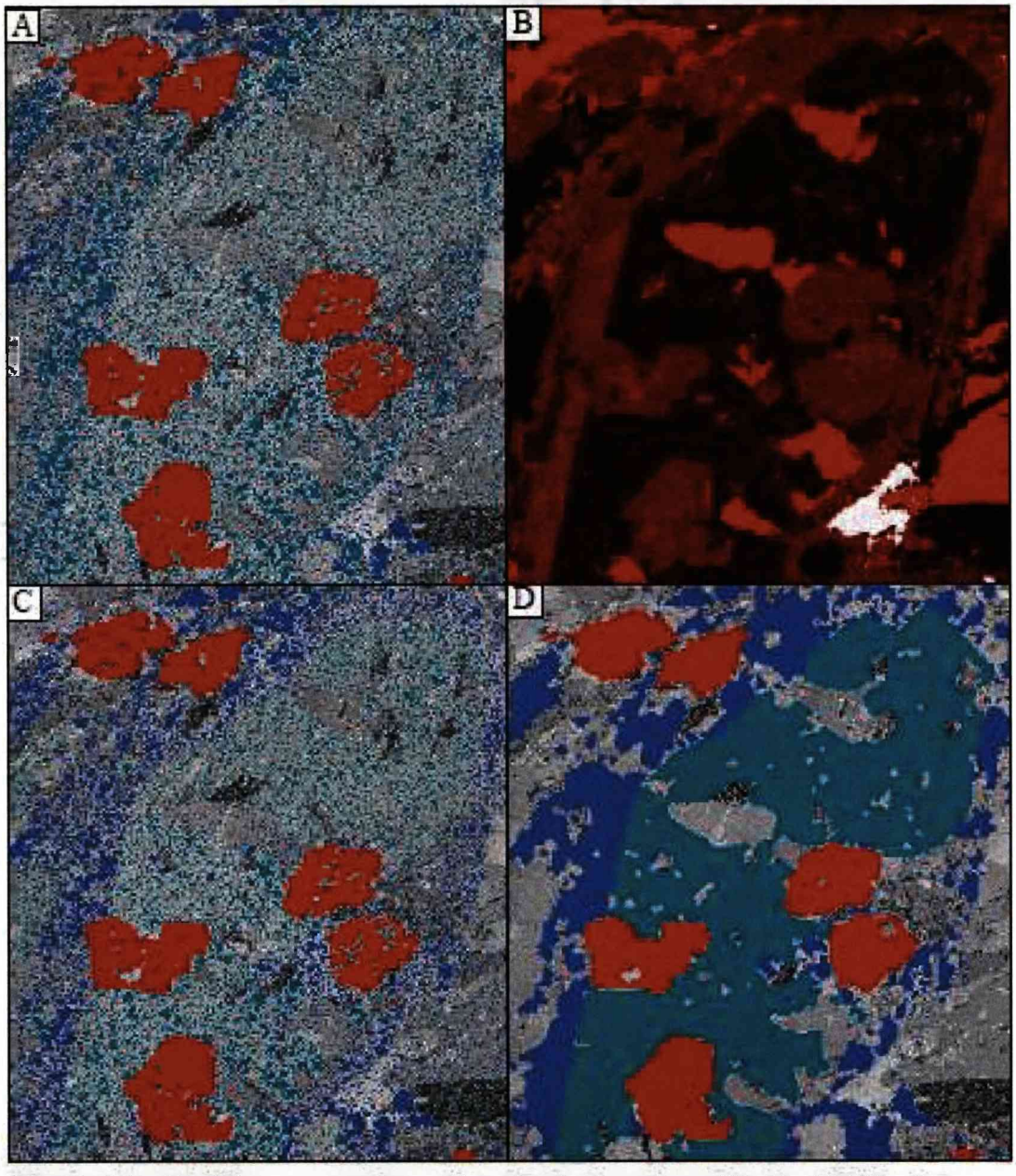

Fig. 3.6 A - Lightly processed raw data displaying phase ID, B - EDX calcium map, C - Phase ID map after the original data has been put through a MATLAB program to reassign phase numbers based on the EDX calcium amounts, D - Phase ID map of the data after significant noise reduction

3.5.4 Pole Figures

Orientation data for pole-figure plotting is produced by two separate methods for this study. One method provides an LPO based on data from a small area of a thin sectioned sample mapped at a small scale. The second method allows for a larger sampling area of orientation points to produce an LPO, as it scans across the entire area of a thin sectioned sample. All samples used for this study have pole figure plots using both procedures outlined here. The first method involves some data manipulation of the EBSD mapped areas (mapped by beam scanning an area or by the FASTRACK stage method) of each sample. Each map undergoes grain detection, a function in the CHANNEL+ v5 software, which separates out grains of each phase based on neighbouring pixels being >10° misoriented from each other. A subset of the data is then created where only one orientation measurement is taken from each of these defined grains. This 'point per grain' data is exported from CHANNEL + v5 and entered into the PFch5.exe program published by D. Mainprice (ftp://saphir.dstu.univ-montp2.fr//pub/TPHY/david/CareWare_Unicef_programs/PC) which creates the pole figures. This method will be referred to as a point per grain scan (PPGscan) in this thesis.

The second method involves the data obtained by mapping the entire thin section at a large spacing using a FASTRACK stage. The spacing for 'stage' maps is determined using the average omphacite grain size in each sample. For example if the grain size is 300μm then this is used as the spacing for each point of data collection. This method provides a large number of points from across an entire thin section, none of which belong to the same grain, for a number of phases. Some problems arise from this due to other phases in the rock (usually glaucophane and garnet) having a larger grain size. To ensure that no one grain of any phase is represented more than once in the dataset, a similar 'point per grain' subset is created the same way it was in the PPGscan method. This data is then also exported for use in the PFch5.exe program. This method shall be referred to as the 'stage' scan (STscan) throughout the thesis. All pole figures are plotted in the same reference frame (Fig. 3.7) where S is the line of foliation and L is the lineation. Benefits of STscans include the ability to collect orientation data from a wider sample area of a rock whereas the PPGscan method provides a smaller amount of grains for LPO investigation.

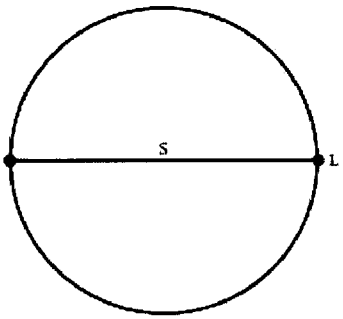

Fig. 3.7 Reference frame for pole figures. L marks the lineation; S marks the plane of the foliation.

3.5.5 SEM, EBSD and EDX Images

The SEM machines used to collect data are capable of producing a variety of images, some of which were utilised in describing sample microstructure and chemistry in this thesis. Also the EBSD processing software package generates a number of possible images, which can be used to explore microstructure in samples. Within EBSD maps each pixel represents a data point which details the crystal orientation, and also contains chemical EDX information where combined maps have been carried out. The various maps (Fig. 3.8) used to present data throughout this thesis are described below.

3.5.5.1 Z-Contrast Images

Z-contrast images, also known as atomic number images are based on the relationship between BSE emission characteristics and sample composition. The BSE signal intensity is proportional to the amount of electrons exiting the sample after interaction with the sample. This signal increases with decreasing depth of electron penetration which in turn is controlled by atomic number, or the z-number of the phase being investigated. Phases with a larger atomic number have greater signal intensity and will appear brighter in z-contrast images and vice versa. This can be used to look at chemical variation within a phase.

3.5.5.2 Band Contrast (BC) Maps

As previously mentioned band contrast (BC) is an EBSP quality number, the higher the value the better the EBSP quality. Low BC values are usually found in deformed

regions and grain boundaries, which thus appear as darker areas on BC maps. BC maps are used primarily in this thesis as the backdrop to other EBSD and EDX maps.

3.5.5.3 All Euler Maps

This map is constructed by using the three different euler angles; φ1, Φ2 and φ3. Euler angles represent spatial orientation as a combination of rotations from a set reference frame. All Euler maps display this information by arbitrarily assigning different colours to various orientations so that areas of variable orientation are clearly defined.

3.5.5.4 Phase Identification (PID) Maps

As mentioned previously EBSD allows the identification of mineralogy based on the EBSPs generated by the technique. Processing software allows various user defined colours to be assigned to the pixels indexed as each phase.

3.5.5.5 Texture Component (TC) Maps

This function of the processing software uses the all Euler data to construct a map that highlights changes in misorientation within a phase and often within one crystal. It often displays orientation change more clearly than All Euler maps do. The user selects a pixel of the phase and grain to display a TC map and the orientation information of this pixel becomes the reference from which all the other pixels of the phase of crystal are coloured. In other words other pixels are coloured based on how misoriented they are from the reference pixel orientation data. Often a rainbow coloured scale is used, the upper and lower limit of which can be determined by the user, to display variations in orientation. Blue usually represents lower changes in misorientation whereas red signifies larger differences in misorientation relevant to the selected reference point.

3.5.5.6 Grain Boundary (GB) Maps

Grain boundary maps use the orientation data of all pixels within a phase to create a set of lines that define boundaries between touching grains, or to highlight subgrain structures within a singular grain. The change in angle of orientation that each line represents can be defined by the user.

3.5.5.7 EDX Element Maps

EDX element maps or 'dot maps' are essentially element intensity maps. The SEM-EDX system scans across a selected area performing analysis on user defined elements. Element amounts are recorded and displayed as coloured maps allowing a qualitative look at chemical variability in a mineral.

3.5.5.8 Combination Maps

Any of the previously described EBSD maps can be overlaid on each other to make any number of combination maps. In addition where EBSD maps have been combined with EDX scans, EDX element maps can be combined with any chosen EBSD maps to display both chemical and orientation data. In addition combined EBSD-EDX data sets allow counts to be displayed on individual phases if desired.

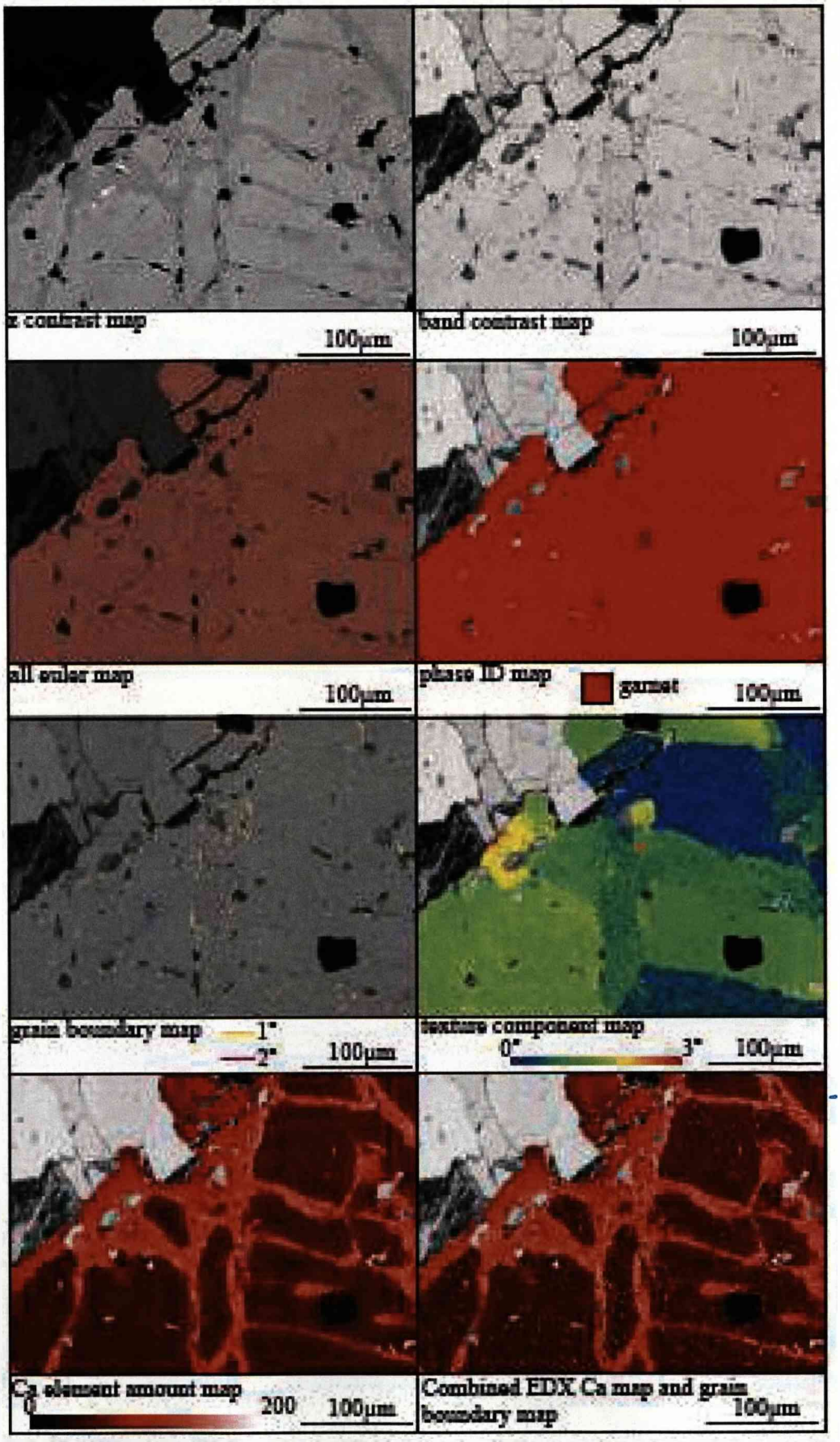

Fig. 3.8 Examples of the various SEM, EBSD and EDX maps that are used to present the data in this thesis

3.5.6 Misorientation Distribution Analysis

For any population of grains the misorientation angle and misorientation axes distribution can be investigated to quantify microstructural features in rocks and to test hypotheses on their formation. Misorientation angle distribution analysis tests neighbour-pair misorientation angle distributions and random-pair misorientation angle distributions for statistically significant differences between them (using the Kolmogorov-Smirnov (K-S) statistical test). Misorientation axes distribution analysis of a population of grains can be represented by a pole figure and/or by an inverse pole figure (IPF) and can be used to highlight whether the misorientation axes of a population of grains shows a crystallographic control (Wheeler et al., 2001).

For misorientation angle distribution analyses a random pair distribution of misorientations is created by relating every grain in a dataset to each other. A neighbour pair misorientation distribution is then calculated from pairs of touching grains in a dataset. These distributions can be represented graphically either as a histogram of misorientation angles or by a cumulative frequency curve. The differences between the two distributions hold important implications for interpreting microstructures (Wheeler et al., 2001).

If a statistically significant difference exists then neighbouring grains have undergone a physical interaction and/or neighbouring pairs have been derived in a significant number of cases from a common parent microstructure: inheritance. In other words neighbouring lattice points know about each other in a way that distant ones do not (Wheeler et al., 2001). Physical interactions include 1) reduction in surface energy by lattice alignment, 2) nucleation, when nuclei affect the orientation of nearby nuclei, 3) mechanical rotations of faceted grains in compacting crystal mushes so faces become parallel and 4) growth twinning. Inheritance can include 1) subgrain rotation recrystallisation in rocks deforming by crystal plastic processes, 2) mechanical and transformation-related twinning and 3) when many grains develop from a few large parent grains.

When using misorientation axes distribution analyses certain restrictions must be taken into account. For each crystal system there is a maximum misorientation angle allowed due to the restrictions of symmetry. For example garnet (Laue group m3m)

has a maximum misorientation angle of 68.2° (Wheeler et al., 2001). For rotations around <100> of more than 45° is equivalent to an alternative rotation of <45° as the <100> axes are tetrads. So, for example, rotations of greater than 50° are forbidden for axes that lie in a region around the <100> direction. Around the <111> axes rotations greater than 60° are forbidden and rotations larger than 68.2° are forbidden altogether (Wheeler et al., 2001). This creates forbidden zones on an IPF diagram for whatever system is being investigated. Due to this misorientation axes distributions on an IPF will show a strong bias due to geometric reasons and interpretations of them must be done bearing forbidden zones and non-uniform axes distributions in mind.

Wheeler et al. (2001) show that misorientation distribution analyses can be used to test hypotheses about which processes contribute to microstructural development in various rocks and minerals. In this investigation we aim to use these analytical tools to investigate possible neighbour correlations in omphacite and garnet from eclogites with the aim of aiding the identification of which process may have produced it.

4 Chapter 4: Eclogite Facies Rock Deformation in the Zermatt-Saas Unit

4.1 Introduction

The deformation of eclogite facies rocks is important as these rocks occur in abundance in the deep crust and upper mantle and in subduction and collision zones. Understanding the processes by which they deform may reveal key information pertaining to the rheology and dynamics of these important geological areas, (Piepenbreier and Stöckhert, 2001, Doin and Henry, 2001).

Omphacite and garnet are the two main mineral constituents of eclogite facies rocks and as such the properties of these minerals will have the most prominent effect on the rock behaviour. In most eclogites omphacite is the framework supporting mineral with garnet usually occurring as isolated porphyroblasts. It is commonly seen that garnet acts as a rigid body in eclogite deformation (Vogelé et al., 1998, Brenker et al., 2003, Kurz et al., 2003) and that omphacite deforms plastically, accommodating any strain within the rock (Godard and Van Roermund, 1995, Mauler et al., 2001, Jin et al., 2001, Piepenbreier and Stöckhert, 2001). However recent studies have suggested garnet may play a more significant role in eclogite deformation than previously thought (Mainprice et al., 2005, Storey and Prior, 2005, Zhang et al., 2007). Thus understanding the mechanisms that control omphacite deformation and contributions made by garnet deformation is essential to understanding models involving high pressure and ultra-high pressure rocks.

The aim of this chapter is to determine how omphacite, and in a briefer study, garnet in eclogite facies rocks of the Zermatt-Saas Unit deformed, in order to gain insight as to how the unit evolved through burial and exhumation. An in-depth investigation of these two minerals is carried out using EBSD and chemical analysis techniques.

The Zermatt-Saas underwent significant retrogression during exhumation (Chapter 2) resulting in the formation of widespread amphibolites in the unit. These rocks are important for understanding certain aspects of the exhumation of this unit and this is explored in detail in Chapter 5, although petrographical descriptions of the rock are included here.

4.2 The Geology of Lago Blu, Punta Telcio

The area of the Zermatt-Saas Unit examined in this study is located at the northern end of Val de Gressoney on Punta Telcio (Fig. 4.1). Punta Telcio is an excellent exposure of the Zermatt-Saas Unit containing a number of lithologies common to ophiolitic bodies. A small mapped area (430m x 210m), centred on Lago Blu, of the Zermatt-Saas Unit on Punta Telcio (Fig. 4.2) displays four lithologies common to the unit; serpentinite, quartz-garnet schist, eclogite and amphibolite (metabasics).

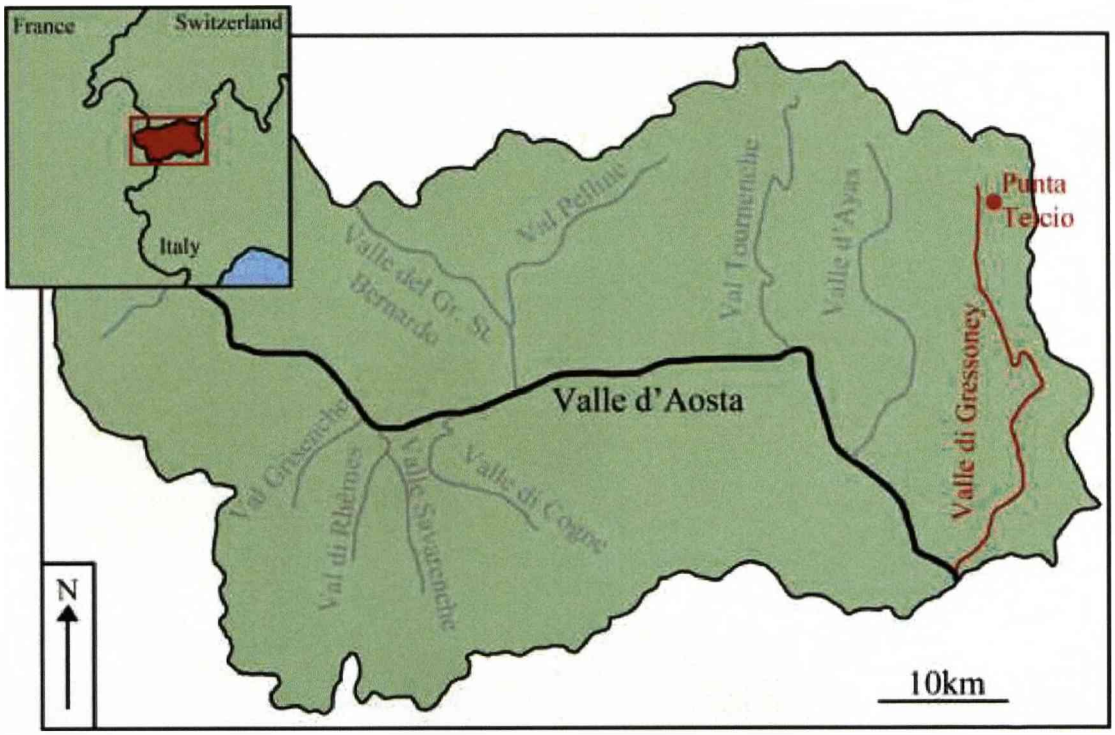

Fig. 4.1 Map of the Val d'Aosta province of Italy showing the location of Valle di Gressoney and the location of Punta Telcio. The inset shows the location of the province in a larger European setting.

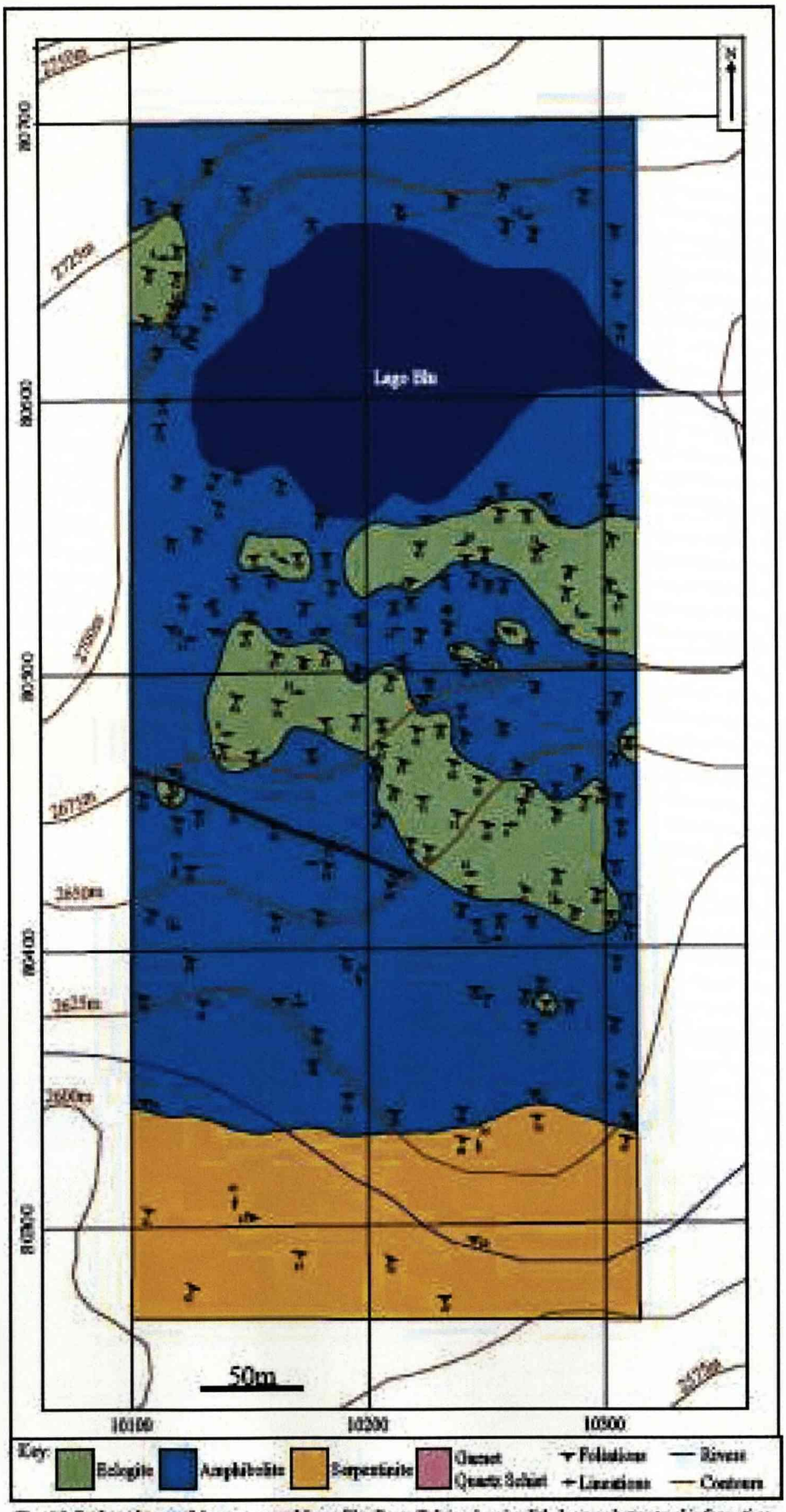

Fig. 4.2 Geological map of the area around Lago Blu, Punta Tolvin, showing lithology and structural information

4.2.1 Eclogite Facies Rocks

Eclogites occur in patches around the Lago Blu area and are in structural continuity with the surrounding amphibolites. They are pale green in colour due to the presence of omphacite as the main mineralogical constituent (Fig. 4.3, Fig. 4.4). Omphacite commonly defines a lineation and a strong shape fabric foliation (Fig. 4.6), although in some areas it poorly developed. Other minerals in the lithology include pink garnet porphyroblasts and atolls (<1-3mm) and large (~1-3mm), blue grains, likely glaucophane (Fig. 4.3 Fig. 4.4). Larger garnet grains are wrapped by the fabrics of the lithology.

Less common minerals within this lithology include white mica and a green amphibole. This amphibole is mainly concentrated within and around fractures in eclogite facies rock outcrops but is also present scattered among the other phases, occasionally within bands (forming a location fabric consistent with the other fabrics previously described) and as rims around garnet porphyroblasts. The amount of amphibole present in the eclogite facies rocks is variable.

Amount and preservation quality of omphacite is variable. Eclogite facies rocks of this unit have undergone partial retrogression with some areas more overprinted than others. The suite of samples used in the study from the Lago Blu area eclogite facies rocks reflects this. The most retrogressed sample investigated (S6.22) shows omphacite exists mainly as small aligned inclusions within large grains of retrogressive clinozoisite, glaucophane and amphibole (Fig. 4.5). In all samples omphacite grains have a symplectite rim which varies in width (<100 μm - ~200 μm) (Fig. 4.6).

Omphacite forms an interconnected, supporting framework in these rocks and grain size is small ranging between ~100 μm and ~1mm. The omphacite shape fabric wraps garnet grains in most cases, though there are examples where omphacite grains truncate against garnet grains as well (Fig. 4.9). Omphacite can also be found as inclusions within garnet grains.

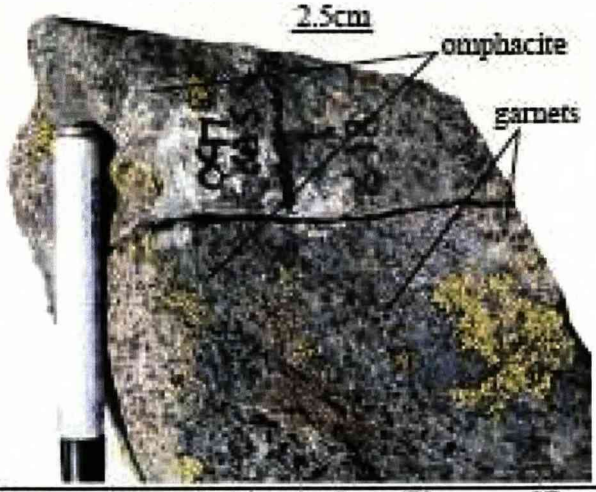

Fig. 4.3 Eclogite facies rock sample from the Lago Blu area of Punta Telcio, showing pale green omphacite and red/pink garnets.

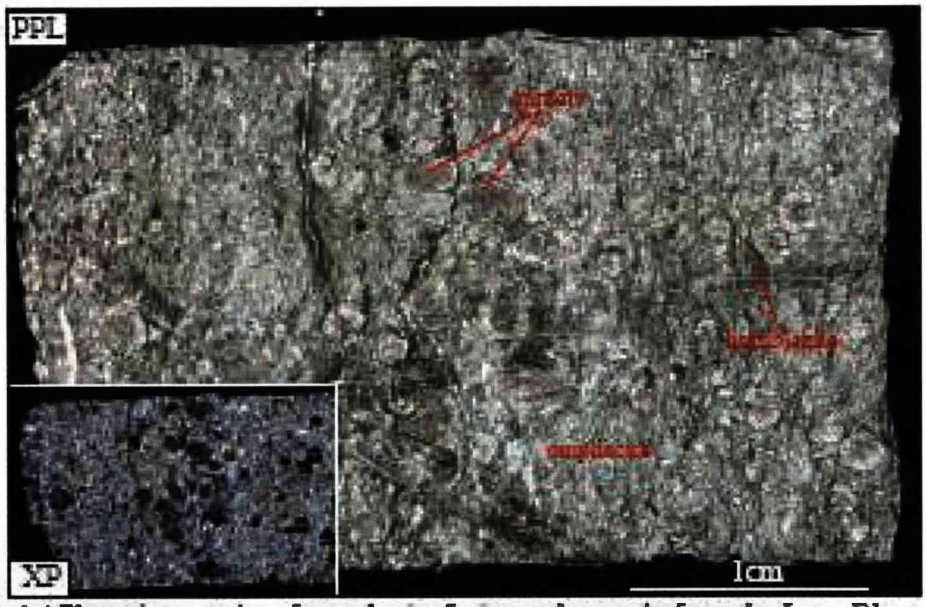

Fig. 4.4 Photomicrographs of an eclogite facies rock sample from the Lago Blu area. Large isolated garnets and clusters of garnets can be seen. The bulk of the rock is composed of pale green omphacite. Amphibole can be seen rimming some garnet grains and fractures in the sample.

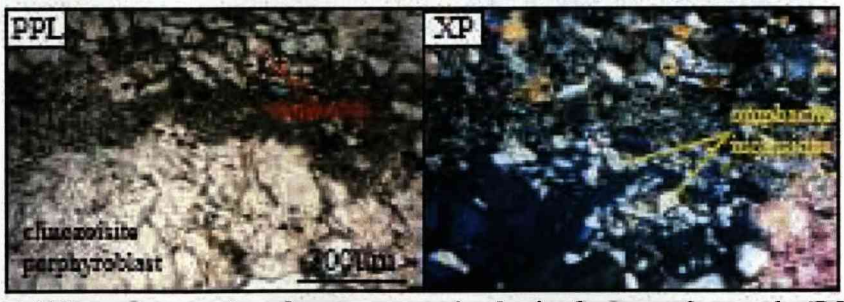

Fig. 4.5 Photomicrographs of a retrogressed eclogite facies rock sample (S6.22) showing a clinozoisite porphyroblast with omphacite inclusions.

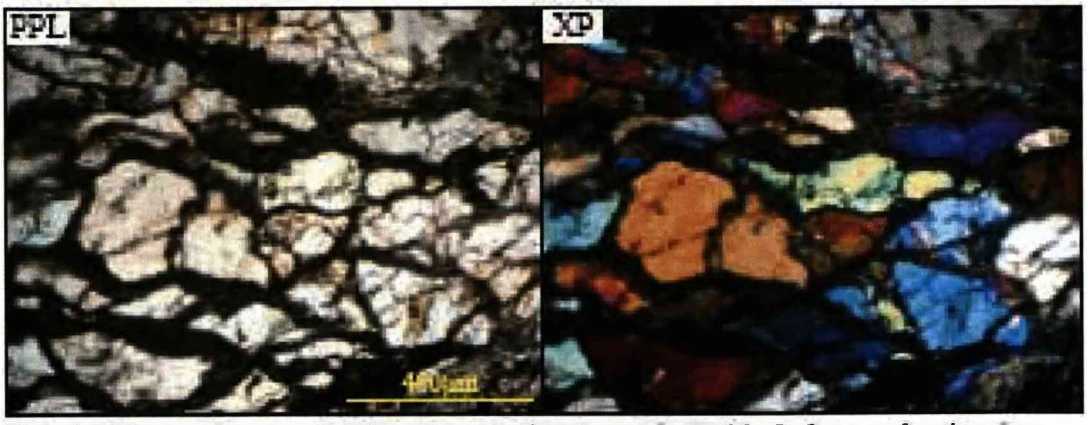

Fig. 4.6 Photomicrographs showing omphacite grains with dark symplectite rims and variable birefringence within single omphacite grains

Fig. 4.7 Photomicrographs (XP) of an omphacite grain showing undulating extinction as the grain is rotated on a light microscope stage

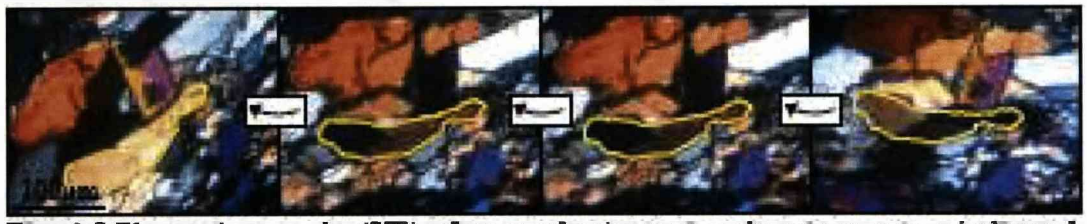

Fig. 4.8 Photomicrographs (XP) of an omphacite grain subgrain structure indicated by changing extinction of areas of the grain as it is rotated on a light microscope stage

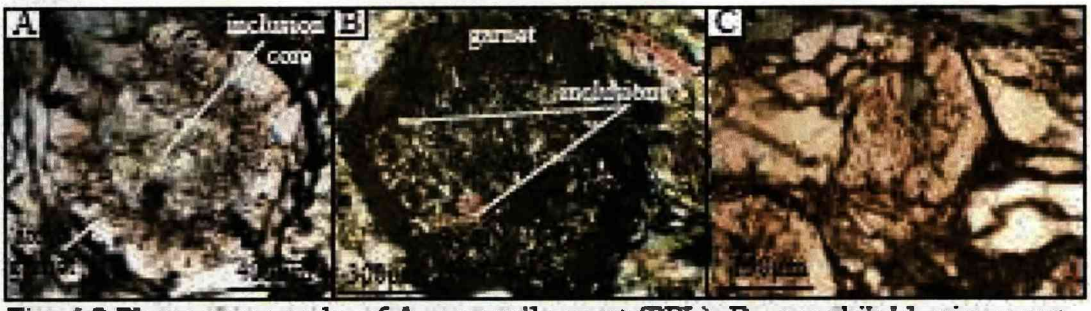

Fig. 4.9 Photomicrographs of A - an atoll garnet (PPL), B - a poikiloblastic garnet (XP) wrapped by an omphacite shape fabric and C - a garnet grain truncating omphacite grains (XP)

Under the light microscope omphacite displays variable birefringence within single grains between high, first order beige and orange and low, second order purple and blue (Fig. 4.6). Some grains show internal features such as undulating extinction and subgrains (Fig. 4.7, Fig. 4.8).

Garnet grain size can range from ~300μm to ~4mm and has irregular to euhedral porphyroblastic forms. These porphyroblasts can be poikiloblastic or atoll shaped. Inclusions usually consist of omphacite, quartz, hornblende, rutile and zoisite (Fig. 4.9). Some atoll garnet grains are ruptured and do not form complete enclosures of their inclusion rich centres. Other garnet porphyroblasts have few or no inclusions. Narrow fractures exist within garnet grains and contain variable amounts of quartz, hornblende and white mica as their fill. Spacing of garnet grains is heterogeneous and some areas of the lithology contain clusters of tightly grouped garnets (Fig. 4.4).

Glaucophane occurs in these eclogite facies rocks and texturally represents the first retrogressive phase in this area. Although prograde glaucophane has been documented in this unit (Fry and Barnicoat, 1987), this is unlikely the case here for a number of reasons. Firstly the prograde glaucophane reported in earlier work occurs as inclusions within the eclogite facies garnet, which is not evident in these samples. Instead the glaucophane here contains eclogite facies garnet as inclusions and some large porphyroblasts cut the fabric formed by the omphacite. Glaucophane displays two separate morphologies, the first being large (~0.5-2.5mm), elongate grains that define a shape fabric parallel to the omphacite shape fabric (Fig. 4.10). These grains can be isolated from each other or form a series of interconnected grains. The second morphology consists of large (~1-3mm), euhedral-subhedral porphyroblasts which cut the omphacite shape fabric obliquely (Fig. 4.11). Glaucophane grains commonly contain garnet, omphacite and zoisite as inclusions.

Green amphibole appears in a variety of places in this lithology and represents a retrogressive event experienced by the Zermatt-Saas Unit. Amphibole forms reaction rims around many of the garnet grains and is also present as inclusions within garnet porphyroblasts (Fig. 4.12).

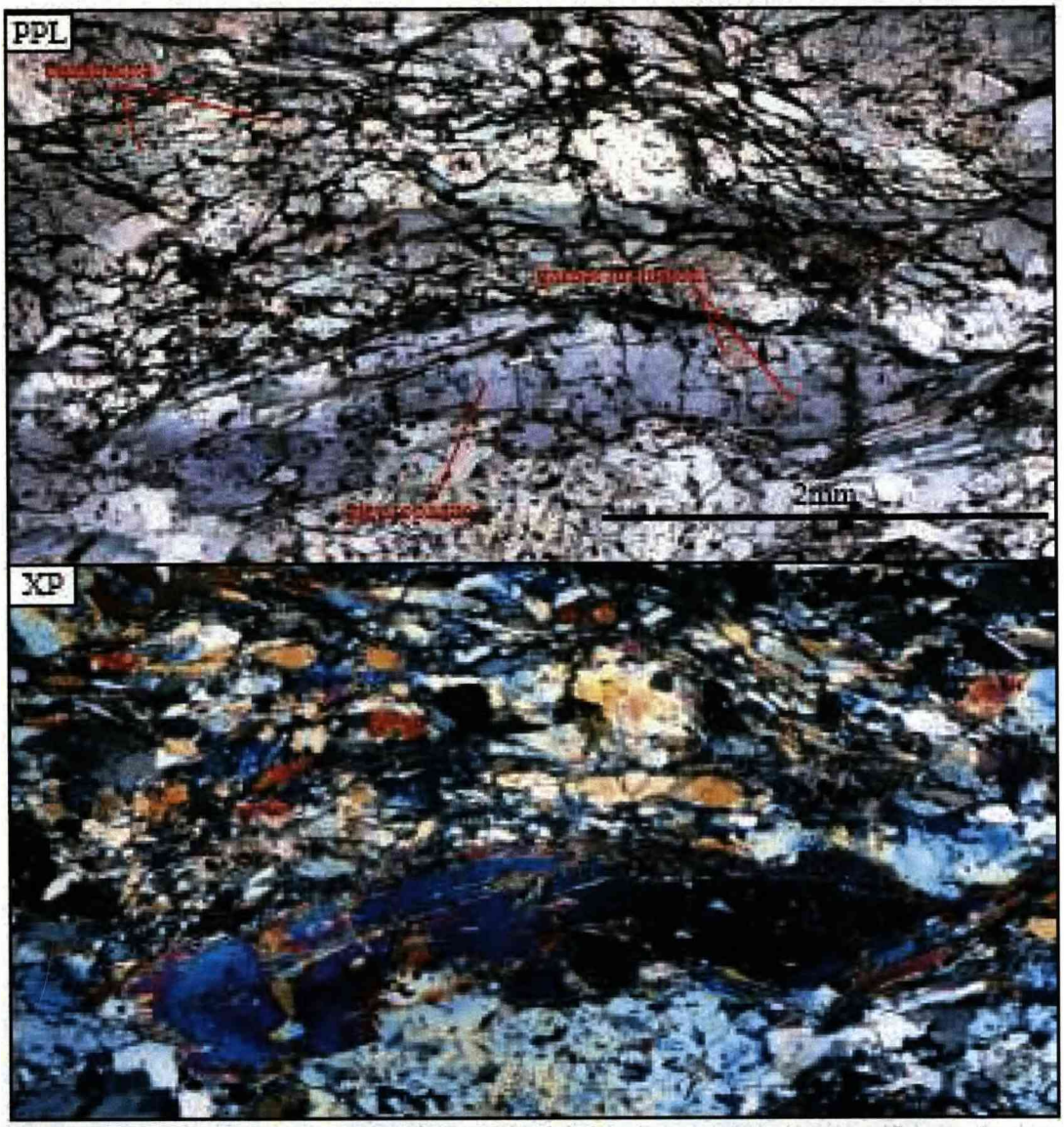

Fig. 4.10 Photomicrograhs of an eclogite facies rock sample showing a large glaucophane porphyroblast, the long axis of which is aligned with the omphacite shape fabric

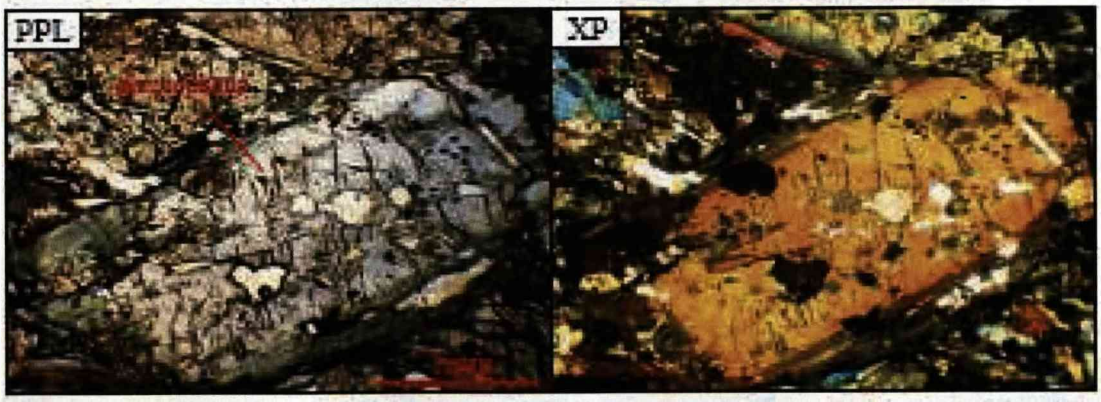

Fig. 4.11 Photomicrographs of a glaucophane porphyroblast in an eclogite facies rock sample showing the grain cutting the foliation obliquely.

Amphibole also forms reaction rims around glaucophane grains and in many places epitactical and topotactical overgrowth of amphibole on glaucophane can be seen quite clearly (Fig. 4.10, Fig. 4.11, Fig. 4.13). Amphibole grains growing around garnet and glaucophane grains and replacing glaucophane grains vary widely in size (~50μm - 1mm). A second stage of amphibole growth seems to occur within the rocks whereby the first stage amphibole is itself replaced by a second stage of amphibole growth. Grain sizes of this second phase of amphibole growth are very small (<100μm) (Fig. 4.13).

Amphibole also occurs as grains within the matrix of the rock. These can be either isolated, single grains or isolated patches of groups of smaller grains. Single grains have sizes between ~200μm and ~1mm and grains in patches have smaller sizes <100μm (Fig. 4.14). Amphibole matrix grains have a shape fabric parallel to the omphacite and glaucophane shape fabrics, though they do not form a similar interconnected network in the rock as omphacite and glaucophane do. The amphibole story is discussed further in Chapter 5.

Other minerals in this eclogite facies rock include quartz, zoisite, rutile and white mica. White mica and zoisite form a shape fabric in the sample, consistent with the one defined by omphacite. Zoisite has a larger grain size than the omphacite (~200μm – 1mm) and occasionally displays zoned extinction patterns. Quartz is usually fine grained (<100μm) except where it appears in strain shadows around garnet grains where grain size is larger (~250μm).

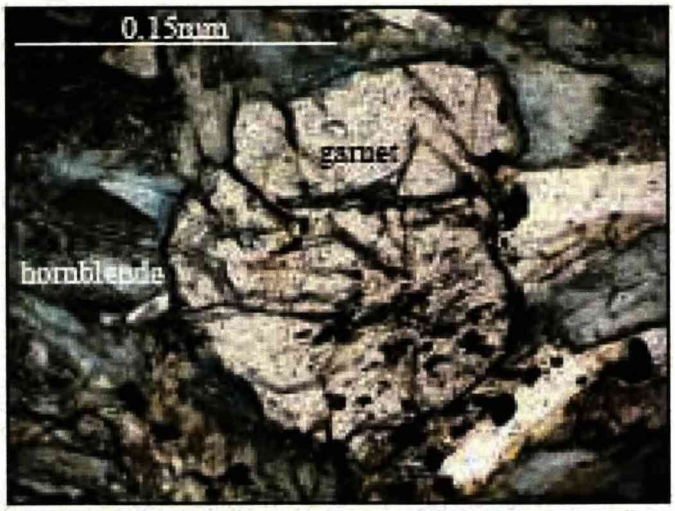

Fig. 4.12 Photomicrograph (PPL) showing amphibole growth around garnet porphyroblasts in an eclogite facies rock from Lago Blu, Punta Telcio.

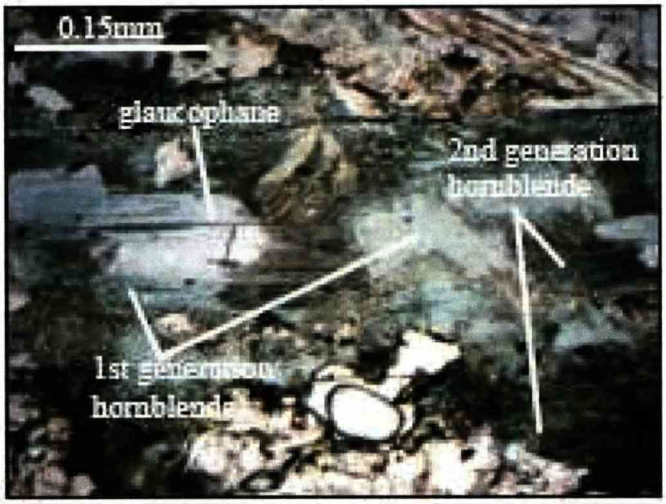

Fig. 4.13 Photomicrograph (PPL) of glaucophane being replaced by first generation green amphibole which in turn in replaced by darker green, finer grained second generation amphibole.

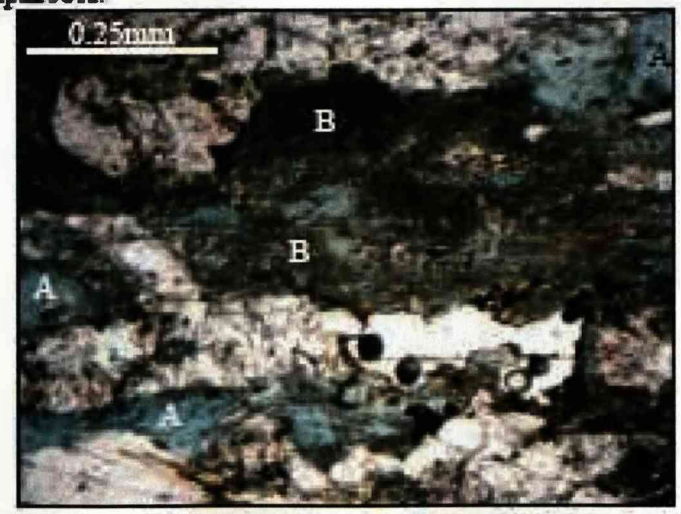

Fig. 4.14 Photomicrograph showing retrogressive amphibole growth in the matrix of the eclogite facies rock. This occurs as both large, isolated, single grains (A) or as isolated patches of smaller grains (B).

4.2.2 Amphibolites

This is the most common lithology found in the field area. The rock is blue/green in colour, and contains dark coloured amphibole, pink garnet and pale coloured minerals. The dark amphibole forms the majority of the lithology and defines a strong shape fabric which wraps garnet grains (Fig. 4.15). Occasionally dark and pale coloured minerals occur in separate bands forming a location fabric consistent with the shape fabric (Fig 4.16). In some areas the pale minerals occur in large (~3mm) polygonal patches (Fig. 4.16).

Garnet can be broadly divided into two types; large porphyroblasts (1-3 mm) with rounded to irregular shapes and occasional euhedral forms, and smaller garnet porphyroblasts (<1 mm) which also display variable grain shape. The large variety can be seen in many areas to form clusters. Large garnet porphyroblasts tend to be mainly poikiloblastic, containing quartz, green amphibole, white mica, zoisite and rutile as inclusions. Large garnet can also be found as atolls occasionally with ruptured sides. Fractures are common within garnet grains and contain quartz, amphibole and white mica as their fill. Both types of garnet have a green amphibole reaction rim and occasionally hornblende filled fractures.

Large garnet porphyroblasts are often surrounded by large patches of quartz which may be pressure shadows. This texture is most common where garnet grains occur in clusters (Fig. 4.16). In some areas garnet grains appear to have grown into clusters such that the morphology of them takes on a jigsaw like appearance. In some of these cases garnet grains have grown so close that only very narrow spaces remain between them causing what often look like wide fractures within a single garnet grain (Fig. 4.15).

Quartz is very fine grained within the lithology or is present within bands and ribbons as part of the pale bands which form a location fabric in this rock. Within these bands quartz is coarser (~100μm - 500μm) and displays internal structures including areas of variable and undulose extinction. Quartz found in patches around garnet clusters is also coarse grained (~0.1 – 1mm) and displays internal structure (Fig. 4.17)

Zoisite (straight extinction) and clinozoisite (inclined extinction) are common in this lithology and in places display a shape fabric consistent with the one defined by the amphibole. These minerals have an average grain size of ~300-600μm. Zoisite grains also occur as large porphyroblasts (~1.5mm) that can either cut across the fabric of the amphibolite or lie parallel to it (Fig. 4.18).

White mica and rutile are present in various amounts, with white mica forming long grains (~300μm - 500μm) that form the same shape fabric defined by other minerals (Fig. 4.17). Rutile (~50μm - 200μm) can occur in the matrix of the rock but is more common as inclusions in other minerals. It occasionally has a reaction rim of sphene (Fig. 4.18).

The transition from eclogite facies rock to this amphibolite lithology, the microstructural and chemical development and consequences for the development of the Zermatt-Saas Unit are explored further in Chapter 5.

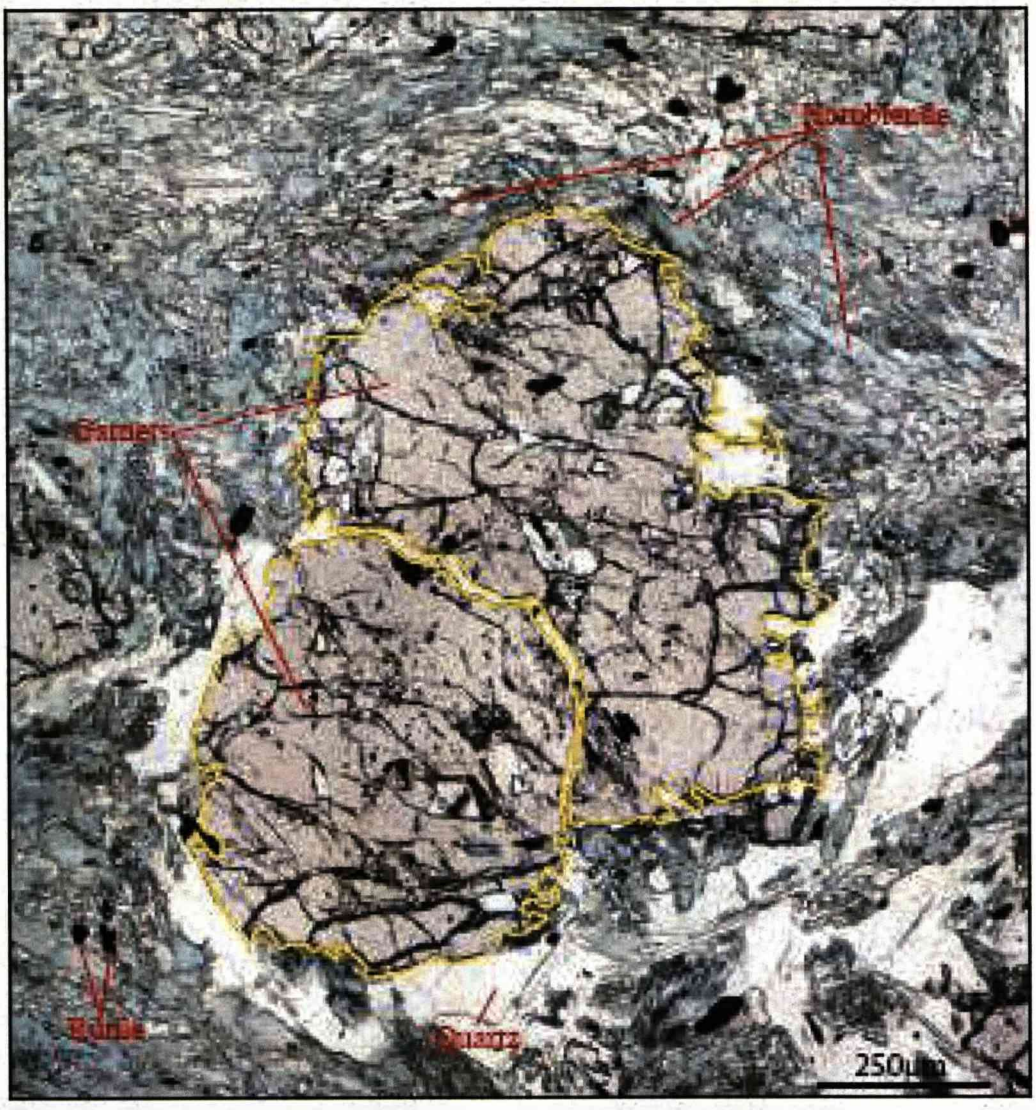

Fig. 4.15 Photomicrograph (PPL) of garnet porphyroblasts in a cluster in amphibolite from Lago Blu, Punta Telcio. Green amphibole forms a shape fabric that wraps the cluster. The two garnets have a jigsaw boundary separated by a thin band of quartz.

Fig. 4.16 Location fabric in amphibolite rocks of the Lago Blu area, Punta Telcio. Pale minerals can also be seen in patches.

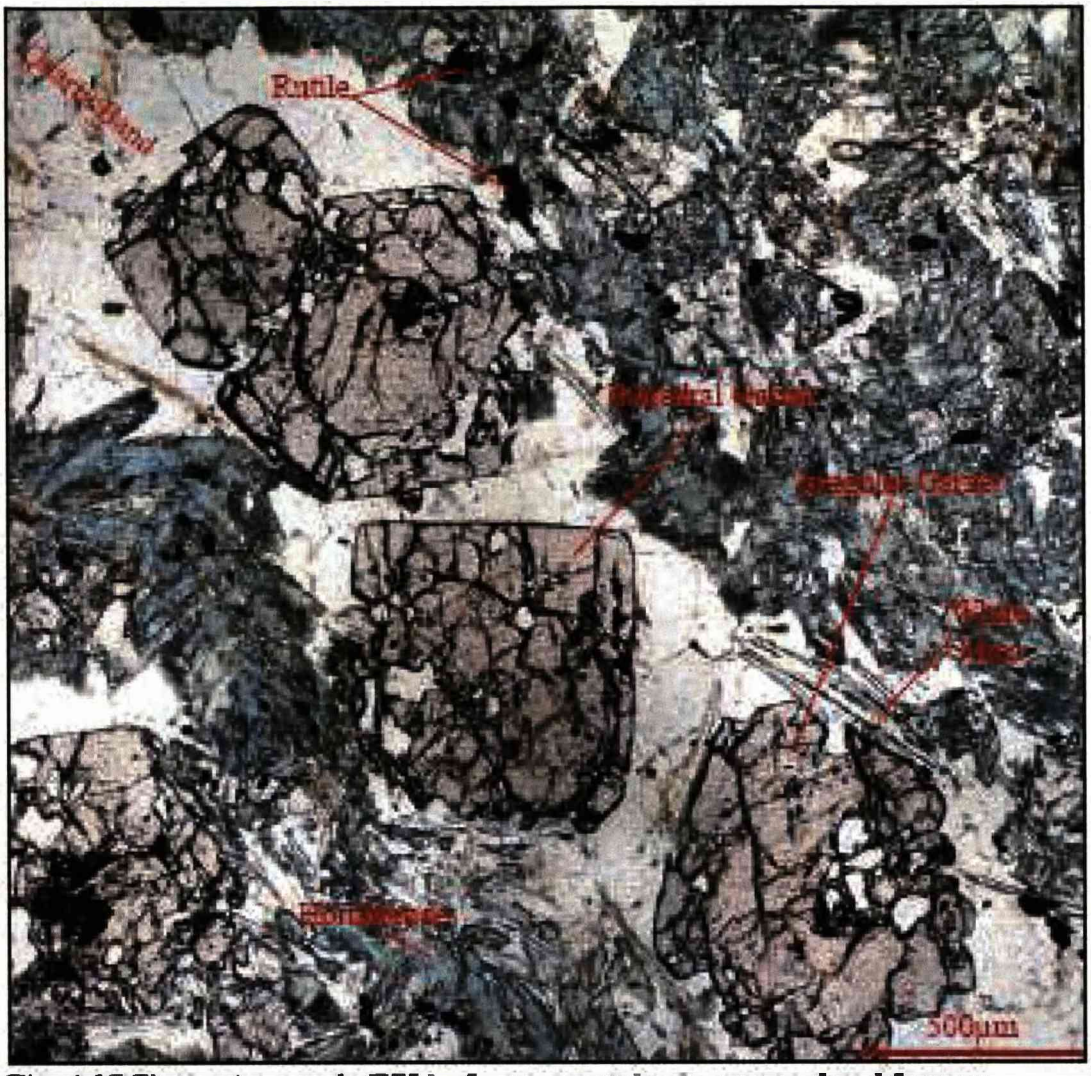

Fig. 4.17 Photomicrograph (PPL) of a garnet grains in a quartz band from an amphibolite from the Lago Blu area, Punta Telcio. Garnets are euhedral or irregular in shape. White mica, amphibole and clinozoisite form a shape fabric.

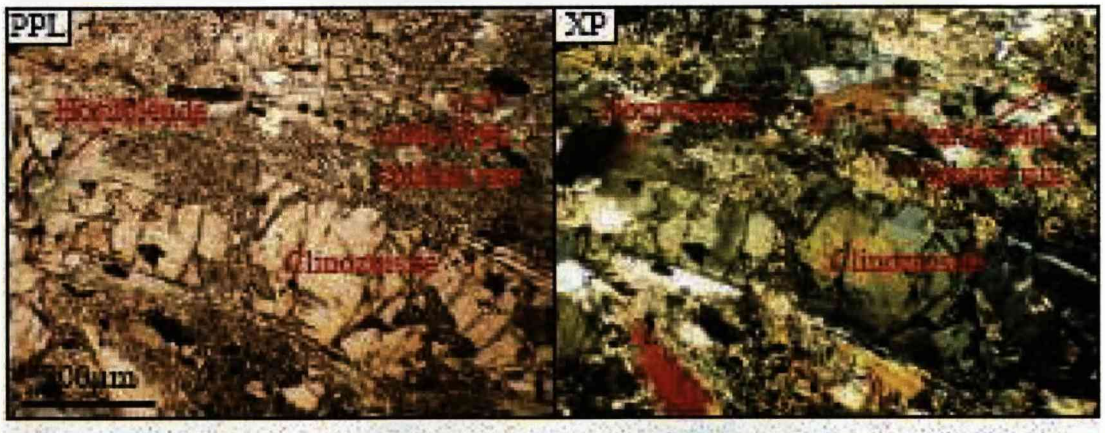

Fig. 4.18 Photomicrographs of a clinozoisite porphyroblast in an amphibolite from the Lago Blu area, Punta Telcio. Sphene rims around rutile grains are also visible.

4.2.3 Other Lithologies

Though not investigated further in this study, a brief description of another two lithologies mapped in the Lago Blu area of Punta Telcio is included here to provide a full geological description of the area.

4.2.3.1 Serpentinite

Serpentinite crops out as a thin, elongate body that tracks across the length of Punta Telcio (Reddy et al., 1999). In the area mapped for this study it forms the southern boundary. This rock is dark green/black in colour and contains a strong foliation (Fig. 4.19) and lineation (Fig. 4.19).

The lithology is composed of a pale green mineral (serpentine) and a black mineral (magnetite) and has a strong magnetic effect on a compass due to the latter. Foliation is defined by a location fabric consisting of alternating black and green layers (~1mm–10mm). Green layers include long (~500μm–2mm), narrow colourless grains (serpentine/brucite) along with small amounts of green serpentine (<100μm). Long axes of these colourless mineral align to form a shape fabric (Fig. 4.20), consistent with the location fabric. Black layers are composed of elongate lenses of serpentine and bands of black magnetite (<100μm-500μm) (Fig. 4.20). Small (0.5-1mm) elongate patches occur throughout the rock containing fibrous material, most likely the fibrous form of serpentine, chrysotile.

This rock also contains augen, composed of green serpentine and black magnetite (Fig. 4.19), and the long axes of these augen align with the foliation. Augen serpentine has a mesh texture (<100μm-200μm), local concentrations of chrysotile, long (~500μm–1.5mm), narrow grains of serpentine/brucite and black grains of magnetite (<100μm–2mm).

4.2.3.2 Quartz Garnet Schist

This lithology occurs as a thin (~1m wide), elongate body that can be traced along strike (bearing -110°) for ~130m. The rock is white being composed mainly of quartz although white mica and large garnet grains (<1mm–6mm) are visible. A foliation is evident, defined by a white mica shape fabric which wraps garnet grains (Fig. 4.22). Crenulations in the foliation are also present (Fig 4.21) as is a quartz lineation.

White mica grains are large (~0.25mm-4mm) and quartz has a variable grain size (<0.25mm – 3mm). Both minerals occur in separate bands forming a location fabric consistent with the white mica shape fabric. Some garnet porphyroblasts contain numerous quartz inclusions that either form concentric ring patterns or sigmoidal patterns possibly representing preservation of an earlier quartz fabrics (Fig. 4.22). Other inclusions in garnet include small biotite needles (<100μm) and white mica. Chlorite is present in this lithology (~1-2mm) and in places forms a shape fabric consistent with that of the white mica (Fig. 4.22). The chlorite can in places be seen to replace or grow around garnet grains (Fig. 4.22) and is representative of the retrogression experienced by the Zermatt-Saas Unit.

Fig. 4.19 A – Location fabric defining foliation in serpentinite and B – serpentine lineations in serpentinite.

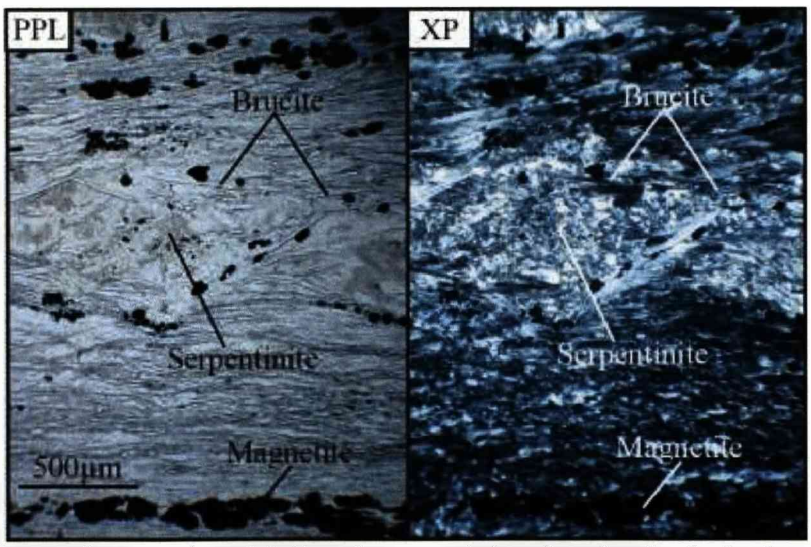

Fig. 4.20 Photomicrographs of foliated serpentinite showing both the location fabric formed by mineral layering and the shape fabric formed by serpentine/brucite.

Fig. 4.21 Cremulation cleavage in the quartz garnet schist lithology.

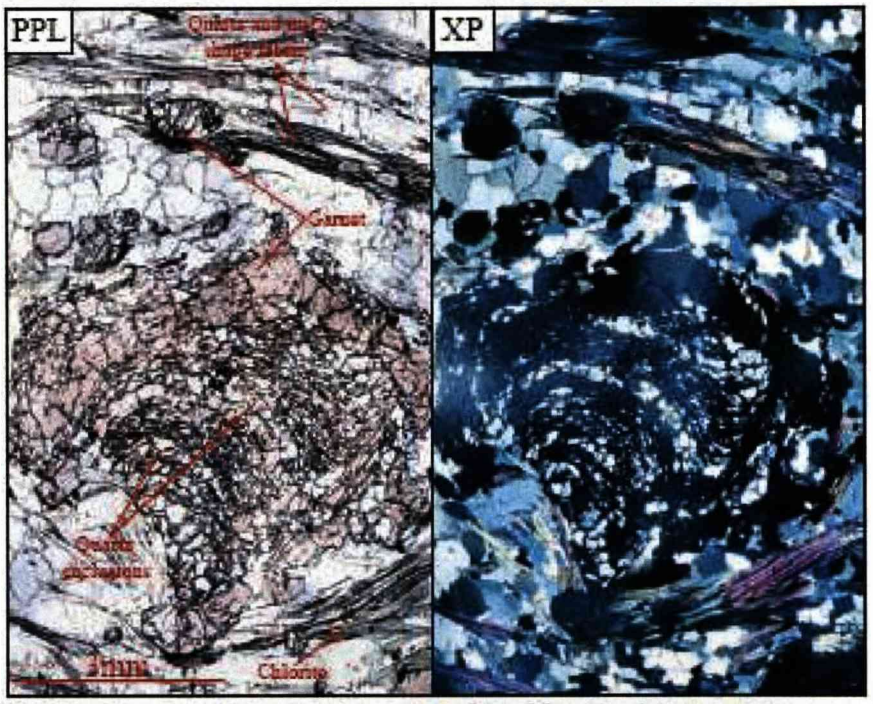

Fig. 4.22 Photomicrographs of a garnet porphyroblast in the quartz garnet schist lithology from Lago Blue, Punta Telcio showing a complicated quartz inclusion pattern. The garnet grain is wrapped by the white mica shape fabric and the white mica and quartz location fabric. Chlorite can also be seen as part of the foliation in this rock.

4.2.4 Structure of Lago Blu, Punta Telcio

What follows here is an introduction and description of the structure of the Lago Blu area of Punta Telcio. A more in depth discussion follows in Chapter 5 as the results from an investigation of the fabrics of the retrogressive mineralogy included there have possible bearings upon the structural evolution of the Zermatt-Saas Unit in Val di Gressoney.

The structure of the Zermatt-Saas Unit of the Lago Blu area, Punta Telcio is relatively simple. A penetrative foliation defined by shape and location fabrics described earlier exists in all lithologies. Foliation geometry is independent of lithological boundaries and is consistent across them. Foliation dip shows a marked, steady increase in angle from the north of the area to the south (Fig. 4.2, Fig. 4.23). Variation in dip angle is a result of the large scale recumbent fold structure apparent in this area (Reddy et al., 1999) and the geology mapped around Lago Blu represents the upper limb of this structure. A stereonet showing poles to planes of foliation defines a great circle the pole to which indicates azimuth and plunge of the hinge line ($5° \rightarrow 274$) of this fold (Fig. 4.24). From foliation measurements and photographs of the larger area the fold is interpreted as having a more open form.

Lineations in eclogite facies rocks of the area are mineral lineations of omphacite and glaucophane. These are recorded as stretching lineations in previous studies of this area (Reddy et al., 1999). Lineations in the amphibolite lithology exist as amphibole mineral lineations. Omphacite and glaucophane lineations are grouped together as these minerals have shown they can be texturally coexistent, representing the late prograde/early retrograde stage of the evolution of the area. Amphibolite lineations are plotted separately as they relate to a later stage of the evolution of the Zermatt-Saas Unit of Punta Telcio. For both groups, most lineation measurements have an easterly azimuth with gentle plunges although at few amphibole measurements have southern azimuths and steeper plunges (Fig. 4.24).

In the serpentinite body, lineations recorded (Fig. 4.24) show two different types. A southward azimuth with a steep plunge is predominant but easterly azimuths with shallow plunges are also noted here. This is similar to what can be found in the amphibolite lithology although the east trending lineations are predominant.

Fig. 4.23 Photograph of an area of Punta Talcio looking eastward showing foliation dip steepening from north to south.

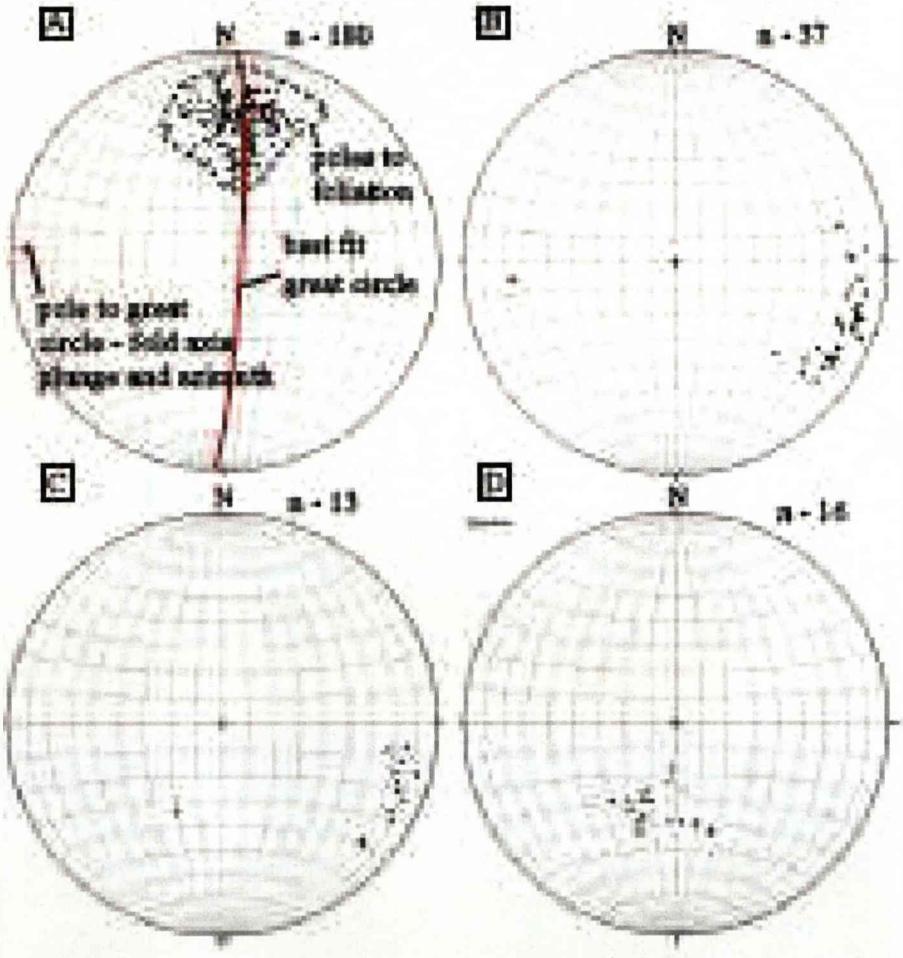

Fig. 4.24 Equal area stereonets showing A - poles to foliation planes, their best great circle and the pole to that great circle, B - orthoclase and plagioclase lineations and C - amphibole lineations, D - serpentinite lineations

4.3 Omphacite Deformation in eclogite facies rocks from the Zermatt-Saas Unit, Lago Blu, Punta Telcio

4.3.1 Introduction

The eclogite facies rocks of the Lago Blu area of Punta Telcio are deformed as is evident by a penetrative foliation and mineral lineations. The mineral omphacite defines these deformation features and is also the framework supporting mineral in this lithology. As such it will have had a significant control on the way this eclogite facies rock behaved during subduction.

Investigation of omphacite lattice preferred orientation and chemistry can provide information on what deformation mechanisms were operating in this mineral during the eclogite facies evolution of the Zermatt-Saas unit. As discussed in Chapter 1 development of an omphacite LPO is mainly attributed to dislocation creep and plenty of evidence exists to suggest so (Godard and van Roermund, 1995, Raterron et al., 2004). However it is theorised that dislocation creep alone cannot be solely responsible for omphacite LPO formation and so other mechanisms must be active, such as diffusive mass transfer processes (Mauler et al., 2001). It is also possible that omphacite LPO patterns can result from preferential growth processes (Godard and van Roermund, 1995). In addition, omphacite LPO, chemistry, space group information and metamorphic conditions it formed under can be used to elucidate whether LPO development in omphacite is related to changes in space group or whether it is solely a result of strain regime.

The purpose here is to determine if omphacite in the deformed eclogite facies rocks of Lago Blu, Punta Telcio, has an LPO and to resolve what mechanism that LPO formed by. LPO data is then used, in conjunction with chemical analyses and structural information, to determine the nature of deformation and metamorphism of this area and to tie this information into existing geological information of this area and on the Zermatt-Saas Unit as a whole. To this end omphacite in samples of Punta Telcio eclogite facies rocks were studied using EBSD, chemical probe analysis and TEM techniques (Chapter 3).

4.3.2 Omphacite LPO

Omphacite orientation data is gathered from thin sections of eclogite facies rock samples from Lago Blu using the STscan procedure (Chapter 3). This is carried out at variable step sizes depending on average omphacite grain size. This produces a data set based upon one omphacite orientation measurement per grain. Table 4.1 summarises information for each sample investigated; omphacite grain size, STscan step size, number of orientation measurements per sample, LPO type and LS index value, Ulrich and Mainprice, (2005) (see Chapter 1 for full explanation).

Omphacite pole figures (Fig. 4.25), and LS-index values (Table 4.1) show that the omphacite in these eclogite samples have a typical S-type LPO pattern based on the classification scheme set out by Helmstaedt at al. (1972) and furthered by Godard and Van Roermund (1995). All omphacite pole figures show <001> poles dispersed in a girdle within the foliation plane, (010) poles forming point maxima normal to the foliation and (100) poles with a random distribution. LS-index values (0.108 - 0.307) are close to the S-type end member value of zero. Larger values indicate that omphacite in some samples have a more intermediate LS-type LPO, although few 010 pole figures show evidence of a girdle distribution normal to the foliation plane.

The presence of an LPO in omphacite is usually taken as evidence that the dominant deformation mechanism in the mineral is dislocation creep (Buatier et al., 1991, Philippot and van Roermund, 1992, Brenker, 1998, Brenker et al., 1999, Bascou et al., 1991, Bascou et al., 2002, Ulrich and Mainprice, 2005). A detailed look at omphacite grain microstructure, misorientation angle distribution analyses and TEM investigations of the omphacite of these samples will shed more light on this possibility. Further evidence is required to confirm this as it is possible to form omphacite LPO patterns by other deformation mechanisms such as diffusion creep or by processes like preferred crystal growth (Helmstaedt, 1972, Godard and van Roermund, 1995, Mauler et al., 2001). Dislocation creep (due to limitations on both single slip and multiple slip models) is unlikely to be solely responsible for LPO creation in omphacite and rather is said to act in conjunction with other processes like those just mentioned. Results of chemical analyses and chemical zoning patterns of omphacite grains showing a strong S-type LPO are presented in an effort to elucidate any contribution made by diffusive mass transfer process or crystal growth.

How the Zermatt-Saas eclogite omphacite developed an S-type LPO is also of interest to this study. As discussed in Chapter 1 two opposing theories exist to explain the cause of variable omphacite LPO type; omphacite space group and strain regime. According to the space group theory an S-type LPO suggests omphacite is of the C2/c (disordered) space group. As previously mentioned, through examination of the evidence for both theories, this study is unconvinced that space group does control LPO type and the more likely control is strain regime. Thus it follows that the strong S-type LPO presented here suggests the omphacite of these Zermatt-Saas eclogites of Punta Telcio is deformed in a flattening strain regime.

TEM investigation of the omphacite will allow identification of the space group of the omphacite in these eclogite samples. Chemical analyses of omphacite grains combined with temperature estimates from literature will allow the omphacite of these eclogites to be plotted on the space group phase diagram. This will allow a direct comparison between space group and LPO type to be made, and conclusions to be drawn on how the S-type LPO formed.

Sample	Average Omphacite Grain Size (μm)	Slide Scan Step Size (μm)	No. of Omphacite Points	LPO Type	LS-Index
5.2	150	300	303	S-type	0.234
5.6	300	400	251	S-type	0.211
6.3	350	350	492	S-type	0.307
6.4	300	350	726	S-type	0.122
6.5	300	400	556	S-type	0.187
6.7	150	300	121	S-type	0.262
6.8	200	350	268	S-type	0.29
6.12	250	350	226	S-type	0.219
6.13	250	300	594	S-type	0.18
6.14	200	300	322	S-type	0.136
6.16	300	350	328	S-type	0.277
6.18	250	400	387	S-type	0.234
6.19	250	300	741	S-type	0.248
6.22	100	300	705	S-type	0.108
S3-50B	200	350	510	S-type	0.218

Table 4.1 FTscan procedure information and omphacite pole figure and LPO information from eclogite facies rocks from Lago Blu, Punta Telcio

(100)
(010)
<001>
S5.2
S5.6
S6.3
S6.4
S6.5
S6.7
S6.8
S6.12

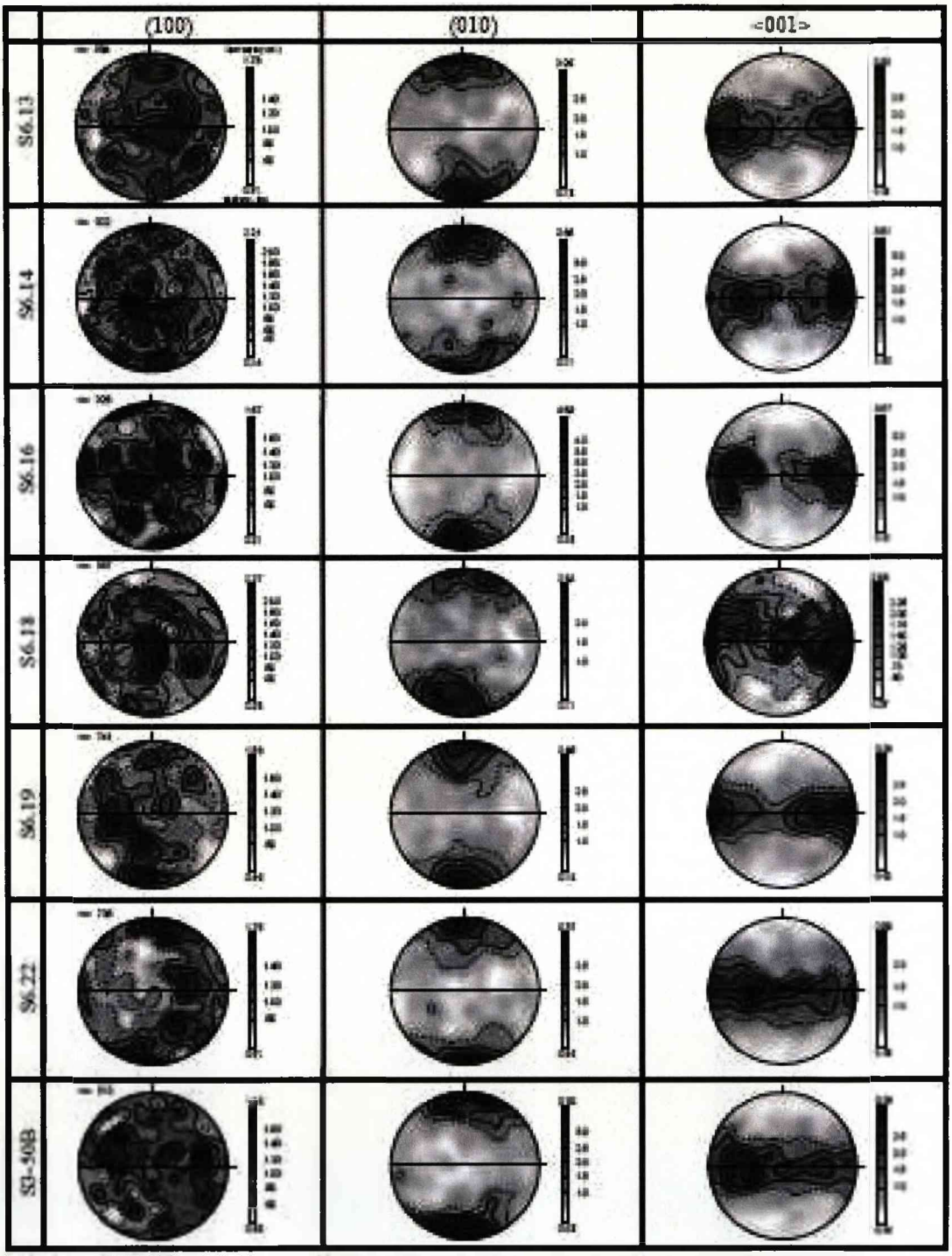

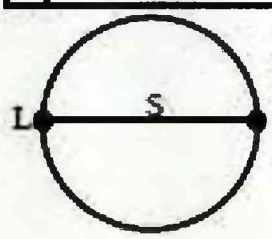

Fig. 4.25 Omphacite pole figures from eclogite facies rock samples from Lago Blu, Punta Telcio. A reference frame for the pole figures is shown to the left, L marking the lineation and S marking the plane of foliation.

4.3.3 Omphacite Misorientation Angle Distribution Analysis and Grain Microstructure

Selected areas of thin sections from eclogite facies rock samples from Lago Blu, Punta Telcio are mapped using EBSD. The aim here is to investigate whether omphacite grains display internal deformation features. Thin section investigation show some omphacite grains have undulating extinction and contain subgrains (Fig. 4.7, Fig. 4.8) and so evidence of this should be apparent in EBSD orientation maps. The presence of subgrains and gradual increases in misorientation across a single omphacite grain can indicate dislocation creep and glide as operating deformation mechanisms (Chapter 1). Misorientation angle distribution analysis, as discussed in Chapter 3, provides a different way of interpreting microstructure and which processes contributed to its development. If omphacite neighbour pair misorientations show a high frequency of low angle (<10°) misorientations it suggests omphacite grains should have numerous subgrain structures thus providing evidence of deformation by dislocation creep.

Misorientation angle distribution analyses (Fig. 4.26) show high frequencies of low angle misorientations (<10°) between omphacite neighbour pair pixels compared to low frequencies between random pair pixels. Higher neighbour pair compared to random pair misorientation frequency persists in misorientations up to about ~20-25° after which the neighbour and random pair misorientations become approximately similar. Cumulative frequency graphs show the neighbour pair misorientation line is significantly shifted to the left compared to the random pair misorientation line reiterating the high frequency of lower angle misorientations.

As stated in Wheeler et al. (2001) a significant difference between the neighbour and random pair distributions (as observed in the omphacite data here) suggests neighbouring grains have undergone a physical interaction and/or neighbouring pairs have been derived in a significant number of cases from a common parent microstructure: inheritance. However before a conclusion can be drawn on which process is likely to have been operating, it is essential to investigate the grain scale microstructures of the omphacite.

Grain boundary maps of selected areas of the eclogite facies rock samples, created from EBSD data, display omphacite subgrain boundaries (<10°) within omphacite grains (Fig. 4.27, Fig. 4.28). Of the subgrain structures observed, a variety of forms are noted. Subgrain boundaries either form across the length or breadth of the omphacite grain they are located within. Others form small islands of misoriented omphacite within a larger grain. While many grains show subgrain formation other grains display none and misorientation profiles across them reveal cumulative misorientation no larger than ~2°.

The presence of subgrain walls within omphacite grains suggests the action of dislocation creep in the deformation of omphacite in these eclogites. In relation to the low angle neighbour pair misorientation in the misorientation angle distribution analyses, this implies the signal is a result of inheritance mechanism; subgrain rotation recrystallisation due to plastic deformation by dislocation creep. The <10° peaks in neighbour pair misorientations are indications of the many subgrain boundaries observed in the omphacite grain boundary maps. Those omphacite grains that display no subgrains yet have cumulative misorientations of ~1.5-2° across them may suggest some dislocation glide may have been active in these grains.

In light of these results the omphacite S-type LPO seems likely to have been formed, at least in part, by dislocation creep. TEM investigations should thus show dislocations organised into subgrain walls given the microstructures described here. Chemical analysis and zoning pattern results still require consideration as most previous studies of the mechanisms contributing to omphacite deformation involve not just the sole action of dislocation creep (Godard and van Roermund, 1995, Mauler et al., 2001). Later this work considers whether diffusive mass transfer processes or crystal growth is a contributing factor.

Misorientation axes distributions were not included here for these samples as they

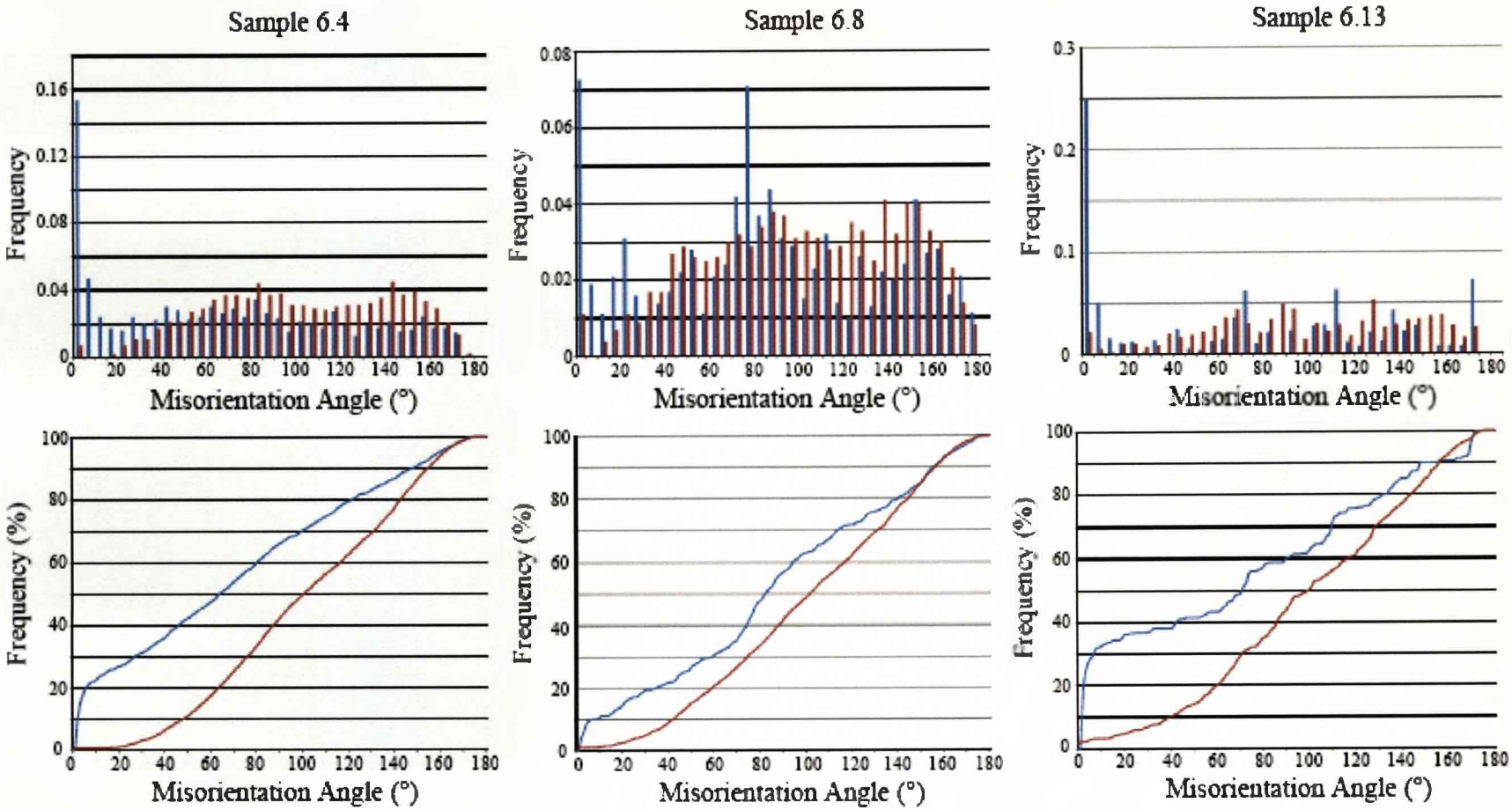

Fig. 4.26 Omphacite misorientation distribution analyses of three eclogite facies rock samples from Lago Blu, Punta Telcio. For each sample the entire omphacite data set is used and a frequency chart and cumulative frequency graph (misorientation angle bin size = 5 degrees) are shown.

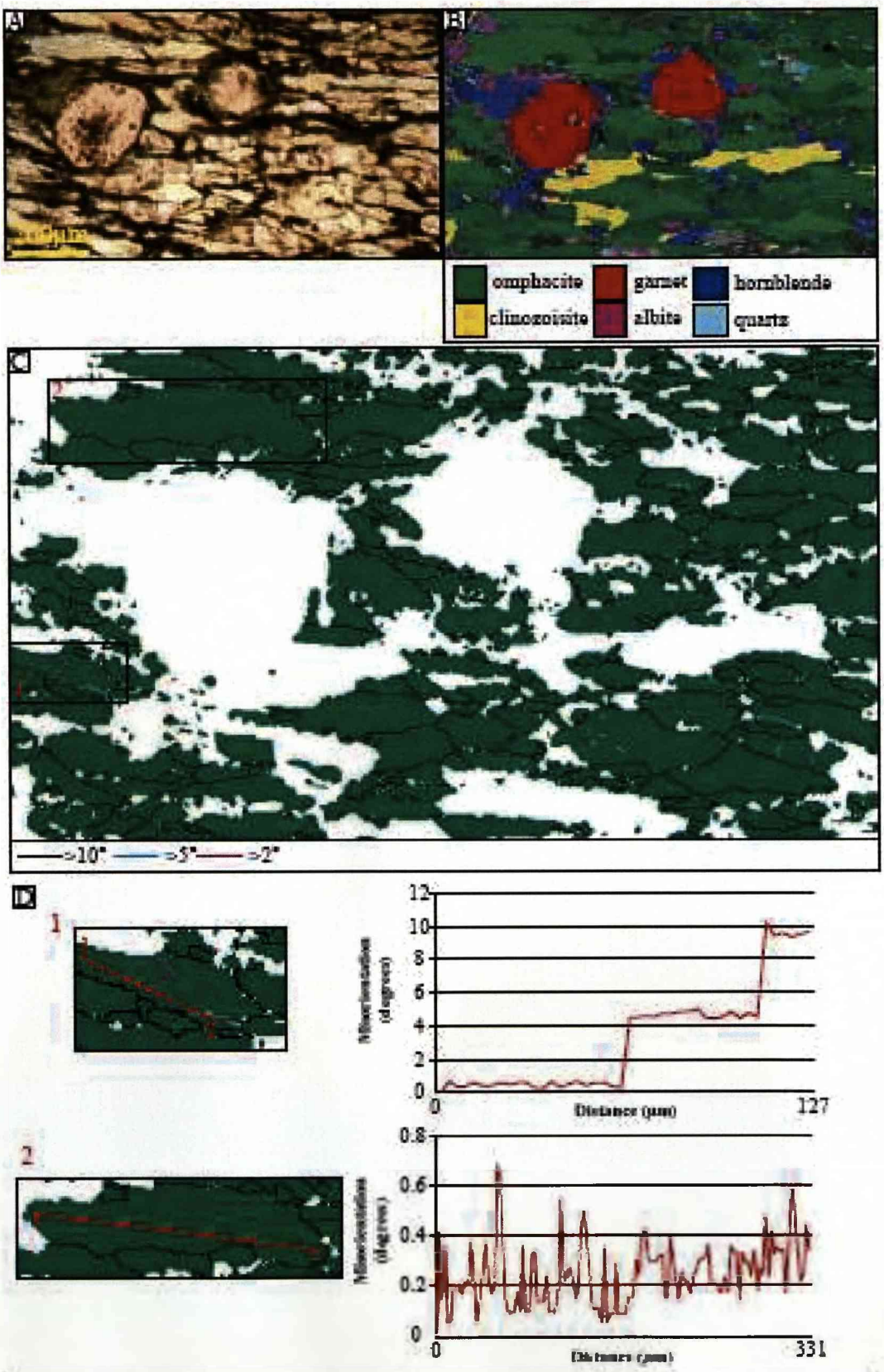

Fig. 4.27 Omphacite grain microstructure images of sample S6.8. A - PPL photomicrograph of the area scanned using EBSD, B - Phase ID map overlaid on a band contrast map, C - Omphacite grain boundary map, D - Two separate enlarged grains from the grain boundary map and associated cumulative misorientation profiles

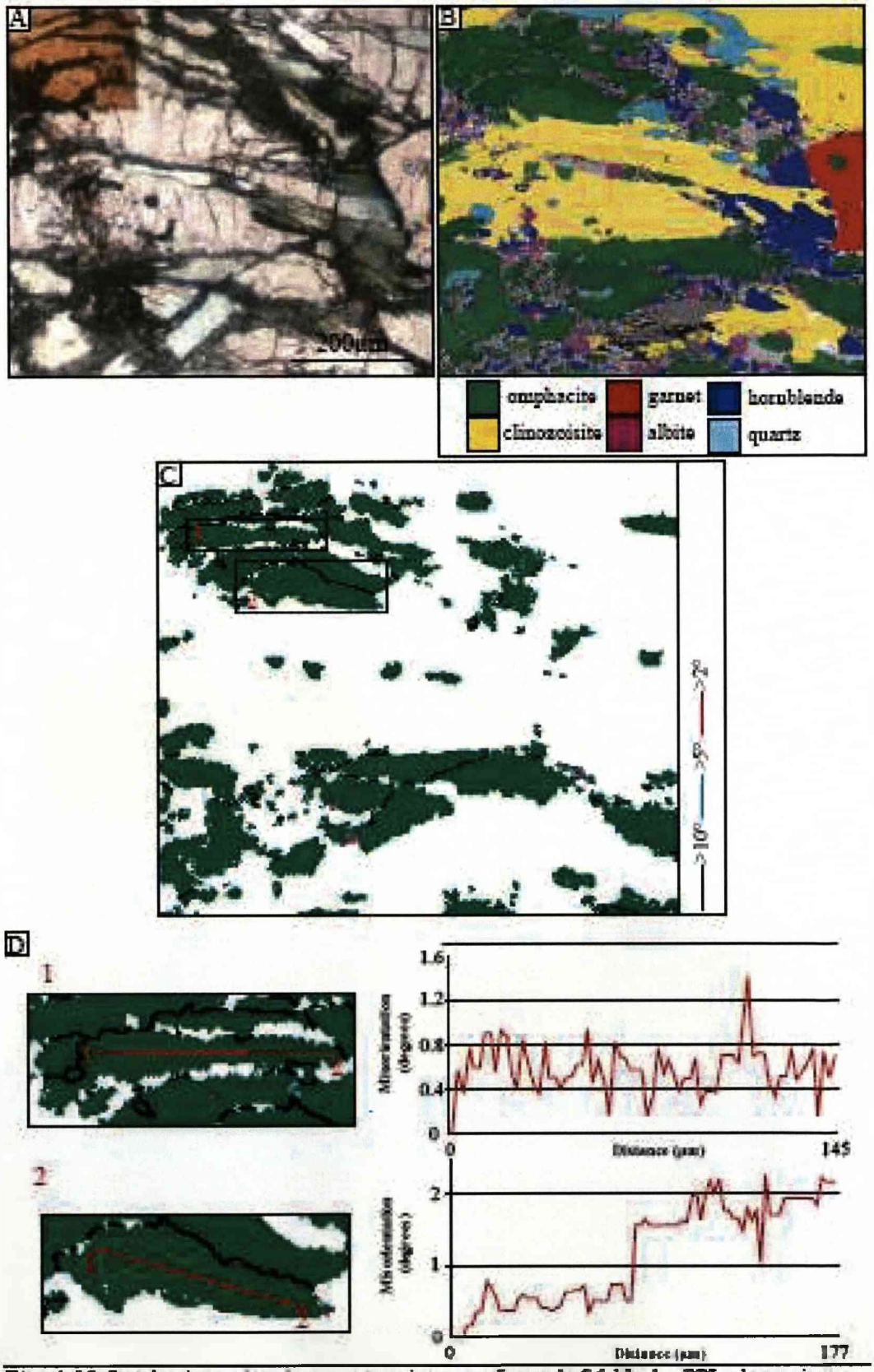

Fig. 4.28 Omphacite grain microstructure images of sample S6.13. A - PPL photomicrograph of the area scanned using EBSD, B - Phase ID map overlaid on a band contrast map, C - Omphacite grain boundary map, D - Two separate enlarged grains from the grain boundary map and associated cumulative misorientation profiles

4.3.4 Omphacite TEM

TEM was carried out on these eclogite facies rocks (by Prof. W. Müller at Technische Universität Darmstadt) in order to determine the space group of omphacite and search for evidence of dislocation creep such as dislocations and subgrain walls. Results should confirm evidence from omphacite EBSD maps and misorientation angle distribution analyses that suggest the action of dislocation creep in omphacite deformation. As such finding direct evidence of dislocations in omphacite with this TEM study is expected. In addition determination of omphacite space group will aid this study in addressing what effect space group has on omphacite LPO formation.

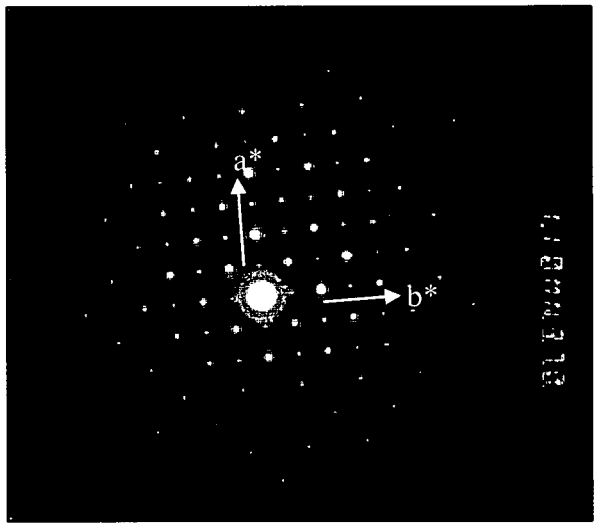

Fig. 4.29 Selected area diffraction pattern showing P2/n omphacite in the [010] orientation

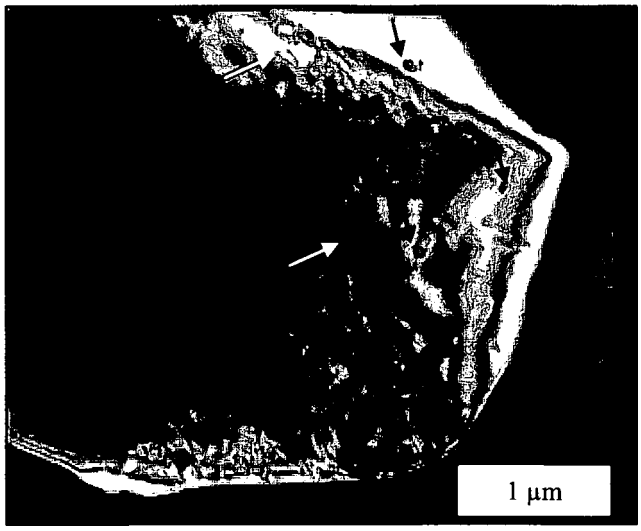

Fig. 4.30 Dark field photomicrograph of ordered omphacite showing rare dislocations (white arrows) and ~30-100nm inclusions, possibly of amphibole (black arrows)

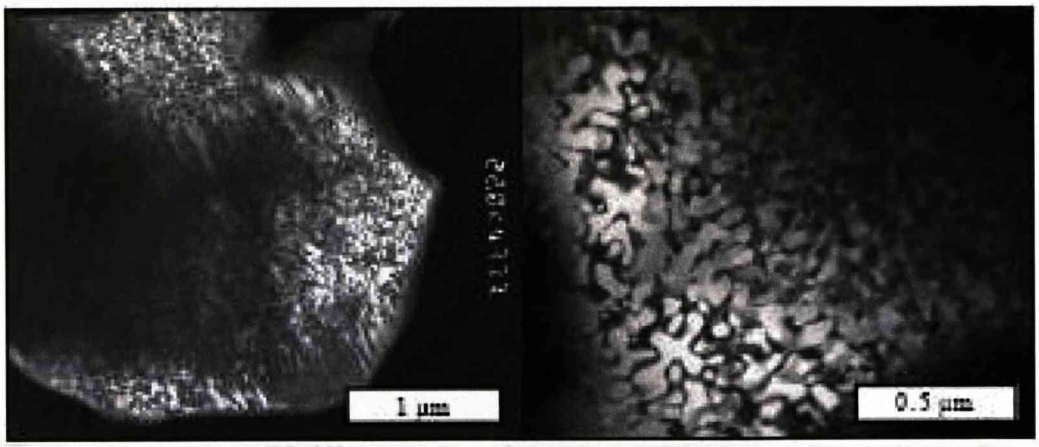

Fig. 4.31 Dark field photomicrographs of antiphase domains in ordered omphacite

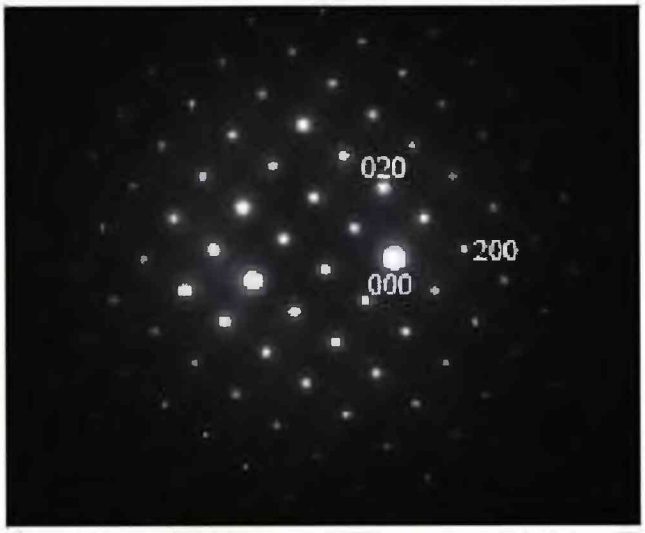

Fig. 4.32 Selected area diffraction pattern of C2/c omphacite in the [010] orientation

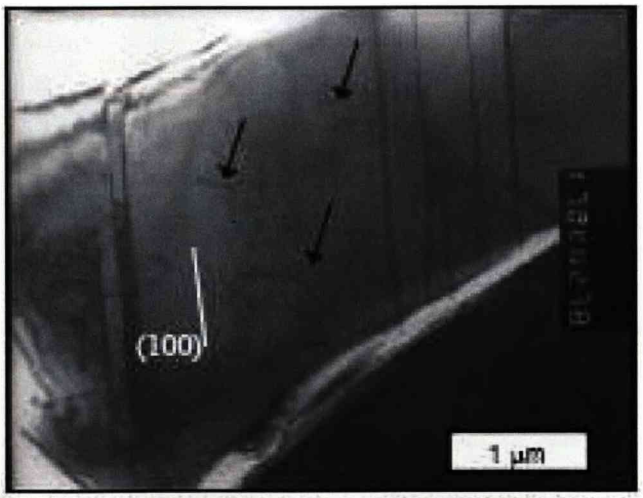

Fig. 4.33 Dark field photomicrograph of C2/c omphacite showing twin lamellae on (100) and dislocations (arrows)

Omphacite from sample S6.4 is mainly of the P2/n space group (ordered) (Fig. 4.29) although some disordered C2/c space group omphacite is present (Fig. 4.32) as are antiphase domains (Fig. 4.31) (Chapter 1). Dislocations are observed (Fig. 4.30, Fig. 4.33) but small angle grain boundaries were not found in omphacite. This may simply be due to the fact some omphacite grains do not display subgrain formation as witnessed in the EBSD grain boundary maps (Fig. 4.27, Fig. 4.28). In addition finding such small structures within grains can be tricky at best and a lack of subgrain wall images is not entirely surprising given the limitations of the technique.

The presence, though rare, of dislocations in omphacite (in both the P2/n and C2/c omphacite) of S6.4 confirms the action of dislocation creep as suggested by EBSD grain maps and omphacite LPO.

The appearance of antiphase domains also bears discussion relevant to the idea that omphacite space group controls omphacite LPO type. Antiphase domains typically appear due to a phase transformation thus providing evidence of post crystallisation structural change. In omphacite the cause of antiphase domain development is due to ordering, a change from the C2/c to the P2/n space group (Carpenter, 1979). This would imply that eclogites were once at a temperature sufficient for the omphacite cations to be disordered. On the other hand studies (Champness, 1973, Brenker et al., 2003) suggest that this transition between stability fields is not needed for antiphase domain formation in omphacite. Rather they can form by omphacite first forming a metastable C2/c form which subsequently starts to order. Based upon the maximum temperatures (not including the ultra-high pressure of the Laghi di Cignana area) for eclogite facies metamorphism in the Zermatt-Saas Unit the latter cause for antiphase domain formation is more likely here. This is discussed further in conjunction with omphacite chemical data later in the chapter.

4.3.5 Omphacite Chemistry

Omphacite chemical data from eclogite facies rocks from Lago Blu, Punta Telcio is essential for a full understanding of how the mineral behaved during the evolution of the Zermatt-Saas Unit. Chemical zoning patterns can shed light on preferential growth of omphacite grains, changing metamorphic conditions of the area and reveal possible evidence for diffusion creep deformation. In conjunction with EBSD and TEM work already presented in this chapter chemical data may provide information as to possible diffusive mass transfer mechanisms operating in omphacite in these rocks and give a clearer picture of any contribution being made by various deformation mechanisms to omphacite microstructure.

Chemical maps, gathered using the EDX system on a CamScan X500 SEM (University of Liverpool) and quantitative chemical data collected using the EDX system on a Philips XL30 SEM (University of Liverpool) and the Cameca SX 100 Electron Microprobe equipment (University of Manchester), are presented here (see Chapter 3 for information in equipment and EDX theory). Quantitative data is recalculated for Fe^{3+} using the stoichiometric method of Droop (1987). Chemical data and maps are gathered from omphacite grains investigated using EBSD, in samples S6.8 and S6.13 for a direct comparison between chemical microstructures and orientation microstructures.

Sample S6.8 (Fig. 4.34, Fig. 4.35, Fig. 4.36) show a preferential chemical zoning pattern in omphacite grains. EDX chemical maps show that zoning is not concentric (as would be expected with simple mineral growth) and rather zoning occurs preferentially along long axes of omphacite grains. EDX maps and EMPA data for selected grains show the most obvious chemical changes occur in Fe, Ca, Na, Al and Mg. Fe, Mg, Al and Ca show zoning patterns that correlate to each other. Na zoning patterns could not be imaged by EDX techniques as the equipment cannot successfully image elements that have the atomic number of sodium or below (see Chapter 3 for an explanation for this). EMPA data and quantitative EDX data however show that Na displays a similar preferential zoning pattern to other zoned elements.

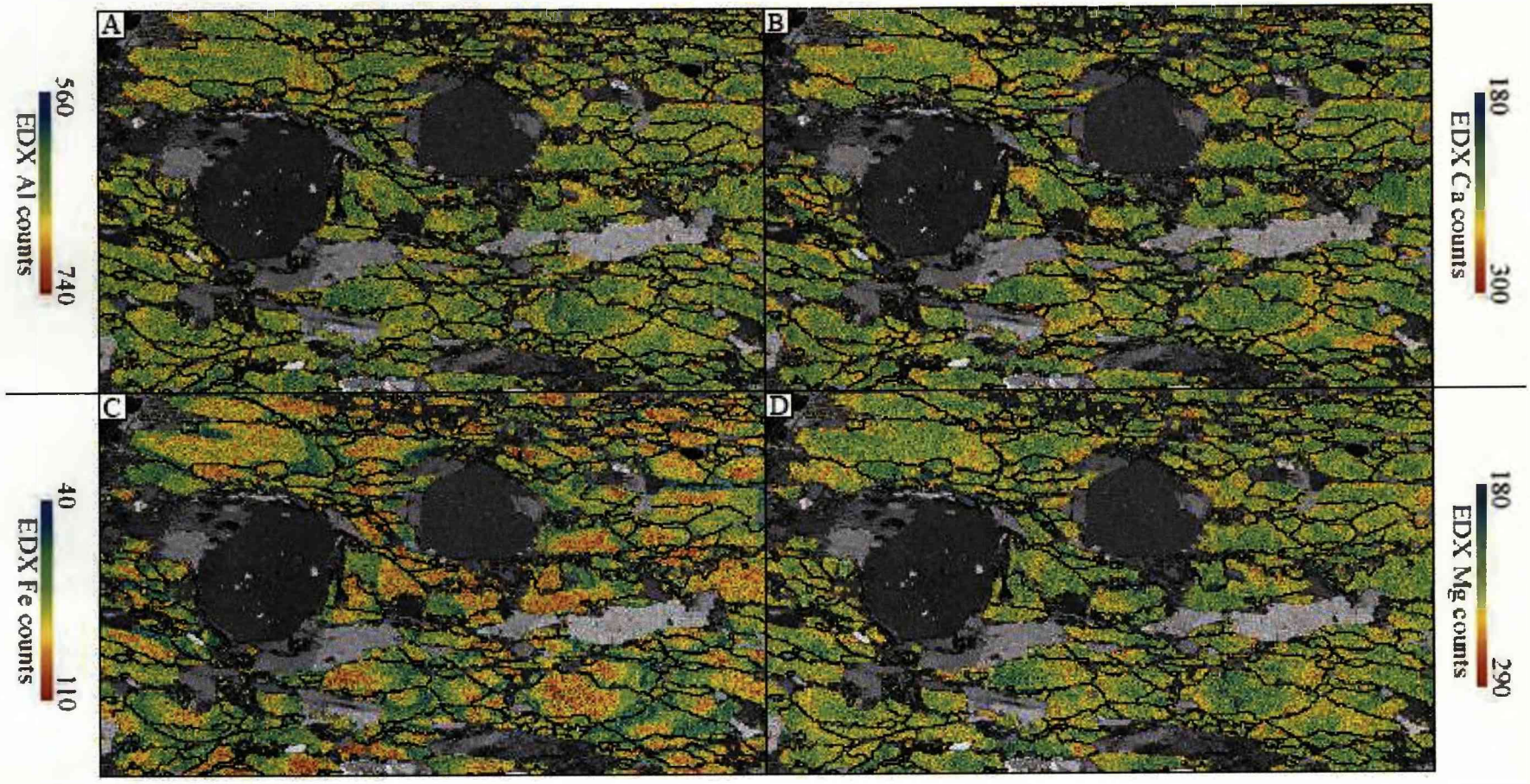

Fig. 4.34 Chemistry maps of omphacite grains in an eclogite facies rock (S6.8) from Lago Blu, Punta Telcio showing A - Al EDX chemistry map, B - Ca EDX chemistry map, C - Fe EDX chemistry map, D - Mg EDX chemistry maps

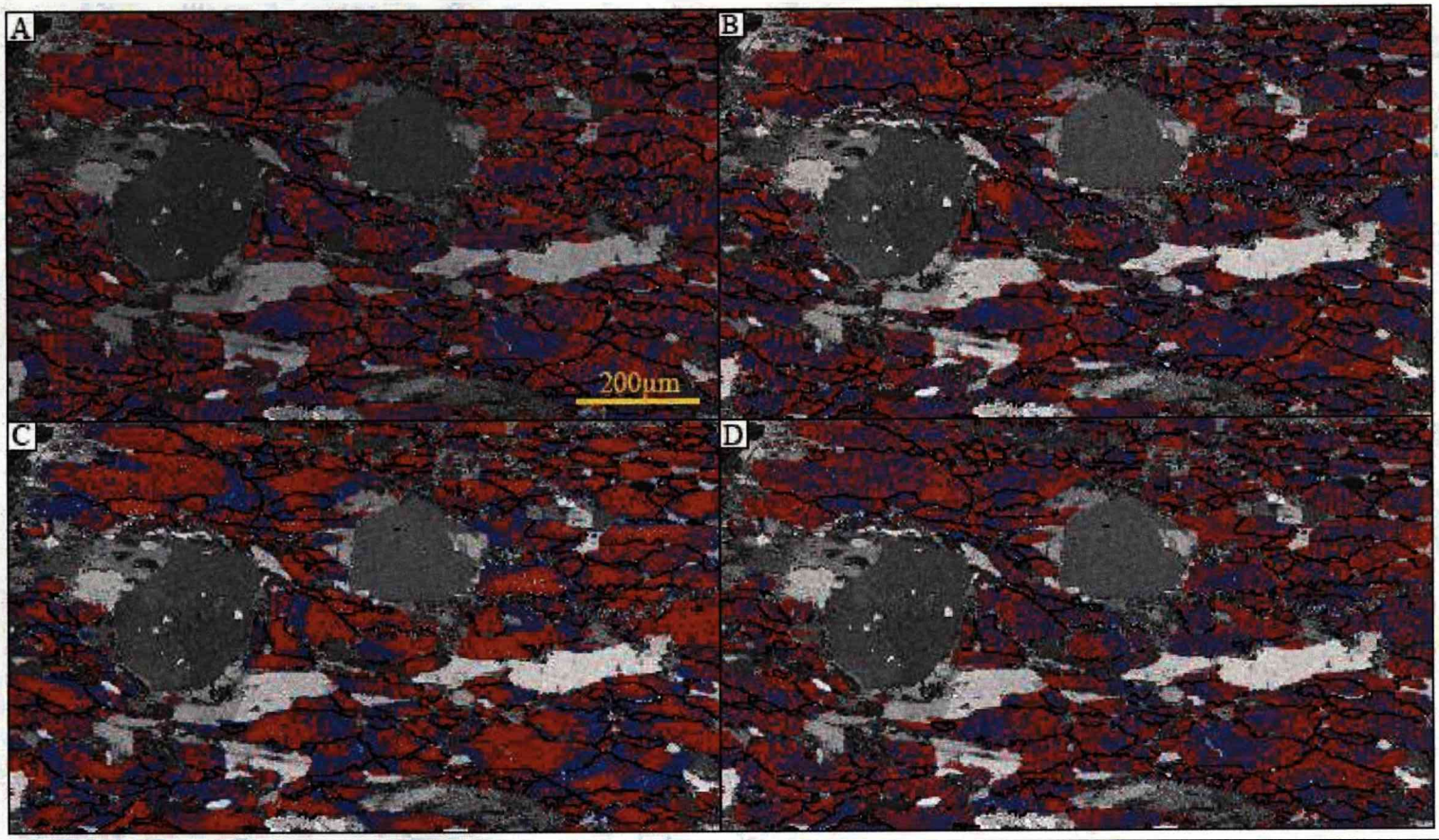

Fig. 4.35 Threshold EDX chemical maps of omphacite grains in an eclogite facies rock sample (S6.8) from Lago Blu, Punta Telcio. A - Al EDX threshold chemical map (blue represents EDX counts of 560-650 and red of 650-740), B - Ca EDX thresgold chemical map (blue = 180-240, red = 240-300), C - Fe EDX threshold chemical map (blue = 40-75, red = 75-110), D - Mg EDX threshold chemical map (blue = 180-235, red = 235-290)

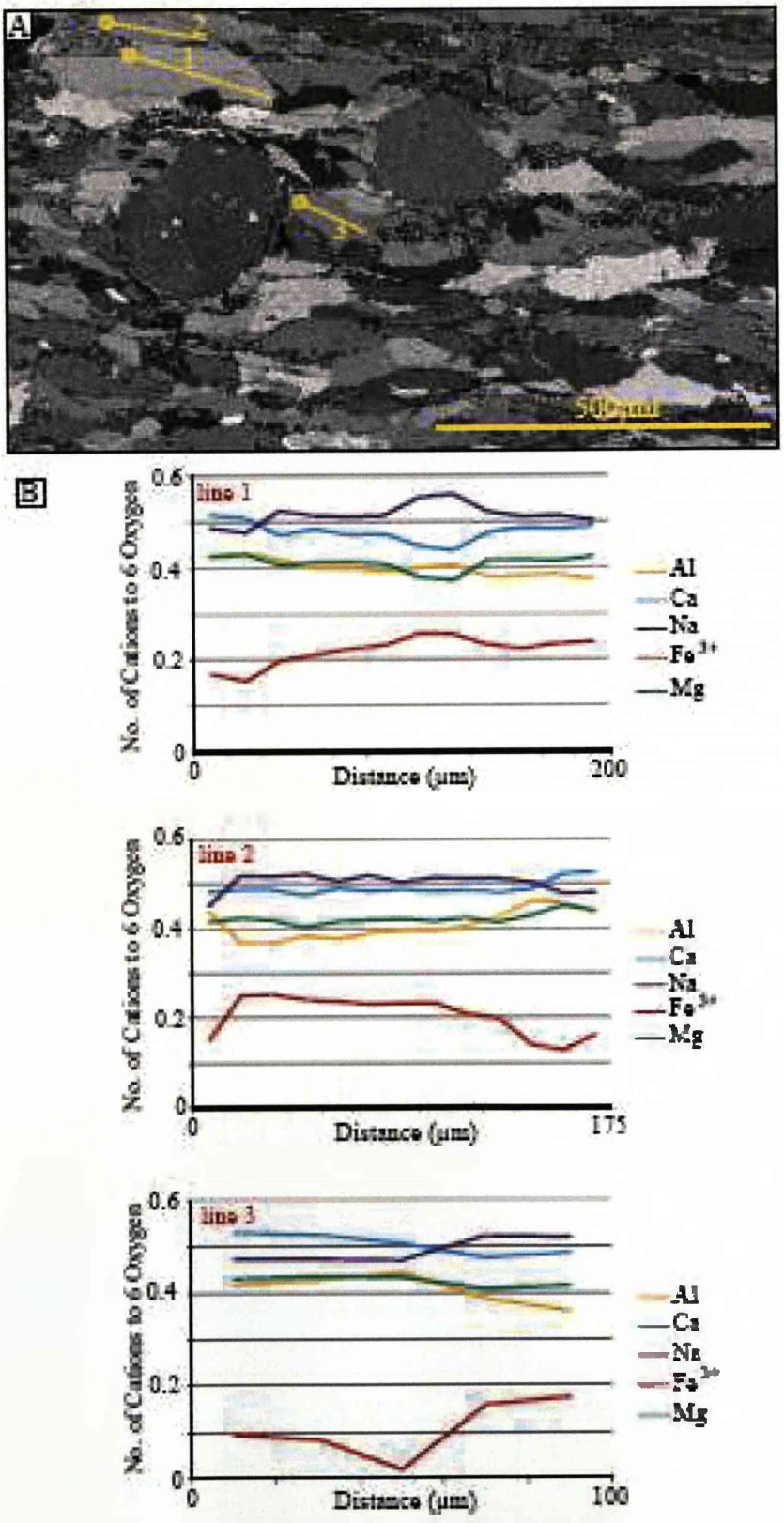

Fig. 4.36 A - Band contrast image of omphacite grains from eclogite facies rock sample S6.8 and chemical transect lines along which quantitative chemical data is collected. B - Chemical profiles along three omphacite grains

Omphacite grains of sample S6.8 show that Fe and Na content decreases from the centre toward the furthest edge of the grain and that Al, Ca and Mg content increases. No significant change in chemistry is noted along the width of omphacite grains. Some grains display a stronger zoning pattern than others with some having a homogeneous chemistry. In some omphacite grains zoning patterns only occur in one direction along the grain length.

Changing patterns in omphacite relate directly to substitutions of various omphacite end member compositions. Decreases in Na and Fe^{3+} coincide with increases in Ca and Mg suggesting substitution of aegirine ($NaFe^{3+}Si_2O_6$) for diopside. Trends in omphacite composition triangles (Fig. 4.43) for individual grains are in agreement with this.

Sample S6.13 (Fig. 4.37, Fig. 4.38, Fig. 4.39) shows elongate, narrow omphacite grains with chemical zoning patterns. The patterns here are similar to those displayed in omphacite grains from sample S6.8 in that Fe and Na content decreases as Al, Ca and Mg content increases. Patterns display sharp boundaries in these grains and are more complicated than those observed in S6.8. Chemical zoning occurs as chemical changes along the length of omphacite grains in one direction rather than in both. No significant chemical zoning occurs along the width of omphacite grains.

Some omphacite grains investigated in detail (Fig. 4.38, Fig. 4.39) show that change in chemistry along the length of some omphacite grains is not one of simple continual or stepped increase or decrease in one direction. One grain (grain 1 in Fig. 4.39, Fig. 4.40A) displays areas of higher aegirine content interspersed with areas of higher diopside content. It is likely these patterns represent broken grains with new omphacite growth forming between broken areas by diffusion, as displayed by the model in Fig. 4.41. EBSD of said grain (Fig. 4.40B) shows a >10° misorientation across the break in the original jadeite/aegirine omphacite grain and subsequent precipitation occurred on the ends of the larger fragment as orientation across the chemical boundaries is constant (Fig. 4.40, Fig. 4.41).

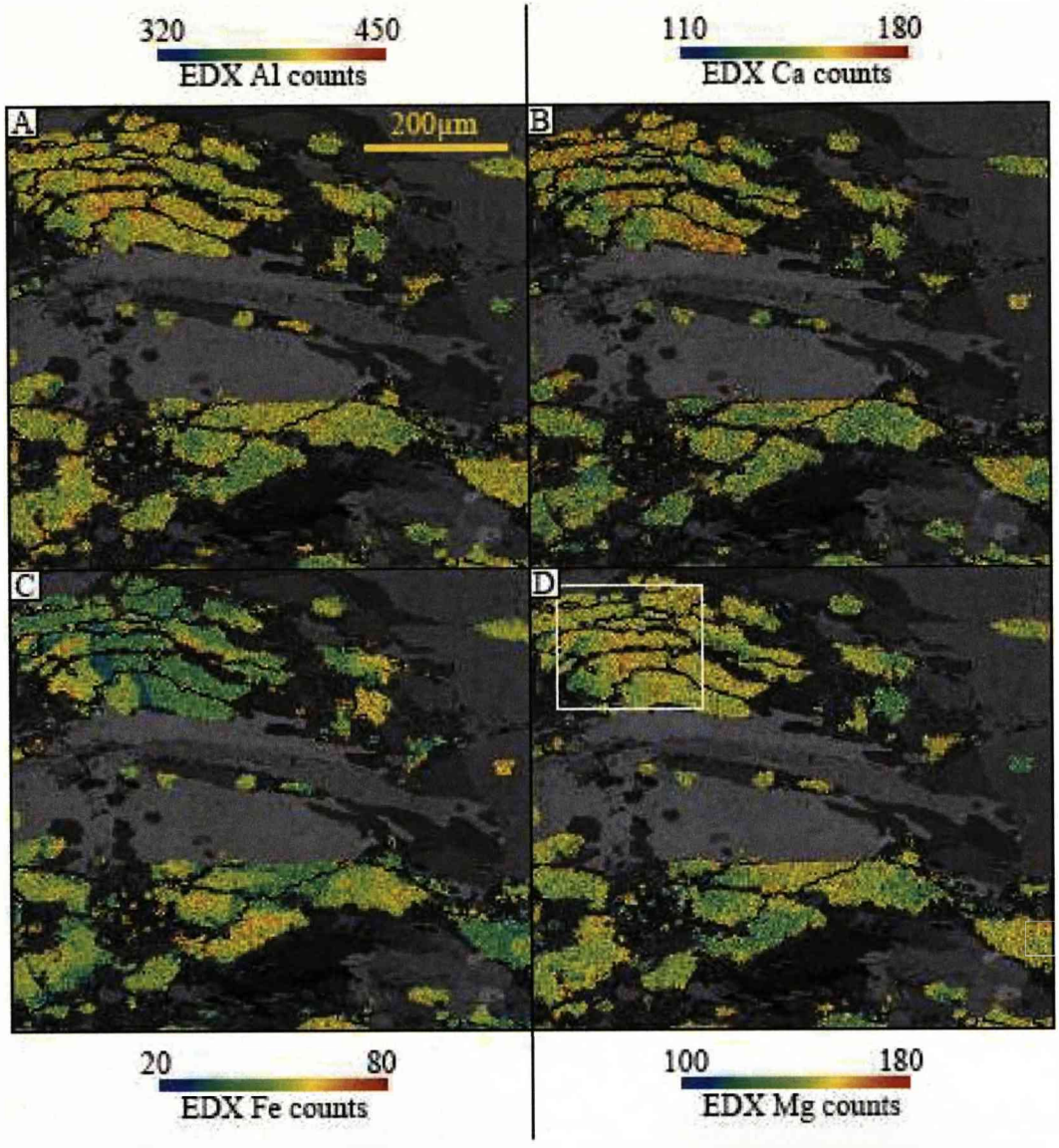

Fig. 4.37 Chemistry maps of omphacite grains in an eclogite facies rock (S6.13) from Lago Blu, Punta Telcio. White square in D represents an area investigated at higher magnification with EDX. A - Al EDX chemistry map, B - Ca EDX chemistry map. C - Fe EDX chemistry map. D - Mg EDX chemistry maps

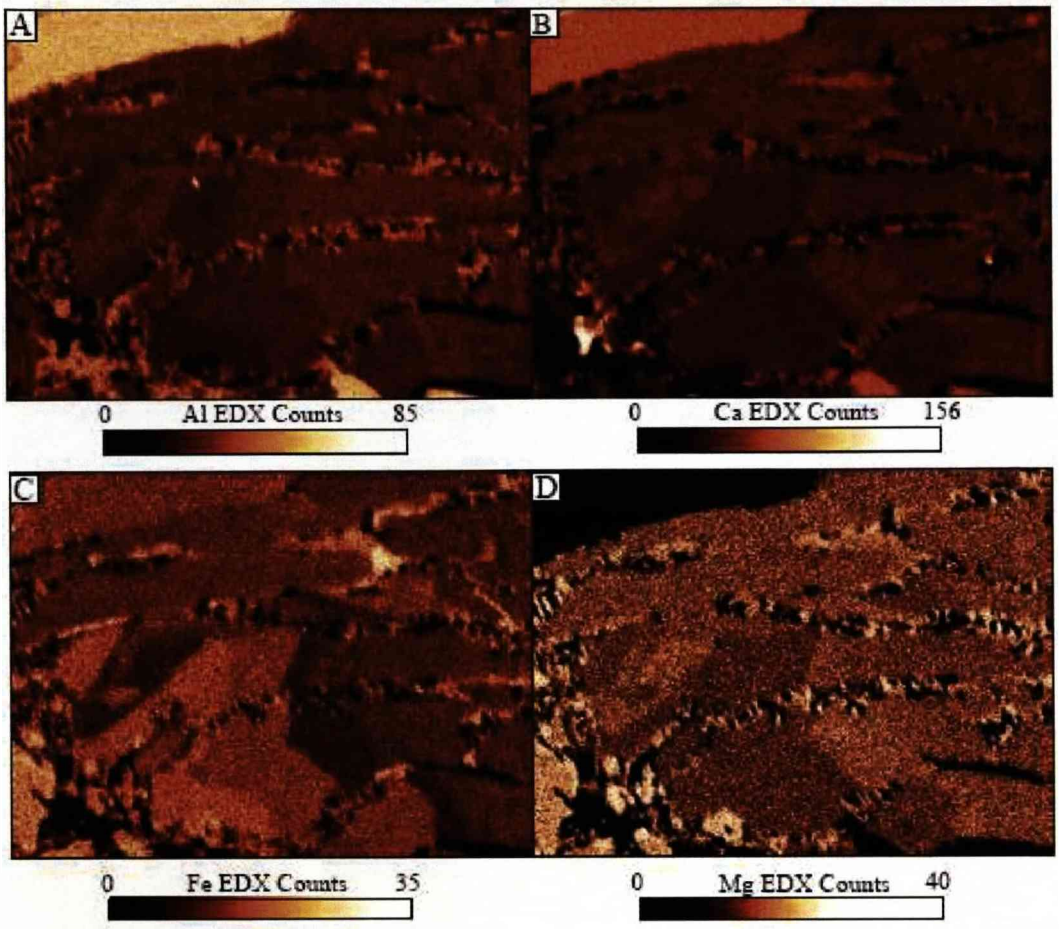

Fig. 4.38 EDX chemistry maps of the white square marked in Fig. 4.37 showing omphacite grains in an eclogite facies rock from Lago Blu, Punta Telcio. A - Al EDX chemistry map, B - Ca EDX chemistry map, C - Fe EDX chemistry map, D - Mg EDX chemistry maps.

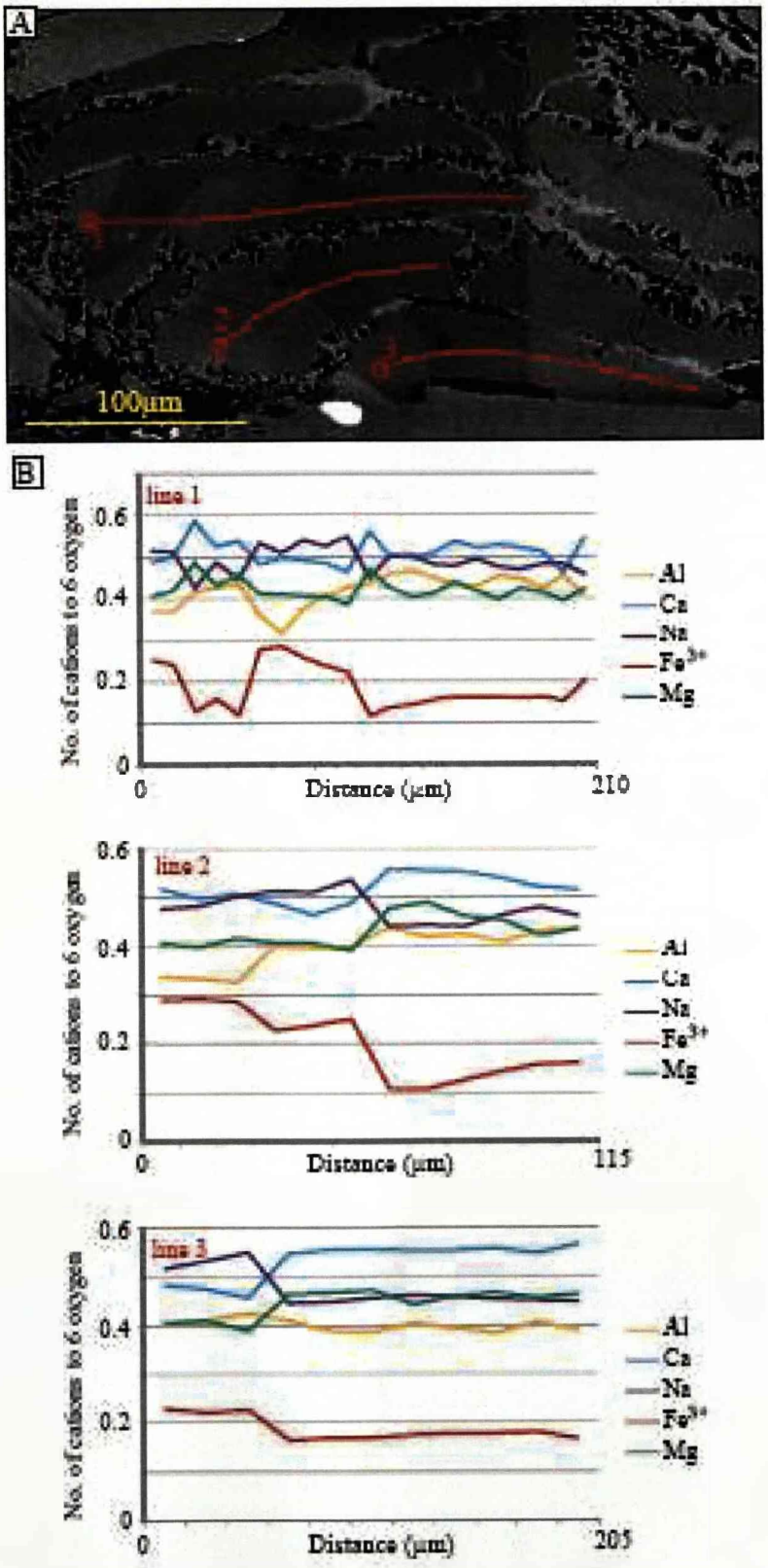

Fig. 4.39 A - SEM BSE image of omphacite grains from eclogite facies rock sample S6.13 and chemical transect lines along which quantitative chemical data is collected (square shaded instrument artifact can be seen). B - Chemical profiles along three omphacite grains

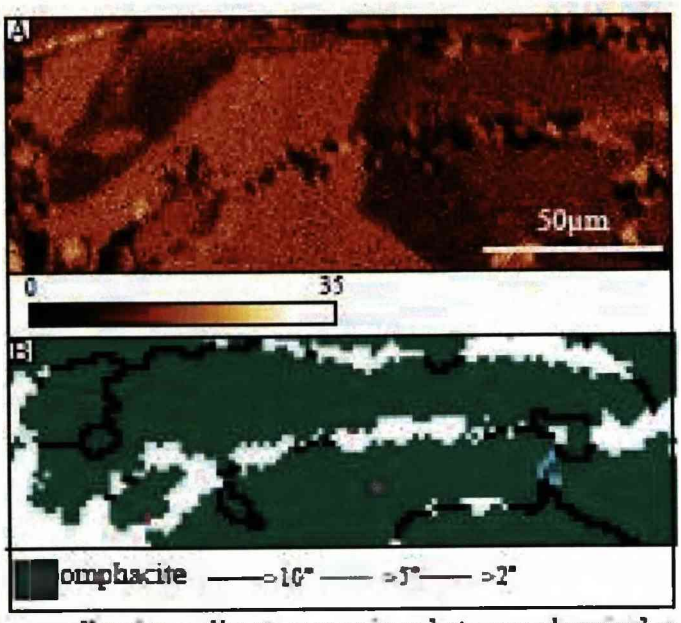

Fig. 4.40 Images allowing a direct comparison between chemical and orientation microstructures in omphacite grain 1 from Fig. 4.39. A - Fe EDX chemistry map, B - Grain boundary map

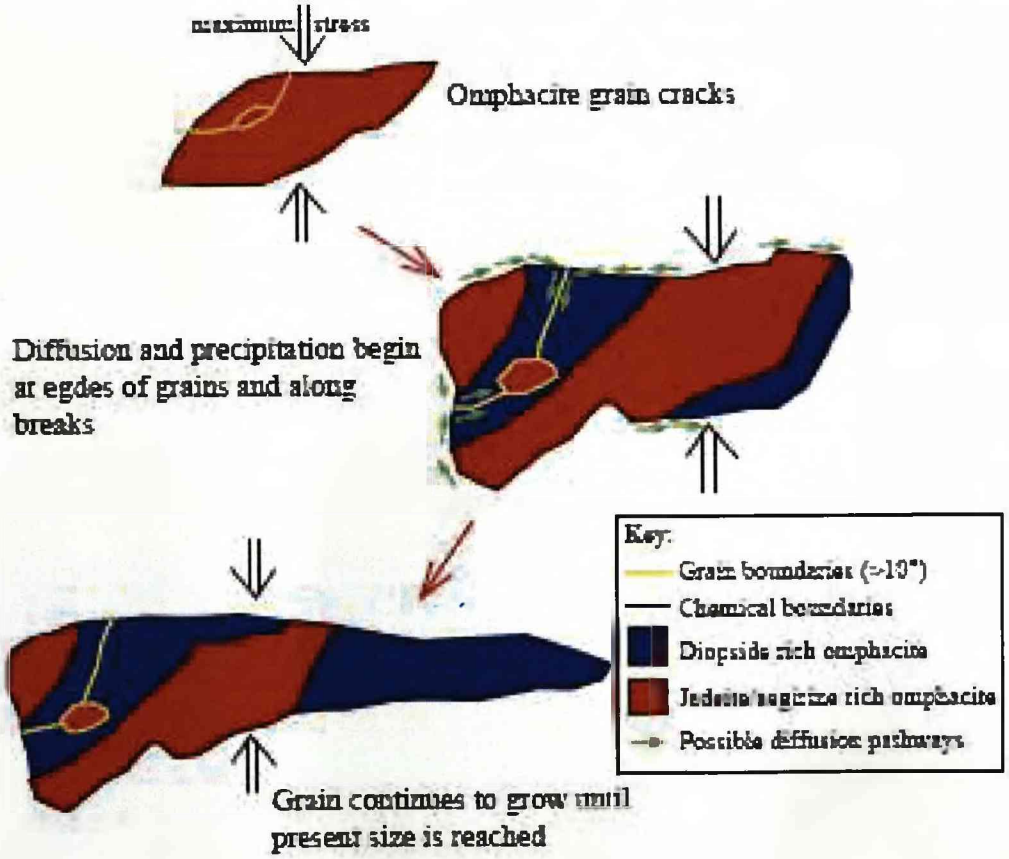

Fig. 4.41 Diagramatical representation of omphacite grain 1 in fig. 4.39 how its microstructure and chemistry have evolved through brittle cracking and diffusion creep

Quantitative data for samples S6.8 and S6.13, when plotted on the Clarke and Papike classification triangle (Fig. 4.43), show that all points measured fall within the omphacite classification field. Data from three grains from each sample are plotted on separate triangle graphs. They show a trend from more aegirine rich omphacite core to more diopside rich omphacite edges.

Zoning patterns from both samples investigated suggest early omphacite had higher amounts of aegirine. In addition Na content is also higher in early omphacite. It is possible that Fe^{3+} and Na in this metamorphic rock are partitioned into omphacite during peak conditions. As retrogression of the Zermatt-Saas Unit occurs Fe^{3+} is partitioned into clinozoisite/epidote instead, leaving Ca, Mg and Al to form omphacite, giving the diopside zoned grains observed here. Zoned changes in interference colours of small zoisite grains may provide evidence of the increased partitioning of Fe^{3+} into clinozoisite (Fig. 4.42), as higher birefringence colours indicate higher iron content. In larger zoisite grains this pattern is not observed and a more random chemical pattern can be inferred from changes in interference colour in these grains. This may be due to larger grains forming statically with little influence from strain.

The loss of Fe^{3+} due to redistribution can be shown by the equation; zoisite + aegirine = iron-epidote + jadeite:

$$Ca_2Al_3(SiO_4)(Si_2O_7)O(OH) + NaFe^{3+}Si_2O_6$$
$$=$$
$$Ca_2Al_2Fe^{3+}(SiO_4)(Si_2O_7)O(OH) + NaAlSi_2O_6$$

Another possible sink for Fe^{3+} may be associated with the growth of glaucophane which from textural observations may have been stable with eclogite facies conditions for some of its development.

As omphacite is the only eclogite facies sodium bearing phase, Na decreases in zoned omphacite may be a symptom of dilution rather than of Na being partitioned into some other phase. Increased production of the diopside component in omphacite due to another reaction occurring in tandem with diffusion creep on omphacite may explain this. One possible reaction that may accommodate this is grossular + pyrope = diopside + Ca-Tschermak:

$$2Ca_3Al_2Si_3O_{12} + Mg_3Al_2Si_3O_{12}$$
$$=$$
$$3CaMgSi_2O_6 + 3CaAl_2SiO_6$$

A combination of these two reactions could explain the chemical patterns observed here. It is also postulated here that Fe^{3+} use for omphacite decreases or stops earlier than the use of Na. Signals of this can be identified in omphacite grain chemical profiles (Fig. 4.36, Fig. 4.39). Fe^{3+} content starts to decrease sooner than Na content as zones of higher diopsidic omphacite is approached. In fact Na profiles often show a plateau from the same point where Fe^{3+} profiles start to show a decline.

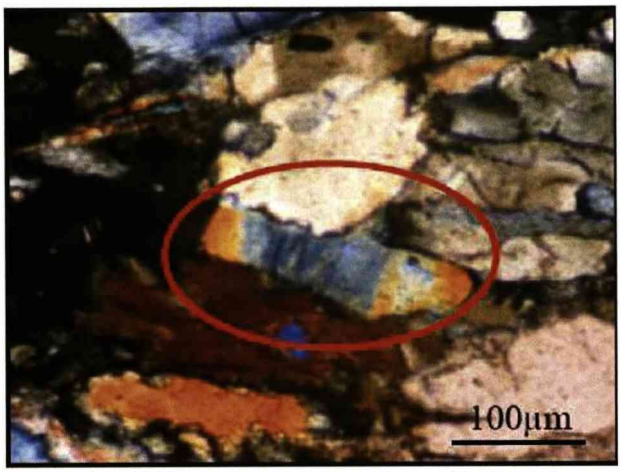

Fig. 4.42 Photomicrograph (XP) of an elongate clinozoisite grain that shows preferential chemical growth indicated by changes in interference colours due to Fe^{3+} increases at the grain edges

Preferential chemical zoning patterns described here for omphacite grains suggest that omphacite in these eclogite facies rocks has had significant contribution made to its deformation by diffusion creep. From EBSD and TEM investigations we also know that dislocation creep was also active. This raises the question of which mechanism is dominant if both are operative at the same time, or are dislocation creep and diffusion creep acting on the omphacite separately?

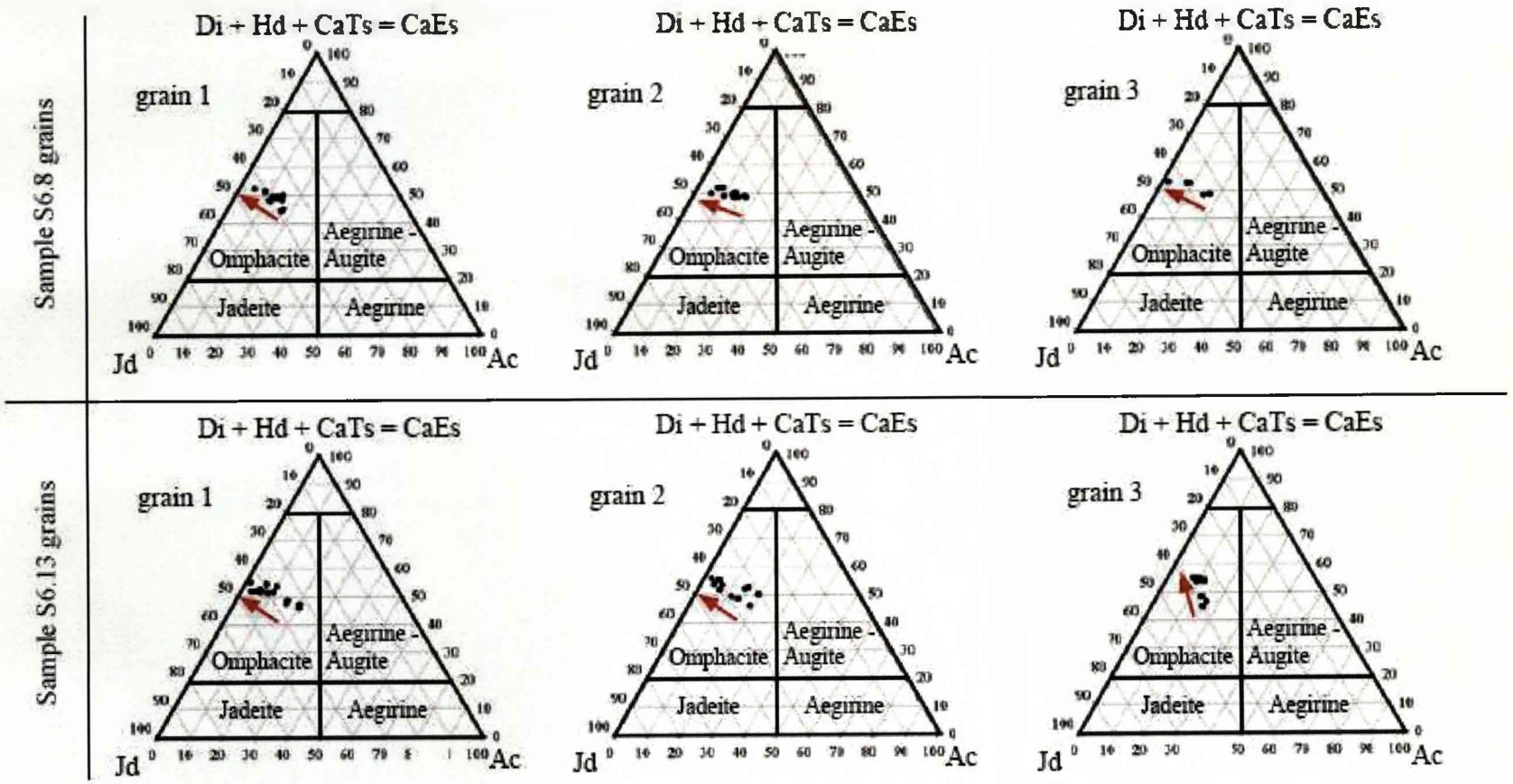

Fig. 4.43 Clark and Papike (168 classification triangular plots for omphacite grains from sample S6.8. and S6.13

Label	Si	Ti	Al	Cr	Mg	Ca	Mn	Fe	Na	K	O	Total
68grain1a	2.00	0.00	0.43	0.00	0.43	0.52	0.00	0.17	0.49	0.00	6	4.0374
68grain1b	2.01	0.00	0.43	0.00	0.43	0.51	0.00	0.16	0.48	0.00	6	4.0201
68grain1c	2.01	0.00	0.42	0.00	0.41	0.47	0.00	0.20	0.52	0.00	6	4.0197
68grain1d	2.01	0.00	0.40	0.00	0.41	0.49	0.00	0.21	0.51	0.00	6	4.0161
68grain1e	2.02	0.00	0.40	0.00	0.41	0.47	0.00	0.23	0.51	0.00	6	4.0303
68grain1f	2.01	0.00	0.39	0.00	0.41	0.48	0.00	0.23	0.52	0.00	6	4.0382
68grain1g	2.02	0.00	0.40	0.00	0.38	0.45	0.00	0.26	0.55	0.00	6	4.0106
68grain1h	2.02	0.00	0.41	0.00	0.37	0.44	0.00	0.26	0.56	0.00	6	4.0172
68grain1i	2.02	0.00	0.38	0.00	0.42	0.48	0.00	0.23	0.52	0.00	6	4.0269
68grain1j	2.02	0.00	0.38	0.00	0.42	0.49	0.00	0.23	0.51	0.00	6	4.0241
68grain1k	2.01	0.00	0.39	0.00	0.42	0.49	0.00	0.24	0.51	0.00	6	4.0576
68grain1l	2.01	0.00	0.38	0.00	0.43	0.49	0.00	0.24	0.50	0.00	6	4.0592
68grain2b	2.02	0.00	0.37	0.00	0.42	0.49	0.00	0.25	0.52	0.00	6	4.0797
68grain2c	2.01	0.00	0.37	0.00	0.42	0.49	0.00	0.25	0.52	0.00	6	4.0577
68grain2d	2.02	0.00	0.38	0.00	0.40	0.47	0.00	0.24	0.52	0.00	6	4.0761
68grain2e	2.02	0.00	0.38	0.00	0.42	0.49	0.00	0.24	0.51	0.00	6	4.0037
68grain2f	2.01	0.00	0.39	0.00	0.42	0.48	0.00	0.23	0.52	0.00	6	4.0295
68grain2g	2.01	0.00	0.39	0.00	0.42	0.49	0.00	0.23	0.50	0.00	6	4.0242
68grain2h	2.01	0.00	0.39	0.00	0.41	0.48	0.00	0.23	0.51	0.00	6	4.0597
68grain2i	2.01	0.00	0.40	0.00	0.42	0.49	0.00	0.21	0.51	0.00	6	4.0556
68grain2j	2.01	0.00	0.43	0.00	0.41	0.48	0.00	0.20	0.51	0.00	6	4.0528
68grain2k	2.00	0.00	0.46	0.00	0.43	0.49	0.00	0.14	0.50	0.00	6	4.0477

68grain2l	1.99	0.00	0.46	0.00	0.45	0.52	0.00	0.13	0.48	0.00	6	4.0697
68grain2m	1.99	0.00	0.43	0.00	0.44	0.52	0.00	0.16	0.48	0.00	6	4.0495
68grain3b	1.99	0.00	0.42	0.00	0.43	0.53	0.00	0.18	0.47	0.00	6	4.0393
68grain3c	1.99	0.00	0.43	0.00	0.44	0.53	0.00	0.17	0.47	0.00	6	4.0731
68grain3d	2.01	0.00	0.44	0.00	0.43	0.51	0.00	0.14	0.47	0.00	6	4.0161
68grain3e	2.01	0.00	0.39	0.00	0.41	0.48	0.00	0.25	0.52	0.00	6	4.0174
68grain3f	2.02	0.00	0.36	0.00	0.42	0.49	0.00	0.26	0.52	0.00	6	4.0068

Table 4.2 Chemical data (cations to 6 oxygen) collected from three omphacite grains from sample S6.8

Label	Na	Mg	Al	Si	K	Ca	Ti	Mn	Fe	O	Total
613grain1a	0.458	0.423	0.406	1.9893	0.008	0.544	0.003	0.0017	0.2	6	4.0374
613grain1b	0.4831	0.417	0.426	2.0108	0.005	0.513	3E-04	0.0032	0.16	6	4.0201
613grain1c	0.4705	0.425	0.45	1.992	-1E-04	0.519	-0.001	0.0065	0.16	6	4.0197
613grain1d	0.4775	0.398	0.455	1.9948	0.003	0.526	0.002	0.0002	0.16	6	4.0161
613grain1e	0.4957	0.419	0.432	1.9987	-0.001	0.521	0.002	0.0024	0.16	6	4.0303
613grain1f	0.4791	0.44	0.433	1.9866	7E-04	0.535	-0.001	0.005	0.16	6	4.0382
613grain1g	0.4823	0.411	0.454	2.0036	-0.003	0.51	-0.001	0.0004	0.15	6	4.0106
613grain1h	0.5032	0.404	0.467	2.0029	9E-04	0.497	-0.002	0.0019	0.14	6	4.0172
613grain1i	0.5009	0.428	0.458	1.9966	0.006	0.502	9E-04	-5E-04	0.14	6	4.0269
613grain1j	0.4488	0.471	0.438	1.9791	0.004	0.56	0.004	0.0027	0.12	6	4.0241
613grain1k	0.5494	0.384	0.427	2.0049	0.003	0.464	3E-04	0.0019	0.22	6	4.0576
613grain1l	0.5247	0.407	0.402	1.9999	-0.002	0.484	0.001	0.0035	0.24	6	4.0592
613grain1m	0.5405	0.407	0.378	2.0031	0.003	0.49	-5E-05	0.0003	0.26	6	4.0797
613grain1n	0.5099	0.408	0.318	2.0393	4E-04	0.497	-0.001	0.0009	0.28	6	4.0577
613grain1o	0.5333	0.412	0.361	2.0126	-5E-04	0.481	-0.003	0.0013	0.28	6	4.0761
613grain1p	0.4479	0.457	0.439	1.9965	-2E-04	0.54	0.004	0.0019	0.12	6	4.0037
613grain1q	0.4872	0.434	0.427	1.9997	-0.002	0.525	-3E-04	0.0014	0.16	6	4.0295
613grain1r	0.4276	0.489	0.418	1.979	-0.002	0.587	7E-04	-0.001	0.13	6	4.0242
613grain1s	0.5118	0.423	0.371	2.0041	0.002	0.5	0.008	-0.002	0.24	6	4.0597
613grain1t	0.5159	0.407	0.369	2.0185	0.001	0.486	-7E-05	0.0046	0.25	6	4.0556
613grain2a	0.4783	0.408	0.341	2.0196	-6E-04	0.519	-0.004	0.0018	0.29	6	4.0528
613grain2b	0.4838	0.402	0.336	2.021	0.002	0.498	0.006	0.0055	0.29	6	4.0477
613grain2c	0.5043	0.42	0.328	2.015	-0.001	0.509	0.003	0.004	0.29	6	4.0697
613grain2d	0.5165	0.409	0.402	2.0016	-0.002	0.488	0.005	0.0019	0.23	6	4.0495
613grain2e	0.5123	0.409	0.399	2.0102	9E-05	0.465	0.007	-0.002	0.24	6	4.0393
613grain2f	0.5388	0.393	0.403	1.994	0.003	0.487	0.002	-1E-04	0.25	6	4.0731

613grain2g	0.4421	0.476	0.439	1.9851	-5E-05	0.558	4E-04	0.0073	0.11	6	4.0161
613grain2h	0.4454	0.49	0.421	1.995	0.002	0.556	4E-04	-9E-04	0.11	6	4.0174
613grain2i	0.4419	0.461	0.425	1.9994	-0.002	0.553	0.002	0.0002	0.13	6	4.0068
613grain2j	0.4658	0.454	0.409	2.0036	6E-04	0.541	0.003	0.0019	0.14	6	4.022
613grain2k	0.4822	0.423	0.431	2.0036	0.002	0.523	3E-04	0.0019	0.16	6	4.0229
613grain2l	0.4623	0.437	0.438	2.0027	7E-04	0.517	-0.003	-9E-04	0.16	6	4.013
613grain3a	0.5179	0.405	0.403	2.0076	3E-04	0.483	0.001	0.0016	0.23	6	4.0487
613grain3b	0.5325	0.41	0.412	2.001	0.003	0.475	0.001	0.0039	0.22	6	4.0595
613grain3c	0.5517	0.39	0.427	2.0053	-3E-05	0.456	-4E-04	0.0018	0.23	6	4.0576
613grain3d	0.447	0.466	0.412	1.9881	5E-04	0.549	2E-04	0.002	0.16	6	4.0293
613grain3e	0.4509	0.466	0.39	1.9966	0.002	0.557	-3E-04	0.002	0.17	6	4.0353
613grain3f	0.4584	0.472	0.387	1.9898	-7E-04	0.557	0.004	0.0035	0.17	6	4.041
613grain3g	0.4634	0.444	0.406	1.9912	-0.001	0.555	0.002	0.0006	0.18	6	4.0354
613grain3h	0.4602	0.459	0.396	1.9883	-1E-05	0.556	0.005	-0.002	0.18	6	4.0386
613grain3i	0.4558	0.468	0.385	1.9919	1E-03	0.559	-8E-04	0.0075	0.18	6	4.045
613grain3j	0.4513	0.457	0.407	1.9871	7E-04	0.549	0.002	0.001	0.18	6	4.0338
613grain3k	0.4503	0.464	0.391	1.9936	-0.002	0.568	-3E-04	0.0046	0.17	6	4.0354

Table 4.3 Chemical data (cations to 6 oxygen) collected from three omphacite grains from sample S6.13

4.3.6 Discussion

The results from optical petrography, EBSD, TEM and chemical analyses of omphacite from the eclogites of the Punta Telcio region of the Zermatt-Saas raise numerous points of interest. One of the aims of this thesis is to further the understanding of omphacite deformation mechanisms and the microstructures they are responsible for, using these techniques. In addition it is hoped that the results and conclusions drawn from such investigations can shed light on the development of the Zermatt-Saas through its burial and exhumation. Here we address those questions dealing solely with omphacite microstructures and deformation. Their bearing on the evolution of the Zermatt-Saas Unit and what they may say about the regional geology of the Punta Telcio area are dealt with in Chapter 5. The reason for this is that the structural evolution of the area is tied to the results presented in both chapters.

4.3.6.1 Omphacite LPO - Dislocation or Diffusion Creep?

EBSD data plotted on pole figures revealed that the omphacite of the Zermatt-Saas eclogites in the Punta Telcio region have a strong S-type LPO. As discussed at length in Chapter 1, LPO in omphacite can be formed by dislocation creep (Buatier et al., 1991, Philippot and van Roermund, 1992, Brenker, 1998, Brenker et al., 1999, Bascou et al. 1991, Bascou et al., 2002, Ulrich and Mainprice, 2005) as well as diffusion creep and preferred crystal growth (Helmstaedt, 1972, Godard and van Roermund, 1995, Mauler et al., 2001), though many authors indicate from their own investigations that a combination of mechanisms is more likely than a single one operating alone.

Optical petrography, EBSD grain maps and TEM investigation of omphacite from the Lago Blu area of the Zermatt-Saas show the presence of subgrain boundaries (<10° misorientations), undulose extinction and dislocations all of which indicate omphacite has deformed by dislocation creep. Omphacite misorientation angle distribution analyses show neighbour pair pixels have a high frequency of <10° misorientation in comparison to random pair omphacite pixels. This is a signal of the subgrain boundaries observed in EBSD grain boundary maps, formed by dislocation

creep. Direct evidence such as this confirms that dislocation creep has had at least some contribution to the creation of the omphacite LPO in these eclogites.

In addition omphacite from these eclogites contains strong evidence for the action of diffusion creep in the form of preferential chemical zoning patterns and overgrowth of broken grains. As observed in omphacite grains from sample S6.8 and S6.13 aegirine/jadeite rich omphacite zone into more diopsidic omphacite often displaying quite sharp chemical boundaries. The preferential patterns observed (zoning occurs along only the long axes of omphacite grains) (Fig. 4.35, Fig. 4.37) and overgrowth of broken grains (Fig. 4.41, Fig. 4.42) suggests the action of a diffusive mass transfer process, likely coble creep or pressure solution. We rule out Nabarro-Herring creep as the acting mechanism, as lattice diffusion through omphacite grains would likely result in more diffuse chemical zoning rather than the sharp zoning patterns observed.

Diffusion creep is highly dependent on grain size as with increasing grain size transport pathways for diffusion creep become longer and dissolution and precipitation sites decrease therefore decreasing flux. The average grain size of omphacite from Punta Telcio eclogites is ~ 250μm and since evidence for diffusion creep in omphacite has been found in grain sizes up to 7mm (Mauler et al., 2001), diffusion creep should not experience grain size limitation in these rocks.

Orientation and chemical microstructures have confirmed the action of both dislocation and diffusion creep in the creation of the S-type omphacite LPO of the Punta Telcio eclogites. This is in agreement with the conclusions of previous work that suggest a combination of deformation mechanisms is responsible for omphacite LPO development (Godard and van Roermund, 1995, Mauler et al., 2001) but provides new types of evidence in both cases. The question remains though of which mechanism is more dominant in omphacite deformation in these eclogites and whether they were operative together or separately.

We suggest here that dislocation creep occurred prior to diffusion creep. The evidence for this lies in the sharp, well defined chemical zoning patterns observed in omphacite grains. If dislocation creep occurred during or after the establishment of these zoning patterns movement of dislocations accompanied by recrystallisation and

recovery in the omphacite grains would have destroyed the sharp chemical patterns, creating a more diffuse zoning profile. Thus any dislocation creep must have occurred prior to omphacite chemical zoning and thus prior to diffusion creep, the mechanism responsible for the zoning patterns. As diffusion creep is a lower stress, lower temperature mechanism than dislocation creep it logically follows that its onset in these eclogite rocks may be tied to the early stages of exhumation of this unit. Chemical profiles in omphacite grains depict chemical changes possibly associated with decreasing pressure and temperature, namely the assumed loss of Fe^{3+} from the aegirine component of omphacite due to retrogressive growth of clinozoisite, Fe-epidote and glaucophane. As these zoning profiles are a direct result of diffusion creep we can assume that this deformation mechanism was active during early exhumation of the Zermatt-Saas eclogites of Punta Telcio. Following logically from this dislocation creep which was active before diffusion creep, may have been the acting deformation mechanism at the unit's peak condition.

The omphacite LPO observed in the Punta Telcio eclogites was created by a combination of dislocation creep and diffusion creep. How much either mechanism contributed to the resulting omphacite LPO is more difficult to assess. At some stage in the evolution of these eclogites dislocation creep either slowed significantly or ceased altogether giving way to diffusion creep.

4.3.6.2 Omphacite LPO Type – Space Group or Strain Regime?

How the Zermatt-Saas eclogite omphacite developed an S-type LPO is also of interest to this study. As discussed in Chapter 1 two opposing theories exist to explain the cause of variable omphacite LPO type; omphacite space group (Brenker et al., 2002) and strain regime (Helmstaedt et al., 1972, Godard et al., 1995, Abalos, 1997, Mauler et al., 2001, Bascou et al., 2002, Kurz et al., 2003, Ulrich and Mainprice, 2005). According to the space group theory S-type LPOs develop in omphacite of space group C2/c (disordered) and L-type LPOs develop in omphacite of P2/n space group. As previously mentioned, critical examination of the evidence for both theories in literature (see Chapter 1) indicates the more likely control is strain regime. Thus S-type LPO patterns form in a flattening strain regime and L-type LPO patterns in a constrictional strain regime.

Using omphacite chemistry (~$Jd_{0.45-0.55}$, $Di_{0.55-0.45}$), TEM, LPO type and eclogite facies temperature conditions of ~550-600°C (Barnicoat and Fry, 1986) a test of the predictions laid out in Brenker et al. (2002) can be performed. TEM investigations of omphacite from the Punta Telcio eclogites show that it is mainly of the P2/n (ordered) space group. Plotting the relevant data on the space group phase diagram (Fig. 4.44), in the same way displayed in Brenker et al. (2002), shows that omphacite from Punta Telcio eclogites lies firmly within the P2/n field. According to the space group theory the P2/n space group is thought to create an L-type LPO in omphacite due to cation ordering affecting dominant slip systems. Omphacite in this study has a clear and strong S-type LPO and so is in contradiction to this theory. If space group is not the control for omphacite S-type LPO development then we assume it formed due to strain regime. This would imply that the eclogites of Punta Telcio were deformed in a flattening strain regime.

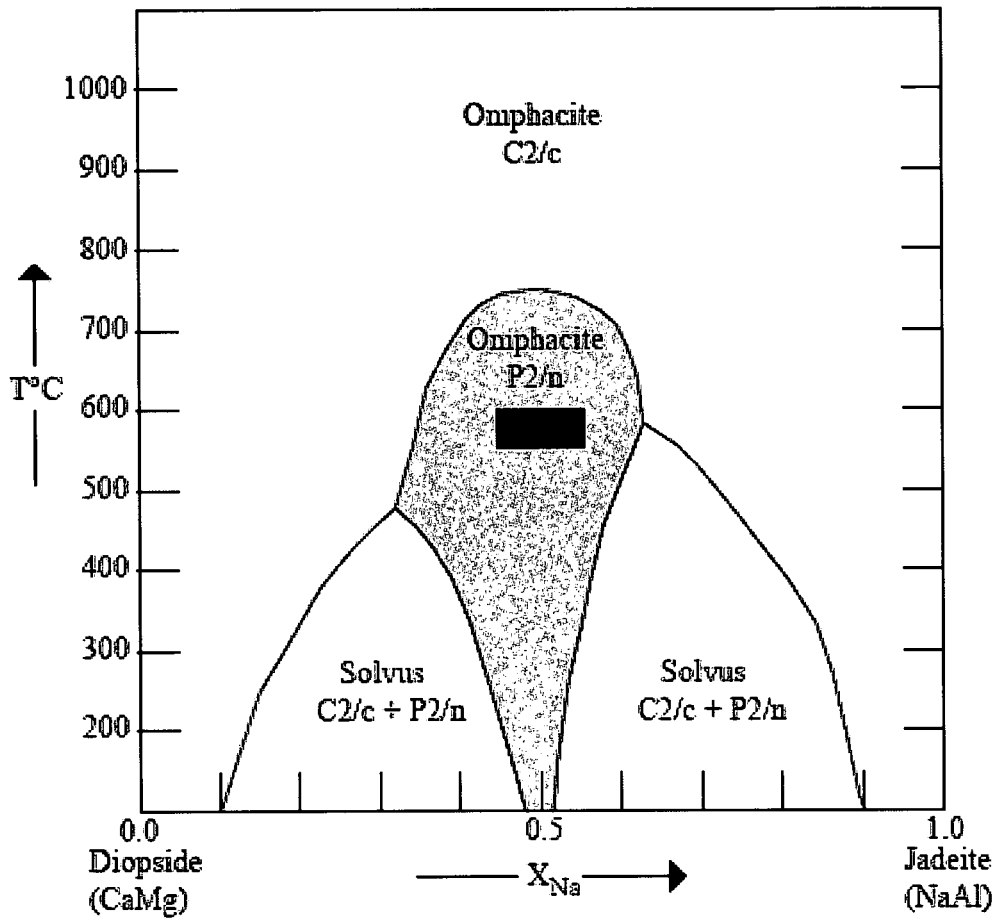

Fig. 4.44 Equilibrium phase diagram of space groups and solvi in the Di-Jd system at pressure exceeding the stability of jadeite (from Carpenter, 1980a). The black rectangle represents the chemistry and temperature range of omphacite from eclogite facies rocks of Lago Blu, Punta Telcio

It is thought that eclogite P-T-t pathways pass through both C2/c and P2/n omphacite stability fields allowing deformation in both (Carpenter, 1979). Thus all P2/n omphacite is thought to have first crystallised with C2/c structure. If deformation corresponds to early stages of omphacite crystallisation even if it is within the P2/n field it will probably show characteristics of the C2/c structure. This is because large strains are needed to overprint pre-existing lattice orientations and cause significant recrystallisation in a sample. Deformation in both diffusion and dislocation creep fields will not rapidly alter the initial LPO (Mauler, 2001). In light of this we must question whether or not the S-type LPO observed in this study is actually due to prior deformation within the C2/c stability field before ordering of cations into the P2/n space group and thus in agreement with the space group control theory.

Omphacite grains from the Punta Telcio eclogites show that, given the chemical range of early omphacite (aegirine/jadeite rich) and maximum temperature of eclogite facies metamorphism for the area, it does not fall into the C2/c at any stage of its evolution. Therefore any omphacite deformation must have been within the P2/n stability field. However, as discussed earlier, antiphase domains typically appear in omphacite due to ordering, a change from the C2/c to the P2/n space group (Carpenter, 1979). This would imply that eclogites were once at a temperature sufficient for the omphacite cations to be disordered. We have already shown that in this case such an assumption is incorrect. We therefore assume that antiphase domains formed in the manner suggested in studies by Champness (1973) and Brenker et al. (2003). This states that antiphase domains form by omphacite first forming a metastable C2/c form which subsequently starts to order. Thus omphacite deformation occurs solely within the P2/n stability field.

In conclusion the temperature range of eclogite metamorphism in the Punta Telcio region, TEM observations, evidence of diffusion creep and chemical composition show that omphacite deformation and S-type LPO formation occurred within the P2/n stability field of the omphacite space group phase diagram. Thus LPO development is not a result of space group control of dominant dislocations but is more likely a result of deformation in a flattening strain regime. In addition, omphacite antiphase domains observed in TEM, formed due to ordering from a metastable C2/c form.

4.4 Garnet Deformation in the Zermatt-Saas Eclogite

4.4.1 Introduction

Any investigation of eclogite deformation is not complete without exploring what the garnet within the rock is doing. As garnet, in conjunction with omphacite, forms the bulk of an eclogite its properties must have some effect on the behaviour of eclogites. Most studies on eclogite deformation write garnet off as behaving in a rigid manner while other minerals accommodate any strain on the rock. But as discussed in Chapter 1, recent studies of garnet (Mainprice et al., 2004, Storey and Prior, 2005, Zhang and Green, 2006, Zhang et al., 2007), garnet may have more influence on the deformation of eclogite facies rocks than previously thought. Orientation and chemical data are considered here for a variety of garnet bearing specimens, with the aim of understanding this mineral's contribution to the story of the Zermatt-Saas Unit. EBSD mapping of garnets can provide us with a way for investigating whether any plastic deformation occurred within the garnets of the Punta Telcio eclogite facies rocks. Chemical patterns in garnet combined with orientation data also reveal certain aspects of garnet deformation and evolution in metamorphic rocks that are rarely explored.

4.4.2 Garnet LPO

Garnet pole figures were calculated from 'point per grain' orientation data sets collected using the STscan method laid out in Chapter 3 to see if this mineral displayed an LPO in the eclogite facies rocks. All samples of eclogite from the Lago Blu area of Punta Telcio show near random LPO patterns examples of which are shown in Fig 4.45.

The lack of LPO here suggests that little plastic deformation has occurred in garnet and thus has not had any significant affect on eclogite deformation in the Punta Telcio region. Omphacite shape fabric can be seen to wrap garnet porphyroblasts and pressure shadows are often present as well, again suggesting garnet behaves passively in these eclogites during deformation. In much of this rock though a direct textural relationship between omphacite and garnet is difficult to ascertain due to retrogressive rims forming around garnet.

A lack of garnet LPO however does not necessarily imply the total absence of plastic deformation in the phase. A closer inspection of individual garnet grains is required to clarify this.

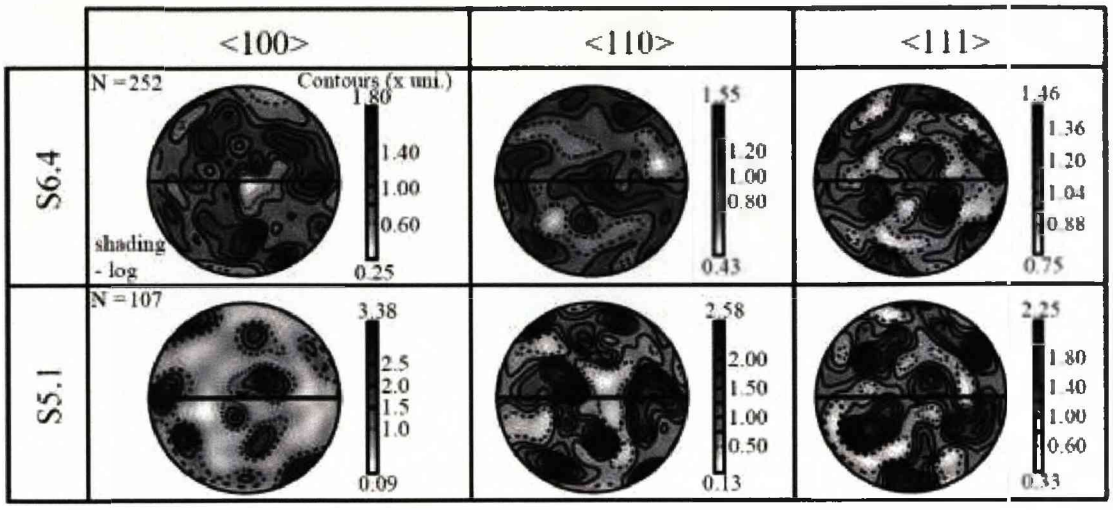

Fig. 4.45 Garnet pole figures from an eclogite sample (S6.4) and an amphibolite sample (S5.1) from the Zermatt-Saas of the Lago Blu area, Punta Telcio showing random LPO patterns

4.4.3 *Examples of Garnet Deformation and Chemistry in the Punta Telcio Region of the Zermatt-Saas Unit*

Chemical and EBSD investigation of individual garnet grains reveal a variety of results, ranging from no notable microstructures (chemical or deformation related) to simple and complicated chemical patterns and evidence of brittle and plastic deformation.

Eclogite samples S6.3 and S6.5 show many atoll garnets. EBSD grain boundary and texture component maps (see Chapter 3) reveal that little deformation occurs within these garnets (~<3-5° cumulative misorientation across grains) and that subgrain boundaries are rare to non-existent (Fig. 4.46). Close inspection of texture component maps show discrete changes in orientation that give the atoll garnets a domainal appearance in terms of orientation though the misorientation between each domain is <2° for each atoll investigated. The boundaries of these discrete domains can be approximately related to fractures within the garnet, as shown when fracture patterns are overlaid on the texture component maps. Thus the low misorientation domainal structure of these garnets is related to fracturing. As the fractures contain retrogressive phases we assume that they formed during retrogression of the Punta Telcio Zermatt-Saas Unit.

A common texture noted in eclogite and amphibolites from the Lago Blu area are jigsaw boundaries and impinging garnets. A jigsaw boundary between two garnets was investigated by EBSD in S5.1 showing that misorientation across the separating quartz grains was >10°. No orientation relationship was noted between the two. An impingement area between two garnet grains in S6.6 was investigated by EBSD and revealed one of the garnet grains has experienced significant plastic deformation near the contact with the other grain, evidenced mainly by the occurrence of subgrain boundaries (Fig, 4.47). This deformation decreases significantly with distance from the impinged area. Pole figures of the deformed garnet no significant rotation around the <100>, <110> and <111> axes. The presence of subgrain boundaries and evidence for rotation shown in the pole figures suggest the action of dislocation creep in this garnet grain. In contrast the neighbouring garnet shows little deformation suggesting orientation of garnet controls deformation here.

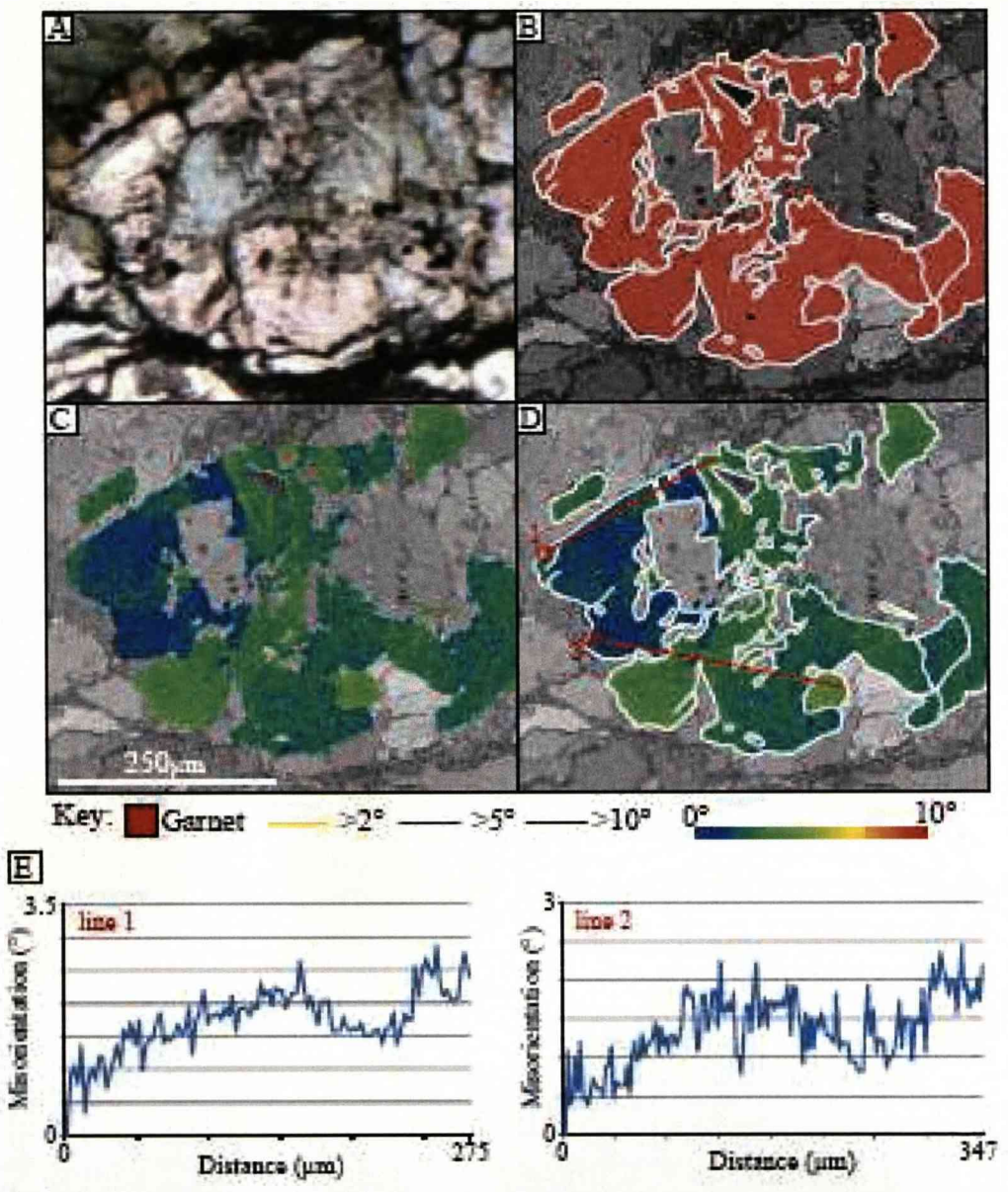

Fig. 4.46 A - Plane polarised light photomicrograph of an atoll garnet from an eclogite sample (S6.5) from Lago Blu, Punta Telcio of the Zermatt-Saas unit, B - An EBSD map of the same garnet with a red phase ID colour on points indexed as garnet and a grain boundary map overlay showing >2°, >5° and >10° misorientation boundaries, white lines show the outline of the atoll garnet and fractures within it, C - A texture component map of the atoll garnet showing domainal areas of lattice misorientation, D - The same texture component map with a fracture overlay (white lines) and misorientation profile lines (red lines), E - Misorientation profiles

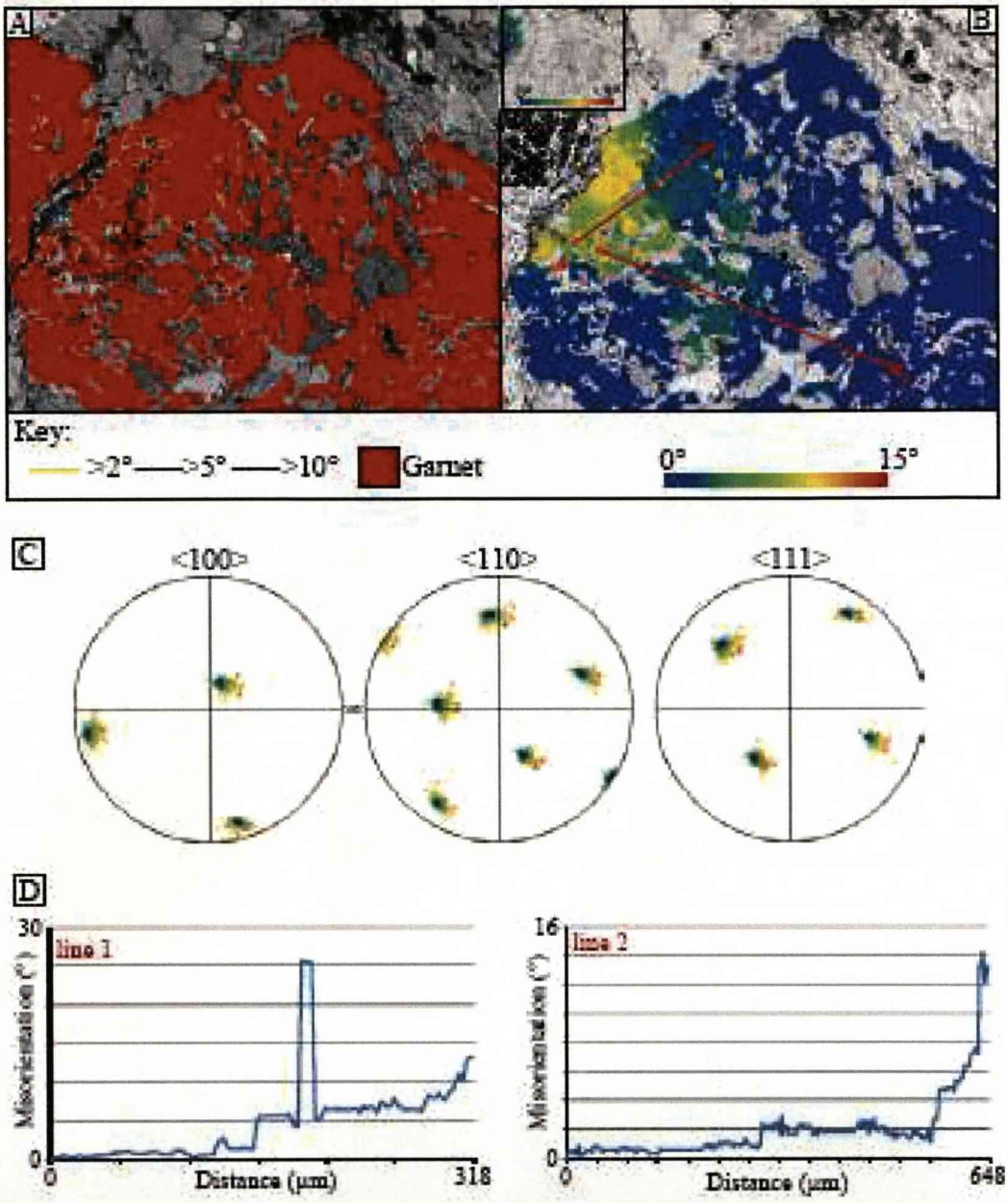

Fig. 4.47 A - Phase ID and grain boundary map for a two impinging garnets in a retrogressed eclogite sample (S6.6) from the Lago Blu Zermatt-Saas. B - Texture component map showing one of the impinged garnets shows significant misorientation near its contact with a second less deformed garnet (inlay - texture component map showing little misorientation in the second garnet). C - Pole figures of the deformed garnet. D - Garnet misorientation profiles

In sample S5.1 combined EBSD and EDX work was carried out on a cluster of garnet grains. These revealed that garnet porphyroblasts contain garnet inclusions with >10° misorientation from their host (Fig. 4.48). One garnet porphyroblast in particular show a four sided euhedral shape with a smaller garnet inclusion with a six sided euhedral shape. Chemical zoning in Mn, Ca, Mg and Fe show correlated patterns such that as Mn decreases so does Mg while Fe and Ca increase (Fig. 4.49). The pattern of zoning however matches the shape of the garnet inclusion which contains the highest Mn concentration, rather than the four sided shape of the larger host garnet. This particular microstructure may have resulted from a number of mechanisms.

1) The 6-sided garnet inclusion represents a garnet formed early during the prograde evolution of the Zermatt-Saas. A pre-eclogite facies metamorphic stage is known to have occurred in the Zermatt-Saas (Fry and Barnicoat, 1987) from inclusion assemblages in eclogite garnet cores. It is possible that this precursor garnet may have acted as a site for future garnet nucleation during a later metamorphic stage, except that the new garnet nucleated and grew in a different orientation. 2) As the 6 sided garnet is a completely separate grain it is possible that it stopped growing at some stage of the rocks evolution and was subsequently enveloped by the growth of a separately nucleated garnet. 3) The six sided garnet was originally a much larger porphyroblast that was recrystallised later with a different orientation, leaving only the small garnet inclusion behind.

Chemical zoning patterns observed here may help elucidate which of these theories is most likely. The fact the pattern of chemical change within the host garnet mimics the 6 sided shape of the garnet inclusion suggests that theory 1 is unlikely. Chemical patterns in a newly nucleating garnet orientation would follow the shape of the newly growing garnet not the one it was nucleated upon. The same reasoning applied to the theory 2 also suggests this was unlikely to be the cause of this garnet microstructure. Theory 3 thus remains as an explanation not only for the orientation microstructures observed but also for the chemical zoning patterns. A later recrystallisation of a garnet porphyroblast into a new garnet with a new orientation potentially may have preserved the zoning pattern.

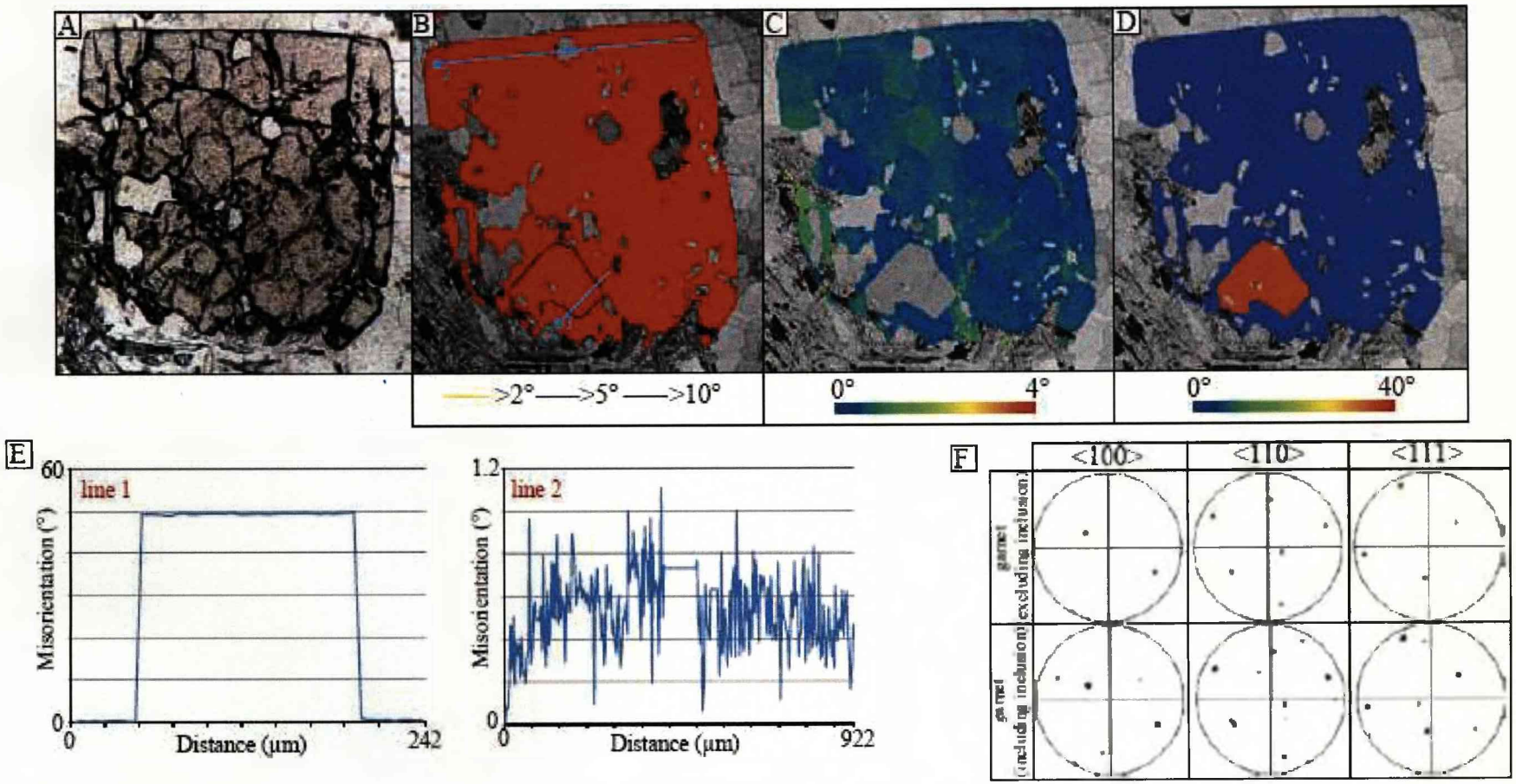

Fig. 4.48 A - Photomicrograph (PPL) of a garnet porphyroblast in a retrogressed eclogite sample (S5.1) from the Punta Telcio area of the Zermatt-Saas, B - Grain boundary map of the same garnet (coloured red), C - Texture component map of the garnet porphyroblast excluding the garnet inclusion within the grain, D - Texture compenent map of the garnet porphyroblast including the garnet inclusion, E - Garnet misorientation profiles, F - Pole figures for the garnet porphyroblast excluding and including the garnet inclusion

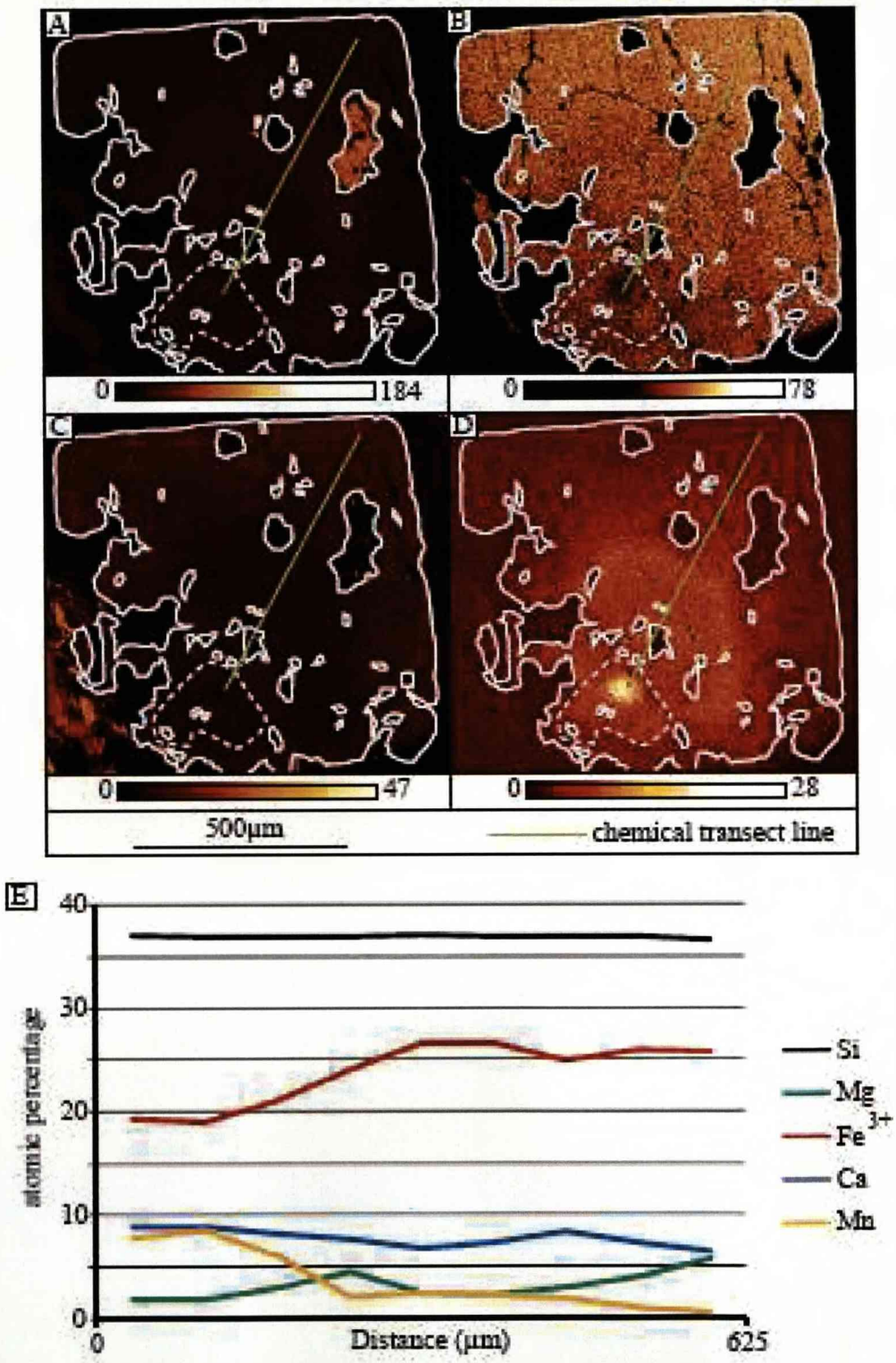

Fig. 4.49 Chemical maps of a garnet porphyroblast from a retrogressed eclogite from the Punta Telcio area of the Zermatt-Saas showing A - Ca map, B - Fe map, C - Mg map and D - Mn map. The white lines on the map mark the outline of the porphyroblast and inclusions within it, the dashed white line marks a garnet inclusion in the porphyroblast. E - Chemical data along the transect marked on the chemical maps

4.4.4 Discussion

Many studies on eclogite deformation state that garnet behaves in a rigid manner while other minerals accommodate any strain on the rock (Vogelé et al., 1998, Brenker et al., 2003, Kurz et al., 2003). From EBSD and chemical studies of garnet from the Punta Telcio eclogites, some of which is presented here, it can be said that garnet is in agreement with this statement. From results already discussed earlier in the chapter we surmise that it is the omphacite that accommodates strain in these eclogites. This study has shown however that garnet is not completely devoid of evidence for deformation. As shown by impinging garnets dislocation creep is active in some porphyroblasts. However not all garnet grains growing in such close proximity display this suggesting for garnet impingement to induce plastic deformation in one of the grains it may need to be in a preferential orientation for slip systems to be easily activated.

EBSD and EDX data on garnet grains containing misoriented garnet inclusions, as depicted in Fig. 4.48 and Fig. 4.49, reveal intriguing chemical and orientation microstructures but it is felt here that the current data is insufficient to propose a method by which it developed. Further work, including detailed chemical probing may provide clarification.

4.5 Conclusions

One of the main goals of this thesis is to determine how much omphacite and garnet contribute to eclogite deformation and what form this deformation takes. Data presented here in this chapter have shown that deformation of eclogites from the Punta Telcio region of the Zermatt-Saas Unit is controlled by omphacite. Garnet shows very little evidence for deformation and hence is assumed to have acted as rigid bodies in these eclogites.

Omphacite deformation and subsequent formation of a strong S-type LPO in the Punta Telcio eclogites is considered to have occurred in two stages. A stage of dislocation creep is evidenced by the occurrence of dislocations by TEM, subgrain boundaries by EBSD and high frequencies of low angle neighbour pair misorientations in omphacite misorientation angle distribution analyses. This is then followed by a stage of diffusion creep, deduced from preferential chemical zoning patterns in omphacite. Decreases in the aegirine and jadeite components of the omphacite and associated increases in diopsidic omphacite define these zoning patterns allowing us to tie diffusion creep to early retrogression/exhumation of the Zermatt-Saas Unit. Therefore, logically, the period of dislocation creep must have occurred prior to this, possibly during peak metamorphism.

A combination of TEM, omphacite chemistry, eclogite facies temperature conditions and omphacite LPO patterns refute the theory that the space group of omphacite alone controls the type of LPO pattern that develops. We assume therefore that strain regime is the likely cause of LPO pattern in the eclogites of the Punta Telcio region of the Zermatt-Saas Unit. Following this theory these eclogites deformed in a flattening strain regime.

5 Chapter 5: Identifying Possible Mimetic Lattice Preferred Orientation in Retrogressed Eclogites from the Zermatt-Saas, Western Alps

5.1 Introduction

The processes by which high pressure rocks reach the surface and what happens to them en route is important in understanding the dynamics of exhumation. Both deformation and metamorphism are likely along an exhumation pathway. Identifying the metamorphic changes, deformation processes and the links between the two is essential to unravel the history of the rocks being exhumed. The structures and fabrics of such rocks contain information on some of the processes at work during exhumation and thus understanding how they form becomes vital. In general many such fabrics are formed by deformation mechanisms such as dislocation creep and diffusion creep. However one aspect of fabric formation remains relatively unexplored: the formation of a lattice preferred orientation (LPO) through mimicry of a pre-existing LPO.

Mimetic LPO transitions are important in metamorphic rocks for a number of reasons. They hold implications for the way an LPO in any phase is interpreted. This is especially evident in those rocks that have undergone multiple metamorphic and deformation episodes, like those involved in a burial – exhumation cycle. There exists the possibility for phases with an LPO to affect the LPO formation of future phases in a later geologic event. Not only does this influence our understanding of the fabrics of a rocks current mineralogy, but there may also be a preserved signal of fabrics formed in earlier events. Retrogressive phases in metamorphic rocks (formed by re-equilibrating during exhumation) often have a fabric. That fabric may have been influenced by the fabric of a pre-existing, higher grade phase. Understanding what contribution earlier phases may have made to retrogressive fabric development clarifies whether the retrogressive event was a static or dynamic one. Knowing this may provide insight into the exhumation pathway of a rock, revealing information about possible hiatuses. Finally, understanding how much fabric mimicry has contributed to LPO formation of a retrogressive phase, allows an assessment of the amount of contribution made to LPO formation by mechanisms such as dislocation

creep or diffusion creep. Understanding the processes involved in this phenomenon and how to investigate it are crucial.

A mimetic LPO forms as a result of a later phase growing on or replacing a pre-existing phase (with an LPO) via epitaxy or topotaxy. Epitaxy refers to an overgrowth, oriented with respect to the reactant, whether the oriented overgrowth is simply growing around the substrate or growing as a result of a reaction with the substrate. Topotaxy on the other hand requires the conversion of a reactant into a new oriented product (Shannon and Rossi, 1964). Topotaxy is any chemical, solid state reaction that leads to the formation of a new material with a crystal orientation that correlates to the crystal orientation of the initial material (Lotgering, 1959) i.e. replacive to some extent. It refers to all oriented conversions of a reactant to a product with the exception of those that are epitactical. Within this definition there exists a continuum of degrees of topotaxy depending on the amount of inherited orientation.

An investigation of partially retrogressed eclogites from the Gressoney Valley area of the Zermatt-Saas unit, Western Alps (Fig. 5.1), attempts to ascertain how much mimicry may have influenced the formation of an LPO in retrogressive barroisite and what this may reveal about the exhumation of the high pressure unit.

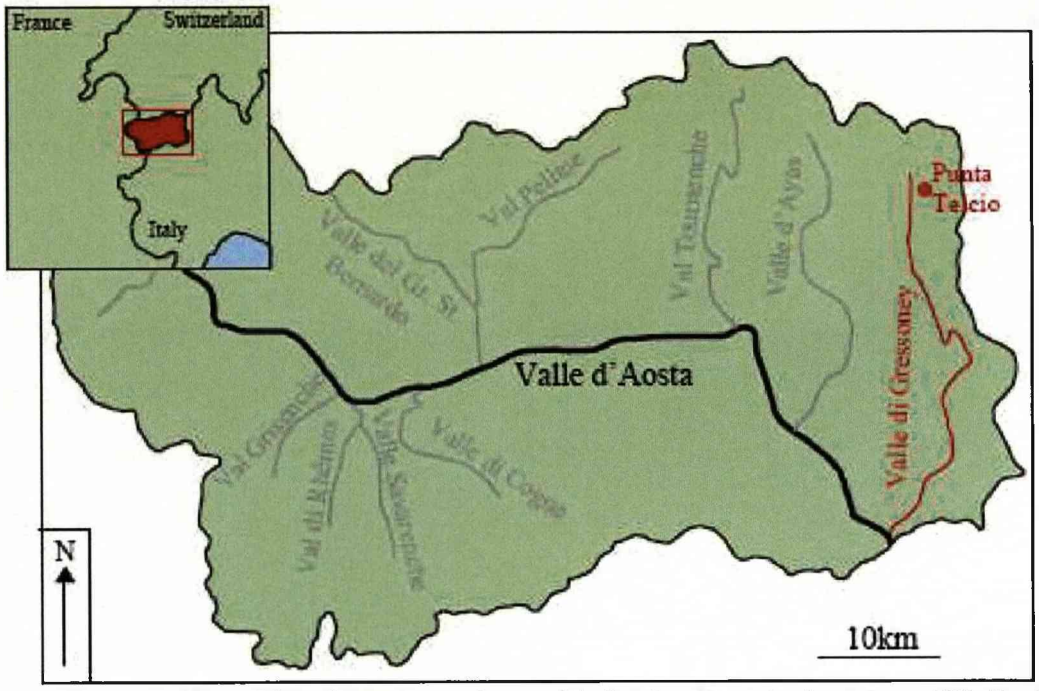

Fig. 5.1 Map of the Val d'Aosta province of Italy showing the location of Valle di Gressoney and the location of Punta Telcio. The inset shows the location of the province in a larger setting.

5.2 Geological Context

The Zermatt-Saas Unit is a layer of ophiolitic material obducted onto the European margin during the Alpine Orogeny. The protolith is Late Jurassic oceanic lithosphere which was the crust of the Piemontese (Tethyan Sea) that originally separated the older continental crust of the European continent and the African margin (Amato et al, 1999).

The unit contains excellent exposure of ultrahigh pressure and high pressure rocks. The ultrahigh pressure rocks exist only in one locality of the unit, at Lago di Cignana and are evidenced by the occurrence of coesite in the assemblage. A detailed P-T-t gives peak pressures of 2.5-3.0 GPa and temperatures of 550-630°C (based on garnet-clinopyroxene pairs, garnet-dolomite-aragonite assemblages and computed assemblage stability diagrams) (van der Klauw et al, 1997, Reinecke, 1998, Bucher et al, 2005).

The entire unit has experienced high pressure metamorphism, at least up to eclogite facies. Pressure and temperature estimates for the high pressure metamorphism are around 1.75-2.0 GPa and 550-600°C (Barnicoat and Fry, 1986). The timing of high pressure, eclogite-facies metamorphism has been well constrained. Tertiary ages of 50-40Ma have been discovered by Lu-Hf dating of garnet (Duchêne et al, 1997), and U-Pb dating of zircon (Rubatto et al, 1998) and Rb/Sr dating (cooling ages) of eclogite facies white mica (Reddy et al. 1999). In the area of the Zermatt-Saas studied here, Punta Telcio, the lithologies are comprised mainly of metabasic and metagabbroic rocks as well as serpentinites and small amounts of metasediments.

The metabasic rocks contain the high pressure minerals omphacite and garnet, though in many areas this assemblage is overprinted by retrogressive assemblages. There are two main retrogressive events noted in the Zermatt-Saas Unit. The first is a blueschist facies overprint at pressures and temperatures of 1.2-1.5 GPa and $\leq$ 500°C and the second event is an amphibolite/greenschist event at pressures <1.0 GPa and temperatures < 550-500°C (Fry and Barnicoat, 1987, van der Klauw et al, 1997, Reinecke, 1998).

This retrogression is due, in part, to the exhumation of these eclogites. The retrograde pathway set out by Fry and Barnicoat (1987) consists of eclogites cooling

into the lawsonite-eclogite field, followed by unloading to conditions of paragonite eclogites, followed by more cooling causing regrowth of glaucophane and then unloading, allowing greenschist facies assemblages to form. The tectonic setting they indicated for such a path involves repeated thrust steps (for a stepped pathway) or continual thrusting (for a smooth pathway) which emplace cool continental crust beneath the ophiolites. This would have the effect of rapid cooling followed by isostatic uplift and pressure decreases attributed to the buoyancy effect of underlying continental crust combined with unroofing either by erosion or extensional tectonics.

Evidence of the latter can be witnessed by the extensional shear zone (Gressoney Shear Zone - GSZ) located mainly in the Combin Zone (Reddy et al, 2003, Reddy at al., 1999), the unit structurally above the Zermatt-Saas. This structure is responsible for the unit's exhumation from ca. 60-100 km to 30km. The contact between the Zermatt-Saas and the overlying Combin Zone represents a significant metamorphic break, between eclogite and greenschist facies respectively. The GSZ has geometry and a kinematic framework consistent with SE directed extensional reactivation of convergent structures (Reddy et al, 1999). Rb/Sr dating of synkinematic recrystallised white mica from the shear zone shows that extension continued from 44 Ma till 36 Ma, unroofing the high pressure Zermatt-Saas footwall from 18kbar to 9kbar (Reddy et al, 1999) and likely contributing to the unroofing of the ultrahigh pressure areas too. $^{40}Ar/^{39}Ar$ dates of white mica from the shear zone indicate cooling after juxtaposition of the different tectonic units and are consistent with the Rb/Sr ages (Reddy et al, 2003).

Similar extensional shear zones are noted in the Täschalp area (Cartwright and Barnicoat, 2002). Rb-Sr data show these shear zones formed at 42-37Ma with the age of shearing becoming younger away from the Zermatt-Saas zone and into the overlying Grand St. Bernhard Nappe. Pressure and temperature estimates record conditions of 400-475°C and 400-500 MPa down to 300-350°C and 300-350 MPa. Subsequent unroofing of the Zermatt-Saas since 36Ma appears to be a result of erosion following uplift caused by further shortening (Reddy et al, 1999).

5.3 Petrography

The Zermatt-Saas unit in the Gressoney Valley, NW Italy, is well exposed on Punta Telcio. There the high pressure assemblages associated with this unit are exposed in patches of fresh eclogite and partially retrogressed eclogites which are surrounded by amphibolites. The samples collected for this study can be assumed to represent the various transitional stages between the conversion of an eclogite facies assemblage, through a blueschist event and into a widespread greenschist facies one. The following is a description of the main petrographical features of these rocks important to the aim of this paper, though fuller lithological descriptions can be found in chapter 4.

Eclogite facies rocks from Punta Telcio are composed mainly of omphacite and garnet. Omphacite typically has a small grain size (100 - 600μm) and has a rim of fine grained symplectite and forms a shape fabric which defines the foliation of the eclogite (Fig. 5.2). This shape fabric wraps around the garnet of the rock. Garnet has a variety of forms with porphyroblastic, poikiloblastic and atoll forms all present either with a euhedral or irregular shape and size varies from 300μm to 2mm.

Glaucophane occurs in many of the samples and is representative of the first retrogressive phase of the Zermatt-Saas. It is unlikely to be prograde glaucophane for a number of reasons. While prograde glaucophane is been documented in this unit (Fry and Barnicoat, 1987) it occurs as inclusions within eclogite facies garnets, a texture which is not evident here. Glaucophane in these samples displays two different morphologies, the first being large (0.5-2.5mm), elongate grains that define a shape fabric parallel to the omphacite fabric (Fig. 5.2). These grains may be isolated or form a series of connected grains. The second morphology consists of large (1-3mm), subhedral porphyroblasts of glaucophane that cut the omphacite fabric obliquely. The glaucophane contains garnet, omphacite and zoisite grains as common inclusions showing it postdates omphacite and is thus unlikely to be prograde.

Barroisite appears in a variety of places in the partially retrogressed eclogite samples and is representative of the second stage of retrogression experienced by the unit. Barroisite forms reaction rims around many of the garnets and also as inclusions

within garnet. It also forms reaction rims around the glaucophane grains and in many places epitactical and topotactical overgrowth of barroisite on glaucophane can be seen quite clearly (Fig. 5.2 and 5.3). Those grains growing around garnet and replacing glaucophane vary widely in size (50μm - 1mm). A second stage of barroisite growth occurs around the glaucophane porphyroblasts. The first stage of barroisite replacement is itself replaced by a second stage of barroisite growth (Fig. 5.3). The grain sizes of this second phase of barroisite are small (≤100μm).

Barroisite also forms grains within the matrix of the rock. These usually occur as completely separate single grains or as patches of smaller grains. The single grains have sizes between 1mm and 200μm. The patches of smaller grains have sizes smaller than 100μm. Matrix grains have a shape fabric that is parallel to the omphacite and glaucophane fabrics, though they do not form an obvious interconnected network in the rock as omphacite and glaucophane do. Rather the barroisite exists as isolated grains or patches that sometimes form discontinuous interconnected networks.

The petrography described here holds the possibility that any LPO found in omphacite may have a mimetic control on any LPO developed in retrogressive glaucophane and barroisite. Likewise any LPO developed in the glaucophane may have a mimetic control on the later appearance of barroisite.

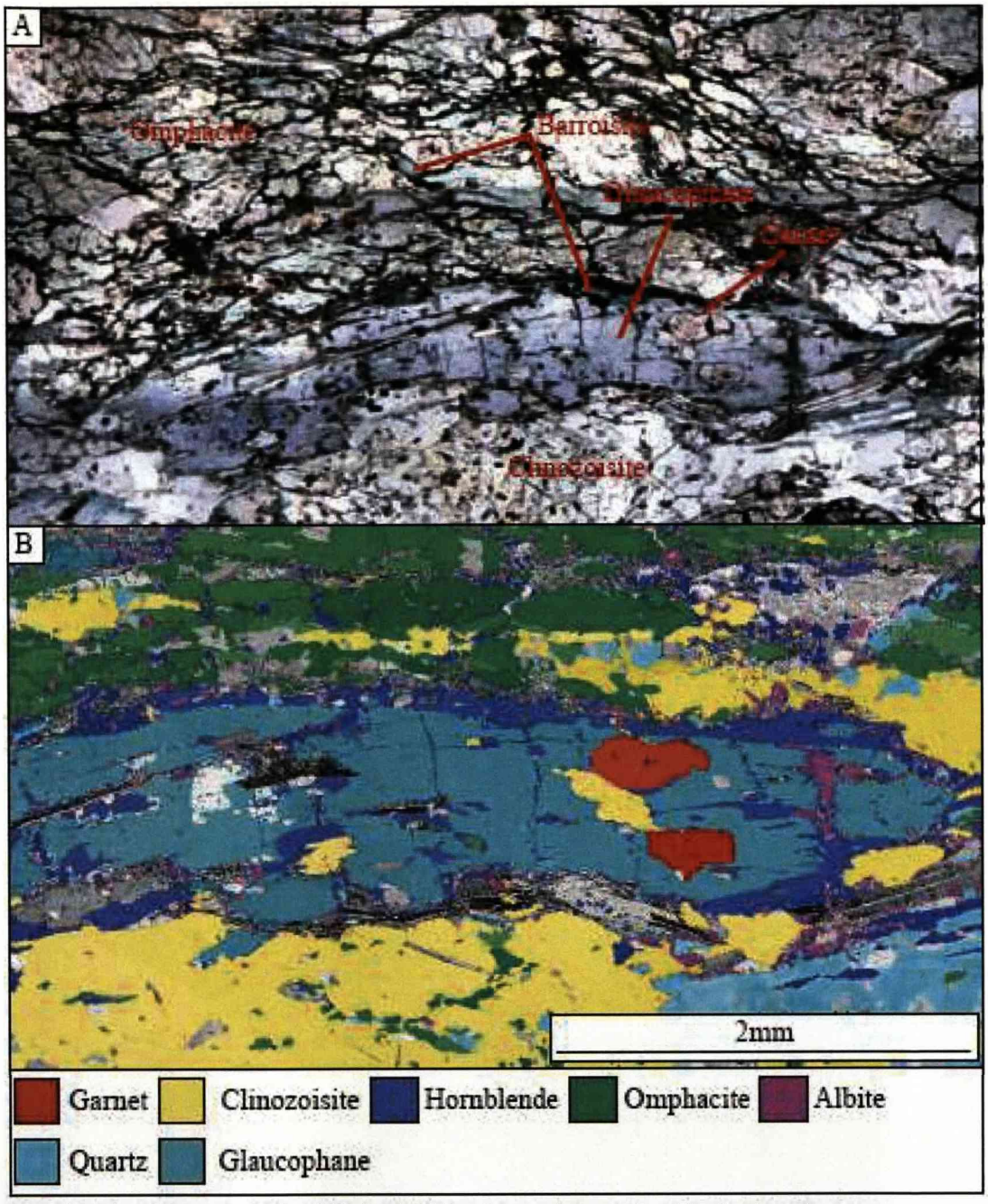

Fig. 5.2 A - Plane polarised light (PPL) photomicrograhs displaying features common to eclogite from the Zermatt-Saas of Punta Telcio (S.6.13) and B - EBSD phase identification map overlaid on a band contrast map showing more clearly the mineralogy and textural relationships

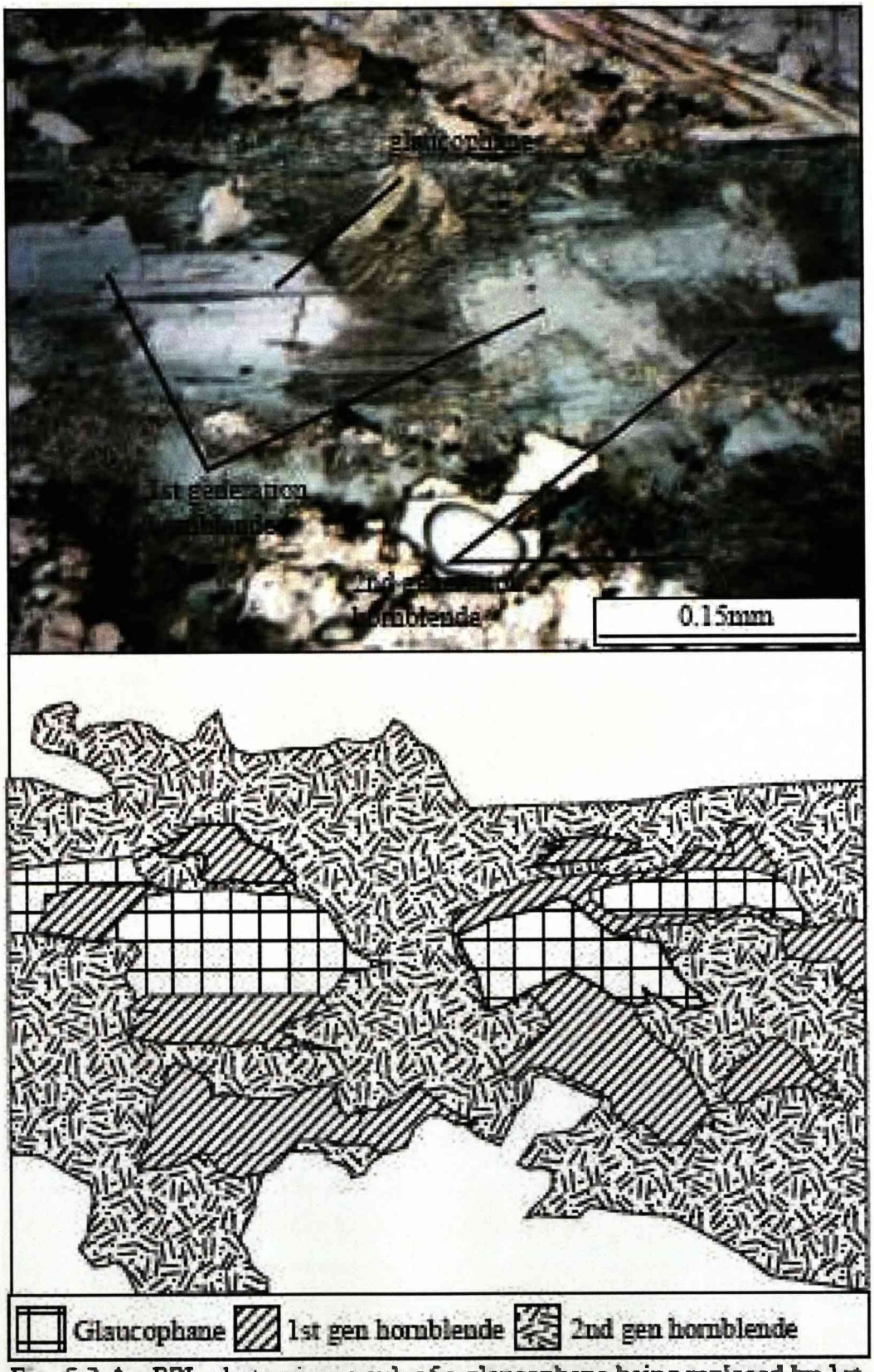

Fig. 5.3 A - PPL photomicrograph of a glaucophane being replaced by 1st generation hornblende which in turn in replaced by a darker, finer grained second generation hornblende. B - schematic diagram of the photomicrograph

5.4 Methods

5.4.1 Sample Preparation

Oriented rock samples collected from the field are re-oriented in the lab and then cut perpendicular to foliation and parallel to lineation. These are then polished to remove saw marks from the desired surface. Cut samples are then made into 30μm think, uncovered thin sections. For electron backscatter diffraction (EBSD), thin sections were polished on a polyurethane lap for three hours each, using a suspension of 0.05μm colloidal silicon (SYTON^{TM}) to remove the amorphous superficial layer (Llyod, 1987, Prior et al., 1996). The samples were given a very thin carbon coat in order to minimise charging effects and maximise the crystallographic signal (Prior et al., 1996).

5.4.2 EBSD Data Collection

All crystallographic orientation data is collected by EBSD using a CamScan X 500 crystal probe scanning electron microprobe (SEM) equipped with a thermionic field emission gun and a FASTRACK stage. An accelerating voltage of 20kV with a typical beam current of ~45-50nA is used for this investigation. The angular resolution of this technique is typically better than 1° and spatial resolution is ~0.1μm. All of the data acquisition is carried out automatically using either a stitched matrix of maps with a typical step size of 1.5-3μm (mapped by moving the electron beam) or by using the FASTRACK stage to collect data on rectangular grids with 2.5-10μm spacing (mapped by moving the stage) (Prior et al., 2002). Also orientation data across an entire thin section is collected using the FASTRACK stage using larger spacing (300-350μm).

5.4.3 EBSD Data Processing

Electron backscatter patterns (EBSP) are indexed using the software package CHANNEL+ v5 from *Oxford Instruments Ltd.* (Prior et al., 1999). Initial processing on beam mapped grains and 'stage' mapped grains (with small spacing between points (≤10μm) involved the removal of isolated points that have been incorrectly indexed (wild spikes). What then follows is the processing procedure laid out in (Prior et al., 2009) which involves manipulating the band contrast (BC) of the

scanned area. For this study most of the EBSD maps have noise reduction carried out for non indexed points that have at least five neighbouring indexed points.

Due to similar crystallography in barroisite and glaucophane, EBSPs for both are indistinguishable (Table 5.1). This results in the automatic indexing software often indexing one phase as the other. While this may result in the wrong phase being assigned to a pixel, it has no effect on the crystallographic orientation measurements (Fig. 5.4). This is confirmed by comparison of the mean angular deviation (MAD) values that accompany each solution. The indexing software will offer both barroisite and glaucophane solutions with approximately the same MAD values. The fact that this indexing problem has no effect on the crystal orientation measurements is further proven by the near identical Euler angles that each solution provides within a 1.5° error bar.

Mineral	a length	b length	c length	β angle (°)
Omphacite	9.646	8.824	5.27	106.59
Glaucophane	9.541	17.74	5.295	103.67
Barroisite	9.87	18.058	5.307	105.2

Table 5.1 Unit cell lengths and β angles used by the indexing software to index the EBSP

To overcome incorrect indexing of barroisite and glaucophane, EBSD scans are performed alongside an energy dispersive X-ray (EDX) scan. This provides each point with orientation data and a phase diagnosis based on the EBSP and also element abundances as well. Chemical maps show a strong difference between the calcium content for barroisite and glaucophane forming a reliable way of distinguishing the two phases. The data is run through a MATLAB program that changes the phase identification number based on upper and lower limits imposed on the calcium counts. The resulting output is then imported back into CHANNEL + v5 with the barroisite and glaucophane points now correctly distinguished. Before and after images and a Ca map for one data set are shown in Figure 5.5.

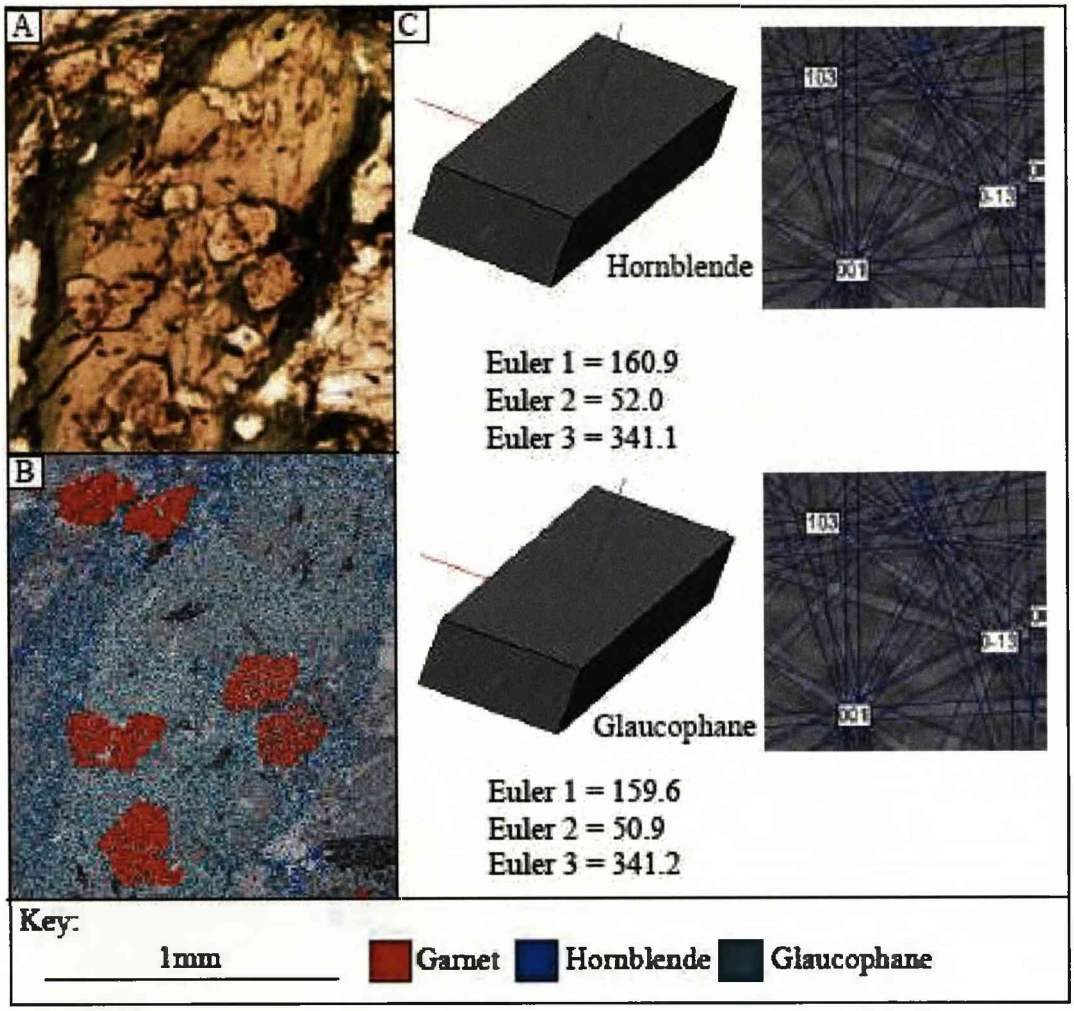

Fig. 5.4 Diagrams showing how hornblende and glaucophane can mis-index as each other due to crystallographic similarities. A - Photomicrograph of a porphryoblast of glaucophane with some hornblende overprint and overgrowth, B - Phase identification map showing the glaucophane area is occasionally indexed as hornblende, C - Euler angles from two neighbouring pixels one of glaucophane and the other of misindexed glaucophane (hornblende), the 3D crystal orientation of those pixels and the indexing patterns of both the pixels.

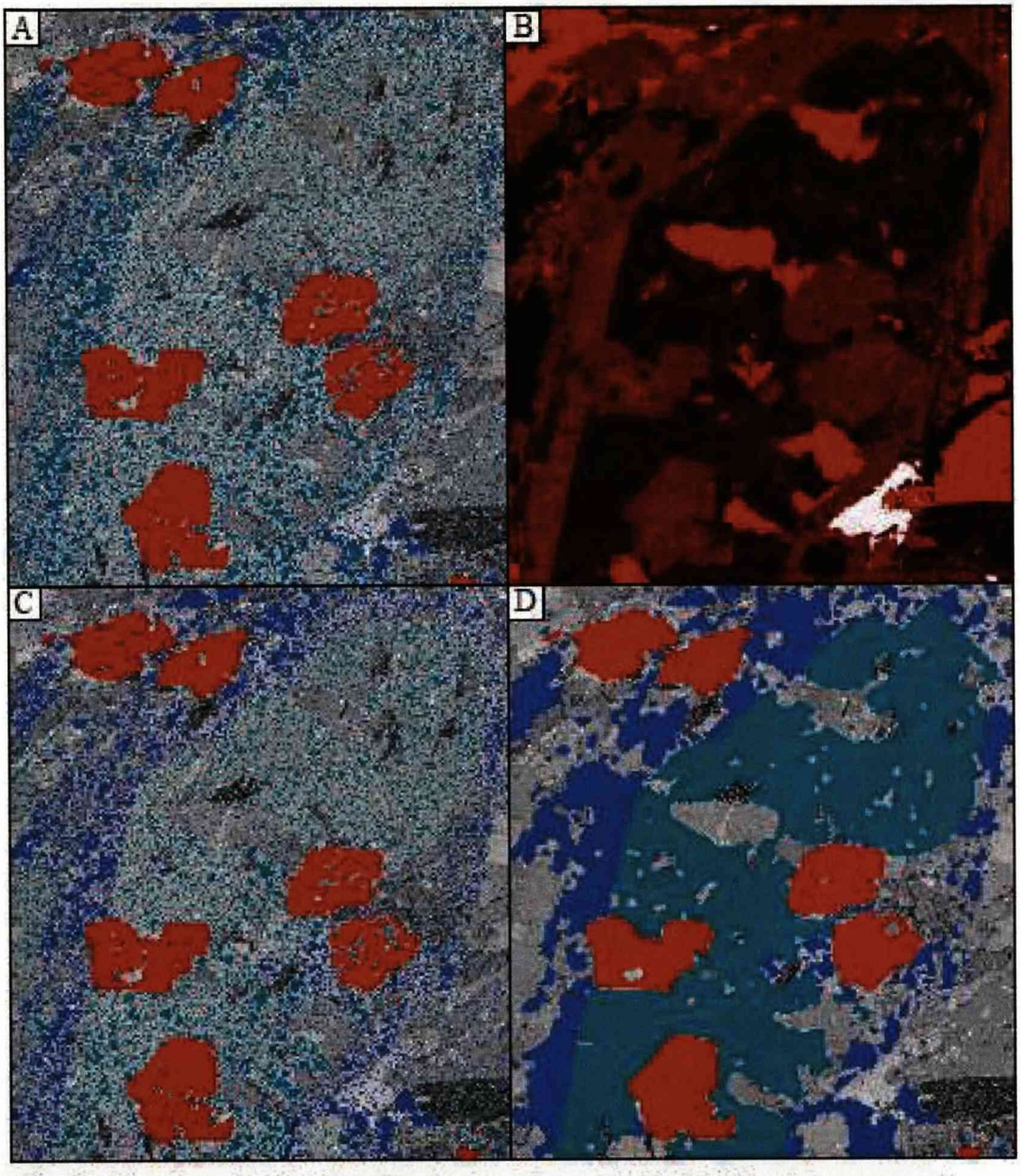

Fig. 5.5 A - Raw EBSD data displaying phase ID, B - EDX calcium map, C - Phase ID map after the raw data has been put through a MATLAB program to reassign phase numbers based on the calcium amounts, D - phase ID map of the data after significant noise reduction

5.4.4 Pole Figures

Orientation data for pole-figure plotting is produced by two separate methods for this study. One method provides an LPO based on data from a small area of a thin sectioned sample mapped at a small scale, though small areas are less reliable for production of representative LPOs. To this end the second method allows for a larger sampling area of orientation points to produce an LPO, as it scans across the entire area of a thin sectioned sample. All samples used for this study have pole figure plots using both procedures outlined here. The first method involves data manipulation of the EBSD mapped areas of each sample. Each map undergoes grain detection, a function in the CHANNEL+ v5 software, which separates out grains of each phase based on neighbouring pixels being more than 10° misoriented from each other. A subset of the data is then created where only one orientation measurement is taken from each of these defined grains. This 'point per grain' data is exported from CHANNEL + v5 and entered into the PFch5.exe program published by D. Mainprice (ftp://saphir.dstu.univ-montp2.fr//pub/TPHY/david/CareWare_Unicef_programs/PC) which creates the pole figures. This method will be referred to as a point per grain scan (PPGscan) in this paper.

The second method involves the data obtained by mapping the entire thin section at a large spacing using a FASTRACK stage. The FASTRACK stage allows automated EBSD mapping by moving the sample by predetermined increments while the electron beam remains stationary. Spacing is determined by average omphacite grain size in each sample. The method provides a large number of points from across an entire thin section, none of which belong to the same grain, for a number of phases. To ensure that no one grain is represented more than once in the data, a similar 'point per grain' subset is created in the same way it was in the first method. The data is then also exported for use in the PFch5.exe program. This method shall be referred to as the 'stage' scan (STscan) for this paper. All pole figures are plotted in the same reference frame where S is the trace of the foliation and L is the lineation.

5.4.5 *Intraphase and Interphase Misorientation*

EBSPs provide the full crystallographic orientation of a point allowing calculation of the rotation required to map the orientation at one point onto the orientation at another point (Prior et al., 1999). Misorientation is the term used to describe this rotation which is achieved via a rotation axis and rotation angle, referred to as misorientation axis and the misorientation angle (Wheeler et al., 2001). The number of misorientation axis and angle solutions that can be calculated from EBSPs depends on the mineral symmetry. The less symmetry a mineral has the fewer misorientation solutions there are. Triclinic minerals will have only one solution whereas cubic minerals have 24 solutions. This study deals with monoclinic minerals and so any one misorientation can have two solutions. When concerned with one phase and the misorientations within that one phase we refer to it as intraphase misorientation.

Interphase misorientation differs from intraphase misorientation in that it is related to a mapping of the crystal orientation at a point of a certain mineral onto the crystal orientation at a point of a different mineral. This also involves a rotation using a misorientation axis and misorientation angle. It is arbitrary which crystal directions are chosen though a choice must be specified. As all minerals considered for this study are monoclinic it is sensible to compare corresponding axes but this is not mandatory. In this study the phases used for interphase misorientation are omphacite, glaucophane and barroisite, all monoclinic minerals. While the unit cell lengths and β angles of all three minerals are similar there are small differences which may influence comparison between them. Table 1 shows the unit cell lengths and β angles used by the software to index the three minerals.

To investigate interphase misorientation, two procedures are followed. The first involves use of the CHANNEL+ v5 software to manipulate processed orientation data, and the second is discussed later. CHANNEL+ v5 software allows investigation of crystal orientation across interphase boundaries: in this study, omphacite/barroisite, and glaucophane/barroisite phase boundaries. This can be done by using 'Lattice Correlation Boundaries' or 'Orientation Relationship Boundaries' as defined by CHANNEL+v5. 'Lattice Correlation Boundaries' display misorientation across phase boundaries between a direction (or plane) in phase A and

a direction (or plane) in phase B. It allows a freedom of rotation about the axes of the plane or direction chosen. This study refers to these maps as direction-direction maps (D-D) and plane-plane maps (P-P) and explores three different D-D relationships <100>, <010> and <001> and three different P-P relationships (100), (010) and (001). 'Orientation Relationship Boundaries' display misorientation across phase boundaries between a specified set of planes and directions (that lie within the planes) defined for both phases. As both the planes and directions are considered together no freedom of rotation is allowed around the axes. Hence there is a complete relationship between the two phases. This study refers to these maps as PD-PD maps and explores six different PD-PD relationships, (100)<010>, (100)<001>, (010)<100>, (010)<001>, (001)<100> and (001)<010>.

Due to the monoclinic symmetry of each of the minerals involved with this study the six PD-PD maps can all be represented by three maps for the following reasons. For example when rotating <001> in (100) in a monoclinic mineral so that it is aligned with <001> in (100) of another monoclinic mineral the <010> automatically becomes aligned as well as the angle between <001> and <010> is always 90°. This means that (100)<010> and (100)<001> PD-PD maps show the same information. The same is true for (001)<100> and (001)<010> PD-PD maps. With (010)<100> and (010)<001> PD-PD maps however slight differences exist between the two as when one direction is lined up between two monoclinic phases the other direction will not due to slight variances in the β angles. As this difference is quite small it produces negligible differences between the two maps and as such both can be represented by one map.

5.4.6 Intraphase and Interphase Misorientation Angle Distribution Analysis

Intraphase misorientation angle distribution analysis takes neighbour-pair misorientation angle distributions and random-pair misorientation angle distributions and tests for statistically significant differences between them. A random pair distribution of misorientations is created by relating every grain in a dataset to every other grain. A neighbour pair misorientation angle distribution is calculated from pairs of touching grains in a dataset. These distribution can be represented graphically either as a histogram of misorientation angles or by a cumulative frequency curve. The differences between the two distributions hold important

implications for interpreting microstructures (Wheeler et al., 2001). If a statistically significant difference exists then neighbouring grains have undergone a physical interaction and/or neighbouring pairs have been derived in a significant number of cases from a common parent microstructure: inheritance.

Here we propose that *interphase* misorientation angle distribution analysis can be conducted in the same fashion and aid in the investigation of mimetic fabrics and LPO by investigating whether there is a statistically significant difference between the neighbour pair and random pair misorientation across a phase boundary. CHANNEL+v5 is not equipped to directly analyse interphase misorientation neighbour and random pairs, though the neighbour pair misorientation data can be acquired indirectly from the software. Interphase neighbour pair misorientation angle distributions are produced through a purpose-made MATLAB program. This program systematically searches the EBSD map for a pixel of a desired phase that has a neighbouring pixel of a desired second phase. Searching continues until all touching pixel pairs of the two desired phases have been found. For this study the phase pairs are omphacite/barroisite and glaucophane/barroisite. The program then takes the orientation data, in the form of Euler angles (Euler 1, Euler 2 and Euler 3), of the touching pixels and converts them to the a, b, and c axes (as unit vectors) of a monoclinic mineral (the crystal system of all phases concerned with this study) with a given beta angle (Table 1.). The calculation is done using the direction cosine matrix (DCM) (Ulrich and Mainprice, 2005) which rotates the direction from the sample to the crystal orientation. The final stage of the program takes this data and calculates the angle between the <100>, <010> and <001> directions of each phase pair.

To acquire an interphase random pair misorientation angle distribution a second MATLAB program is used. From a dataset the program selects a random pixel of a desired phase and then selects a random pixel of a second desired phase, combining them into a random pair. It continues to do this for a preset number of random pixel pairs. The program then takes the orientation data from both randomly selected pixels (one of each phase) and performs the same processes carried out in the interphase neighbour pair misorientation angle distribution program to determine the misorientation between them.

For each sample an interphase neighbour and interphase random misorientation angle distribution is are obtained. These are then displayed as cumulative frequency curves on the same graph for each sample. The distributions, if necessary, can be tested to determine whether they are significantly different using the Kolmogorov-Smirnov test. Here, the Kolmogorov-Smirnov statistic quantifies the distance between the interphase neighbour and interphase random misorientation angle distributions. The maximum distance between the two cumulative frequency distributions is calculated. The larger this value is the less likely the two distributions are the same.

It is worth noting here that interphase misorientation axes distribution analysis would be a useful tool for investigating and defining possible mimetic boundaries over interphase boundaries, but currently no software exists for plotting the inverse pole figures (IPFs) required.

5.5 Results

5.5.1 Pole Figures

Omphacite pole figures (Fig. 5.6) show that (010) poles form point maxima normal to foliation and the <001> poles are dispersed in a girdle within the foliation plane. The (100) poles have a random distribution. There is little difference between pole figures obtained from STscans and PPGscans for omphacite.

Glaucophane pole figures (Fig. 5.6) show that an LPO also exists within this mineral. This commonly takes the form of point maxima in the <001> poles parallel to the lineation. Variation in the <001> poles occurs as weak girdles within the foliation plane (sample S5.2). The (100) poles form a girdle distribution perpendicular to the foliation plane and the (010) poles tend to form point maxima also normal to the foliation. More random distributions are also observed in the (010) poles in sample S5.2 and S6.13.

Barroisite pole figures (Fig. 5.6) show (010) poles form point maxima normal to the foliation and the <001> poles are dispersed in a girdle within the foliation plane. A slight departure from this pattern occurs when samples show a stronger girdle distribution within the foliation plane of (010) poles and stronger point maxima parallel to the lineation in the <001> poles. The strength of observed patterns varies from sample to sample and also between STscan and PPGscan methods for each sample. Sample S5.2 shows strong (010) maxima and a clearly defined girdle in the <001> poles in the PPGscan pole figures. The STscan pole figures for the same sample show no point maxima in (010) and a very weakly defined girdle in <001>. The (100) pole figures show a variety of patterns. Sample 5.2 shows the (100) poles in a random distribution but for some other samples (S6.8, S6.14 and S6.18), the (100) poles form incomplete or weak girdles normal to the foliation plane.

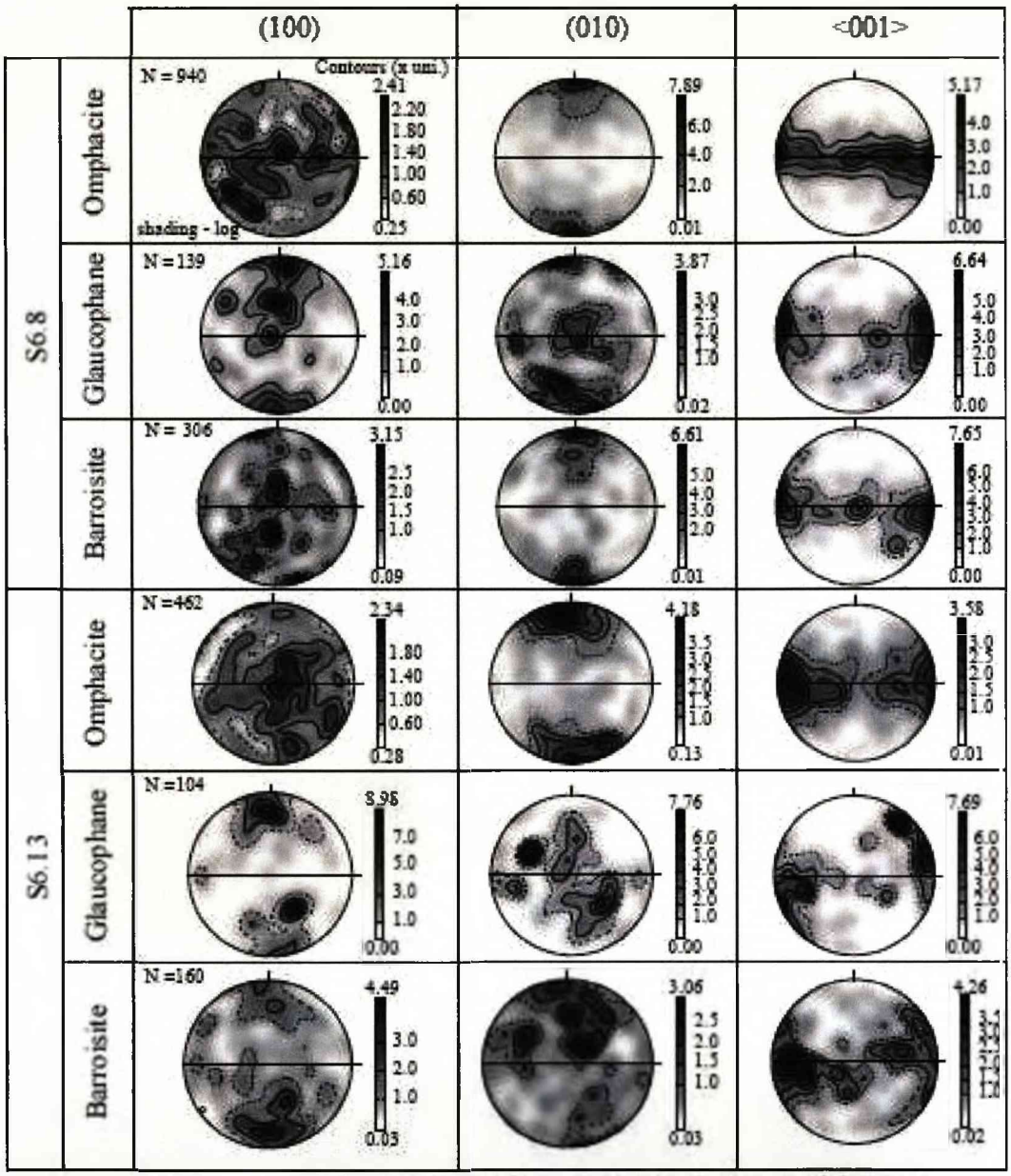

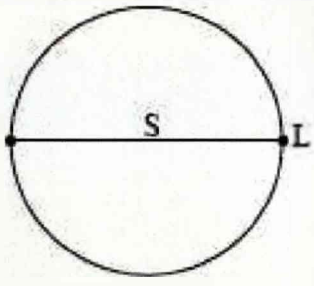

Fig. 5.6 Omphacite, glaucophane and barroisite pole figures for two samples used in this study collected via the 'stage' scan method. The plane of foliation (S) and lineation (L) references are shown on a reference pole figure

5.5.2 P-P, D-D and PD-PD Maps and Interphase Misorientation Angle Distribution Analysis

5.5.2.1 Omphacite/barroisite

P-P maps for all data sets show that misorientation of (100) across omphacite and barroisite phase boundaries have a large frequency of low angle misorientations (<10°). For (010), misorientations across the phase boundary are >10° with a large proportion of these ~180°. (001) misorientations are also >10° with a significant proportion at ~30°. Conversely D-D maps for all samples show the misorientation of <100> across omphacite-barroisite phase boundaries to be >10° with a large proportion of ~30° misorientations. The <010> shows misorientations >10° across omphacite-barroisite boundaries with a high frequency of them at ~180°. The <001> D-D map is the only one to show a large proportion of <10° misorientations across this phase boundary. P-P and D-D maps for omphacite/barroisite phase boundaries are shown for sample S5.2 (Fig. 5.7).

PD-PD maps for all samples show that misorientation across omphacite/barroisite phase boundaries is >10°. A high frequency of 170-180° misorientations is noted on all PD-PD maps. Fig. 5.8 shows an example of a PD-PD omphacite/barroisite map for sample S6.18.

Misorientation angle distribution analysis of D-D maps for omphacite/barroisite misorientation confirms what is noted visually in the maps. Histograms for <100> show a peak in omphacite/barroisite neighbour pair misorientation at ~30°. For <010> a peak in the neighbour pairs occurs at 180° and for <001> a peak occurs at misorientations <5°. Cumulative histograms for all samples show the same 30° neighbour pair misorientation peak for <100>, an anti-correlation pattern for the neighbour pair misorientations of <010> with a sharp increase at 180° and a high frequency of low angle misorientation (<5°) for <001>. Cumulative frequency graphs and corresponding D-D maps are shown in Fig. 5.7.

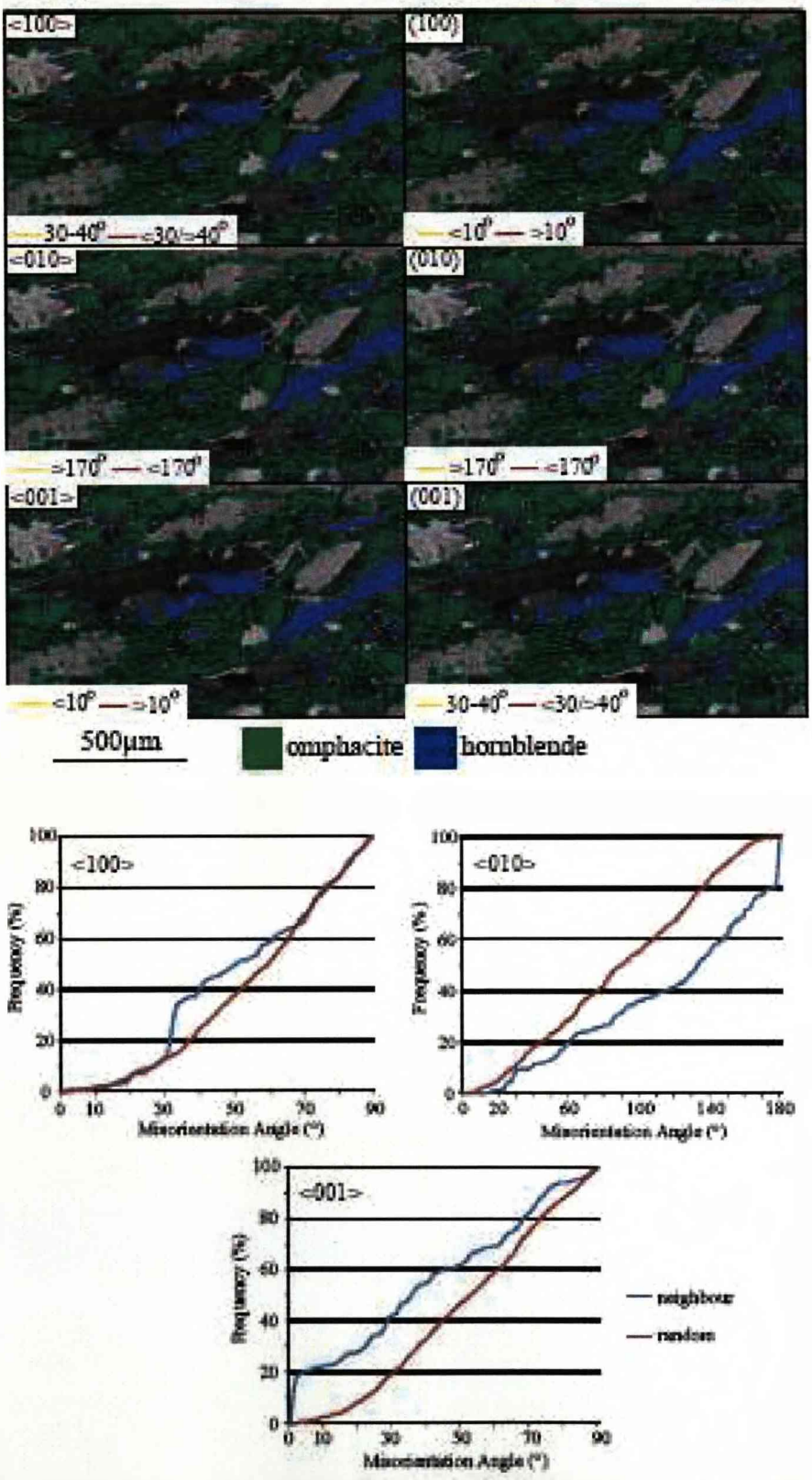

Fig. 5.7 D-D and P-P maps for omphacite hornblende phase boundaries in sample S5.2 for the three principal directions and planes and the cumulative frequency graphs showing interphase neighbour and random misorientation distribution analyses for the three principal directions

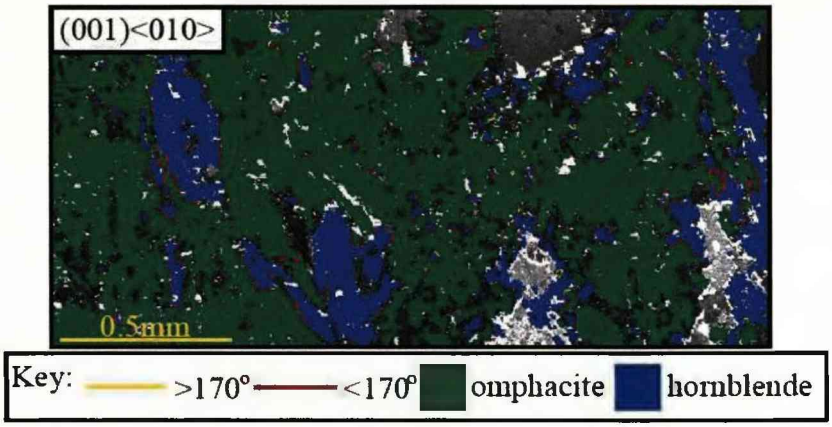

Fig. 5.8 PD-PD map showing misorientation across omphacite/hornblende boundaries in sample S6.18 for the combination (001)<010>. Other PD-PD combinations are not displayed for reasons mentioned earlier.

5.5.2.2 Glaucophane/barroisite

D-D and P-P maps for all samples show misorientation across the majority of glaucophane/barroisite phase boundaries is <10° for all directions and planes. In few areas where the glaucophane grain is bordered by more than one grain of barroisite the interphase misorientation between the glaucophane grain and some of the barroisite grains is >10°. D-D and P-P maps for glaucophane/barroisite phase boundaries are shown for a glaucophane porphyroblast from sample 6.8 (Fig. 5.9).

PD-PD maps for all samples show that the interphase misorientation patterns are exactly the same as they are in P-P and D-D maps. For some areas the interphase misorientation is >10° and in others areas it is <10°. PD-PD maps are shown for sample S.6.14 (Fig. 5.10).

Interphase misorientation angle distribution histograms for glaucophane/barroisite boundaries show the neighbour pixel pairs have a high frequency of low misorientation angles (<10°) for <100>, <010> and <001> but the random pairs have a low amount with higher frequencies of higher misorientation angles. Interphase misorientation graphs for glaucophane/barroisite in S6.14 are shown in Fig. 5.9.

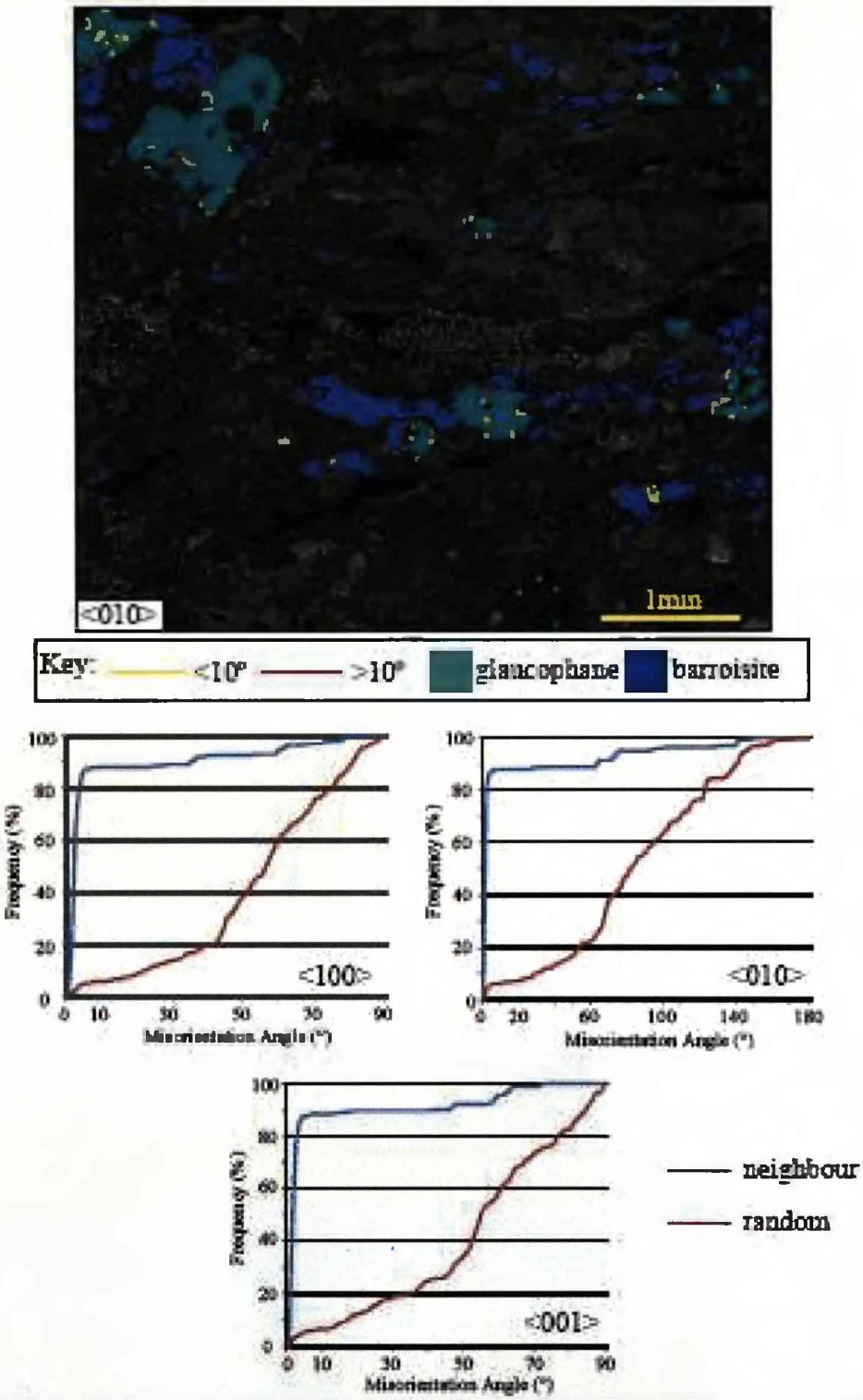

Fig. 5.9 <010> D-D maps showing misorientation across glaucophane-hornblende boundaries for sample S6.14. D-D maps for the other two principle directions and principle planes show the exact same pattern. Also shown are interphase misorientation distribution cumulative frequency graphs for the three principle directions.

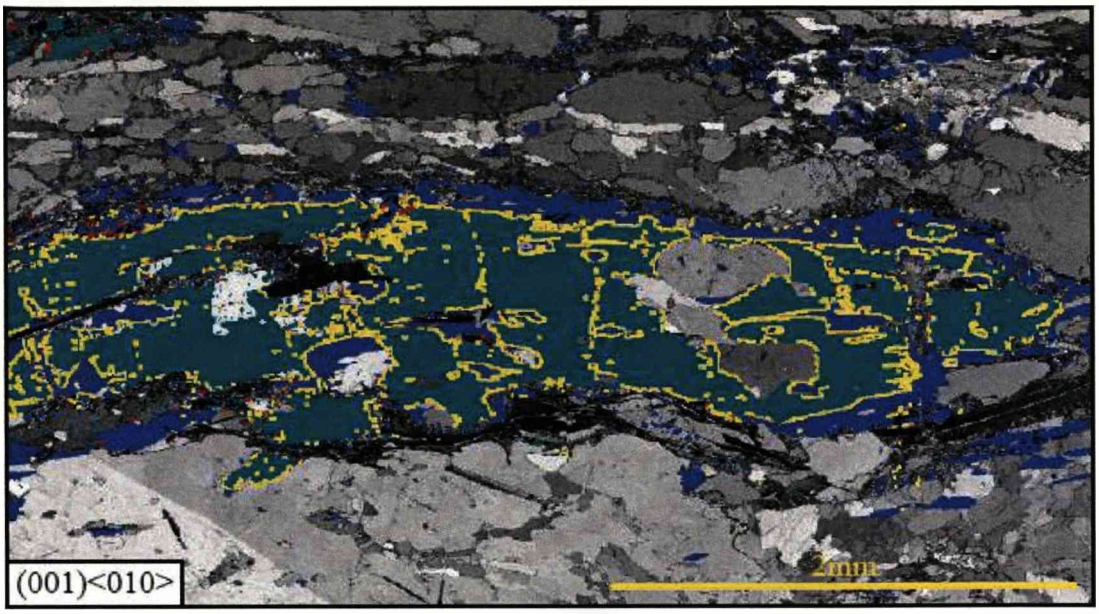

Fig. 5.10 PD-PD map showing misorientation across glaucophane/hornblende boundaries in sample S6.13 for the combination (001)<010>. Other PD-PD maps are not displayed for reasons mentioned earlier.

5.6 Discussion

The crystallography of omphacite, glaucophane and barroisite already provide us with an intuitive idea of whether they may be mimetic on each other (Deer et al., 1992). All three minerals are monoclinic with very similar crystal lattice parameters. An important difference is that omphacite has a shorter 010 length than glaucophane or barroisite. Also, while all three are monoclinic, omphacite is a clinopyroxene (single chain) and glaucophane and barroisite are amphiboles (double chain). This would suggest that an amphibole would find it difficult to directly mimic the crystal lattice of a clinopyroxene. Between amphiboles the idea of mimicry seems much more plausible.

Omphacite has a strong LPO in these rocks as has the retrogressive barroisite. The two minerals cannot be in equilibrium with each other and thus have developed their LPOs during separate events in the evolution of this unit. The omphacite will have formed its LPO during the prograde or early retrograde portion of the metamorphic history of the unit. The barroisite, which did not appear in the mineral assemblage till later exhumation of the unit, will have formed its LPO then through a variety of means which we attempt to identify here.

5.6.1 Mimicry of Omphacite

Comparison of the pole figures between omphacite and barroisite show some strong similarities but also some important differences in LPO patterns. Similar elements can be recognised such as the formation of girdle distributions of the <001> poles within the foliation and point maxima formed by the (010) poles normal to the foliation. However this pattern is only evident in some of the samples and others will show that the barroisite pole figures have a more variable pattern than the consistent one described by omphacite.

Rather than the <001> girdle and (010) point maxima described the barroisite can often develop more of a girdle distribution in the (010) poles normal to the foliation and a stronger point maxima signature in the <001> poles parallel to the lineation. This pattern is not seen in any of the omphacite pole figures. Further differences between omphacite and barroisite pole figures lie with the (100) patterns. All samples show that omphacite has a random pattern in the (100) poles whereas the

barroisite (100) poles tend to form a girdle distribution perpendicular to the foliation. So while some samples show barroisite and omphacite to have similar pole figures others do not, meaning that omphacite may be having some mimetic control but it is far from the complete story.

Insight into the possible crystallographic relationship between omphacite and barroisite is revealed though the D-D and P-P maps and misorientation angle distribution analyses. High frequencies of 30° misorientations are noted for <100>, >170° misorientations for <010> and <10° misorientations for <001> across omphacite/barroisite phase boundaries. When exploring a single neighbour pair set of axes misorientations, these three high frequency misorientations coincide. The high frequency misorientation signals represent a 'special relationship' between the crystallography of omphacite and barroisite (Fig. 5.11). Where barroisite has formed around omphacite due to retrogression it has taken on an orientation that has resulted in these specific misorientations with the omphacite crystal lattice. In other words it suggests that the omphacite lattice has a strong effect on the orientation of forming barroisite grains.

Similar 'special orientation relationships' are noted in material science studies in materials such as Nb solid solution precipitates, Nb5Si3 intermetallics, materials in the Zr-ZrB2 system and WC-Co alloys (Cheng et al., 2009, Bounhoure et al., 2008, Champion and Hagège, 1992). Many composite metals in alloys are investigated to see how they join together to form a new material. In these studies local interfacial configurations between materials organise to minimise interfacial energies resulting in special orientation relationships forming. It has even been shown that orientation can be predicted in epitaxial growth in fcc-bcc interfaces (Gotoh and Arai, 1986). The relationship described here would be expressed so:

$$<001>_{omp} \parallel <001>_{barr}$$

$$<010>_{omp} \text{ 180 degrees to } <010>_{barr}$$

$$<100>_{omp} \text{ 30 degrees to } <100>_{barr}$$

Large barroisite grains are often surrounded by smaller omphacite grains in the eclogites of Punta Telcio. This grain size discrepancy between the two phases would suggest that barroisite is not completely mimicking the omphacite grains, though this

can be explained. Some of these bordering omphacite grains have the special relationship boundary with the barroisite whereas others do not. It is likely that the barroisite grain nucleated on a certain omphacite grain creating the 'special relationship' misorientation and then grew in that same orientation, engulfing and destroying other omphacite of varying orientation. Occasionally other omphacite grains oriented in the same way as the 'nucleation' omphacite grain are encountered and the 'special relationship' misorientation boundary is achieved again. These can be seen in texture component maps of omphacite and using misorientation profiles between relative omphacite grains, showing there is low misorientation between omphacite grains across a large barroisite grain (Fig. 5.12).

Taking this 'special relationship' into consideration the patterns shown on omphacite/barroisite PD-PD maps can be rationalised. A strong misorientation angle frequency at around 170-180° is noted in all PD-PD maps. The way the barroisite crystal structure likes to replace the omphacite one can be simplified as a 180° rotation around the omphacite <001> axis.

This signal of a crystallographic special relationship between omphacite and barroisite indicates that there is some mimetic control on the growth of barroisite and thus on the development of its LPO. As mentioned though comparison of pole figures shows that there are significant differences that need to be explained by other methods of LPO formation.

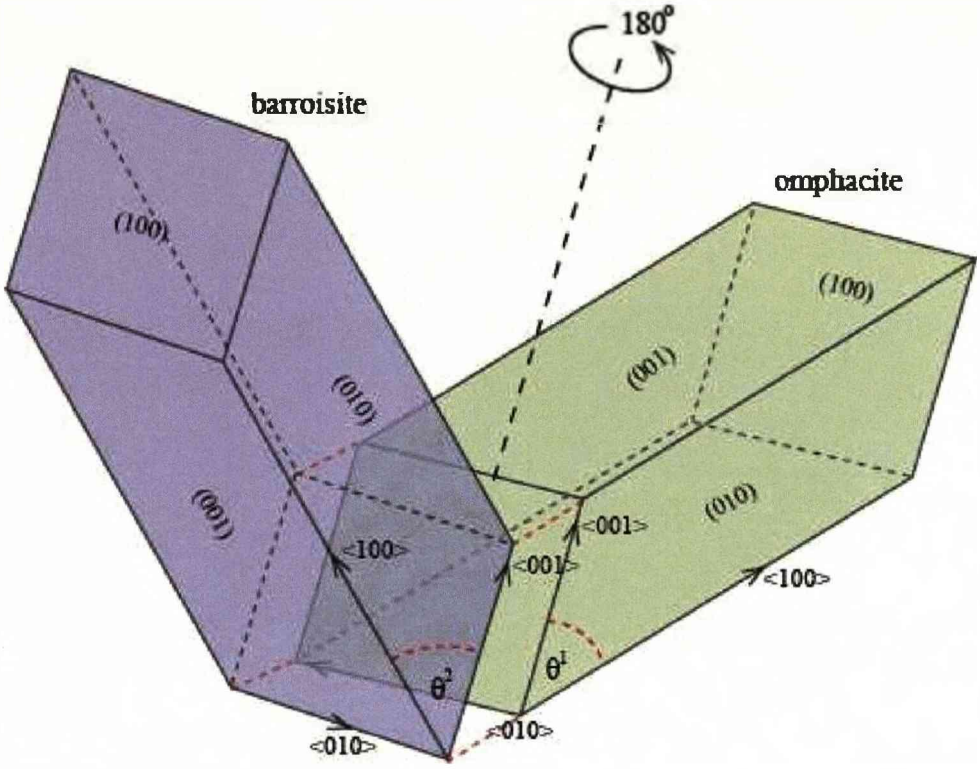

$\theta^1 = 180 - \beta = 73.41$

$\theta^2 = 180 - \beta = 74.8$

$180 - 73.41 - 74.8 = 31.79$

Fig. 5.11 Diagram to show the 'special orientation relationship' that barroisite uses to replace omphacite, and the 180 degree rotation axis about <001>

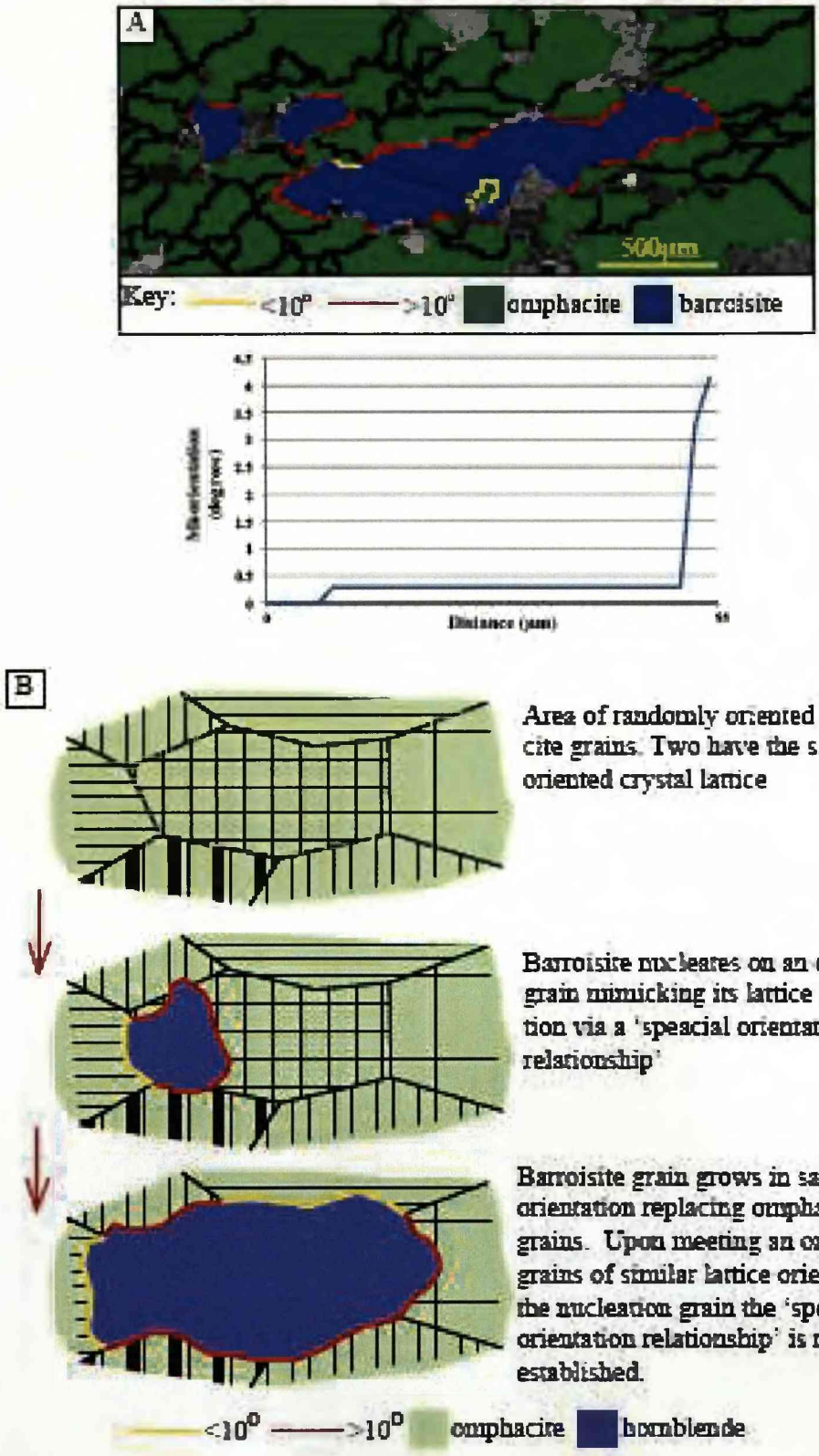

Fig. 5.12 A - <001> D-D map showing large barroisite grain bordered by many omphacite grains, two of which are similarly oriented as shown by the misorientation profile. B - Schematical diagram of how such a microstructure forms

5.6.2 *Mimicry of Glaucophane*

The mimetic affect of omphacite orientation on barroisite growth suggests that the barroisite LPO may be partially derived from the omphacite LPO. It can only be partially derived due to the variation displayed between (100) pole figures for omphacite and barroisite. While some barroisite (100) pole figures display the same random pattern as omphacite (100) pole figures other samples display girdle patterns perpendicular to the foliation. These girdles cannot be explained by mimicry of omphacite LPO thus there is still scope for other mechanisms to be involved in barroisite LPO formation.

From field and thin section observations it is known that glaucophane growth occurred either during the eclogite facies conditions or in a separate retrogressive blueschist facies event, before the amphibolite/greenschist facies event that resulted in barroisite formation. Large grains of glaucophane grew and formed an LPO here. The glaucophane in some places forms an interconnected network but there are isolated grains still aligned as part of the shape fabric. It is possible that the glaucophane was deformed at the same time as the omphacite and formed its LPO via crystal plasticity. Large glaucophane grains contain little to no internal strain or sub-structure, certainly not enough to have caused a strong LPO. This rules out dislocation creep as a deformation mechanism, unless there was significant recovery removing such sub-structures. Other mechanisms such as diffusion creep are difficult to obtain evidence for but as discussed in Chapter 4 this deformation mechanism is thought to be a significant contributing mechanism to the creation of the omphacite LPO. If glaucophane deformed at the same time as omphacite creating its LPO in tandem, then it is possible diffusion creep played an important role in its LPO development.

It is possible that after glaucophane deformed in tandem with omphacite a period of static glaucophane growth occurred with existing grains growing larger. Evidence for a further period of static glaucophane growth comes from large glaucophane porphyroblasts cutting the fabric of the rock. Either these grains nucleated and formed after those that did so during deformation or they represent preferential growth of glaucophane in a certain orientation.

Thin section evidence shows that glaucophane is directly being replaced as well as being overgrown by barroisite. This is likely to be topotactical and epitactical growth which may mean that barroisite LPO is mimetic on that of glaucophane. This would mean that there is the possibility, through topotaxy and epitaxy, for complete replacement of the glaucophane by barroisite.

Comparison of barroisite and glaucophane LPO patterns shows they are quite similar. Glaucophane and barroisite both display point maxima or weak girdles normal to the foliation in the (100) poles, point maxima or weak girdles normal to the foliation in the (010) poles and point maxima parallel to the lineation or weak girdles within the foliation plane in the <001> poles. Pole figures for single crystal glaucophane with barroisite replacement show that glaucophane and barroisite plot in the exact same places on (100), (010) and <100> pole figures.

P-P, D-D and PD-PD map results show that there is no change at all in the crystal orientation across glaucophane/barroisite boundaries. Interphase misorientation angle distribution analysis show high frequencies of low angles (<5°) for the neighbour pair distributions, while the random distributions show a much smaller frequency of them. For this mineral pair LPO mimicry seems to provide an important contribution to the formation of the barroisite LPO where barroisite is directly copying the crystal orientation of glaucophane. Thus we suggest the barroisite LPO patterns are a composite of elements from omphacite and glaucophane LPO patterns. This is based on comparative LPO patterns of the three elements from the same sample and the fact that evidence exists for mimicry of barroisite on both omphacite and glaucophane.

There are problems however with the idea of barroisite mimicry of glaucophane. In most of the samples taken from the area little glaucophane is present. Modal abundances of eclogite facies rocks from the area show this quite well (Table 5.2). This raises a question as to how much effect glaucophane LPO may have had on the barroisite LPO development given that glaucophane may not be a widespread phase. It is possible only some areas of Punta Telcio preserve this blueschist event marker or, on the other hand, areas of the unit have been retrogressed so much all glaucophane has been replaced, leaving no trace of it.

Sample	Garnet %	Omphacite %	Glaucophane %	Amphibole %	Other %	Total
S5.2	11.5	23.1	12.7	14.4	38.3	100
S6.8	15.6	32.4	19.7	25.2	7.1	100
S6.13	7.7	34	7.6	11.8	38.9	100
S6.14	4.6	30.4	25.2	14.2	25.6	100
S6.18	10.29	35.9	0	13	40.81	100

Table 5.2 Modal abundances of mineral phases from selected samples of eclogite facies rocks of Punta Telcio. Calculated from EBSD maps using Channel+ v5.

The problem with complete glaucophane replacement in some areas of the Punta Telcio lies with a grain size discrepancy between large glaucophane and the small barroisite. Complete replacement of large glaucophane porphyroblasts (Fig. 5.2) would logically result in large barroisite porphyroblasts. While large barroisite grains are noted there are none with the size and texture displayed by glaucophane. A possible explanation for this lies with retrogressive textural relationships noted in these rocks (Fig. 5.3). A second phase of green amphibole growth is noted in these rocks and texturally it can be seen to replace barroisite, which was already replacing glaucophane. Chemical analyses show these green amphiboles to be representative of lower grade mineralogy such as magnesio-hornblende, actinolitic-hornblende and actinolite, suggesting it formed later in the exhumation of this unit. Grain sizes of this second stage amphibole growth are smaller than barroisite grains. Replacement of barroisite by this second generation amphibole may explain why large barroisite grains (that have completely replaced large glaucophane porphyroblasts) are not observed.

5.6.3 Crystal Plasticity

As mentioned earlier, one of the main causes of LPO formation in a phase is crystal plasticity. The barroisite here may have had some element of this contributing to its formation. This involves the build up of strain during the greenschist facies event in this unit providing the means for crystal plastic processes to reorient the barroisite crystal lattice into an LPO. However there are often areas where groups of isolated barroisite grains still display a strong LPO. The lack of interconnectivity between them rules out mechanisms associated with crystal plasticity as the cause of the LPO. It also could not have deformed plastically with omphacite as the phases are not stable and develop at different stages in the evolution of this unit.

Conversely grain boundary maps shows that barroisite grains in these rocks have subgrain walls (Fig. 5.13). Intraphase misorientation angle distribution analyses from all samples shows high frequencies for low angle (<10°) misorientation for amphibole (Fig. 5.13). This would suggest that some plasticity (likely dislocation creep) is involved in the formation of the barroisite LPO. This would suggest that the barroisite LPO is formed in a possible two stages, the first involving mimicry of omphacite and glaucophane, the second involving a bit of plastic strain (dislocation creep) creating subgrain walls.

However other theories for the barroisite microstructural observations are possible, including the idea that said microstructures are inherited from earlier phases. As suggested by the interphase misorientation work presented here, much of the barroisite in these rocks grows mimetically on both omphacite and glaucophane, likely inheriting its LPO in this fashion. We suggest here that it may be possible that subgrains and low angle neighbour misorientation signals in barroisite may also be a function of crystal mimicry. In Chapter 4 it was shown that omphacite contains subgrain walls as well as high low angle intraphase neighbour angle misorientation frequencies and it may simply be this signal that is picked up and copied by the barroisite as it replaces omphacite.

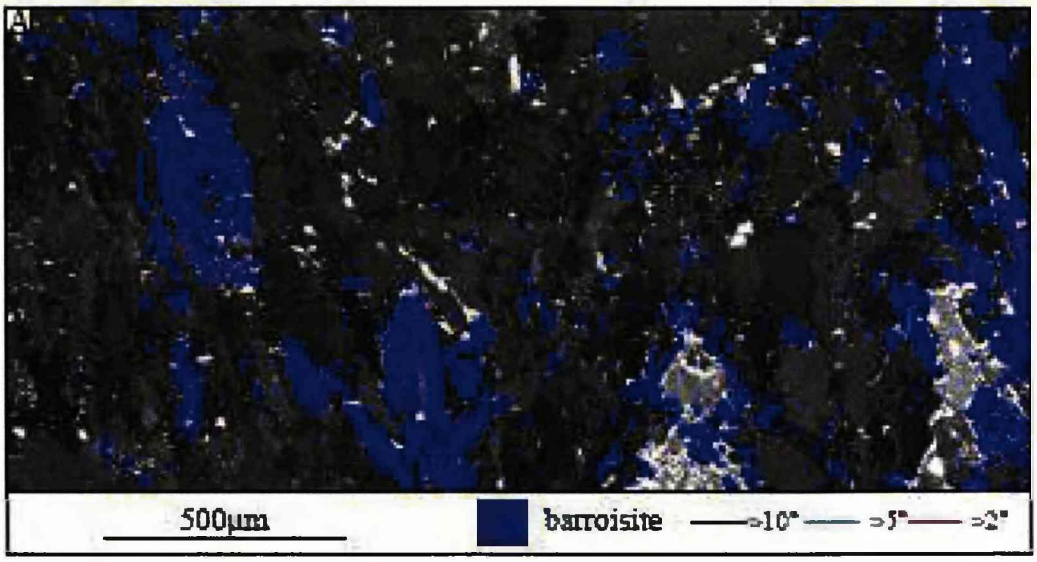

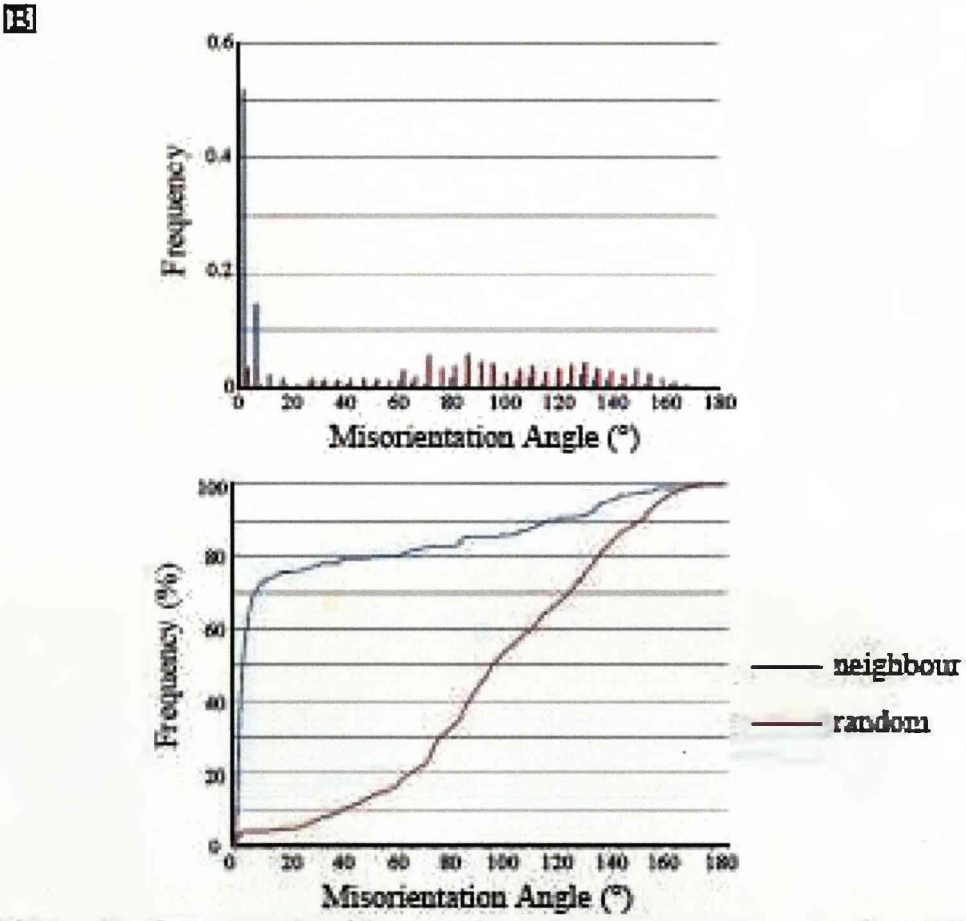

Fig. 5.13 A - Barroisite grain boundary map showing grains contain subgrain walls. B - Barroisite intraphase misorientation distribution graphs

5.6.4 Regional Implications

The data presented here is consistent with development of a barroisite LPO forming through mimicry of a pre-existing omphacite and glaucophane LPO. This has certain meaning for the interpretation of not only the exhumation pathway of this eclogite facies unit but also for how some structural aspects of the Punta Telcio region are considered.

5.6.4.1 Punta Telcio Structure Summary

A penetrative foliation defined by shape and location fabrics described in Chapter 4 exists in all lithologies and foliation geometry is consistent across lithological boundaries. Foliation dip shows a steady increase in angle from the north of the area to the south (Fig. 4.24). This is a result of a large scale recumbent fold structure apparent in this area (Reddy et al. 1999). Azimuth and plunge of the hinge line of this fold is 5° → 274 (Fig. 4.24). Lineations in eclogite facies rocks are omphacite and glaucophane mineral lineations, recorded as stretching lineations in previous studies (Reddy et al., 1999). Lineations in amphibolites are amphibole mineral lineations. Omphacite and glaucophane lineations represent the late prograde/early retrograde stage of the evolution of the area. Amphibolite lineations are plotted separately as they relate to retrogression of the Zermatt-Saas Unit of Punta Telcio. For both groups, most lineation measurements have an easterly azimuth with gentle plunges although at few amphibole measurements have southern azimuths and steeper plunges (Fig. 4.24). In the serpentinite body, serpentine mineral lineations recorded (Fig. 4.24) show southward azimuths with steep plunges are predominant are but easterly azimuths with shallow plunges are also noted.

5.6.4.2 Structural Interpretation

The kilometre scale recumbent fold in this area is part of an isoclinal folding event that affects both the Zermatt-Saas Unit and Monte Rosa Nappe and the contact between the two units. Folding is associated with retrograde growth of glaucophane and titanite, post-dating peak metamorphic assemblages (Reddy et al., 1999). Folds rarely show axial planar fabrics although when found they are defined by greenschist facies minerals indicating folding occurred during greenschist facies retrogression (Reddy et al., 1999). This would suggest folding is contemporaneous with

exhumation, accomplished in this area initially by the extensional Gressoney Shear Zone (Chapter 2). As previously mentioned this shear zone was active around 44-36Ma starting when the area was still experiencing eclogite facies metamorphism (Reddy et al., 1999). Lineations with southward azimuths noted in the serpentinite and amphibolite are thought to be related to flexural slip on foliation surfaces as the rocks folded.

The fold hinge measurement is parallel to the stretching lineations found in most of the lithologies involved in this structure. There are numerous ways in which such a relationship can come about. 1) An array of folds with random or common orientation may be subjected to strain large enough to rotate the folds towards parallelism with subsequent stretching direction (Escher and Watterson, 1974, Sanderson, 1972, Skjernaa, 1980), 2) where the intermediate strain, Y, is perpendicular to the original layering of the fold and deformation takes place under plane strain conditions, buckle folds can develop with axes parallel to the stretching direction and any stretching linear features that form (Grujic and Mancktelow, 1995), 3) a pre-existing well defined linear fabric may exert a mechanical control on a developing fold causing the hinge line to form parallel to the fabric, a process referred to as 'bending anisotropy' (Cobbold and Watkinson, 1981), 4) folds may begin with hinges perpendicular or oblique orientations to the regional transport direction of a shear plane and experience passive rotation to that they become parallel to the transport direction (and subsequently stretching lineations) with increasing strain intensity (Coward and Potts, 1983), 5) stretching lineations and fold hinges may form simultaneously with a common orientation within a constrictional strain field (Krabbendam and Dewey, 1998).

The third process for creating parallelism between stretching lineations and a fold hinge is unlikely to apply here. This model requires the linear feature causing the bending anisotropy to be deformation resistant rods or fibres embedded in a 'weaker' matrix. Here linear features consist of mineral lineations of omphacite, glaucophane and amphibole, the same phases that make up the bulk of the rock they are found in. Although this model could simply require a rock with a strong LPO (making it anisotropic in itself) this still fails to apply to this situation.

It is also unlikely that the parallelism noted here is a cause of simultaneous development of lineation and folding in a constrictional strain field (Mechanism 5). This is due to results described in Chapter 4 associated with the type of LPO formed in the omphacite of the eclogite facies rocks from this area. A strong S-type fabric is recorded in the omphacite of these eclogite facies rocks. It is determined in Chapter 4 that this LPO pattern is not controlled by space group and as such we assume it is created by the strain regime the eclogites were deformed in. As S-type fabrics are thought to form in compressional strain regimes this means that the structural observations made in Punta Telcio cannot be a result of simultaneous folding and lineation development in a constrictional strain field.

Mechanism 2 is unlikely to apply here as the stretching lineation and fold hinge that form in this case do not develop parallel to the principal stress direction X, rather forming parallel to Z. The geometry of the area, structural measurements and previous work show that the fold hinge, lineations and shear indicators are all parallel.

More likely interpretations of this phenomenon lie with the models 1 and 4. As previously mentioned the folding event that produced the structure mapped here took place during greenschist facies conditions as evidenced by greenschist facies axial planar fabrics. This timing does not resolve the coincident stretching omphacite lineation which must have formed during peak metamorphic conditions that also lies parallel to the fold hinge. Exhumation of this area of the Zermatt-Saas Unit occurs due to SE directed extension along the GSZ. If the fold formed during this exhumation the omphacite and likely the glaucophane lineation too would have been folded. Subsequent rotation of the fold hinge into parallelism with the later developing amphibole lineation would rotate the previous lineations into a non parallel orientation.

The possibility exists that the fold actually initiated during eclogite facies conditions due to evidence of fabric mimicry in the greenschist phases presented here. Exhumation of the Zermatt-Saas along the extensional Gressoney shear zone initiated while eclogite facies conditions were still in effect. This fold may have formed during this initial stage and the hinge may have rotated into the SE transport direction matching the SE stretching omphacite and glaucophane lineations.

This leaves us with how the amphibole lineations formed in a parallel direction to the fold hinge. As previously mentioned, in Earth Science, LPO formation is commonly thought to be the result of some plastic deformation event, which if true in this case would imply strain during the greenschist facies retrogression event of the Zermatt-Saas. It is suggested here that this stage of retrogression was static rather than dynamic with most of the barroisite LPO a result of LPO mimicry. Mimetic replacement of omphacite and glaucophane by barroisite may extend to omphacite and glaucophane lineations thus explaining the parallelism of the fold hinge and greenschist lineations.

This leaves the problem of explaining the previously mentioned greenschist facies axial planar fabric used to time the formation of this fault. In light of this area showing amphibole copying fabrics set out by pre-existing eclogite facies minerals means the interpretation of this axial planar fabric must be carefully considered. It is possible that it was originally defined by omphacite and glaucophane but was since replaced statically by amphibole, suggesting in turn that fold development may have been associated with eclogite facies conditions during the burial or early exhumation stage (when movement on the GSZ began) of this tectonic unit.

5.6.5 *Evolution of the Zermatt-Saas Unit in Punta Telcio*

What follows here is a summation of the evolution of the eclogite facies rocks of the Punta Telcio region of the Zermatt-Saas Unit combining results obtained in both this chapter and Chapter 4.

Subduction leads to eclogite facies metamorphism developing common eclogite minerals; omphacite and garnet. Omphacite accommodates the majority of the strain on the rock during this period with garnet behaving passively. Omphacite first deforms by dislocation creep followed by diffusion creep to create an S-type LPO. From this we assume this area of the Zermatt-Saas Unit was experiencing a flattening strain regime at this period of its evolution. Diffusion creep occurs in tandem with early exhumation of the unit as evidenced by retrogressive preferred chemical zoning patterns. Retrogression through blueschist facies conditions results in the growth of glaucophane which also forms an LPO possibly through plastic deformation likely in tandem with omphacite.

As exhumation begins along the Gressoney Shear Zone, folding of the Punta Telcio region begins, creating a large kilometre scale recumbent fold in the area. Omphacite and glaucophane stretching lineations develop parallel to the fold hinge due to large enough strains rotating the fold hinge parallel to the stretching direction.

Further exhumation leads to greenschist facies conditions. Green amphibole develops as the predominant phase here. Barroisite growth occurs early in this stage, mimetically replacing both omphacite and glaucophane, developing an LPO that incorporates components of both pre-existing LPO patterns. This stage of exhumation is static rather than dynamic though it is likely a small amount of strain occurred late in this stage forming subgrain walls in barroisite. Lower greenschist conditions occur with further exhumation noted by the change in amphibole chemistry from barroisite to magnesio-hornblende and actinolite. This latter stage partially replaces the barroisite grains in this rock.

5.7 Conclusions

From the results presented in this chapter it is shown that orientation data can be successfully used to identify the existence of mimetic LPO formation. D-D, P-P and PD-PD maps as well as interphase misorientation angle distribution analysis are excellent tools to investigate this phenomenon.

Applying these techniques to an investigation of retrogressive barroisite in the eclogite facies rocks of the Zermatt-Saas has resulted in the discovery of a 'special orientation relationship' of barroisite on omphacite such that it preferentially replaces the mineral through a 180° rotation around the <001> axis of omphacite. The same techniques show that this retrogressive barroisite also shows a direct crystal orientation replacement of pre-existing glaucophane, copying the crystal lattice exactly. Therefore the resulting barroisite LPO is mainly formed in these rocks by mimicry of both a pre-existing omphacite and glaucophane LPO, combining elements of each with the possibility that some crystal plasticity was involved also. <001> and (010) pole figures contain elements found in omphacite and glaucophane LPO patterns and (100) pole figures contain patterns common to glaucophane LPO patterns but not omphacite LPO patterns.

Assuming the barroisite LPO develops via mimicry of a pre-existing omphacite and glaucophane LPO leads to the suggestion that greenschist retrogression and exhumation of the Zermatt-Saas Unit in this area was at least for a time static. Possible implications for the structural interpretation of a kilometre scale fold in this area show also that mimetic fabrics must be carefully considered in any microstructural interpretation of a polymetamorphic rock when attempting to interpret its metamorphic and structural evolution.

6 Chapter 6: Microstructures of the 'Streaked Eclogite' Lithology and Eclogite Pods of Colle della Barme d'Oropa, Sesia-Lanzo Zone

6.1 Introduction

The Sesia-Lanzo Zone is an eclogite facies, tectonic slice of continental crust, one that has previously experienced a significant tectonic and metamorphic history prior to the Alpine Orogeny, as discussed in chapter 2. As emphasized throughout the thesis deformation of eclogite facies rocks may play a key role in understanding the rheology and dynamics of the geological environments they are formed in. As omphacite and garnet are typically the two main mineral constituents of eclogite facies rocks the properties of these minerals will make a significant contribution to the behaviour of the rock.

As the Sesia-Lanzo Zone is a unit with a long tectonic and metamorphic history it is important to determine how much of the deformation features observed in eclogite facies rocks of this unit may have been inherited from deformation features of previous tectonic events. In other words how much pre-Alpine deformation is preserved but modified during the Alpine Orogeny in the Sesia-Lanzo Zone.

With this in mind the aim of this chapter is to determine how the streaked eclogite lithology of the Colle della Barme d'Oropa area of the Sesia-Lanzo Zone developed its eclogite facies location fabric. The rock is noted for its banded appearance which defines a strong location fabric, the main component of foliation in this lithology. Alternating pink and green bands relate to layers of garnet and omphacite respectively. Is this location fabric related to inheritance from an earlier location fabric or did it form during Alpine deformation and eclogite facies metamorphism?

In addition this chapter will also aim to investigate omphacite and garnet microstructure to resolve what, if any, deformation mechanisms were in operation in these minerals and to determine the implications they may have on the behaviour of this area of the Sesia-Lanzo Zone during burial and exhumation.

6.2 Geological Setting

A full and detailed summary of the geology of the Sesia-Lanzo Zone in contained in Chapter 2 of this thesis. What follows here is a brief description of the geology of the Sesia-Lanzo Zone as found in the study area of Colle della Barme d'Oropa. It is located in the Monte Mars nature reserve on the mountain ridge between Val di Gressoney and Val Sesia (Fig 6.1). The area contains excellent exposure of rocks associated with the Eclogitic Micaschist Complex (EMC) sub division of the Sesia-Lanzo Zone (Chapter 2).

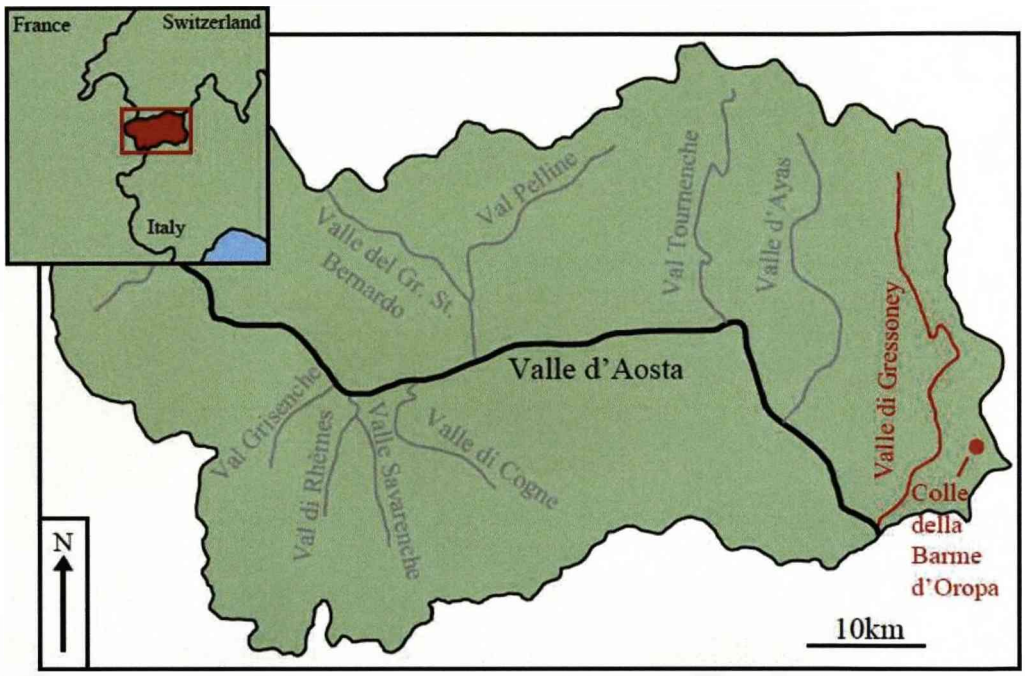

Fig. 6.1 Map of the Val d'Aosta province of Italy showing the location of Valle di Gressoney and the location of Colle della Barme d'Oropa. The inset shows the location of the province in a larger European setting.

The Eclogite Micaschist Complex (EMC) is the main lithology exposed in this study area but other lithologies such as streaked eclogite, aplite sheets and undeformed eclogite pods, occur within it in various amounts. The EMC contains a pervasive foliation defined by both a white mica shape fabric and by quartz and white mica bands forming a location fabric. In places the bands responsible for the location fabric bands are quite thick (~2-15cm) giving the rock a more gneissic appearance (Fig 6.2).

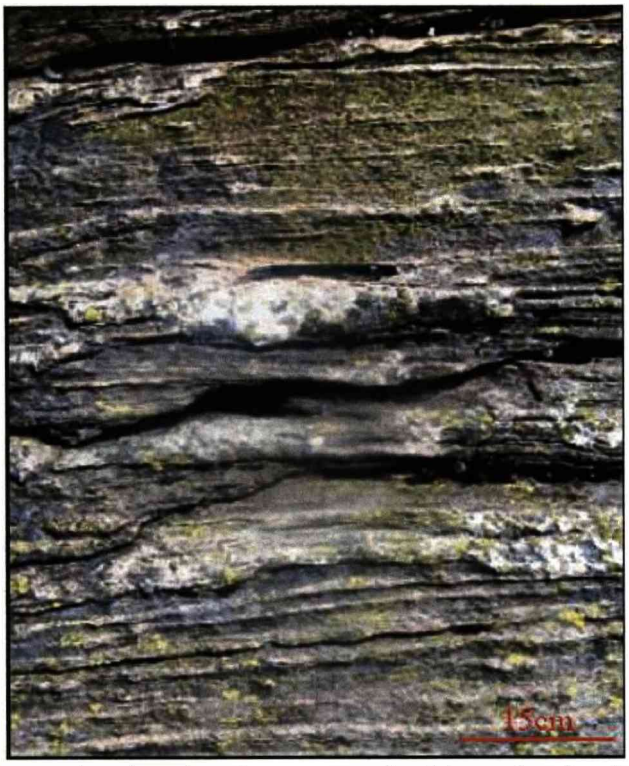

Fig. 6.2 Thick alternating bands of quartz and white mica in the EMC giving it a gneissic appearance

Though this lithology is predominantly composed of white mica and quartz, pink garnet and pale green omphacite can also be distinguished. Omphacite preservation within the lithology is variable, with most grains showing some degree of symplectite replacement. Omphacite forms a shape fabric consistent with previously described foliation fabrics in this lithology. In some areas omphacite occurs in bands forming another component of the previously mentioned location fabric.

Other features of the lithology include large white/buff coloured patches, likely feldspar or zoisite, and large dark grains of glaucophane. It is difficult to define texturally whether glaucophane grains formed contemporaneously with high pressure phases (white mica, omphacite and garnet) or if it represents a later blueschist retrogressive event as noted in other areas of the Sesia-Lanzo Zone (Williams and Compagnoni, 1983). Rutile is present as an accessory mineral, occasionally rimmed by sphene. Other minerals are retrogressive in origin including green amphibole and biotite.

The structural geology of Colle della Barme d'Oropa consists mainly of a complicated series of folds and refolded folds defined by the foliation fabrics of the previously described EMC, and to a lesser extent by the foliation fabrics of the other lithologies (Fig. 6.3). In addition folds also contain parasitic folding with classic, s, m and z forms (Fig. 6.4). Foliation geometry is independent of lithological boundaries in the study area and measurements of strike and dip are consistent across them. In exception to this are the rare eclogite pods which remain undeformed within the lithologies that contain them.

Aplite in Colle della Barme d'Oropa occurs as intrusive pale white rocks in the EMC. Cross cutting relationships vary throughout the area with some aplite intrusions appearing to cut the foliation of the EMC and others appearing to run parallel to it (Fig. 6.5). White mica forms a shape fabric defining a foliation in this lithology. Foliation geometry is consistent across EMC/aplite contacts regardless of cross cutting relationship between the two.

Omphacite in aplite sheets is rare and relics mostly remain as polycrystalline polymorphs and patches (~1mm) composed of microcrystalline mica, plagioclase and quartz. Where actual omphacite grains are found they have elongate shapes defining a shape fabric which is consistent with previously described shape and location fabrics. Garnet is rare and grains have sizes between ~200μm-2mm. Dark green amphibole occurs throughout the aplites and is likely an indication of the greenschist facies event that occurred throughout the entire Sesia-Lanzo Zone.

Structural features of aplite intrusions, such as its crosscutting relationships with the country rock and an Alpine planar shape fabric, are relevant to the idea that location fabrics in the country rock (EMC and streaked eclogite) may be inherited from fabrics formed during previous deformation events of the Sesia-Lanzo Zone. Location fabrics can form due to 1) inheritance of banded chemical heterogeneity in the protolith, 2) shearing of chemically distinct objects into layers (probably implying high strains) 3) metamorphic segregation such as the process which forms crenulation cleavage and 4) other poorly understood metamorphic segregation processes such as that discussed by Robin (1978). Mechanisms two and three likely require significant strain. If location fabrics described in the EMC and streaked eclogite (see 6.2.2) are Alpine in origin then significant strain would have occurred

during the Alpine Orogeny. If so observed crosscutting relationships between aplite sheets and the country rock in this study area would be less likely to be preserved rather the aplite sheets would tend to be transposed during high strain. Also a location fabric would likely have developed in the aplite rather than just the observed white mica shape fabric. Thus we must consider the possibility that the location fabric in streaked eclogite and EMC is inherited from pre-Alpine fabrics and subsequently modified during the Alpine Orogeny (eclogite facies mineral development and folding). If so it is hoped omphacite and garnet in the streaked eclogite lithology may show microstructural evidence to support this theory. To determine this EBSD and EDX techniques are carried out on these two minerals.

In addition EBSD and EDX analysis were carried out on omphacite in undeformed eclogite pods. This latter lithology may contain information on omphacite microstructures that develop solely due to grain growth. Comparison of microstructures in omphacite of both lithologies may provide insight as to whether the eclogite facies location fabric is inherited, if they prove to be similar.

Fig. 6.3 Field photographs of tight recumbent fold structures in Colle della Barme d'Oropa. A - a larger scale fold B - a smaller scale fold

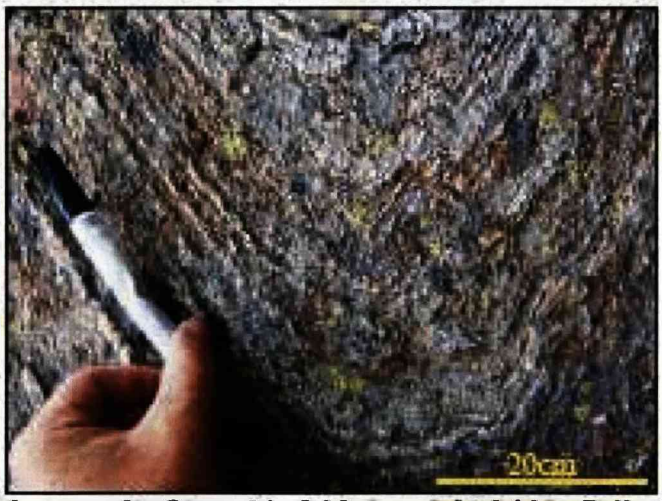

Fig. 6.4 Field photograph of parasitic folds in a tight fold in Colle della Barme d'Oropa

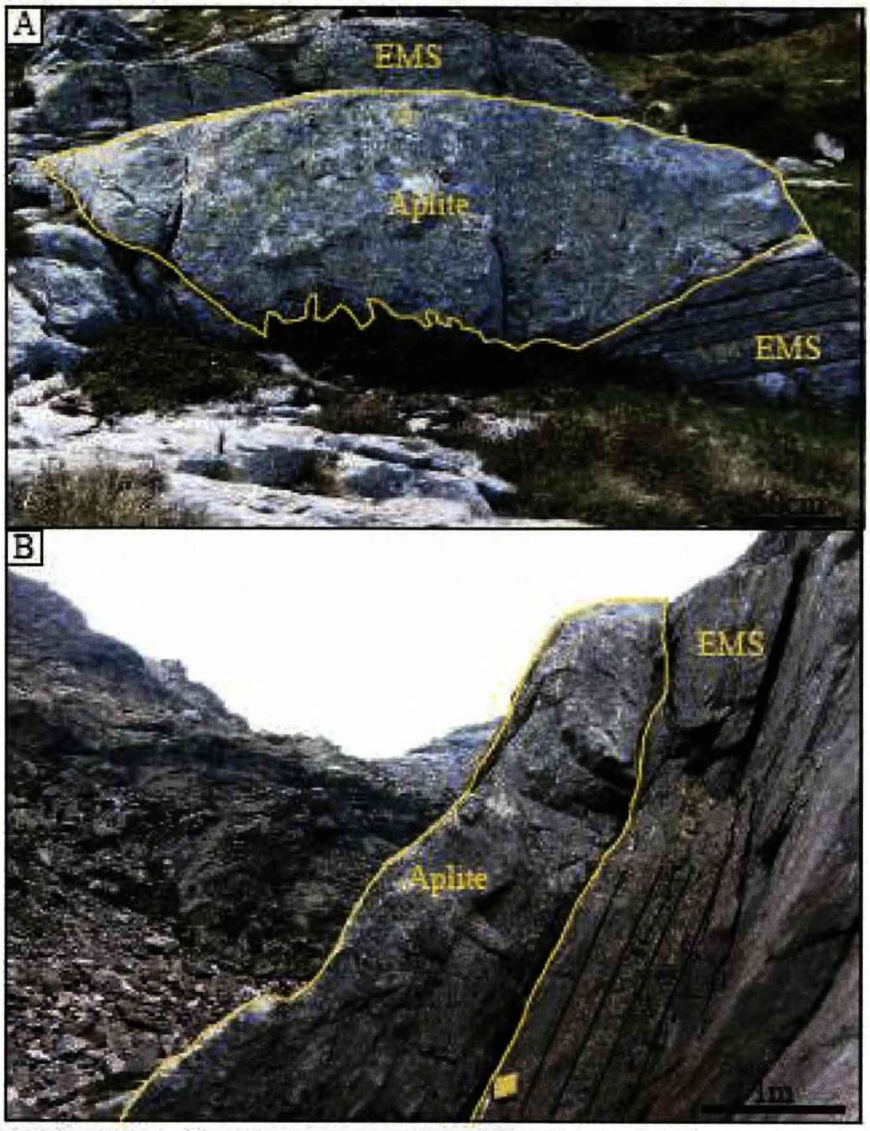

Fig. 6.5 Photographs of aplite cross cutting relationships in Colle della Barme d'Oropa. A - cutting across foliation in the EMC lithology and B - parallel to the foliation in the EMC lithology

6.2.1 Eclogite Pod Petrography

Eclogite pods, consisting solely of garnet and omphacite, are dotted throughout the EMC lithology. They appear undeformed, lacking the foliations and lineations evident in the lithologies that contain them. Foliation of lithologies containing these pods can be seen to be deflected around them (Fig. 6.6).

Large slightly elongate, grains of pale to dark green omphacite dominate the rock. These elongate grains appear to be randomly oriented. Large (~1cm) and small (~1-2mm), dark red/pink garnet grains are present and are euhedral to subhedral in shape. Larger garnet shows numerous, green coloured inclusions, likely omphacite. Quartz veins occasionally run though both phases of this lithology.

Large (~1mm-5mm) omphacite grains observed in thin section display fan like forms, with each fan randomly oriented within the pod (Fig. 6.7). Fans appear to be made of a composite of narrow, elongate, aligned, omphacite grains or subgrains inferred from variation of extinction angle and birefringence within each single fan like grain. Omphacite fans abruptly terminate at contact with garnet grains. In thin section smaller, irregular shaped omphacite grains are also present and contain irregular shaped areas of variable extinction. The occurrence of what may be subgrain boundaries within omphacite grains possibly indicates a microstructure that can form from omphacite growth free of strain.

Garnet grains are poikiloblastic and heavily fractured with aligned, elongate omphacite grains as the dominant inclusion. These elongate inclusions are oriented identically to the elongate direction of omphacite fans bordering garnet grains suggesting garnet grew later or in tandem with their growth (Fig. 6.8A). Other inclusions include quartz and a dark green amphibole. Small quartz fractures occasionally cut through garnet grains.

Retrogressive amphibole and biotite are present throughout the eclogite pods mainly concentrated around the garnet or as inclusions within the garnet (Fig. 6.8B). This is representative of the greenschist facies event that pervasively overprinted eclogite mineralogy of the Sesia-Lanzo Zone.

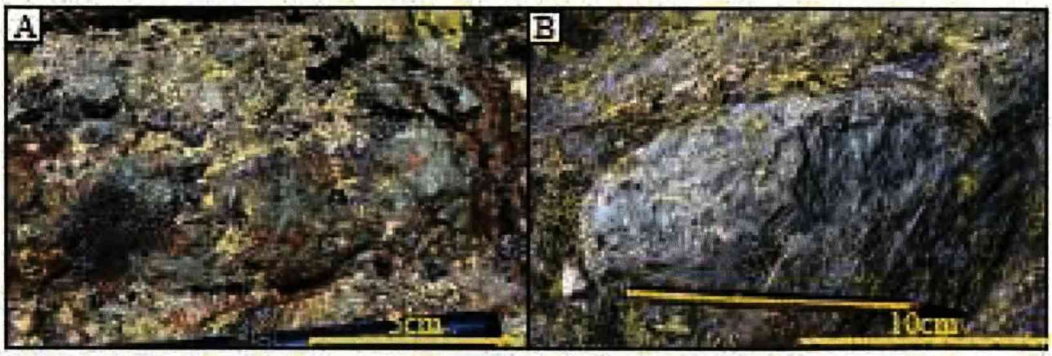

Fig. 6.6 Photographs of two eclogite pods within the EMC lithology. A - Pod with large garnets easily visible B - Pod with little to no garnet content, composed primarily of green omphacite

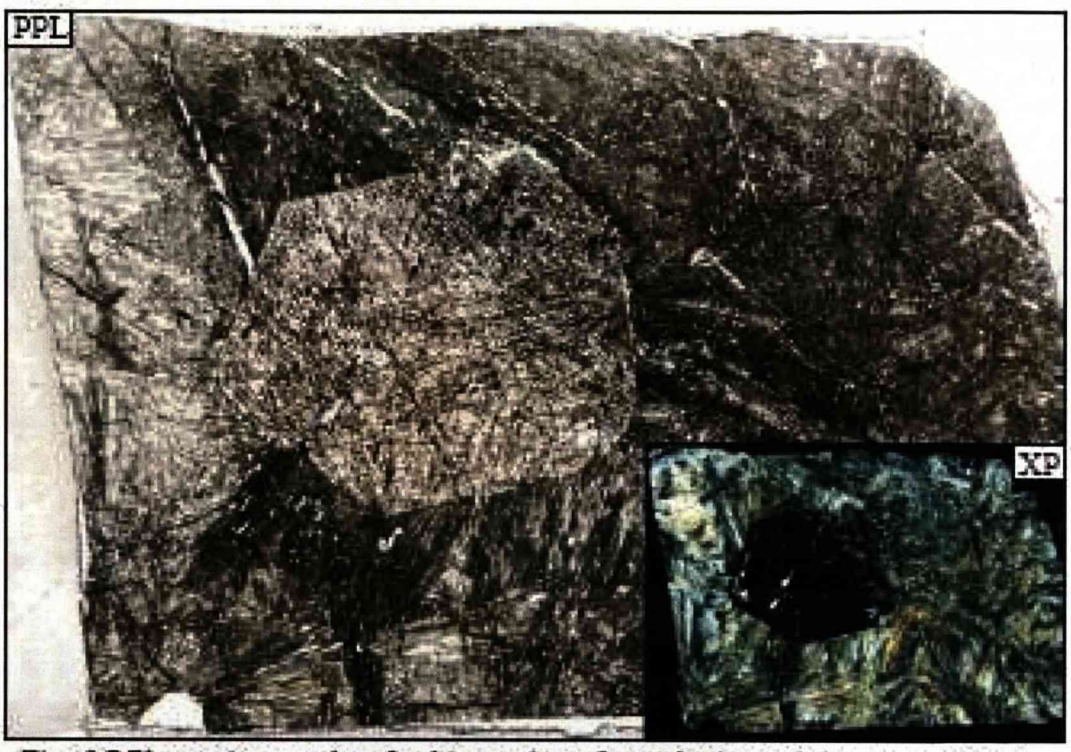

Fig. 6.7 Photomicrogrpahs of a thin section of an eclogite pod showing a single large garnet porphyroblast and many randomly oriented omphacite fans

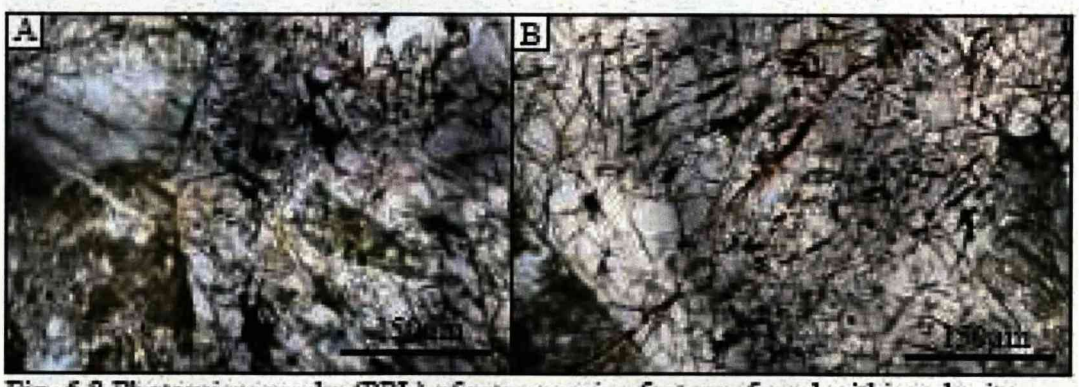

Fig. 6.8 Photomicrogrpahs (PPL) of retrogressive features found within eclogite pods. A - amphibole growth on garnet, B - biotite growth along fractures in the pod

6.2.2 Streaked Eclogite Petrography

The 'streaked eclogite' lithology occurs mainly in the eastern area of the colle and becomes less common further west. Lithological boundaries between this lithology and the EMC are difficult to observe and no definite contact is noted. Foliation and lineation measurements from neighbouring outcrops of EMC and streaked eclogite are unchanging, although the minerals and fabrics defining these structural elements do.

This eclogite facies rock earns its 'streaked' prefix from its appearance in the field (Fig. 6.9). It consists of alternating green and pale pink bands corresponding to concentrations of omphacite and garnet respectively. These bands create a location fabric in this lithology defining the foliation. Quartz and white mica are also present with the latter forming a shape fabric parallel to the location fabric. Mineral lineations of quartz are observed.

Omphacite bands are composed of large, elongate omphacite crystal laths that in some cases taper to a point (Fig. 6.10). When viewed on foliation surfaces the long axes of these omphacite grains are seen to have variable orientation. Inclusions within the omphacite grains consist mainly of small crystals of garnet and quartz. Large omphacite crystals have well defined, elongate areas of variable extinction and birefringence (Fig. 6.11) suggesting a polycrystalline or subgrain nature. The long axes of these elongate grains/subgrains create an omphacite shape fabric parallel to the long axis of the overall large omphacite grain. In some cases however these large elongate omphacite grains do not display much internal detail and the whole grain will go into extinction under crossed polars at the same orientation and birefringence will vary only slightly. Smaller, irregular shaped patches of omphacite occur but are less common (Fig. 6.12). As with the larger, elongate grains, these patches display variable extinction suggesting a polycrystalline or subgrain internal structure for them as well. Another similarity that the irregular omphacite grains share with the elongate grains is that occasionally these grains display little internal structure.

Garnet layers of 'streaked eclogite' are composed of large amounts of fine grained (~250μm), euhedral-subhedral, touching garnets with quartz, omphacite, zoisite and

white mica scattered randomly within the layers (Fig. 6.13). Also present in this rock are small (~250μm), isolated garnets, or isolated clusters of small garnets.

Layers of quartz and white mica also form a location fabric consistent with that defined by omphacite and garnet layers. Quartz has irregular grain shapes whereas white mica defines a shape fabric as previously mentioned. White mica is partially replaced by retrogressive biotite in places. Rutile is also present as an accessory mineral in this rock, occasionally with a retrogressive sphene rim.

The large, elongate omphacite grains occasionally have fractures that cross their width containing retrogressive fills of green amphibole and chlorite (Fig. 6.14). These fractures can be quite wide (~1mm) and amphibole and chlorite grow across them as fibrous, elongate growths. In places omphacite grains are rimmed by green amphibole and chlorite.

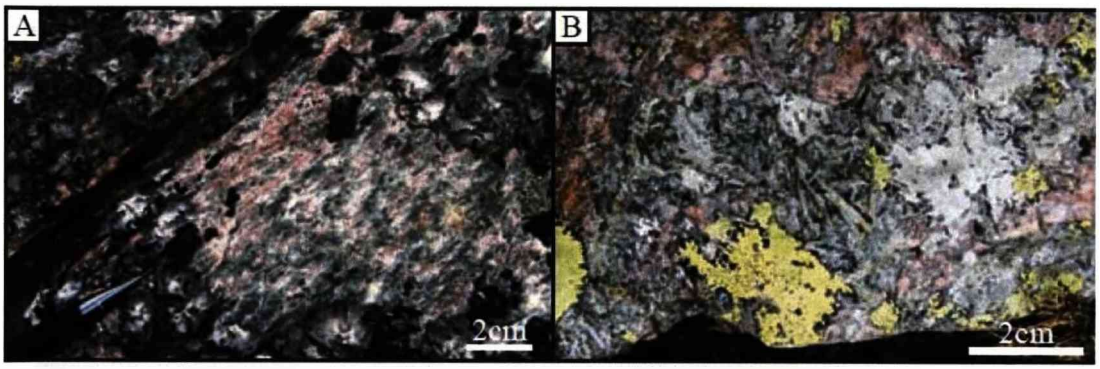

Fig. 6.9 A – Streaked eclogite showing pink garnet and green omphacite banding, B – Large elongate omphacite grains of the streaked eclogite lithology

An investigation of the large grains of omphacite described here is integral to understanding how this eclogite facies rock may have deformed during burial and exhumation. From optical microscopy omphacite in this lithology appears to contain interesting microstructures. The occurrence of what may be numerous subgrains is often indicative of the action of dislocation creep (Godard and Van Roermund, 1995, Mauler et al., 2001, Jin et al., 2001, Piepenbreier and Stöckhert, 2001). However it is noted that the shape and microstructure of omphacite grains in this lithology closely resembles those described from omphacite in undeformed eclogite pods of this area. It is vitally important for understanding the evolution of this rock to determine whether omphacite microstructures are similar enough to those in omphacite of

undeformed eclogite pods to suggest they are a result of grain growth or whether they formed by crystal plastic processes.

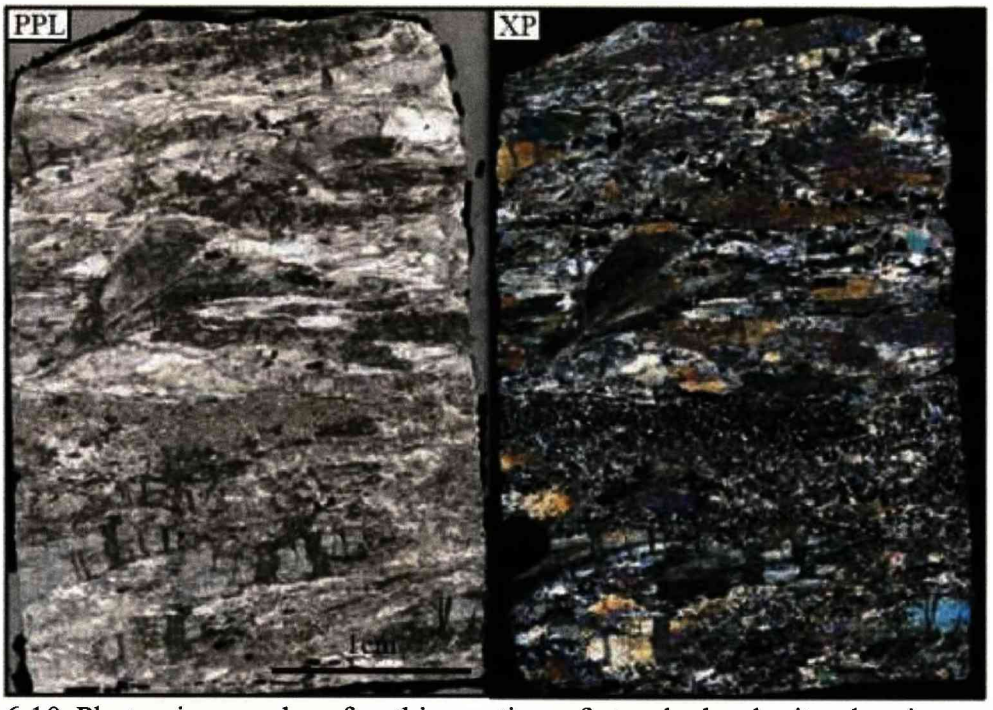

Fig. 6.10 Photomicrographs of a thin section of streaked eclogite showing garnet layers and large elongate grains of omphacite

To determine what mechanism created observed omphacite microstructures EBSD and EDX was carried out on a number of omphacite grains from this lithology. A similar study was performed on a sample of an undeformed eclogite pod. The eclogite pod is intended as a control for this study as omphacite grain size within it is comparable to that found in the streaked eclogite lithology. As already mentioned the pod has not experienced any significant deformation, as it contains no foliation or lineation, although the surrounding more quartz-rich rocks locally display a strong foliation which wraps the pod.

In addition to the omphacite study EBSD and EDX work is carried out on the layers of small, tightly packed garnet grains. As previously discussed (chapter 1) garnet is thought to contribute little to eclogite deformation, though recent studies have shown plastic behaviour and grain boundary sliding can be quite common. Orientation and chemical data are used here to determine whether deformation mechanisms were acting in garnet grains and whether these may be responsible for garnet concentration in layers. In addition such a study may reveal implication for the behaviour of this lithology during burial and exhumation.

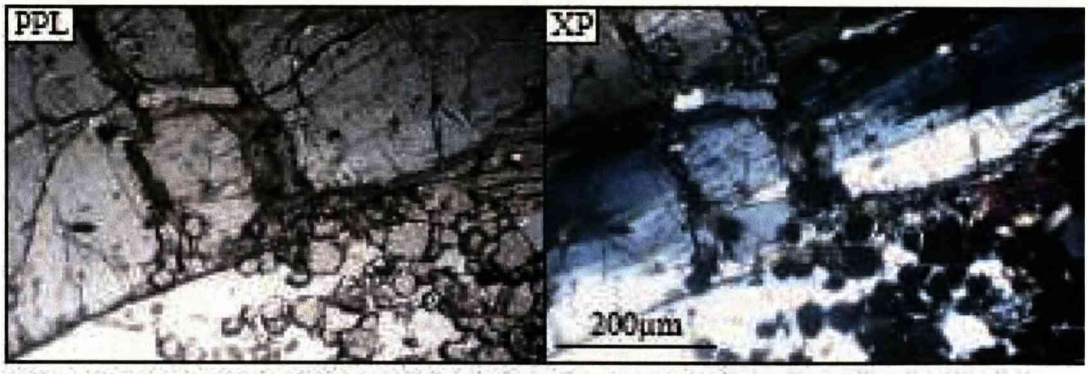

Fig. 6.11 Photomicrographs of elongate areas of variable extinction within large omphacite grains of the streaked eclogite lithology

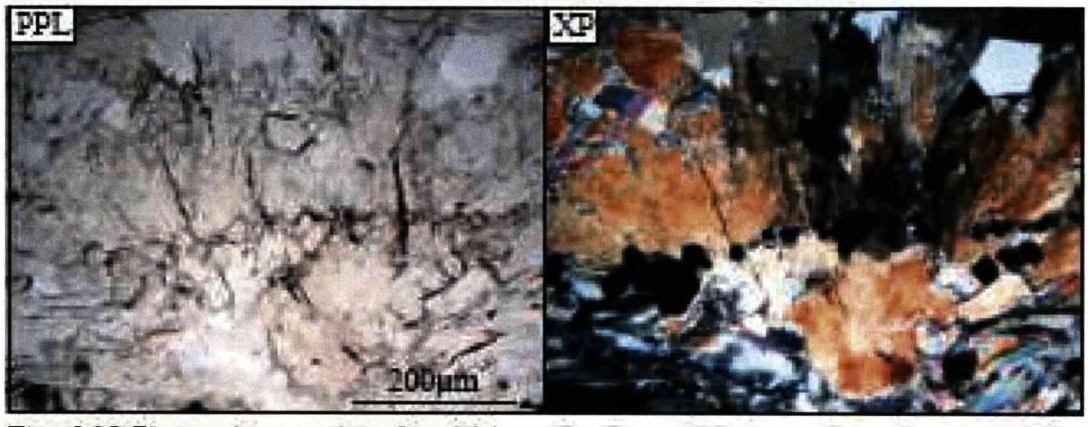

Fig. 6.12 Photomicrographs of variable extinction within large, irregular, rounded omphacite grains of the streaked eclogite lithology

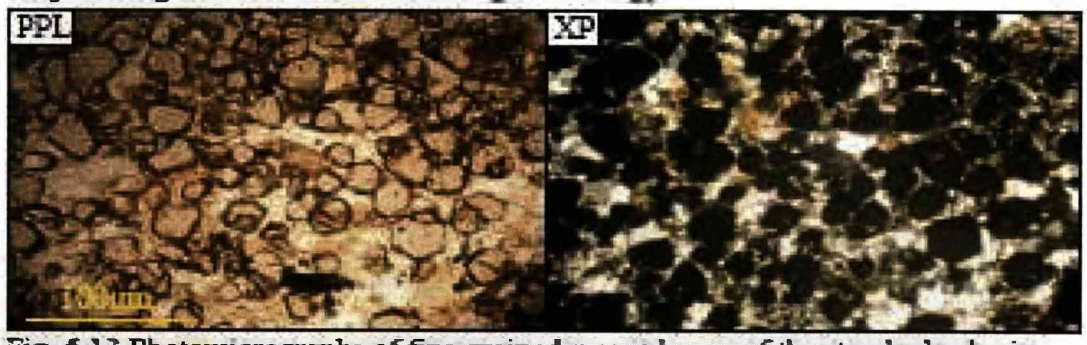

Fig. 6.13 Photomicrographs of fine grained garnet layers of the streaked eclogite lithology

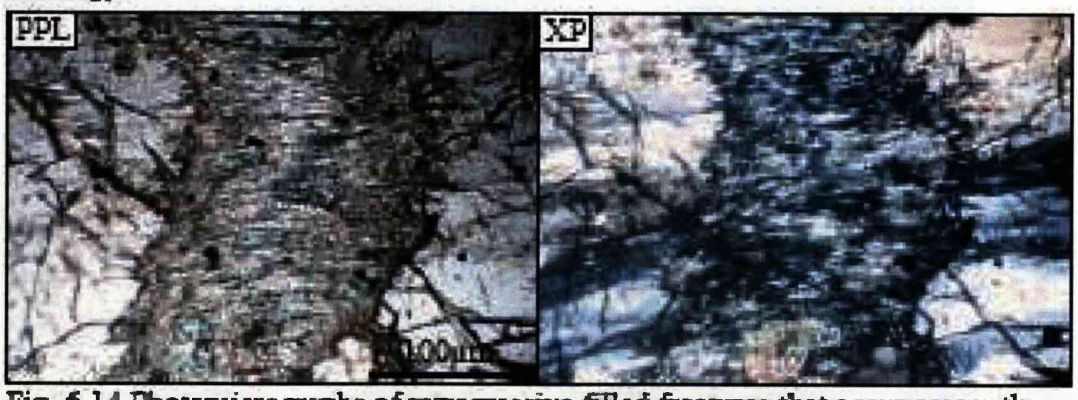

Fig. 6.14 Photomicrographs of retrogressive filled fractures that occur across the width of large, elongate omphacite grains of the streaked eclogite lithology

6.3 Omphacite Microstructure and LPO in the Streaked Eclogite Lithology and Undeformed Eclogite Pods from the Colle della Barme d'Oropa

6.3.1 Eclogite Pod Results

6.3.1.1 Omphacite LPO

Pole figures for eclogite pod sample S7.1 are shown in Fig. 6.15 and were created by scanning a thin section of the undeformed eclogite pod using the STscan method (Table 6.1) and show that omphacite has an LPO pattern. However this apparent LPO pattern must be analysed in context to the overall observations made on this lithology, namely that coarse grained omphacite grains have random shape orientations as observed in pod hand specimens. Given the large grain size of omphacite in this lithology, the thin section, from which omphacite orientation is derived to plot pole figures, may not contain a sufficient sample size of omphacite grains to give an overall picture of the omphacite texture of this lithology. A key feature of this apparent LPO pattern is that it is not aligned parallel to specimen axes which are linked to the fabrics in surrounding lithologies. As explained in the following section, c-axes of the omphacite grains are parallel to the omphacite grain length. A significant portion of the thin section used here to generate these pole figures happens to be dominated by a large grain, the long axis of which is oriented roughly perpendicular to the structural framework of the fabric in the surrounding lithology.

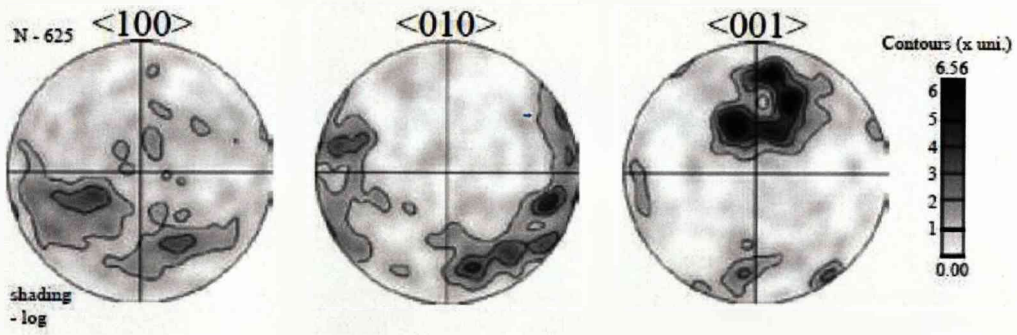

Fig. 6.15 Omphacite pole figures for eclogite pod sample S7.1

6.3.1.2 Omphacite Grain Microstructure, Single Grain Pole Figures and Misorientation Angle Distribution Analyses

Fig. 6.16 shows EBSD maps of an area of eclogite pod sample S7.1 contains a number of omphacite grains. Both large omphacite grains with fan like microstructural textures and smaller, irregular omphacite grains are evident. A grain boundary map of this area reveals large numbers of grain (>10°) and subgrain (2-10°) boundaries within single omphacite grains. Boundaries in omphacite grains that display fan like textures (indicated by variable extinction and birefringence) define parallel, elongate shapes which correlate with this fan like microstructure. In the rounded, irregular grains they display more irregular shapes. A texture component map shows sharp colour changes that replicate the patterns observed in thin section and grain boundary maps.

Pole figures (with the data points coloured to match the texture component map) for both a large omphacite grain with a fan like texture and an rounded grain with irregular grain and subgrain boundary shapes show that <100> and <010> poles display significant rotation around the <001> axis. Misorientation profiles across the fan like omphacite grains, perpendicular to subgrain boundary traces, show misorientations of ~50°. Misorientation profiles parallel to subgrain boundaries in the same grain show smaller misorientations of ~10°. Misorientation profiles across the rounded omphacite grain in various directions show cumulative misorientations of up to 120°.

Omphacite misorientation angle distribution analysis of the eclogite pod shows high frequencies of low angle misorientations (<10°) between omphacite neighbour pair pixels compared to low frequencies between random pair pixels. This pattern persists up to ~20° misorientation after which random misorientation angle frequency is higher than neighbour pair angle frequencies. Cumulative frequency graphs show neighbour pair misorientation lines shifted to the left compared to random pair misorientation lines, reiterating the high frequency of lower angle misorientations.

As stated in Wheeler et al. (2001) a significant difference between the neighbour and random pair distributions (as observed in the omphacite data here) suggests neighbouring grains have undergone a physical interaction and/or neighbouring pairs

have been derived in a significant number of cases from a common parent microstructure: inheritance. Further investigation is required to determine which mechanism produces the pattern observed for omphacite here.

Usually the occurrence of omphacite subgrain boundaries and a high frequency of low angle neighbour pair misorientations would suggest the action of dislocation creep (Buatier et al., 1991, Philippot and van Roermund, 1992, Brenker, 1998, Brenker et al., 1999, Bascou et al. 1991, Bascou et al., 2002, Ulrich and Mainprice, 2005) possibly operating in tandem with a diffusive mass transfer process or anisotropic grain growth. However as mentioned the eclogite pod is undeformed and so the microstructures displayed here by omphacite must be growth related. This leaves the question of how the multiple subgrain boundaries and significant rotation around the <001> axis formed within the omphacite grains.

As discussed in chapter 1, omphacite growth is affected by anisotropic growth and dissolution rates (Van Panhuys-Sigler and Hartman, 1981, Godard and van Roermund, 1995). Dissolution/growth rates are faster for the <001> direction than in the <100> direction which is faster again than the <010> direction. As the <001> direction is parallel to alignment of omphacite fans (as can be seen from single grain pole figures) it can be assumed that this process is likely strongly involved in creating the observed microstructural texture in the omphacite grains in this eclogite pod.

There are a few theories that may explain the formation of subgrain boundaries due to omphacite grain growth. The first involves the possibility of lineage structures or lineage boundaries in omphacite. Lineage structures are noted in other minerals such as quartz (Carstens, 1967) and pyrite and beryl (Petreus, 1978) and are crystalline growth structures that divide a crystal into separate parts that are slightly misoriented relative to each other. In quartz these lineage structures form in grains with high dislocation densities which are rearranged into low angle boundaries. These dislocations are produced where non-structural impurities are trapped during rapid grain growth. The microstructural textures and misorientation patterns described here for omphacite may represent similar growth structures for this mineral with dislocations supplied by small garnet and quartz inclusions. These lineage boundaries combined with preferential growth in the <001> direction would result in the fan like

omphacite grain forms (Fig. 6.17A). In quartz lineation boundaries are noted to be sub-parallel to the c axis direction (Carstens, 1968) which is also the faster growth direction in quartz (Shelley, 1983).

A second possibility may involve multiple omphacite nucleations on a grain of a protolith phase. Orientation of these omphacite nuclei may have been similar but not identical thus creating low angle subgrain boundaries between neighbouring areas of omphacite growth (Fig. 6.17B). Grains continue to grow and again, due to anisotropic omphacite grain growth, results in the elongate grains parallel to the faster growing <001> direction.

A final theory for production of the observed omphacite microstructure may be that as omphacite first began to develop it was in fact subjected to some deformation and subgrains developed as a result of plastic deformation processes (Fig. 6.17C). Deformation on the eclogite pod then ceased and anisotropic grain growth took over resulting in large randomly oriented grains growing into the current observed texture.

Which of these theories explains the microstructure of omphacite in this eclogite pod is however difficult to ascertain. The first theory may indeed be possible though it has not been documented in omphacite before. The second theory cannot be exclusively proven as there are no textural observations of what the parent material may have been previous to omphacite development. The third theory is possibly least likely as even some deformation during the early development stages of omphacite has the potential to create even a weak preferred orientation within the omphacite grains which is completely lacking in the eclogite pod pole figures.

6.3.1.3 Chemistry

The area of the undeformed eclogite pod investigated using EBSD (Fig. 6.18) is mapped chemically to see if the undeformed omphacite grains displayed any chemical growth zoning or whether any chemical patterns associated with the various microstructural textures existed. EDX Al, Ca, Fe and Mg chemical maps show that there are no significant chemical variation within them and no discernable chemical zoning patterns. Lack of zonation in omphacite chemistry holds possible implications for the evolution of this area of the Sesia-Lanzo Zone and these are addressed later in the chapter.

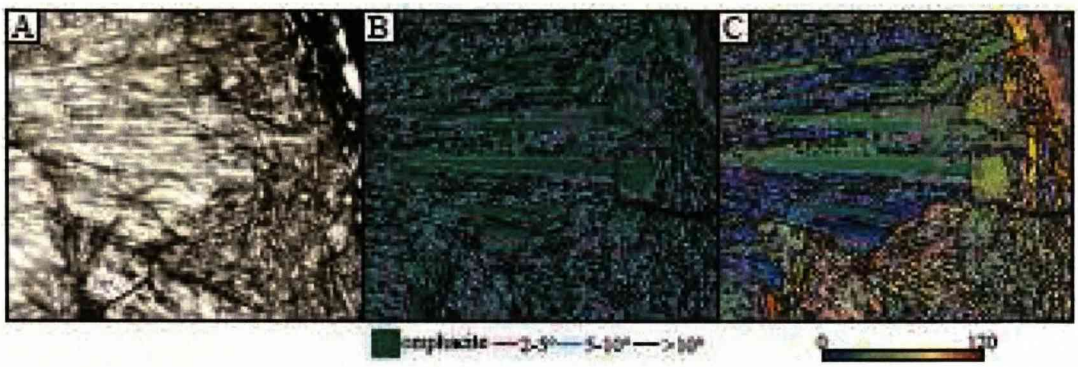
A
B
C
2-5°
5-10°
>10°
0
120

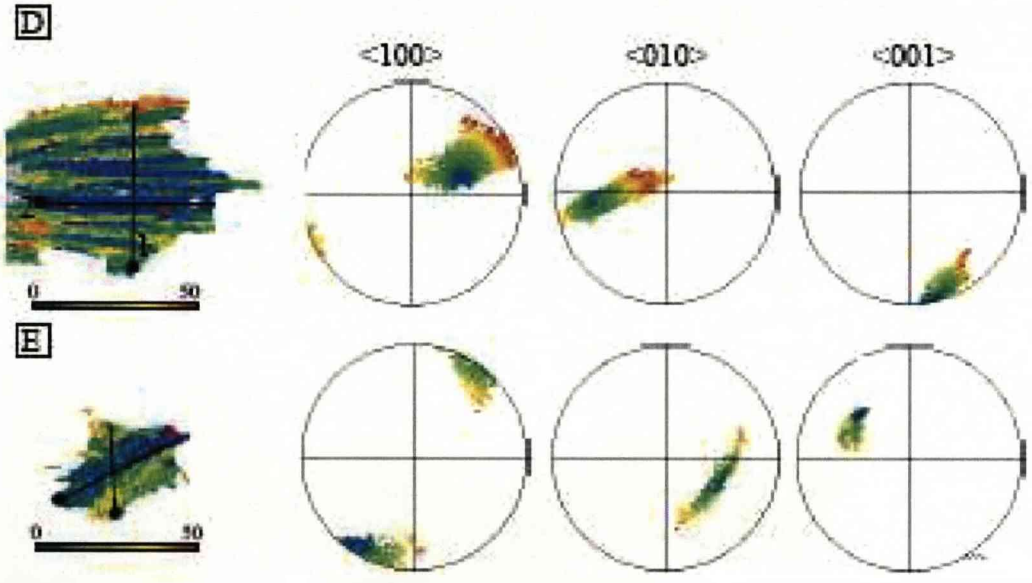
D
<100>
<010>
<001>
0
50
E
0
50

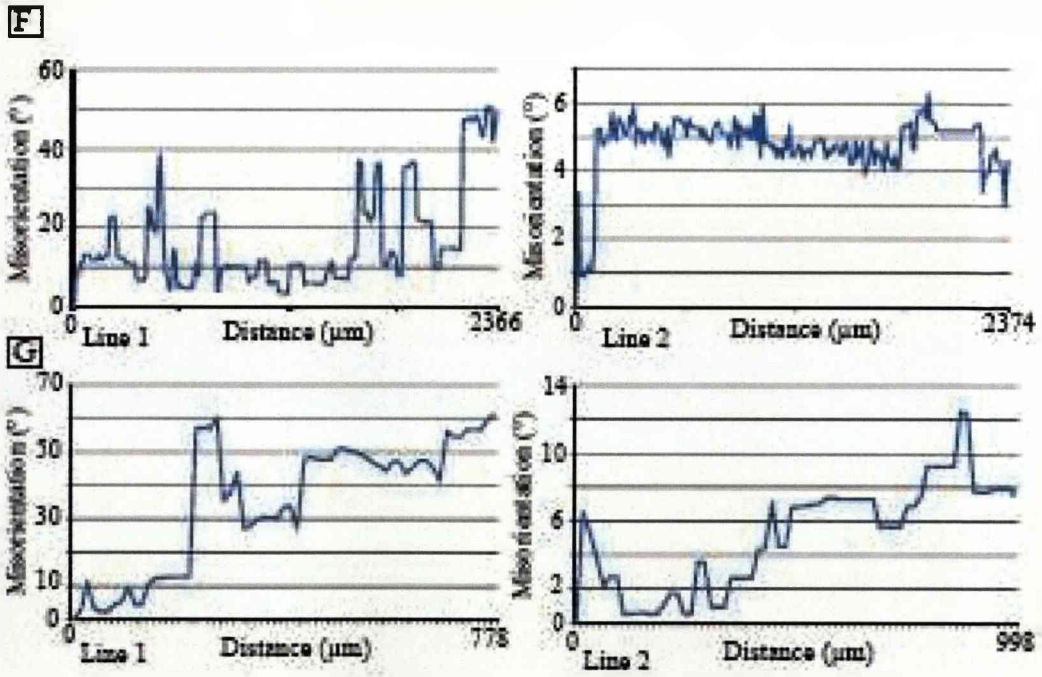
F
Misorientation (°)
60
40
20
0
Line 1
Distance (µm)
2366
Misorientation (°)
6
4
2
0
Line 2
Distance (µm)
2374
G
Misorientation (°)
70
50
30
10
0
Line 1
Distance (µm)
778
Misorientation (°)
14
10
6
2
0
Line 2
Distance (µm)
998

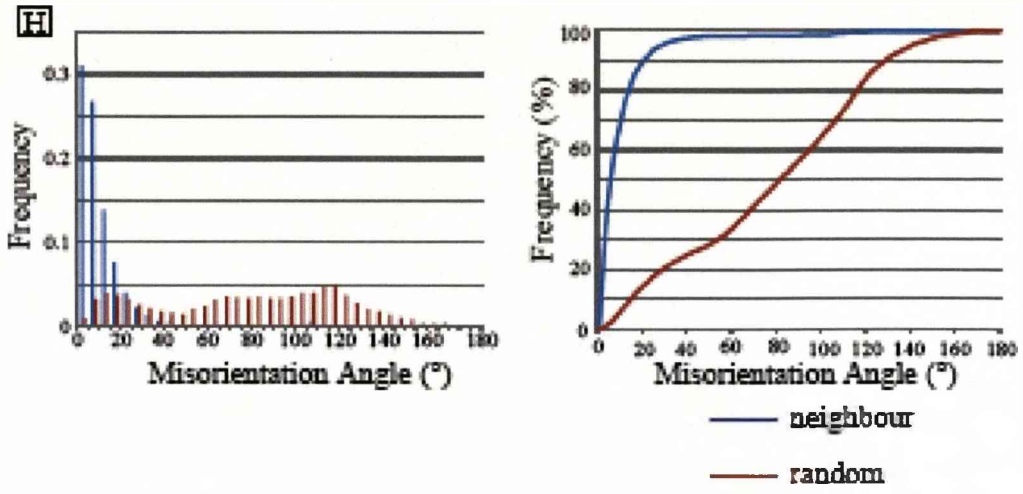

Fig. 6.16 EBSD results for sample S7.1, an undeformed eclogite pod from the Colle della Barme d'Oropa. A - Photomicrograph (PPL) of omphacite grains in sample S7.1, an undeformed eclogite pod. B - Grain boundary map showing subgrain (<10°) and grain (>10°) boundaries. C - Texture component map showing omphacite misorientations (from 0-120°) from the red dot combined with a grain boundary map. D - Texture component map and pole figures with corresponding colours for an elongate omphacite grain with fan like microstructural texture. E - Texture component map and pole figures with corresponding colours for a rounded omphacite grain. F - Misorientation profiles (black lines starting from black dots) across the fan omphacite grain. G - Misorientation profiles (black lines starting from black dots) across the rounded omphacite grain. H - Omphacite misorientation distribution analyses. Frequency chart and cumulative frequency graph are shown. Neighbour pair misorientations are shown in blue, random pair misorienrations in red

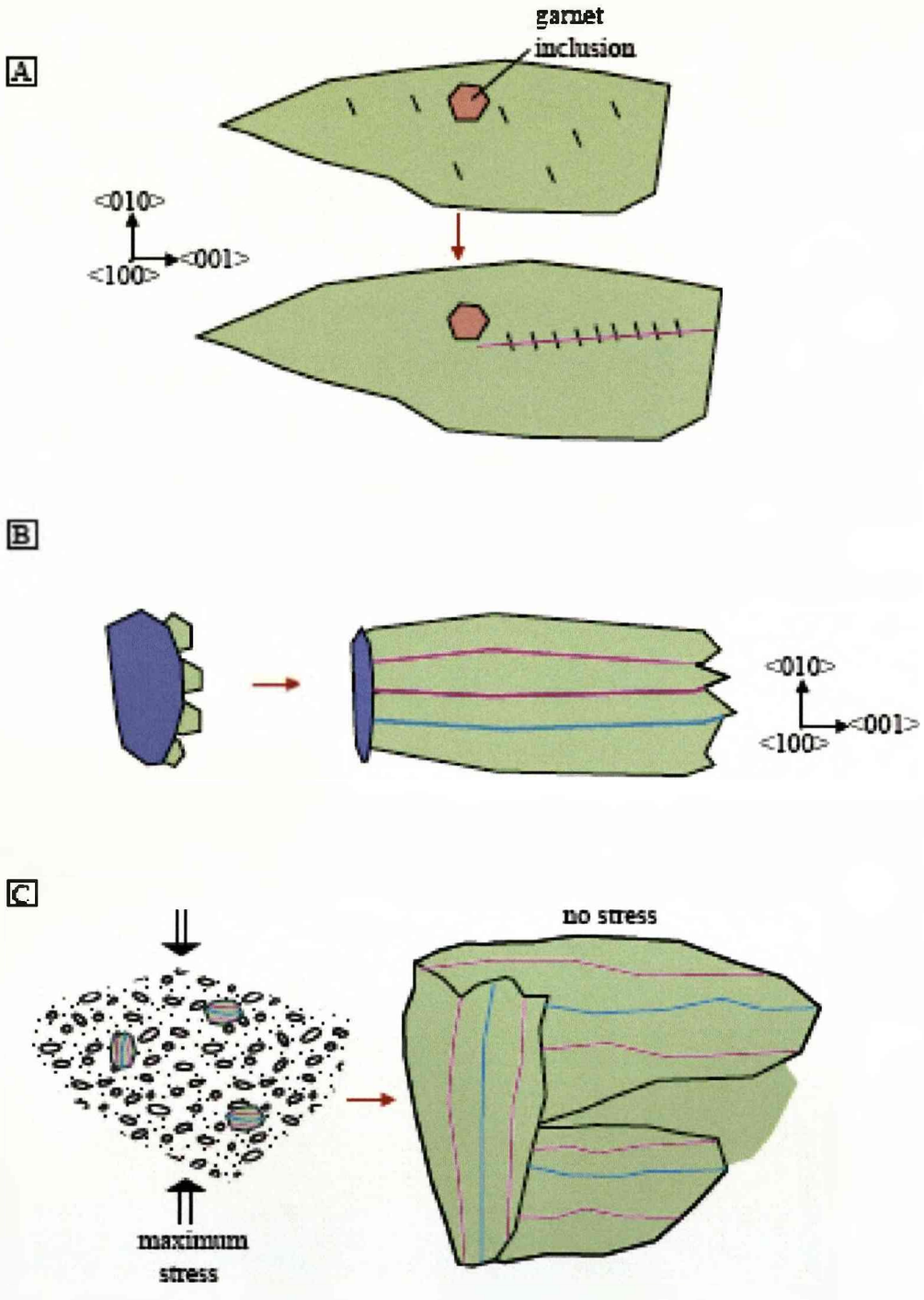

Fig. 6.17 Schematic diagrams showing possible mechanisms for creating microstructural textures described in omphacite from an undeformed eclogite pod. A - formation of lineage boundaries parallel to the omphacite <001> axis during grain growth, B - multiple nucleation of omphacite on a protlith phase of similar orientations followed by anisotropic grain growth, C - plastic deformation during early omphacite formation creates subgrain boundaries then deformation ceases and subsequent omphacite anisotropic grain growth takes over

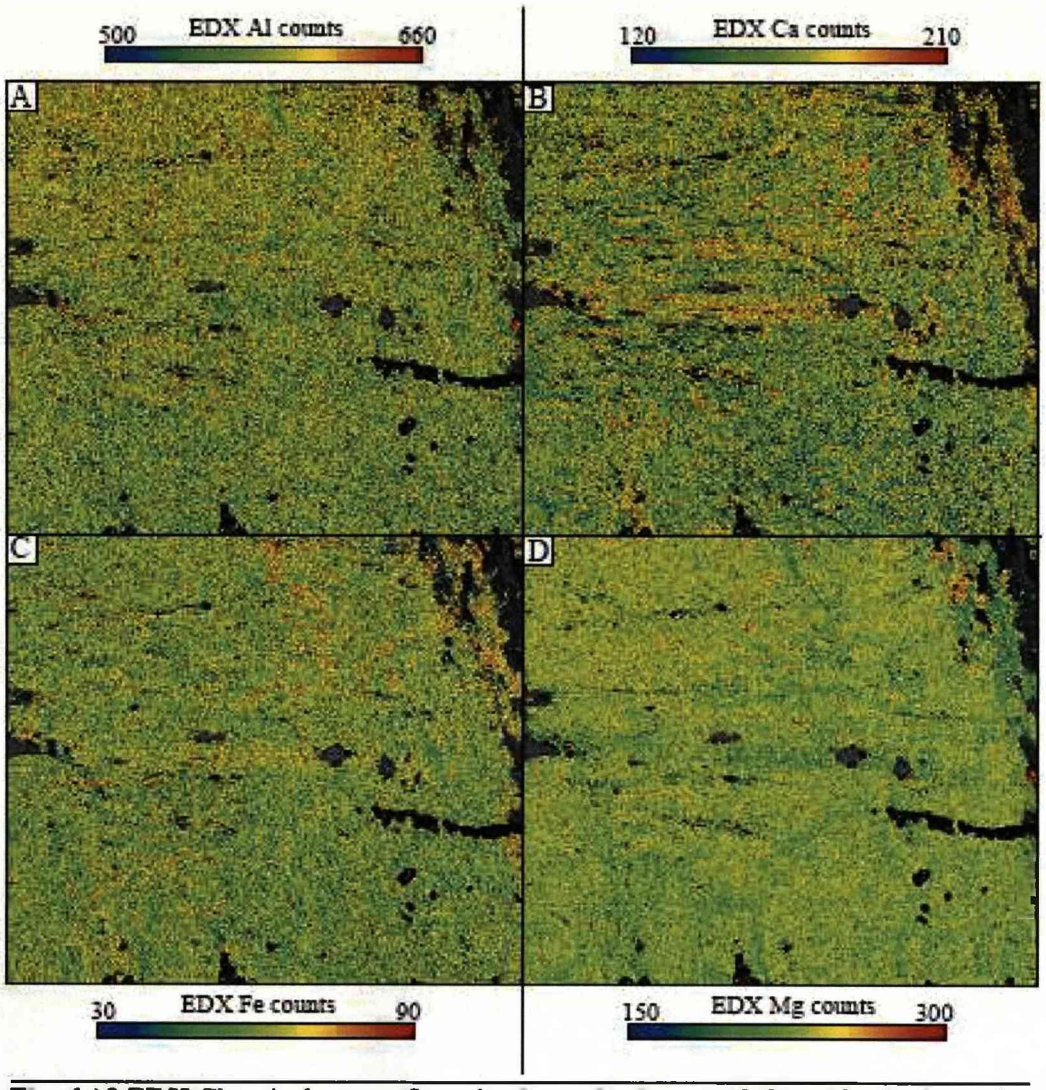

Fig. 6.18 EDX Chemical maps of omphacite grains in an undeformed eclogite pod (S7.1) from Colle della Barme d'Oropa. A - Al EDX chemical map, B - Ca EDX chemical map, C - Fe EDX chemical map, D - Mg EDX chemical map

6.3.2 Streaked Eclogite Results

6.3.2.1 Omphacite LPO

A selection of streaked eclogite thin sections underwent the STscan method for generating pole figures (Chapter 3). In this way only one 'point per grain' orientation measurement is gathered from multiple omphacite grains across a thin section. Streaked eclogite samples show a mix of omphacite LPO types. Pole figures for all samples are shown in Fig. 6.19. Table 6.1 summarises information for each sample investigated; omphacite grain size, STscan procedure step size, number of omphacite orientation measurements collected per sample, LPO type and LS index value (Ulrich and Mainprice, 2005).

Samples S5.9 and S7.8 show an L-type omphacite LPO, where strong point maxima of <001> poles are located parallel to lineation and the (010) poles are distributed in a girdle perpendicular to the plane of foliation. LS index values for these two samples are 0.706 and 0.752 respectively which is close to the L-type end member value of 1.

Streaked eclogite sample S7.7 has an omphacite LPO that describes an LS-type or intermediate pattern. Point maxima are noted parallel to the lineation for the <001> axes and also normal to the foliation plane for the (010) axes. A slight tendency toward a weak girdle is noted in the (010) axes. The orientation data provides an LS index value of 0.561, firmly in between the end member values for S-type = 0 and L-type = 1 omphacite LPO patterns.

Sample S5.8 shows an S-type omphacite LPO pattern with <001> poles distributed in a girdle within the foliation plane and point maxima (010) poles perpendicular to the foliation plane. It has an LS value of 0.397 which is close to the end member S-type vale of 0.

The LS index value for sample S6.42 shows an S-type value (0.377) but the pole figures do not describe such a fabric. The <001> pole figure shows a few point maxima dispersed in a girdle within the foliation plane and the (010) pole figure shows point maxima roughly perpendicular to the foliation plane. The (100) pole figure however instead of showing a random distribution shows a couple of point

maxima. This pattern of S6.42 pole figures suggests a few single grains of omphacite are dominating the data (more than one orientation measurement per grain). Comparison of omphacite grains in thin section and distribution of indexed data points on a corresponding orientation map reveals a possible explanation. Non - indexing of sections of large omphacite grains can cause the same grain (which shows no variation in extinction or birefringence) to appear as two or more separate grains on an orientation map. Thus the STscan will contain data that includes more than one point for some grains due to areas of the overall grain not indexing. This highlights a certain lack of precision in LPO information for this lithology. Due to the large grain size of the omphacite grains fewer orientation measurements than the number desired for plotting LPOs (~ 300) are not achieved and there are some issues with multiple readings from single grains due to indexing errors (a result of either thin section quality or ability of the indexing software to correctly identify Kikuchi bands). When interpreting the LPO patterns reported here these limitations must be taken into consideration.

Variable LPO patterns noted within the omphacite of the streaked eclogite lithology may result from a possible variety of mechanisms. As discussed frequently throughout this thesis omphacite LPO type is thought to be controlled by either the space group of the omphacite or the strain regime it is deforming in. Due to critical analysis of the arguments against the space group theory (chapter 1) and the findings of this thesis in chapter 4 we assume that it is strain regime and not space group that controls the type of omphacite LPO that develops in a rock. Applying this to the results presented here for omphacite of the streaked eclogite lithology would suggest that the small area of sampling experienced a combination of flattening and constriction strain regimes. This may be possible due to folding of the lithology in this area. The garnet and omphacite location fabric is folded thus fold development occurred either contemporaneously or with eclogite facies metamorphism in order to influence omphacite LPO pattern development. In this way S-type (flattening) LPO types would form on fold limbs and L-types (constriction) would form in fold hinges, with LS-types possibly somewhere in between. However lack of structural information from this area hinders further exploration of this theory.

This theory however assumes omphacite LPO in the streaked eclogite lithology is related to deformation. While the presence of an omphacite LPO is normally an indication for the action of dislocation creep, diffusion creep, preferred crystal growth or some combination of these mechanisms (Chapter 1) there are other possible explanations. This study has also shown LPO can be inherited by mimicry of a pre-existing LPO of a mineral phase in the protolith (chapter 5).

Given the long history of pre-Alpine deformation in the Sesia-Lanzo Zone, and the already mentioned idea that the location fabrics in this study area may be inherited (from field observations of aplite sheets), could very well mean that the omphacite LPO is mimetic on an LPO of a possible pre-existing granulite/amphibolite facies mineral LPO. In addition preliminary comparison of omphacite textures in streaked eclogite and undeformed eclogite pods suggest similar microstructures. While the appearance of what seem to be multiple subgrains may be commonly associated with the significant action of dislocation creep in omphacite, eclogite pod EBSD has shown they may also develop from omphacite grain growth. This may imply that the LPO observed here is not a result of eclogite facies deformation and is instead the result of inheritance. Further EBSD and chemical data is explored to investigate which mechanisms have contributed to the development of these LPO patterns.

Sample	Average Omphacite Grain Size (mm)	Slide Scan Step Size (μm)	No. of Omphacite Points	LPO Type	L-S Index
5.8	5mm	450	163	S-type	0.397
5.9	7mm	500	179	L-type	0.706
6.42	6mm	300	146	N/A	N/A
7.7	8mm	300	236	LS-type	0.561
7.8	6mm	400	165	L-type	0.752

Table 6.1 STscan procedure information and omphacite pole figure and LPO information from streaked eclogite samples and an eclogite pod sample from Colle della Barme d'Oropa

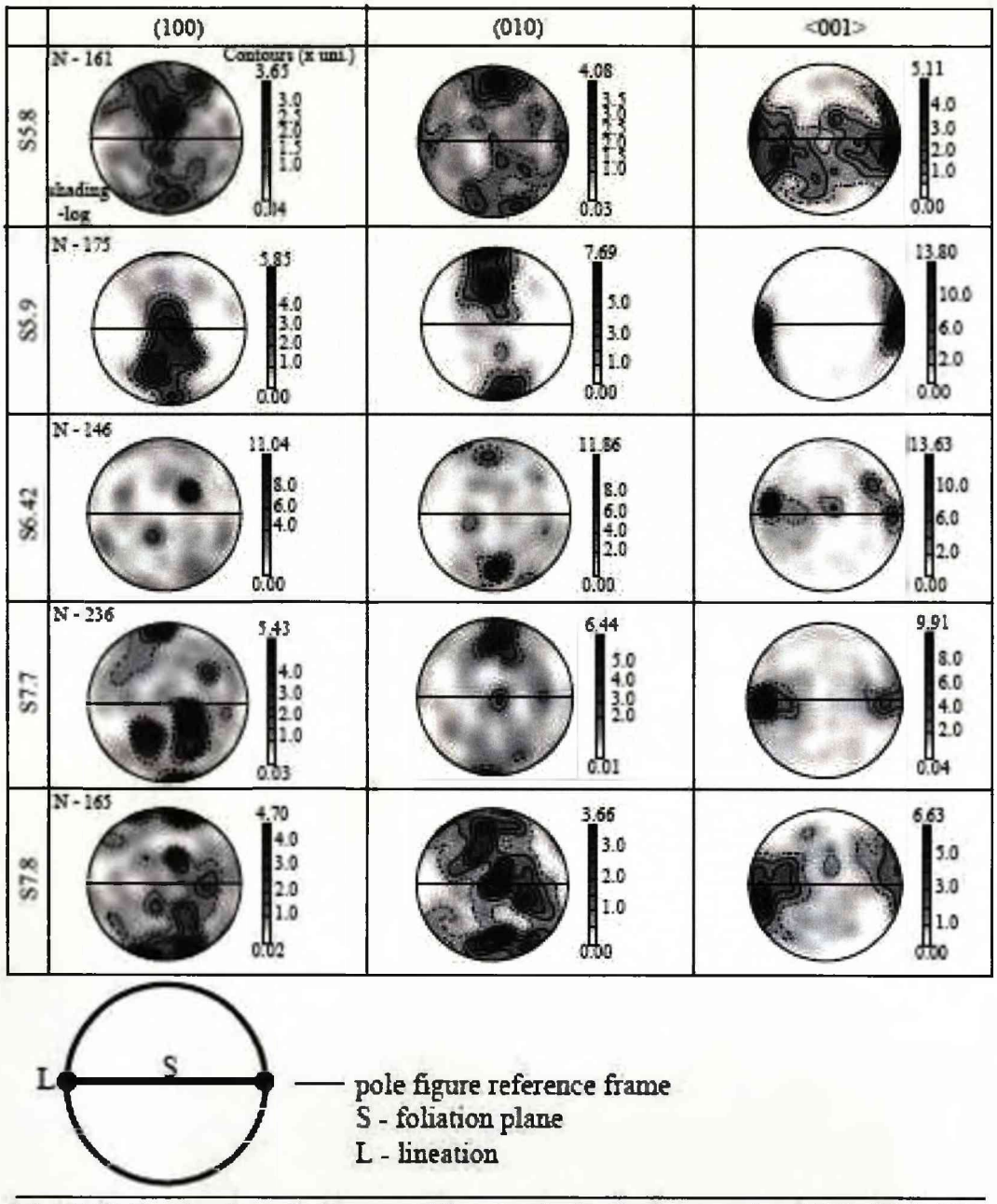

Fig. 6.19 Omphacite pole figures of five streaked eclogite samples (S5.8, S5.9, S7.7, S7.8 and S6.42) from Colle della Barme d'Oropa. Pole figures were created following the FTscan method (see Chapter 3)

6.3.2.2 Omphacite Grain Microstructures, Single Grain Pole Figures and Misorientation Angle Distribution Analyses

EBSD data sets are collected from the various omphacite grain morphologies observed in the streaked eclogite omphacite layers to investigate the microstructures observed in thin section. Omphacite morphology is divided into three types here; 1) large, elongate grains with variability in extinction and birefringence creating fan like textures within them, 2) rounded omphacite grains with variability in extinction and birefringence and 3) large, elongate omphacite grains that show only slight sweeping extinction and no variability in birefringence.

1) Fig. 6.20 shows EBSD results from an elongate omphacite grain in sample S5.9. A grain boundary map (Chapter 3) of the omphacite grain reveals large numbers of grain (>10°) and subgrain (2-10°) boundaries within the overall, large omphacite grain. Both grain and subgrain boundaries define elongate forms matching the variable extinction and birefringence patterns observed in optical microscopy. Long axes of subgrains and grains are parallel to the long axis of the overall large omphacite grain. A texture component map (Chapter 3) shows sharp colour changes (representing changes in orientation based on a reference orientation) matching the patterns displayed by grain and subgrain boundaries. Pole figure patterns (with data points coloured to match the texture component map) show (100) and (010) poles are distributed such that they express a rotation around the clustered pattern of the <001> poles. Misorientation profiles across the width of the grain show a maximum cumulative misorientation of ~30° and across the length of the grain misorientations are ~10°.

2) EBSD results for a rounded, irregular shaped omphacite grain from sample S7.8 are shown in Fig. 6.21. A grain boundary map reveals large numbers of grain (>10°) and subgrain (2-10°) boundaries. These boundaries match up to areas of variable extinction and birefringence noted in optical microscopy as do patterns displayed on texture component maps. Pole figures (with data points coloured to match the texture component maps) show similar patterns to those observed for the previously described texture (1). As with the fan like texture of the elongate omphacite grains pole figures for the rounded, irregular omphacite grains show

rotation of the <100> and <010> poles around <001>. Misorientation profiles across the grain in any direction show cumulative misorientations of ~20°.

3) Fig. 6.22 shows a large, elongate omphacite grain from sample S6.42. This grain shows none of the variance in extinction or birefringence noted in other elongate omphacite grains. A grain boundary map shows very little internal structure such as grain or subgrain boundaries; rather it is one large, coherent grain. Some subgrain boundaries are noted most of which have ~2-5° misorientation across them though a few have <5-10° misorientation. A texture component map shows gradual colour changes across the width of the grain rather than the sharp patterns observed in other omphacite morphologies. Similar to the other morphologies pole figures for this omphacite grain show rotation of the <100> and <010> poles around <001>. Misorientation profiles show cumulative misorientation across the breadth of the grain of ~9° in total while along the length misorientation is ~4°.

Due to the large grain size of omphacite in the streaked eclogite lithology, misorientation angle distribution analyses are created from EBSD scans of entire thin sections. This way orientation information from numerous omphacite grains from each sample is used to compile more representative misorientation angle distribution analyses of the samples. The analyses (Fig. 6.23) show high frequencies of low angle misorientations (<10°) between omphacite neighbour pair pixels compared to low frequencies between random pair pixels. Higher neighbour pair misorientation frequency compared to random pair misorientation persists in misorientations up to ~20° after which the neighbour pair misorientation frequencies become similar to random pair misorientation frequencies. Cumulative frequency graphs show neighbour pair misorientation lines significantly shifted to the left compared to random pair misorientation lines, reiterating the high frequency of lower angle misorientations.

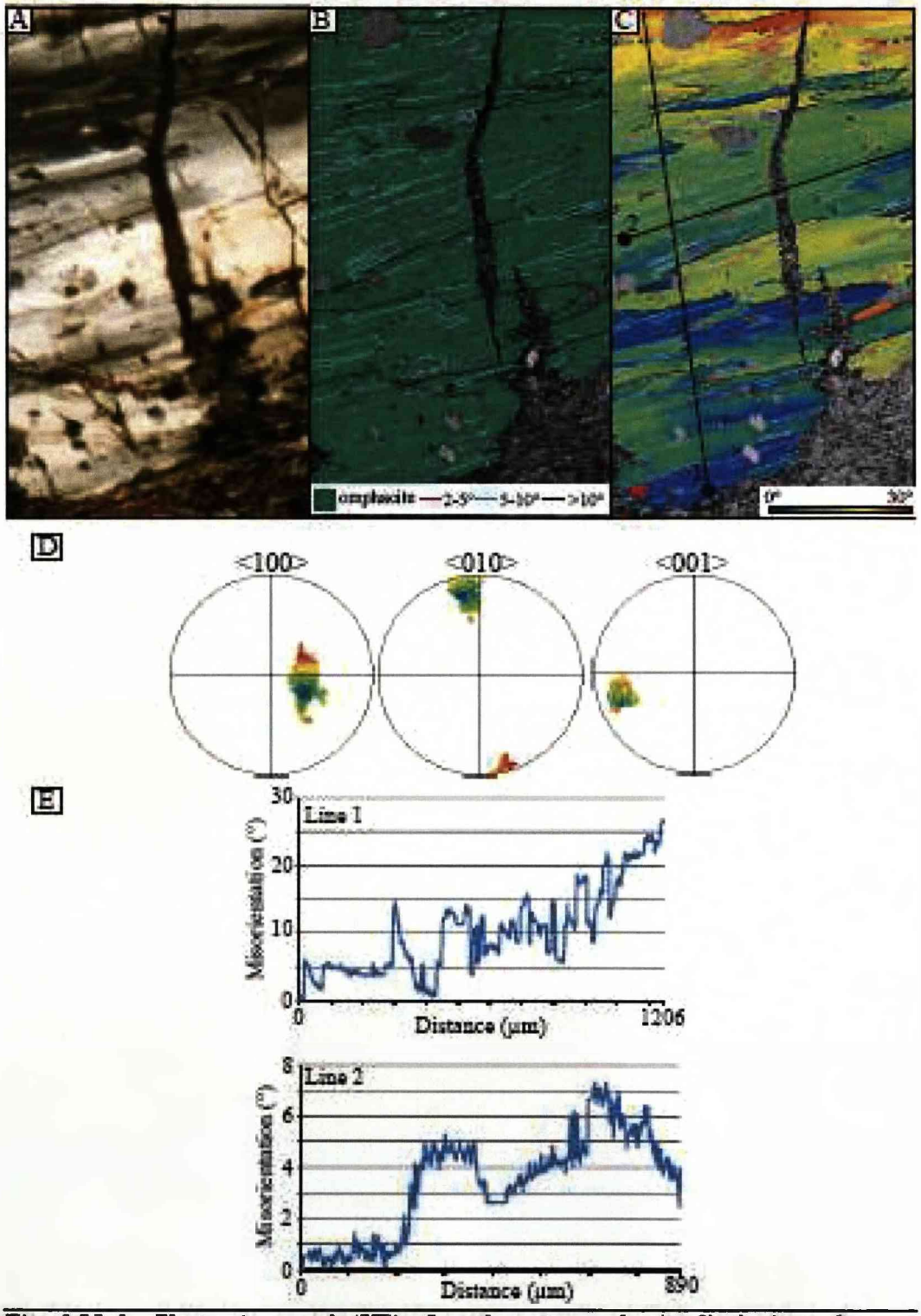

Fig. 6.20 A - Photomicrograph (XP) of an elongate omphacite displaying a fan texture from streaked eclogite sample S5.9 B - Grain boundary map showing subgrain boundaries of 2-5° and 5-10° and grain boundaries (>10°), C - Texture component showing misorientations from 0-30° from the red dot combined with the grain boundary map, D - pole figures for the omphacite grain showing significant rotation around <001> , E - Misorientation profiles (black lines starting from black dots) across the omphacite grain showing ~30° across the grain width and ~8° along the grain length

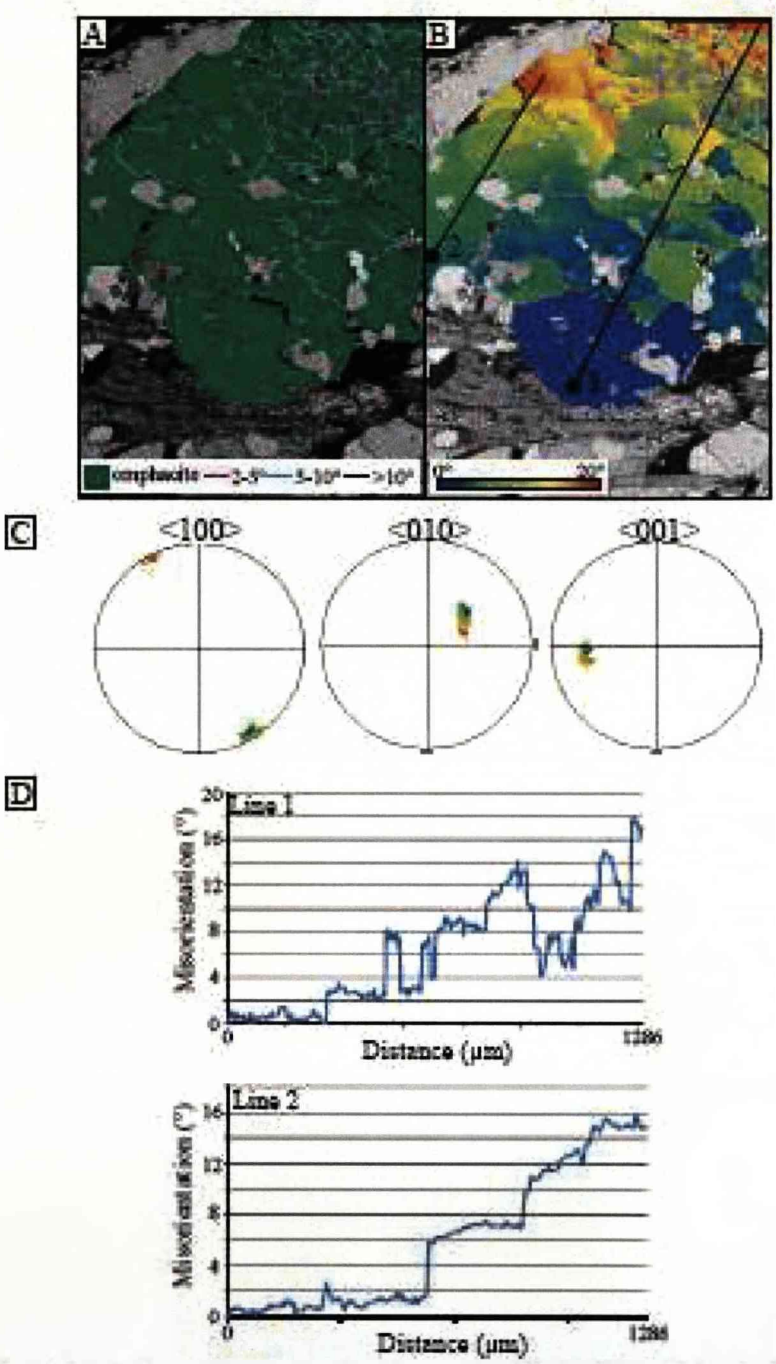

Fig. 6.21 A - Grain boundary map showing subgrain (<10°) and grain (>10°) boundaries, B - Texture component showing misorientations from 0-20° from the red dot combined with the grain boundary map, C - pole figures for the omphacite grain showing rotation around <001>, D - Misorientation profiles (black lines starting from black dots) across the omphacite grain showing ~20° across the grain

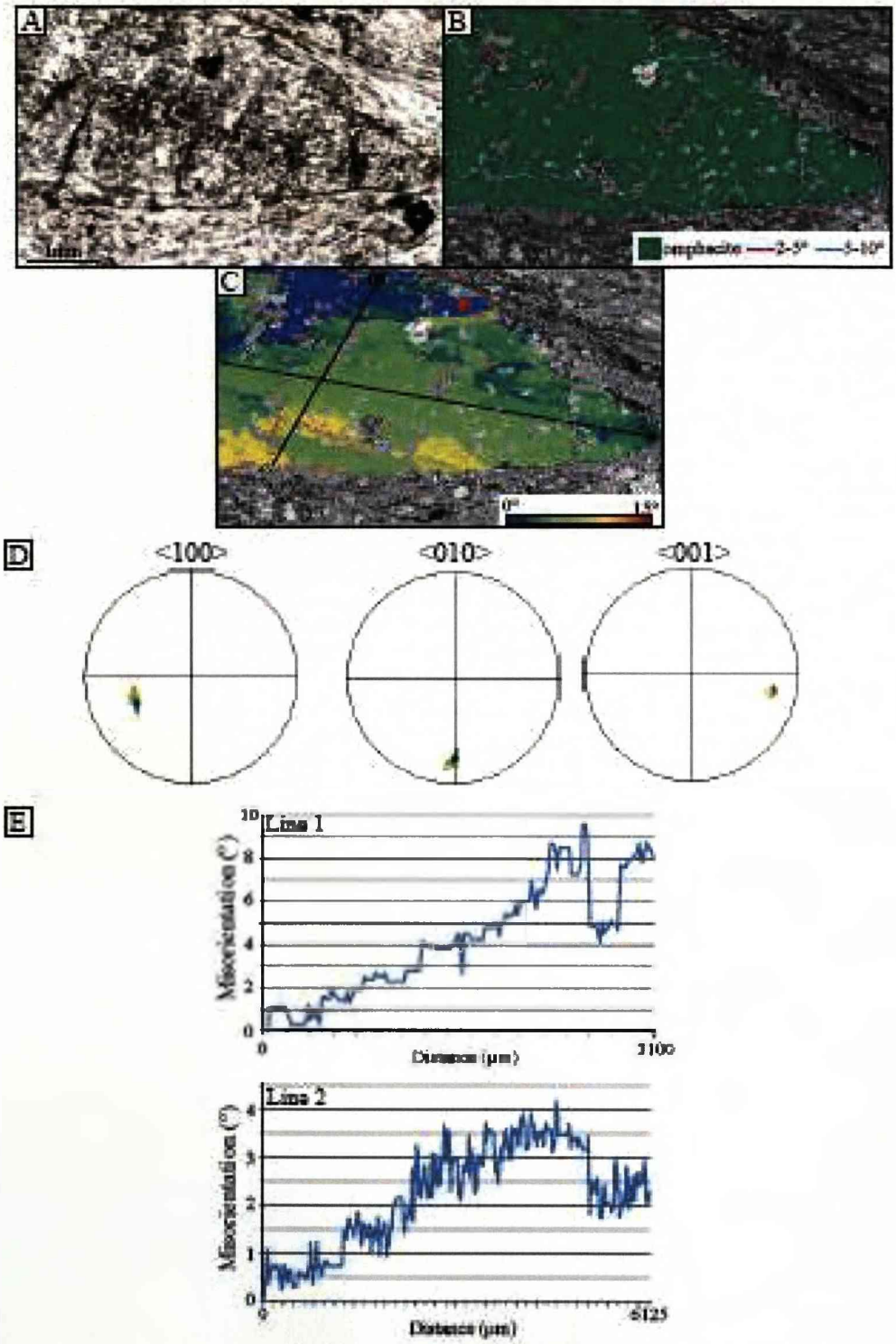

Fig. 6.22 A - Photomicrograph (PPL) of an omphacite grain in streaked eclogite sample S6.42. B - Grain boundary map showing subgrain boundaries of 2-5° and 5-10°, C - Texture component showing misorientations from 0-15° from the red dot combined with the grain boundary map. D - pole figures for the omphacite grain showing rotation around <001> , E - Misorientation profiles across the omphacite grain showing ~10° across the grain width and ~5° along the grain length

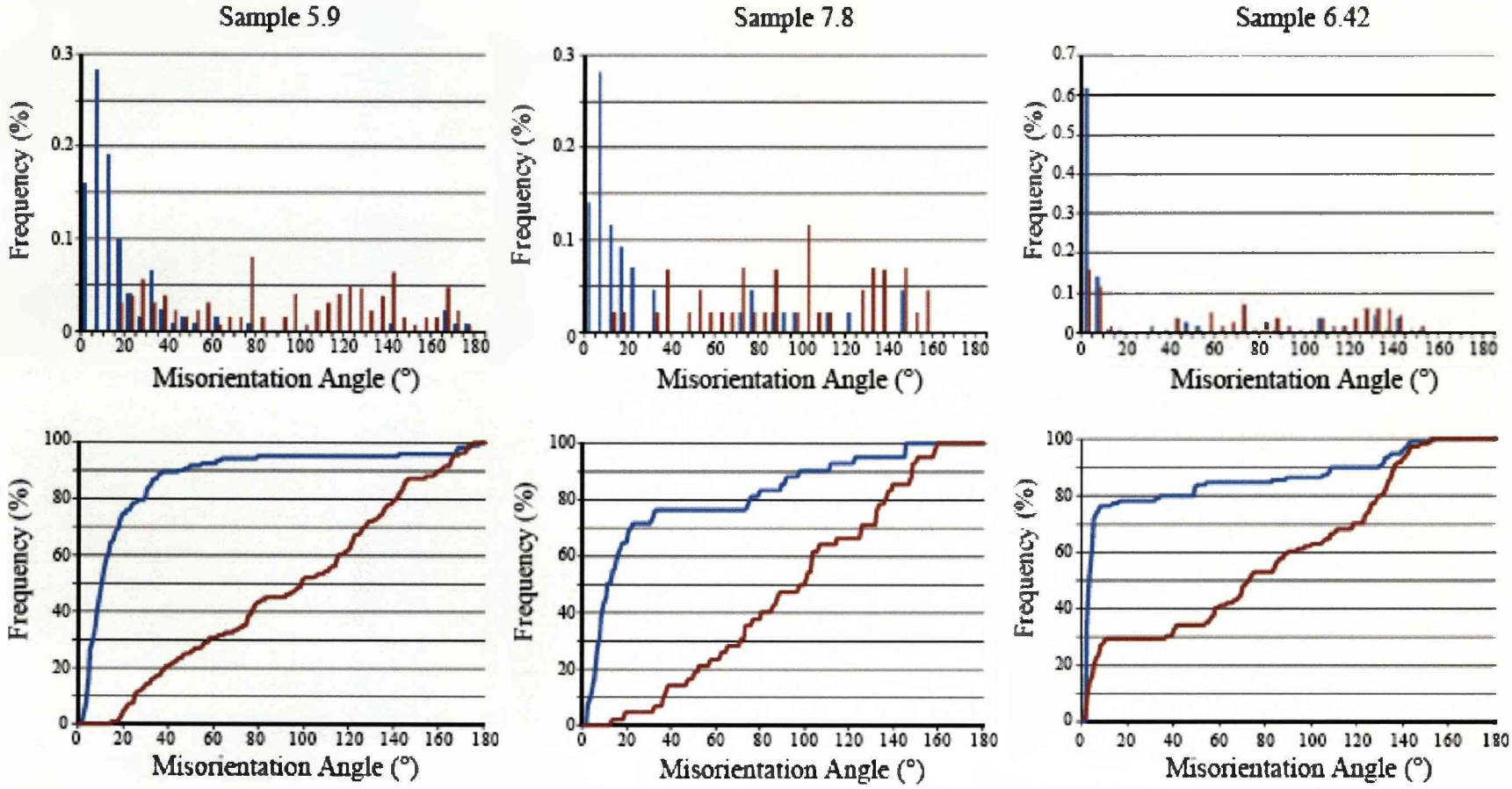

Fig. 6.23 Misorientation distribution analyses of omphacite from three streaked eclogite samples from Colle della Barme d'Oropa. For each sample a frequency chart (bin size 5) and cumlative frequency graph are shown. Neighbour pair misorientations are shown in blue, random pair misorientations in red

Observations of omphacite single grain microstructures and pole figures allow certain assumptions to be made about the distribution of omphacite grains within the omphacite layers of the streaked eclogite lithology. Large, elongate omphacite grains displaying the fan like microstructural texture and rounded omphacite grains which also show significant internal structure both display significant rotation of the <100> and <010> poles around the <001> axis. In a three-dimensional context there may be a link between these two omphacite morphologies. Here we imply that these two omphacite textures are simply a result of the 3D orientation of omphacite grains within omphacite layers of the lithology. Both can occur within the same sample as the long axes of omphacite grains are randomly oriented and thus the observed rounded omphacite grains may simply be cross section cuts of the large, elongate grains (Fig. 6.24).

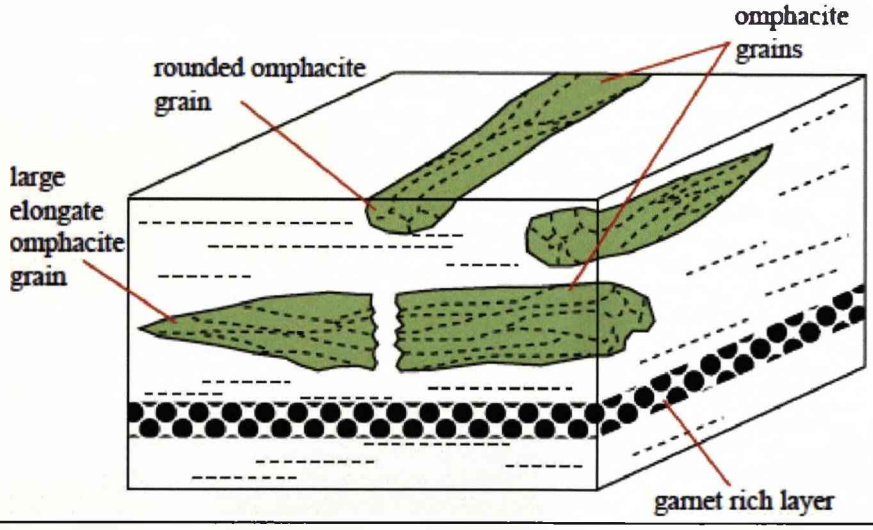

Fig. 6.24 Diagrammatical cross-section through a sample of streaked eclogite depicting how the rounded and elongate omphacite grains and their microstructures may be related to orientation of omphacite grain within the foliation plane

Presence of an LPO, subgrain boundaries and a high frequency of low angle neighbour misorientations normally suggest the action of dislocation creep and diffusive mass transfer in omphacite. However comparison to microstructures and single grain pole figures from omphacite in the undeformed eclogite pod reveals a striking similarity to what is observed here in the streaked eclogite omphacite. As previously discussed the microstructures in undeformed omphacite are growth related though the exact growth mechanism that created them remains uncertain. The similarity between the results from both lithologies thus suggests that omphacite in

the streaked eclogite lithology has microstructures that are growth related and formed, at least in part, in the absence of deformation.

While microstructures here in the streaked eclogite are likely to be growth related the occurrence of an omphacite LPO still needs to be resolved. If omphacite here grows free from strain as with the eclogite pod then a random LPO pattern is expected. If however early during omphacite formation in this lithology there was an element of deformation followed then by subsequent anisotropic grain growth free of deformation it may explain observed LPO patterns.

Another possible cause of LPO formation in omphacite here is that of inheritance. As mentioned earlier due to structural observations of aplite and assumptions of inherited location fabrics in the EMC and streaked eclogite it is entirely possible that omphacite LPO may be a result of mimicry of a pre-existing phase LPO. As detailed in chapter 2 the Sesia-Lanzo contains various evidence for granulite to amphibolite facies metamorphism occurring prior to Alpine deformation and metamorphism. It is possible that some pyroxene or amphibole layer contained an LPO before eclogite conditions began. Static omphacite growth then began on these grains and developed an LPO accordingly. Chapter 5 has already shown evidence for the barroisite developing an LPO from mimicry of omphacite and glaucophane LPO patterns, so it is not far from the realm of possibility that omphacite may form one from amphibole LPO patterns.

6.3.2.3 Chemistry

Chemical analyses of omphacite grains of the streaked eclogite lithology is important for understanding the rock's development and how the phase behaved during the evolution of this area of the Sesia-Lanzo Zone. Chemical zoning patterns can shed light on preferential growth of omphacite grains, changing metamorphic conditions of the area and reveal possible, diffusion controlled omphacite growth. From EBSD results and comparison to microstructure observed in an undeformed eclogite pod we assume omphacite has developed free from deformation and that LPO development is a result of mimicry of a pre-alpine LPO. Chemical data is considered here with the aim of investigating whether any diffusive mass transfer mechanisms may have been operating in the streaked eclogite omphacite and to look for zoning patterns that may

provide further evidence of deformation free, anisotropic grain growth. Chemical maps, gathered using the EDX system on a CamScan X500 SEM (University of Liverpool) are presented here. In order to attain a direct comparison between chemical microstructures and orientation microstructures EBSD was performed alongside the chemical mapping procedure in these same samples.

A large, elongate omphacite grain from sample S7.7 contains an excellent example of the fan like microstructural texture common in the streaked eclogite lithology. A grain boundary map shows similar patterns to those previously described for an omphacite grain of similar texture from S5.9 (Fig. 6.20). EDX chemical maps for Ca, Fe, Al and Mg show no discernable, significant chemical changes within this omphacite grain and it appears to have uniform chemistry across its entirety (Fig. 6.25).

The chemistry of the large, elongate omphacite grain from sample S6.42 (EBSD data shown in Fig. 6.22) is also investigated by EDX. Results for this grain are included here to provide a comparison between elongate omphacite grains with fan like microstructures and those with little internal microstructure. The possibility exists that these two different omphacite textures represent a sequence of development with the simple grain in S6.42 being a precursor to complicated grain structures shown by omphacite in other samples (S7.7, S5.9). Chemical maps (Mg, Ca, Fe and Al) of this grain (Fig. 6.26) show no chemical zoning patterns across the whole of this large omphacite grain in Mg, Ca, Fe and Al.

The homogeneous chemistry of the omphacite grains in the streaked eclogite unfortunately lends little to our understanding of how omphacite microstructures in the streaked eclogite formed. Homogeneous chemistry of the omphacite grains suggest they grew quickly with respect to the changing metamorphic conditions of this area.

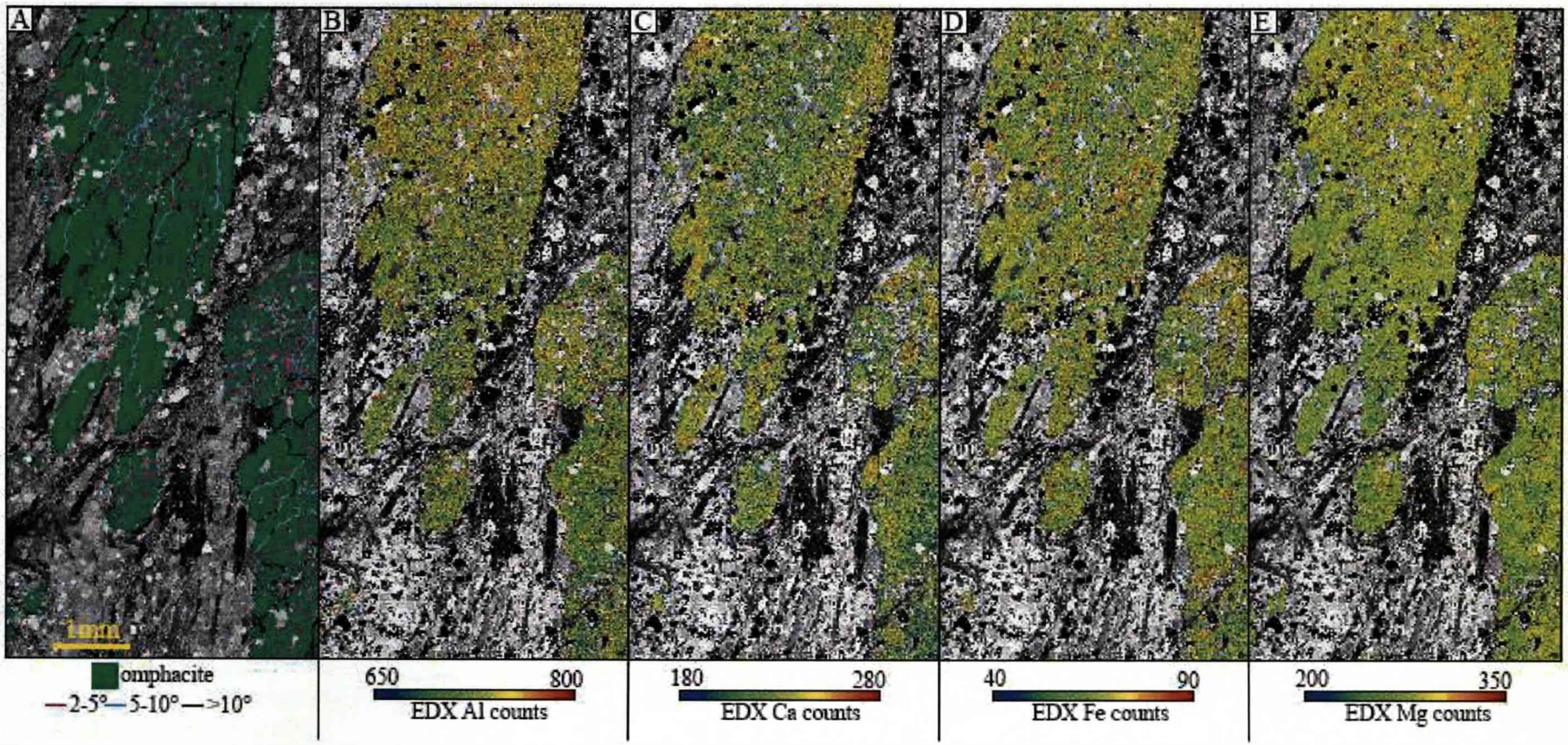

Fig. 6.25 A - Grain boundary map on omphacite grains that display both the large, elongate grains with fan like microstruictures and rounded grains with significant internal microstructure. These grains are from streaked eclogite sample S7.7 from Colle della Barme d'Oropa. B - Al EDX chemical map, C - Ca EDX chemical map, D - Fe EDX chemical map, E - Mg EDX chemicai map

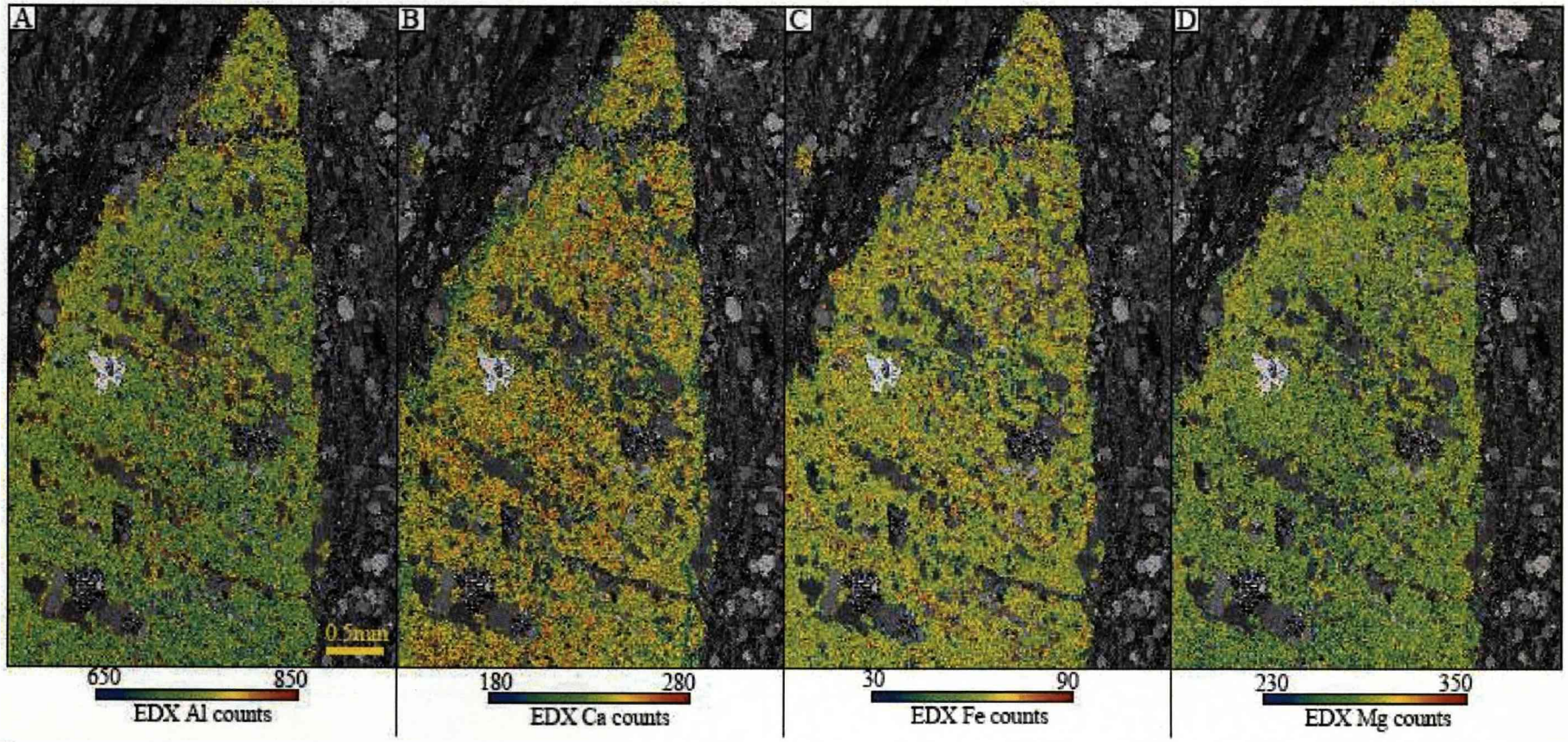

Fig. 6.26 Chemistry maps of an elongate omphacite grain with little microstructure. This grain is from streaked eclogite sample S6.42 from Colle della Barme d'Oropa. A - Al EDX chemical map, B - Ca EDX chemical map, C - Fe EDX chemical map, D - Mg EDX chemical map

6.3.3 Discussion

Results of optical petrography, EBSD and chemical analyses from omphacite in the streaked eclogite lithology and an eclogite pod from the Colle della Barme d'Oropa area of the Sesia-Lanzo Zone provide insight as to what deformation mechanisms or lack thereof are in operation in this mineral phase. One aim of this thesis is to further the understanding of omphacite deformation mechanisms and the microstructures they are responsible for creating, as well as to investigate the effect of pre-existing microstructures on later developed minerals. It is hoped that results drawn from such investigations can shed light on the development of this area of the Sesia-Lanzo Zone through its burial and exhumation.

6.3.3.1 Development of Omphacite Microstructures in Streaked Eclogite and Eclogite Pods of Colle della Barme d'Oropa

The undeformed eclogite pods and streaked eclogite lithology contain omphacite microstructures (LPO, subgrain boundaries and high frequencies of low angle neighbour pair misorientation angles) normally associated with the combined action of dislocation creep and diffusive mass transfer (Buatier et al., 1991, Philippot and van Roermund, 1992, Brenker, 1998, Brenker et al., 1999, Bascou et al. 1991, Bascou et al., 2002, Ulrich and Mainprice, 2005, Helmstaedt, 1972, Godard and van Roermund, 1995, Mauler et al., 2001).

However as previously mentioned eclogite pods are undeformed and as such the microstructures apparent within them must be related to some growth process. Three separate mechanisms have been suggested for creating the omphacite microstructures observed here (Fig. 6.17) but which one of these is in operation is still uncertain. The mineral johannsenite ($4(CaNaSi_2O_6)$) and diopside are shown to be isostructural (Schaller, 1938) and lineage structures have been noted in johannsenite in the b and c directions (Freed and Peacor, 1967) possibly suggesting similar structures would not be uncommon in diopside and other pyroxenes. The formation of multiple omphacite nuclei on a grain of a protolith phase may be a possible mechanism to create the observed microstructure although as previously mentioned no textural relationships remain preserved in the eclogite pod to suggest this. And as previously mentioned

the theory assuming a small amount of deformation at the start of omphacite development followed by anisotropic growth seems less likely.

While the precise mechanism for creation of these omphacite microstructures cannot be ascertained here, the fact they are formed during grain growth free of strain is still an important observation. As mentioned comparison of the omphacite microstructures between the undeformed eclogite pod and the streaked eclogite show marked similarities. So while the streaked eclogite lithology is obviously deformed (shape fabric and folding) the omphacite grains within it appear to have grown free from strain, developing microstructures associated with a growth mechanism.

6.3.3.2 Streaked Eclogite Omphacite LPO

While omphacite microstructures described here for the streaked eclogite are likely to be growth related the occurrence of an omphacite LPO still needs to be resolved. If omphacite here has indeed developed free from strain as with the eclogite pod then a random LPO pattern would be expected, due to omphacite crystal lattices being free to grow in any direction. However as noted in the streaked eclogite through hand specimen, thin section and EBSD observations omphacite grains do not have a random orientation within the omphacite layers (Fig6.24). To have the omphacite grain arrangement a few possibilities must be explored.

As discussed in chapter 1 anisotropic growth and dissolution rates in omphacite (Fig. 1.7) can be responsible for creating both S and L-type LPO patterns. Long grains parallel to the <001> direction suggest anisotropic growth has had a significant effect on omphacite grain development in these rocks. If it were occurring during stress on these rocks it is possible that the omphacite LPOs were created by this process. Assuming the white mica shape fabric in the aplite sheets of the area were developed during Alpine deformation we have possible evidence for deviatoric stress during eclogite facies conditions.

Another possibility involves deformation in the unit during the beginning of omphacite growth. This would create a number of small deformed omphacite grains with subgrains and a lattice preferred orientation. Deformation on the unit then ceases though omphacite grain growth continues and due to anisotropic grain growth develops the large elongate omphacite grains parallel to the <001> crystal direction.

If however early during omphacite formation in this lithology there was an element of deformation followed then by subsequent anisotropic grain growth free of deformation it may explain observed LPO patterns.

The possibility that the omphacite LPO patterns are a product of inheritance of a pre-existing LPO must also be considered here given that the Sesia-Lanzo Zone has experienced a long tectonic history prior to the Alpine Orogeny. As mentioned earlier due to structural observations of aplite and assumptions of inherited location fabrics in the EMC and streaked eclogite it is entirely possible that omphacite LPO may be a result of mimicry of a pre-existing phase LPO. As detailed in chapter 2 the Sesia-Lanzo contains various evidence for granulite to amphibolite facies metamorphism occurring prior to Alpine deformation and metamorphism. It is possible that some pyroxene or amphibole layer contained an LPO before eclogite conditions began. Static omphacite growth then began on these grains and developed an LPO accordingly. Chapter 5 has already shown evidence for the barroisite developing an LPO from mimicry of omphacite and glaucophane LPO patterns, so it is not far from the realm of possibility that omphacite may form one from amphibole LPO patterns.

Subsequent omphacite nucleation on this preferentially oriented phase may explain why only certain omphacite grain orientations are observed in the streaked eclogite omphacite layers as opposed to the random orientations seen in the undeformed eclogite pod. This mimetic replacement followed by anisotropic grain growth of omphacite (free of strain) would create an inherited omphacite LPO pattern.

While it can be said that the omphacite microstructures are related to some grain growth mechanisms and not to deformation what exact set of events caused the mineral to form an LPO pattern remains unclear. Saying this, due to deformation in the Alpine Orogeny it is likely more reasonable to envision that deformation at least in a small part is responsible for omphacite LPO in this unit.

6.4 Microstructural Investigation of Garnet Layers in the Streaked Eclogite of Colle della Barme d'Oropa

Garnet is often considered to act as a rigid body in eclogite facies rocks, contributing little toward deformation (Vogelé et al., 1998, Brenker et al., 2003, Kurz et al., 2003). But as discussed in chapter 1, recent studies (Mainprice et al., 2004, Storey and Prior, 2005, Zhang and Green, 2006, Zhang et al., 2007) suggest dislocation creep and grain boundary sliding mechanisms assisted by subgrain formation are important for garnet deformation. Of particular interest to this study is work showing fine grained garnet layers deforming by grain boundary sliding (Terry and Heidelbach, 2004). One of the definitive features of the streaked eclogite lithology, are the garnet layers that define part of the location fabric and as such bear closer inspection to see how garnet formed layers and may have behaved throughout the evolution of this lithology.

6.4.1 Garnet Layer LPO

Garnet LPO patterns are gathered using the STscan data from the same thin sections used to investigate omphacite microstructure in the streaked eclogite lithology. Pole figures for all samples show <100>, <110> and <111> patterns are random meaning garnet has no LPO. An example of the observed pattern is shown in Fig. 6.27. The absence of LPO may suggest there was no deformation within the garnet rich layers of this rock. There are however examples of garnet that has undergone deformation yet shows a random LPO pattern (Storey and Prior, 2005, Zhang and Green, 2006), so LPO patterns observed here may not necessarily mean garnet has contributed little to the deformation of this eclogite facies rock. In an effort to explore this problem further EBSD data is considered as are EDX chemical analyses of garnet layers.

6.4.2 Garnet Layer Grain Microstructure and Misorientation Angle Distribution Analysis

EBSD of garnet grains in garnet rich layers of the streaked eclogite lithology reveal some grains contain subgrain boundaries (Fig. 6.27). Grain boundary maps reveal various amounts of 2-5° and occasional 5-10° misorientation boundaries within individual garnet grains. These subgrain boundaries either run across the entire width or length of a garnet grain or occasionally form small rounded areas within garnet

grains. Cumulative misorientation across any chosen garnet grain can lie anywhere between ~3-9°.

Garnet misorientation angle distribution analyses for garnet layers from samples S5.9 and S7.8 shows slightly higher frequencies of low angle misorientations (<10°) between garnet neighbour pair pixels compared to low angle misorientation frequencies between random pair pixels (Fig. 6.28). This slightly higher frequency persists up to ~10° misorientation after which the neighbour pair angle frequencies more closely match the random ones. Cumulative frequency graphs show neighbour pair misorientation lines shifted a little to the left compared to random pair misorientation lines, reiterating what is seen in the frequency bar charts.

It is possible this misorientation angle distribution is a signal of the presence of the subgrain boundaries noted in the garnet grains. However the difference between the neighbour and random misorientation angle distributions is not very large suggesting no significant physical interaction between neighbouring garnet grains occurred. This supports the lack of LPO in the garnet layers.

The small amount of subgrains noted in the garnet grains may explain the small higher amount of low angle neighbour misorientations, possibly showing the action of dislocation creep here. This makes the lack of garnet LPO odd but as already stated (chapter 1) the presence of deformation microstructures and an LPO in garnet can be mutually exclusive. However as mentioned the difference between the neighbour and random pair misorientation angle distribution is small and as such supports the random LPOs observed, possibly suggesting garnet layers formed grain boundary sliding.

6.4.3 Garnet Chemistry

Chemical maps of garnet grains in streaked eclogite garnet layers from sample (S6.44) show that occasional garnets show chemical zoning in Ca and Fe (Fig. 6.29). Most grains show high Ca in their cores with lower Ca in rims. The opposite pattern is observed for Fe. EDX chemical maps of garnet grains (Fig. 6.30) in a layer from sample S7.8 show weaker zoning patterns in grains and that some other grains have no zoning whatever. Zoning is concentric for the most part suggesting no diffusion creep or preferential growth was in operation during garnet development.

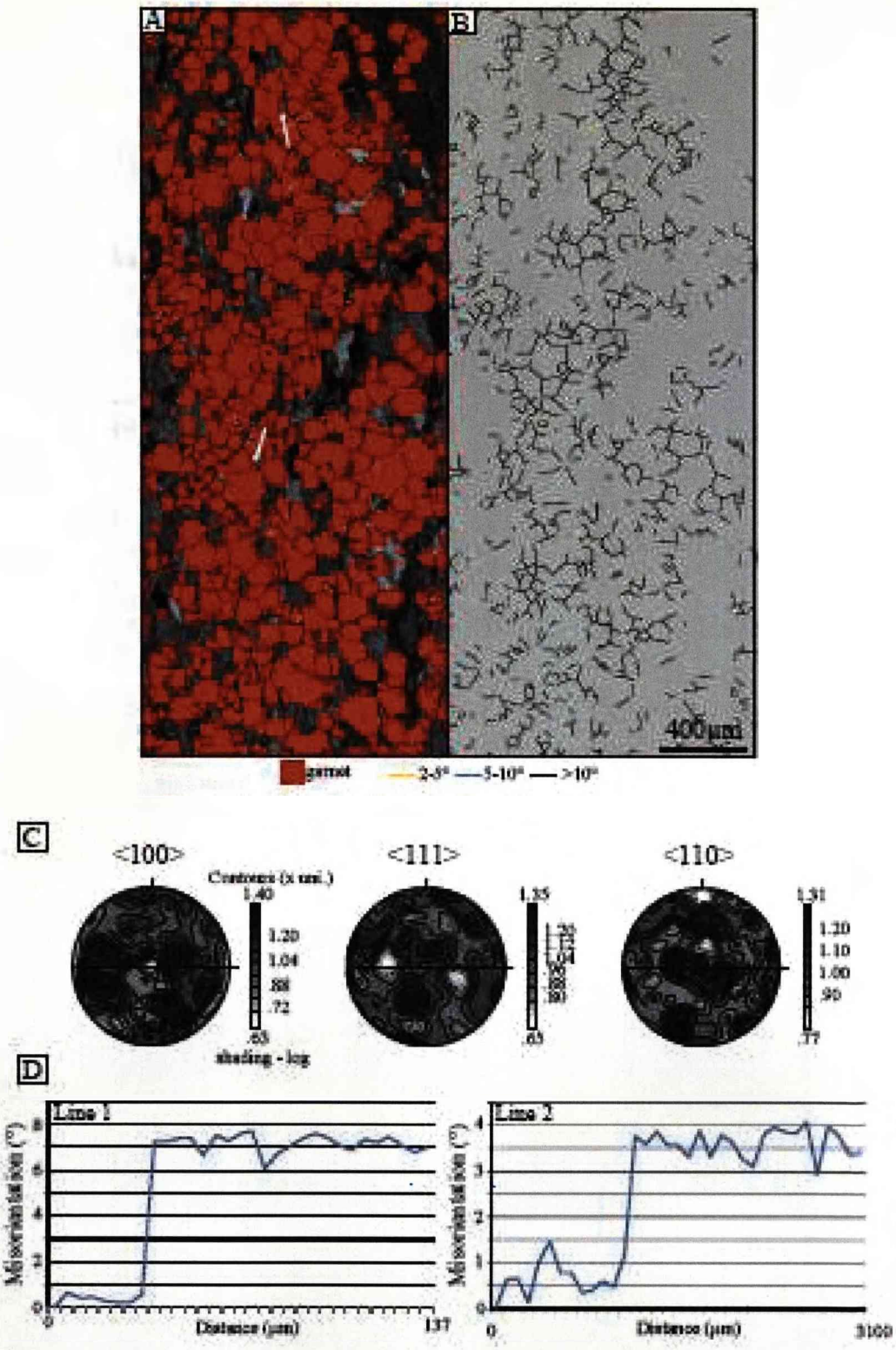

Fig. 6.27 EBSD results for a garnet layer from streaked eclogite sample S5.9 from Colle della barme d'Oropa. A - Grain boundary map of garnet grains (red) with 2-5° misorientation boudaries (yellow), 5-10° misorientation boundaries and >10° boundaries. B - EBSD map showing just the garnet grain boundaries on a grey background. C - Point per grain pole figures for the garnet layer. D - Misorientation profiles across two garnet grains (white lines starting from white dots)

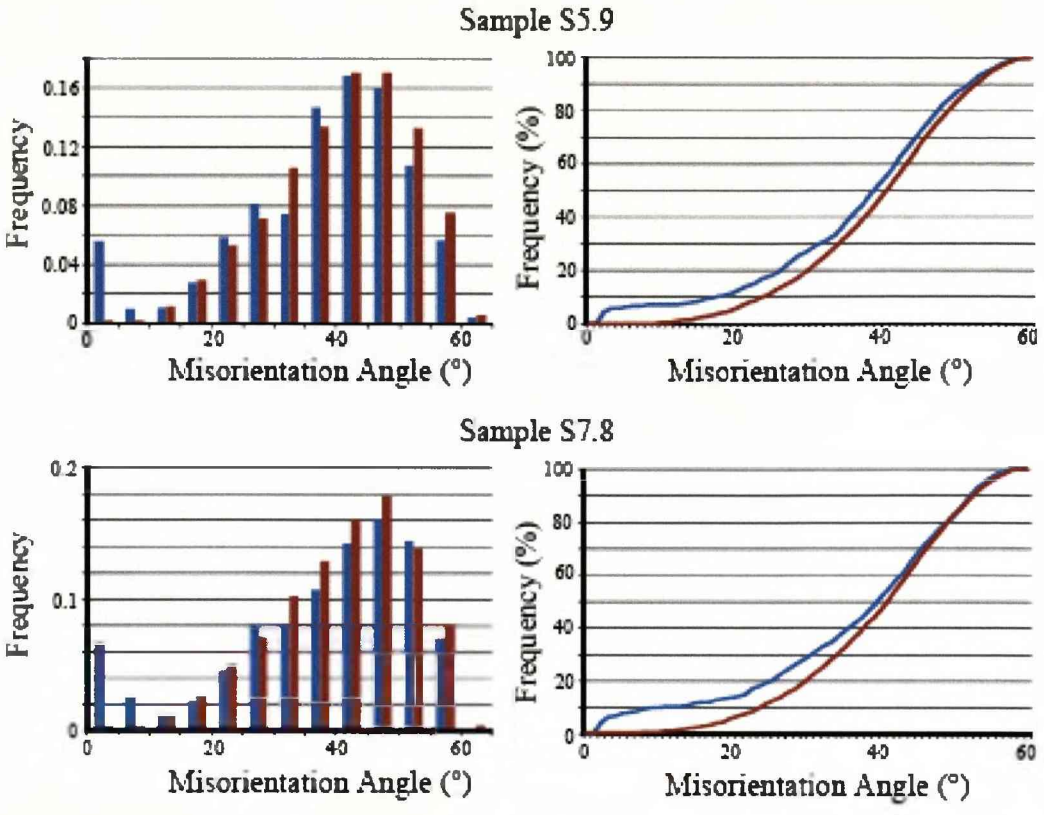

Fig. 6.28 Misorientation distribution analyses of garnet grains in garnet rich layers from streaked eclogite samples S5.9 and S7.8. Frequency bar chart data is displayed in bins of 5° misorientation.

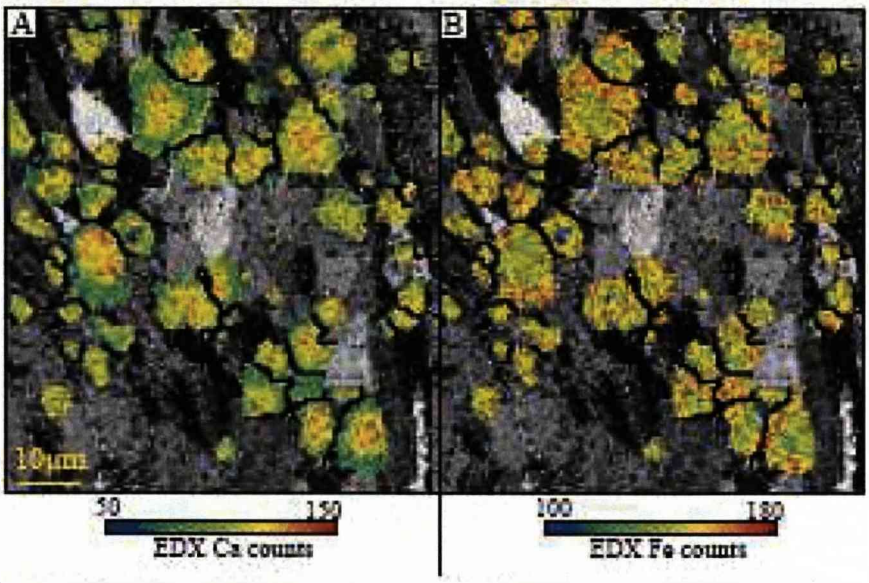

Fig. 6. 29 EDX chemical maps of garnet grains in a garnet rich layer of streaked eclogite sample S6.43. A - Ca EDX map, B - Fe EDX map

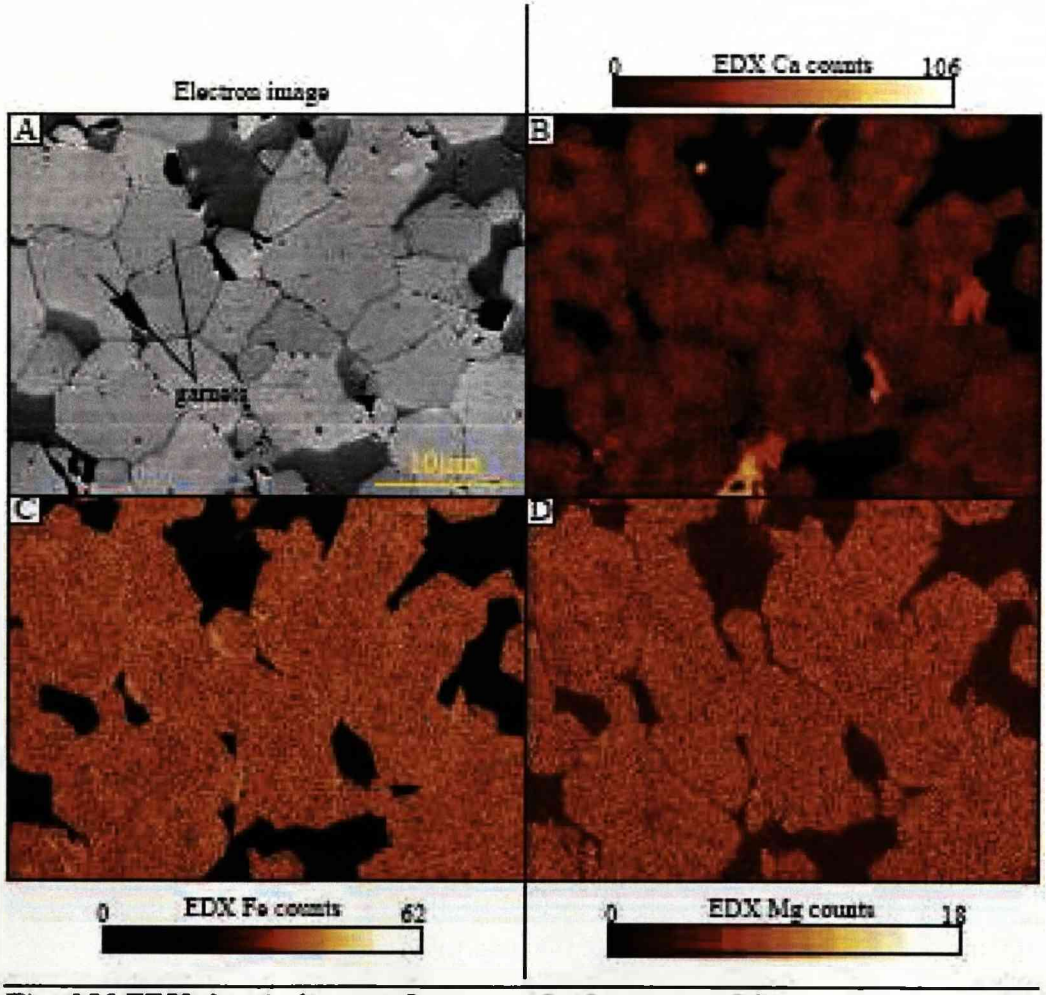

Fig. 6.30 EDX chemical maps of garnet grains in a garnet rich layer from streaked eclogite sample S7.8. A - Electron image of chemically mapped area, B - Ca EDX map, C - Fe EDX map, D - Mg EDX map

6.4.4 Discussion

As discussed in detail in chapter 1 many studies on eclogite deformation take the view that garnet often behaves as a rigid body contributing little to the overall deformation of the rock. It is worth noting that most studies that conclude or suggest this are of garnet porphyroblasts within a matrix of more deformed mineralogy. In the streaked eclogite lithology garnet occurs in fine grained layers. Previous studies (Wang and Ji, 2000, Ji et al., 2003, Terry and Heidelbach, 2004) show that deformation by various processes is common in garnet when concentrated in layers.

The occurrence of subgrain boundaries, in garnet grains of this lithology, possibly indicate the action of dislocation creep in this mineral. If dislocation creep is indeed the mechanism responsible for formation of subgrain boundaries a signature of this is expected in the misorientation angle distribution analysis. In the neighbour pair misorientation angle distribution there is a slightly higher frequency compared to the random distribution, which may be such a signal. This makes the lack of garnet LPO odd but as already stated (chapter 1) the presence of deformation microstructures and an LPO in garnet can be mutually exclusive.

However dislocation creep may not be the only process by which subgrain boundaries and high frequencies of neighbour pair low angle misorientations may have formed in this garnet layer. In the Schneeberg Complex of the Italian Alps garnet grains are thought to have rotated toward coincident orientations once they came into contact with each other as suggested by microstructures observed in amalgam garnet porphyroblasts (Spiess et al., 2001, Wheeler et al., 2001). These microstructures include garnet with domainal orientation characterised by small misorientations across domain boundaries and misorientation axes randomly oriented with respect to crystallographic orientations (Spiess et al., 2001). Garnet rotation is driven by subgrain boundary energy reduction associated with misorientation loss and accommodated by diffusion along subgrain boundaries, diffusion creep and rigid body rotation of other minerals around garnet grains. This model allows for a physical neighbour interaction between garnet grains satisfying the trend seen in the misorientation angle distribution analysis results for garnet layers here (Wheeler et al., 2001). In reference to the occurrence of subgrain boundaries present within garnet of the streaked eclogite garnet layers, it is unlikely a similar process is

occurring mainly because the garnet porphyroblasts in the Schneeberg Complex have an LPO and here the garnet layers of the streaked eclogites do not. In addition chemical zoning patterns noted for the garnet grains in the streaked eclogite do not match those described for the process occurring in the Schneeberg complex.

As mentioned earlier and in chapter 1 lack of a garnet LPO does not necessarily mean that garnet has not deformed. Terry and Heidelbach (2004) shows that initial fine grained garnet, due to its formation being concurrent with deformation, deformed by grain boundary sliding and associated grain boundary migration in high pressure shear zones, creating garnet layers with an SPO but not an LPO in the Haram Gabbro, Haramsøya, Norway.

However these garnet grains displayed an SPO and garnet layers in the streaked eclogite do not. This does not however rule out the possibility that these garnet layers formed by grain boundary sliding. As previously said, the small difference in neighbour and random pair misorientation angle distributions may possibly represent the presence of subgrains in the garnet grains and thus the action of dislocation creep. However this difference between the misorientation angle distributions is very small suggesting that dislocation creep may not be as important a mechanism as originally thought. This leaves the possibility of grain boundary sliding as a possible mechanism for the formation of garnet layers. If, as with the Haram Gabbro, this is assisted by grain boundary migration then an explanation for the occurrence of a small amount of subgrain boundaries in garnet exists.

The garnet layers in the Haram Gabbro are thought to have formed contemporaneously with deformation. As already discussed the location fabric of the streaked eclogite lithology is thought to have been inherited from previous tectonic events prior to that of the Alpine Orogeny. Given that the location fabric of this lithology may be inherited, it is possible that garnet layers are a product of an inherited location fabric, forming by garnet nucleation and growth.

6.4.5 Evolution of the Streaked Eclogite Lithology of Colle della Barme d'Oropa

What follows here is a summation of the possible evolution of the streaked eclogite lithology of Colle della Barme d'Oropa based on the results and conclusions of this chapter.

As discussed in chapter 2 the Sesia-Lanzo Zone displays evidence for amphibolite/granulite facies metamorphism. In fact in some areas of the EMC hornblende aggregates can be seen to be overprinted by eclogite and greenschist facies assemblages (Williams and Compagnoni, 1983). Pre-Alpine deformation creates a location fabric in the protolith of the EMC and streaked eclogite lithology. These rocks are then intruded by aplite sheets some of which crosscut the pre-Alpine fabrics some run parallel to them.

Subduction leads to eclogite facies metamorphism developing eclogite facies minerals, omphacite and garnet in all lithologies. Garnet and omphacite develop in layers of variable bulk composition on the thin section scale. Small amounts of strain accompany early omphacite growth creating an LPO in the omphacite layers. Subsequent anisotropic growth created large oriented omphacite grains which display microstructures associated with omphacite grain growth suggesting some of the eclogite facies metamorphism is static rather than dynamic. Garnet forms showing variable zonation representing growth through changing temperature conditions. After a period of garnet growth dislocation creep creates small amounts of subgrain walls within separate garnet grains. Dislocation creep was however not prolific as chemical zonation is quite sharp hence dislocations must not have been highly mobile otherwise this chemical microstructure would not exist.

Alpine deformation is defined in the Sesia-Lanzo Zone in this area by the development of a white mica shape fabric in aplite sheets, eclogite facies and retrogressive facies folding and as mentioned earlier some small amount of deformation in the EMC and streaked eclogite as evidenced by the development on an omphacite LPO in the streaked eclogite. Retrogression to amphibolite facies conditions then occurred creating the amphibole filled fractures across omphacite grains and amphibole growth near garnet grains.

6.5 Conclusions

From the results presented in this chapter it is shown that omphacite not only develops subgrain boundaries through deformation but can also generate specific microstructures through some growth mechanism. EBSD has been key in identifying these structures but has proven limited in elucidating the mechanism by which they form.

An investigation into what mechanisms may have been responsible for LPO development in the streaked eclogite lithology have shown that microstructures normally associated with dislocation creep must be carefully considered relevant to omphacite grain form so as not to confuse growth microstructures with deformation microstructures. In addition anisotropic grain growth of omphacite may play a large role in LPO development in eclogite facies rocks under stress. Whether it was the sole mechanism forming the observed omphacite LPO patterns or whether it represents a period of static eclogite metamorphism after some small amount of early deformation remains unresolved.

Unlike the eclogite facies rocks of the Zermatt-Saas Unit, garnet in the streaked eclogite lithology may contribute to the deformation of this rock either through some small amount of dislocation creep or grain boundary sliding. Contrary to this though is the possibility that garnet layers are a result of nucleation and growth in a pre-existing layer of a location fabric formed in a pre-Alpine deformation event meaning no Alpine deformation mechanism is required to form them.

Of significant importance to this study is the possibility that the location fabric of the streaked eclogite lithology is possibly inherited from a location fabric that formed in the Sesia-Lanzo Zone's pre-Alpine tectonic history. Possible evidence lies in aplite sheet structural relationships with the shape fabric of the country rock and the likelihood that garnet and omphacite layers grew at least in part statically meaning their layer segregation is not due to a large amount of strain. This holds implications for the way the structural geology and microstructural development of newly forming mineralogy is interpreted in a tectonic unit that has experienced a long metamorphic and structural history.

7 Chapter 7: Synthesis and Further Work

7.1 Summary of Aims

In this chapter the conclusions and assumptions made from the data presented in the previous three chapters is summarised and considered in relation to how the overall aims of this thesis are met:

1. To understand the deformation mechanisms responsible for LPO development in omphacite in both monometamorphic and polymetamorphic terrains, using electron backscatter diffraction data (EBSD) and chemical data.
2. To understand the role of garnet, if any, in the deformation of eclogite rocks in monometamorphic and polymetamorphic rocks, using EBSD and chemical data.
3. To examine the effect of pre-existing microstructure on later forming mineral phases.
4. To link microstructural findings to the overall regional evolution of eclogite facies tectonic units.

In addition to this, further avenues or research and possible additional future work on the conclusions and ideas outlined by this thesis are suggested.

Aims 1 and 2 are addressed in chapters 4 and 6, aim 3 in chapter 5 and aim 4 is addressed in chapters 4, 5 and 6.

7.2 Deformation Mechanisms Responsible for LPO Development in Omphacite (Aim 1)

Careful examination of omphacite microstructures, using a combination of techniques, from both monometamorphic and polymetamorphic eclogite facies rocks reveal that not only do omphacite LPO patterns develop through a combination of deformation mechanisms but that they can also form from some omphacite growth mechanism.

Omphacite in eclogite facies rocks from the Punta Telcio region of the Zermatt-Saas Unit show a strong S-type LPO. This LPO formed through a combination of dislocation creep followed by a period of diffusion creep. This is ascertained by a combination of EBSD, TEM and chemical zoning data. The preferential sharp chemical zoning observed in omphacite grains and preferred growth on broken omphacite grains suggests that diffusion creep was in operation. Dislocation creep, evident due to the occurrence of subgrain boundaries and misorientation angle distribution patterns, is determined to have occurred prior to diffusion creep as otherwise the sharp chemical patterns observed in omphacite grains would not exist, rather more diffuse zoning profiles would likely be evident.

In contrast omphacite from the streaked eclogite lithology of the Colle della Barme d'Oropa is thought to have developed an LPO through significant action of anisotropic grain growth under static conditions, possibly preceded by small amounts of dislocation creep. Investigation of omphacite microstructures in the streaked eclogite lithology and comparison to omphacite growth microstructures in an undeformed eclogite pod reveal that growth mechanisms are strikingly similar and care must be taken not to mistake them for the action of dislocation creep.

In addition TEM investigation of omphacite in the Zermatt-Saas combined with temperature conditions for eclogite facies metamorphism taken from previous studies and omphacite chemistry suggest that it is not omphacite space group that dictates which LPO pattern develops. We assume therefore that LPO type is determined by the strain regime the eclogite is deforming in. As the eclogites from the Lago Blu area of Punta Telcio display an S-type LPO pattern we argue for deformation in a flattening strain regime.

7.2.1 Further Work on omphacite LPO

What seems to be lacking in omphacite deformation studies is the construction of a deformation mechanism map. This thesis has shown that omphacite LPO can be generated from a combination of a variety of mechanisms. The evidence for dislocation creep, diffusion creep and anisotropic grain growth in the development of omphacite LPO now needs further consideration as to how large or small the limits

of controlling factors, such as grain size, stress and temperature, are, given the action of these mechanisms in omphacite of eclogite facies rocks described here.

In addition further work is required to determine if indeed it is strain regime and not space group that controls the omphacite LPO pattern formation in these eclogite facies rocks. For omphacite of the Zermatt-Saas eclogite facies rocks an SPO study would help shed some light on possible strain regime controls. It has been noted that a relationship exists between the shape fabric of omphacite and its LPO (Helmstaedt et al., 1972, Godard et al., 1995, Abalos, 1997, Mauler et al., 2001). If indeed an S-type LPO implies a flattening strain regime an expected oblate SPO in omphacite should also be observed.

Similarly further work like this is required on omphacite from the streaked eclogite lithology of the Sesia-Lanzo Zone. TEM work to determine the space groups of omphacite with variable LPO patterns and a more tightly constrained pressure and temperature for the eclogite facies metamorphism in the Colle della Barme d'Oropa area would shed some light on this situation. As mentioned the variable LPO noted in the omphacite of the streaked eclogite samples may be due to eclogite facies folding. What is needed to explore the theory of strain regime controlled LPO more soundly in these rocks is detailed structural analysis of the folds found within this lithology.

A useful microstructural tool not utilised in this thesis is misorientation axes distribution analysis. Application of this to the current EBSD data set for omphacite in the rocks investigated in this thesis may show whether a certain misorientation axis is common to omphacite deformation by dislocation creep in the Zermatt-Saas Unit and may also help characterise the growth structures noted in the omphacite of the streaked eclogite lithology from the Sesia-Lanzo Zone.

A final piece of further work that remains important to this study is anything that may further our understanding of what mechanisms are responsible for the development of growth microstructures in omphacite as displayed by omphacite in an undeformed eclogite pod. It is thought possible that experimental work on omphacite grain growth and TEM investigation on the subgrain boundaries that result from some growth mechanism may provide useful insight.

7.3 Role of Garnet in the Deformation of Eclogite Facies Rocks (Aim 2)

Study of possible garnet deformation within eclogite facies rocks from oceanic and continental tectonic units shows that garnet has a variable contribution to the deformation of these rocks. In the Zermatt-Saas garnet is seen to contribute very little to the deformation in the rock with most of the strain being accommodated by omphacite. Rare impinged garnet grains occasionally displayed evidence of plastic deformation but most deformation in garnet is evidenced by slight orientation differences related to the action of brittle fracturing.

In contrast to this fine grained garnet layers within the streaked eclogite lithology of the Sesia-Lanzo Zone show possible evidence for the action of dislocation creep or grain boundary sliding. This may suggest that when garnet is concentrated in a non-porphyroblastic way it may contribute more to eclogite deformation. It is concluded here that any contribution garnet makes to the overall deformation of an eclogite facies rock depends on the distribution of garnet within the rock and its grain size. As a more variable distribution can be expected in eclogitised continental rocks due to variable parent lithology we assume garnet has more contribution to eclogite rheology there than in 'normal' eclogite facies rocks that arise from eclogitised oceanic rocks.

7.3.1 Further work on garnet

Further work is required to explain some of the rare garnet microstructures observed in some of the eclogite facies rock samples from the Punta Telcio region of the Zermatt-Saas. It is felt that further detailed chemical analysis of these garnets combined with the already existing EBSD work and a search for similar structures within these rocks would go a long way to achieving this.

Garnet layers in the streaked eclogite lithology display the possible action of dislocation creep and further understanding of what composes these boundaries would be useful. To this end TEM study of these subgrain walls would allow us to see what slip systems were in operation during the deformation of this eclogite facies unit. In addition further chemical analysis including quantitative data would aid in constructing a more complete story for the growth and development of this mineral and aid in developing the story of the evolution of this eclogite facies unit as whole.

As previously mentioned for the omphacite work, misorientation axes distribution analysis on the existing garnet EBSD data would be useful for the same reasons mentioned there.

7.4 Effect of Pre-existing Microstructure on Later Forming Mineral Phases (Aim 3)

Results presented in chapter 5 have shown that fabrics created in eclogite facies mineral phases have the potential to significantly affect fabric development in phases developing in retrogressive stages of a tectonic unit's evolution. EBSD orientation data can be successfully used to identify the existence of mimetic LPO formation. D-D, P-P and PD-PD maps as well as interphase misorientation angle distribution analysis are excellent tools to investigate this phenomenon.

In the Zermatt-Saas Unit retrogressive barroisite in eclogite facies rocks shows a 'special orientation relationship' to omphacite such that it replaces the mineral through a 180° rotation around the <001> axis of omphacite. This retrogressive phase also shows an exact crystal orientation replacement of pre-existing glaucophane. The resulting LPO that develops in barroisite has thus formed by mimicry of pre-existing omphacite and glaucophane LPO patterns, combining elements of each.

In the Sesia-Lanzo Zone the possibility that the location fabric of the streaked eclogite lithology being inherited from a pre-existing location fabric formed during an earlier stage of the Sesia-Lanzo Zone's tectonic history is explored. Possible evidence comes in from structural observations of aplite sheet relationships with the shape fabric of the country rock and the likelihood that garnet and omphacite layers grew, at least in part, statically suggesting their segregation into separate layers is not due to a large amount of strain. In addition to this the suggestion is made that the omphacite LPO in this lithology is a mimetic LPO on a pre-existing granulite/amphibolite facies mineral LPO. Though there exist some suggestion that the eclogite facies location fabric is inherited from earlier structures and that omphacite LPO may be mimetic it is not as clear cut as that of retrogressive mimetic LPO development in the Zermatt-Saas Unit.

7.4.1 Further Work on the Effect of Pre-existing Phases

Results from this work have shown that mimetic fabrics have the potential to be a common microstructural feature in crustal rocks. The techniques used here in this study have also proven themselves to be very useful in identifying the microstructural and orientation relationships involved in this mechanism.

In light of this further development of the techniques used here would be useful. This study makes use of interphase misorientation angle distribution to distinguish a 'special orientation relationship' between neighbouring omphacite and barroisite grains and a direct crystal lattice replacement of barroisite on glaucophane grains. However it does so by considering each crystallographic axis separately. Intraphase misorientation can be done using the Channel software which considers a full three dimensional misorientation within a phase. Development of a similar process for interphase misorientation would be another useful tool in these kinds of investigations.

In addition to the further development of interphase misorientation angle distribution analysis, development of a program to investigate interphase misorientation axes distributions (currently not possible with existing software) would prove useful for characterising the 'special relationship' misorientation boundary that exists between omphacite and barroisite as well as other interphase relationships (glaucophane/barroisite).

This study deals solely with comparisons between monoclinic minerals all of which have similar lattice parameters. In addition to this, interphase misorientation investigations would benefit from development of this technique so that orientation comparisons between minerals of different crystal systems could be performed. Also further investigation into how the actual atomic structures of interphase boundaries align would provide a complete definition of mimetic relationships between omphacite/barroisite and glaucophane/barroisite.

The eclogite facies rocks studied in this thesis contain a number of potential case studies for investigating the effect of pre-existing minerals on the development of new ones. The breakdown of jadeite and quartz to albite during retrogression of the Zermatt-Saas unit provides such an example. This would require an investigation of

orientation between minerals of different crystal symmetries. In the Sesia-Lanzo Zone retrogression may provide further examples of eclogite facies minerals controlling the growth of retrogressive ones. For example, retrogressive fracture fills across large, elongate omphacite grains show fibrous like growths of green amphibole (Fig. 6.11). This fracture fill texture holds the potential to have formed due to retrogressive minerals forming a preferential orientation on omphacite.

7.5 Implication of Microstructural Findings to the Evolution of Eclogite Facies Tectonic Units (Aim 4)

7.5.1 Zermatt-Saas Unit

What follows here is a summary of what the microstructural evidence suggests about the evolution of the Zermatt-Saas Unit using the combined results of chapters 4 and 5. The unit experienced eclogite facies metamorphism due to subduction and develops common eclogite mineralogy. As shown by lack of garnet deformation omphacite is considered to accommodate the majority of the strain on the rock during this period. Omphacite deforms first by dislocation creep as evidenced by the occurrence of subgrain boundaries and low angle neighbour pair interphase misorientation angle distributions. This is then followed by a period of deformation where diffusion creep is the dominant mechanism as evidenced by preferential chemical zoning. The combined efforts of dislocation and diffusion creep create an S-type omphacite LPO pattern. From this we assume this area of the Zermatt-Saas Unit experiences a flattening strain regime at this period of its evolution.

Retrogression due to extension along the Gressoney Shear Zone, through blueschist facies conditions results in the growth of glaucophane. This phase also forms an LPO possibly through plastic deformation likely in tandem with omphacite and subsequent grain growth on the glaucophane grains during a static period of exhumation creates large porphyroblasts, some of which cross cut eclogite facies fabrics. As exhumation continues, folding of the Punta Telcio region begins, creating a large kilometre scale recumbent fold in the area. Omphacite and glaucophane stretching lineations develop parallel to the fold hinge due to large enough strains rotating the fold hinge parallel to the stretching direction.

Eventually exhumation leads to greenschist facies conditions. Green amphibole develops as the predominant phase here. Barroisite growth occurs early in this stage, mimetically replacing both omphacite and glaucophane, developing an LPO that incorporates components of both pre-existing LPO patterns. <001> and (010) pole figures contain elements found in omphacite and glaucophane LPO patterns and (100) pole figures contain patterns common to glaucophane LPO patterns but not omphacite LPO patterns. This stage of exhumation is static rather than dynamic though it is possible a small amount of strain occurred late in this stage forming subgrain walls in barroisite. Lower greenschist conditions occur with further exhumation noted by the change in amphibole chemistry from barroisite to magnesio-hornblende and actinolite. This latter stage partially replaces the barroisite grains in this rock.

7.5.2 Sesia-Lanzo Zone

What follows here is a summary of the possible evolution of the streaked eclogite lithology of Colle della Barme d'Oropa based on the results and conclusions of chapter 6. The Sesia-Lanzo Zone displays evidence for amphibolite/granulite facies metamorphism prior to the eclogite facies event. Pre-Alpine deformation created a location fabric in the protolith of the EMC and streaked eclogite lithology. These rocks are then intruded by aplite sheets some of which crosscut the pre-Alpine fabrics some run parallel to them.

Eclogite conditions occur as subduction of this tectonic unit begins and common eclogite mineralogy develops. Garnet and omphacite develop in layers due to pre-existing layers having variable bulk composition on the thin section scale. Small amounts of strain accompany early omphacite growth creating an LPO in the omphacite layers. Subsequent anisotropic growth then creates large oriented omphacite grains which display microstructures associated with omphacite grain growth suggesting some of the eclogite facies metamorphism is static rather than dynamic. Meanwhile garnet forms in its separate layers showing variable zonation possibly representing growth through changing temperature conditions. Dislocation creep then occurs in the garnet grains creating small amounts of subgrain walls. Dislocation creep was however not prolific as chemical zonation is quite sharp hence

dislocations must not have been highly mobile otherwise this chemical microstructure would not exist.

7.5.3 Further Work on the Implications of Eclogite Microstructure

As already mentioned further work is required in the Sesia-Lanzo Zone to determine the cause of variable omphacite LPO patterns. If LPO is linked to strain regime careful structural mapping of fold structures and sampling of streaked eclogite on fold limb and hinges should show a correlation between S-type LPOs on the fold limbs (flattening strain regime) and L-type LPO on the hinges (constrictional strain regime). If such results were found folding events in the streaked eclogite lithology could be linked to eclogite facies metamorphism. In the Zermatt-Saas an investigation into SPO of omphacite will provide another test of whether the S-type LPO is related to the eclogite facies rocks deforming in a flattening strain regime. If it is then we would expect to see an oblate SPO.

Again as already mentioned, further investigation into mimetic microstructures in eclogite facies mineralogy in the Sesia-Lanzo Zone may further the idea of the streaked eclogite location fabric being an inherited feature. Further sampling of the streaked eclogite lithology and investigation of omphacite and garnet microstructures in the EMC lithology (which also contains a potentially pre-Alpine location fabric) may shed more light on this.

References

Abalos, B. (1997). Omphacite fabric variation in the Cabo Ortegal eclogite (NW Spain): Relationships with strain symmetry during high-pressure deformation. Journal Of Structural Geology **19**(5): 621-637.

Alam, M. N., M. Blackman and D. W. Paschley (1954). High-angle kikuchi patterns. Proceedings of the Royal Society **221A**: 224.

Amato, J., M., C. Johnson, M., L. Baumgartner, P. and B. Beard, L. (1999). Rapid exhumation of the Zermatt-Saas ophiolite deduced from high-precision Sm-Nd and Rb-Sr geochronology. Earth And Planetary Science Letters **171**: 425-438.

Ando, J., K. Fujino and T. Takeshita (1993). Dislocation microstructures in naturally deformed garnet. Physics Of The Earth And Planetary Interiors **80**: 105-116.

Argand, E. (1911). Les nappes de recouvrement des Alpes penniques et leurs prolongments structuraux. Beitraege zur Geologischen Karte der Schweiz **31**: 1-26.

Atherton, M. P. and W. M. Edmunds (1966). An electron microprobe study of some zoned garnets from metamorphic rocks. Earth And Planetary Science Letters **1**: 185-193.

Avé Lallement, H. G. (1978). Experimental Deformation Of Diopside And Websterite. Tectonophysics **48**(1-2): 1-27.

Azough, F. and R. Freer (2000). Iron diffusion in single-crystal diopside. Physics And Chemistry Of Minerals **27**(10): 732-740.

Babaie, H. A. and T. E. La Tour (1994). Semibrittle and cataclastic deformation of hornblende-quartz rocks in a ductile shear zone. Tectonophysics **229**: 19-30.

Baratoux, L., K. Schulmann, S. Ulrich and O. Lexa (2005). Contrasting microstructures and deformation mechanisms in metagabbro mylonites contemporaneously deformed under different temperatures (c. 650oC and c. 750oC). Deformation Mechanisms, Rheology and Tectonics: from Minerals to the

Lithosphere. D. Gapais, J. P. Brun and P. R. Cobbold, Geological Society, London, Special Publications. **243:** 97-125.

Barnert, E. B., W. F. Muller, E. Schmadicke and G. Fabries (2001). Transmission electron microscopy on eclogites from the Lower Schist Cover and the Eclogite Zone (Tauern Window, Austria). Mitteilungen der Österreichischen Mineralogischen Gesellschaft **146**: 31-33.

Barnicoat, A., C. and N. Fry (1986). High-pressure metamorphism of the Zermatt-Saas ophiolite zone, Switzerland. Journal of the Geological Society, London **143**: 607-618.

Bascou, J., G. Barruol, A. Vauchez, D. Mainprice and M. Egydio-Silva (2001). EBSD-measured lattice-preferred orientations and seismic properties of eclogites. Tectonophysics **342**(1-2): 61-80.

Bascou, J., A. Tommasi and D. Mainprice (2002). Plastic deformation and development of clinopyroxene lattice preferred orientations in eclogites. Journal Of Structural Geology **24**(12): 1357-1368.

Beccaluva, L., G. V. Dal Piaz, G. Macciotta and O. Zeda (1978). The austroalpine harzburgite body of the Artogna Valley (Italian Western Alps). Memorie degli Istituti di Geologia e Mineralogia dell' Università di Padova **33**: 173-181.

Bell, P. M. and B. T. C. Davis (1969). Melting relations in the system jadeite-diopside at 30 and 40 kilobars. American Journal of Science **267-A**: 17-32.

Berger, A. and H. Stünitz (1996). Deformation mechanisms and reaction of hornblende: examples from the Bergell tonalite (Central Alps). Tectonophysics **257**: 149-174.

Biermann, C. (1981). (100)-deformation twins in naturally deformed amphiboles. Nature **292**: 821-823.

Biermann, C. and H. L. M. Van Roermund (1983). Defect structures in naturally deformed clinoamphiboles - a TEM study. Tectonophysics **95**: 267-278.

Bocquet, C., M. Delaloye, J. Hunziker and D. Krummenacher (1974). K-Ar and Rb-Sr dating of blue amphiboles, micas and associated minerals from the Western Alps. Contributions To Mineralogy And Petrology **47**: 7-26.

Boland, J. N. and T. E. Tullis (1986). Deformation Behaviour of Wet and Dry Clinopyroxenite in the Brittle to Ductile Transition Region. Mineral and Rock Deformation: Laboratory Experiments; the Patterson Volume. Hobbs and Heard, *Geophys. Monogr. Am. Geophys. Union* 35-49.

Borghi, A., R. Cossio, F. Olmi, R. Ruffini and G. Vaggelli (2002). EPMA major and trace element analysis in garnet and its petrological application. Mikrochimica Acta **139**(1-4): 17-25.

Bounhoure, V., S. Lay and M. Loubradou (2008). Special WC/Co orientation relationships at basal facets of WC grains in WC-Co alloys. Journal of Materials Science **43**: 892-899.

Brenker, F. E. (1998). Mikrogefügethermochronometrie für Eklogite. Frankfurt, J.W. Geothe Universität **Thesis**.

Brenker, F. E., W. F. Müller and G. P. Brey (2003). Variation of antiphase domain size in omphacite: A tool to determine the temperature-time history of eclogites revisited. American Mineralogist **88**(8-9): 1300-1311.

Brenker, F. E., D. Prior and W. F. Müller (1999). Cation ordering in omphacite and effect on deformation and lattice preferred orientation, Nuestadt an der Weinstrasse, Germany.

Brenker, F. E., D. J. Prior and W. F. Muller (2002). Cation ordering in omphacite and effect on deformation mechanism and lattice preferred orientation (LPO). Journal Of Structural Geology **24**(12): 1991-2005.

Brodie, K. H. and E. H. Rutter (1985). On the relationship between deformation and metamorphism, with special reference to the behaviour of basic rocks. Metamorphic Reactions: Kinetics, Texture and Deformation. A. B. Thompson and D. C. Rubie, Advanced Physical Geochemistry. **4:** 138-179.

Buatier, M., H. L. M. van Roermund, M. R. Drury and J. M. Lardeaux (1991). Deformation and recrystallisation mechanisms in naturally deformed omphacites from the Sesia-Lanzo zone; geophysical consequences. Tectonophysics **195**(1): 11-27.

Bucher, K., Y. Fazis, C. de Capitani and R. Grapes (2005). Blueschists, eclogites, and decompression assemblages of the Zermatt-Saas ophiolite: High-pressure metamorphism of subducted Tethys lithosphere. American Mineralogist **90**: 821 - 835

Bystricky, M. and S. Mackwell (2001). Creep of dry clinopyroxene aggregates. Journal Of Geophysical Research-Solid Earth **106**(B7): 13443-13454.

Carlson, W., C. Denison and R. A. Ketcham (1995). Controls on the nucleation and growth of porphyroblasts: Kinetics from natural textures and numerical models. Geological Journal **30**(3-4): 207-225.

Carlson, W. D. (1989). The significance of intergranular diffusion to the mechanisms and kinetics of porphyroblast crystallization. Contributions To Mineralogy And Petrology **103**(1): 1.

Carlson, W. D. and C. Denison (1992). Mechanisms of porphyroblast crystallisation - results from high-resolution computed x-ray tomography. Science **257**: 1236-1239.

Carpenter, M. A. (1979). Contrasting properties and behaviour of antiphase domains in pyroxenes. Physics And Chemistry Of Minerals **5**: 119-131.

Carpenter, M. A. (1980). Mechanisms of exsolution in sodic pyroxenes. Contributions To Mineralogy And Petrology **71**: 289-300.

Carpenter, M. A. (1981). Omphacite Microstructures As Time-Temperature Indicators Of Blueschist-Facies And Eclogite-Facies Metamorphism. Contributions To Mineralogy And Petrology **78**(4): 441-451.

Carpenter, M. A. (1981). Time-Temperature-Transformation (Ttt) Analysis Of Cation Disordering In Omphacite. Contributions To Mineralogy And Petrology **78**(4): 433-440.

Carstens, H. (1968). The lineage structure of quartz crystals. Contributions To Mineralogy And Petrology **18**: 295-304.

Cartwright, I. and A. Barnicoat, C. (2002). Petrology, geochronology, and tectonics of shear zones in the Zermatt-Saas and Combin zones of the Western Alps. Journal Of Metamorphic Geology **20**: 263-281.

Chakraborty, S. and J. Ganguly (1992). Cation diffusion in aluminosilicate garnets: experimental determination in spessartine-almandine diffusion couples, evaluation of effective binary diffusion coefficients and applications. Contributions To Mineralogy And Petrology **111**: 74-86.

Champion, Y. and S. Hagège (1992). A study of composite interfaces in the Zr-ZrB_2 system. Journal of Materials Science Letters **11**: 290-293.

Champness, P. E. (1973). Speculation on an order-disorder transformation in omphacite. American Mineralogist **58**: 540-542.

Cheng, G. M., Y. X. Tian and H. L. L. (2009). Orientation relationship and interfacial structure between Nb solid solution precipitates and a-Nb_5Si_3 intermetallics. Journal of Materials Research **24**: 192-197.

Chopin, C. and P. Monié (1984). A unique magnesiochloritoid-bearing, high-pressure assemblage from the Monte Rosa, Western Alps: petrologic and $^{40}Ar - ^{39}Ar$ radiometric study. Contributions To Mineralogy And Petrology **87**: 388-398.

Clark, J. R. and J. J. Papike (1968). Crystal-chemical characterization of omphacite. American Mineralogist **53**: 840-868.

Cobbold, P. R. and A. Watkinson (1981). Bending anisotropy: a mechanical constraint on the orientation of fold axes in an anisotropic medium. Tectonophysics **72**: T1-T10.

Coleman, R. G., D. E. Lee, L. B. Beatty and W. W. Brannock (1965). Eclogites and eclogites: Their differences and similarities. Geological Society of America Bulletin **76**: 483-508.

Compagnoni, R. (1977). The Sesia-Lanzo Zone: high pressure-low temperature metamorphism in the Austroalpine continental margin. Rendiconti della Società Italiana di Mineralogia e Petrologia **33**: 335-374.

Compagnoni, R., G. Dal Piaz, J. Hunziker, G. Gosso, B. Lombardo and P. Williams (1977). The Sesia-Lanzo Zone, a slice of continental crust with alpine high pressure-low temperature assemblages in the Western Italian Alps. Rendiconti della Società Italiana di Mineralogia e Petrologia **33**: 281-334.

Compagnoni, R. and B. Maffeo (1973). Jadeite-bearing metagranites l.s. and related rocks in the Monte Mucrone area (Sesia-Lanzo Zone, Western Italian Alps). Schweizerische Mineralogische und Petrographische Mitteilungen **53**: 355-378.

Coward, M. P. and G. J. Potts (1983). Complex strain patterns developed at the frontal and lateral tips to shear zones and thrust zones. Journal Of Structural Geology **5**: 383-399.

Cox, S. F. and M. A. Etheridge (1983). Crack-seal fibre growth mechanisms and their significance in the development of oriented layer silicate microstructures. Tectonophysics **92**: 147-170.

Cuthbert, S. J. and J. O. Buckman (2005). Charge contrast imaging of fine-scale microstructure and compositional variation in garnet using the environmental scanning electron microscope. American Mineralogist **90**(4): 701-707.

Dachs, E. and A. Proyer (2002). Constraints on the duration of high-pressure metamorphism in the Tauern Window from diffusion modelling of discontinuous growth zones in eclogite garnet. Journal Of Metamorphic Geology **20**(8): 769-780.

Dal Piaz, G. (1966). Gneiss ghiandoni, marmi ed anfiboliti antiche del ricoprimento Monte Rosa nell'alta Valle d'Ayas. Bollettino della Societa Geologica Italiana **85**: 103-132.

Dal Piaz, G. (1971). Nuovi ritrovamenti di cianite alpina nel cristallino del Monte Rosa. Rendiconti della Società Italiana di Mineralogia e Petrologia **27**: 437-477.

Dal Piaz, G., A. Bistacchi and M. Massironi (2003). Geological Outline of the Alps. Episodes **26**: 175-180.

Dal Piaz, G., V. and W. Ernst, G. (1978). Areal geology and petrology of eclogites and associated metabasites of the Piemonte ophiolite nappe, Breuil-St. Jacques area, Italian Western Alps. Tectonophysics **51**: 99-126.

Dal Piaz, G., G. Gosso and G. Martinotti (1971). La II Zona Diorito-Kinzigitica tra la Valsesia e la Valle d'Ayas. Memorie Società Geologica Italiana **10**: 257-276.

Dal Piaz, G., J. Hunziker and G. Martinotti (1972). La zona Sesia-Lanzo e l'evoluzione tettonico-metamorfica delle Alpi nordoccidentali interne. Memorie Società Geologica Italiana **11**: 433-460.

Daniel, C. G. and F. S. Spear (1998). Three-dimensional patterns of garnet nucleation and growth. Geology **26**(6): 503-506.

Darco, P., F. F. Fava, R. Dovesi and V. R. Saunders (1996). Structural and electronic properties of pyrope garnet (Mg3Al2Si3O12): An ab initio study. Journal Of Physics-Condensed Matter **8**(45): 8815-8828.

Deer, W. A., R. A. Howie and J. Zussman (1992). An Introduction to the Rock-Forming Minerals, Pearson Education Limited.

DenBrok, B. and J. H. Kruhl (1996). Ductility of garnet as an indicator of extremely high temperature deformation: Discussion. Journal Of Structural Geology **18**(11): 1369-1373.

Desmons, J. and E. Ghent (1977). Chemistry, Zonation and Distribution Coefficients of Elements in Eclogitic Minerals from the Eastern Sesia Unit, Italian Western Alps. Schweizerische Mineralogische und Petrographische Mitteilungen **57**: 397-411.

Desmons, J, O'Neil, J.R., (1978). Oxygen and Hydrogen Isotope Compositions of Eclogites and Associated Rocks from the Eastern Sesia Zone (Western Alps, Italy). Contributions to Mineralogy and Petrology **67**: 79-85.

Diaz Aspiroz, M., G. E. Lloyd and C. Fernandez (2007). Development of lattice preferred orientation in clinoamphiboles deformed under low-pressure metamorphic

conditions. A SEM/EBSD study of metabasites from the Aracena metamorphic belt (SW Spain). Journal Of Structural Geology **29**: 629-645.

Dimanov, A. and O. Jaoul (1998). Calcium self-diffusion in diopside at high temperature: Implications for transport properties. Physics And Chemistry Of Minerals **26**(2): 116-127.

Dimanov, A., O. Jaoul and V. Sautter (1996). Calcium self-diffusion in natural diopside single crystals. Geochimica Et Cosmochimica Acta **60**(21): 4095-4106.

Dimanov, A. and V. Sautter (2000). Average interdiffusion of (Fe,Mn)-Mg in natural diopside. European Journal Of Mineralogy **12**(4): 749-760.

Dingley, D. J. (1984). Diffraction from sub-micron areas using electron backscattering in a scanning electron microscope. Scanning Electron Microscopy **2**: 569-575.

Dingley, D. J. and V. Randle (1992). Microtexture determination by electron back-scatter diffraction. Journal of Materials Science **27**: 4545-4566.

Dobbs, H. T., L. Peruzzo, F. Seno, R. Spiess and D. J. Prior (2003). Unravelling the Schneeberg garnet puzzle: a numerical model of multiple nucleation and coalescence. Contributions To Mineralogy And Petrology **146**(1): 1-9.

Doin, M.-P. and P. Henry (2001). Subduction initiation and continental crust recycling: the roles of rheology and eclogitisation. Tectonophysics **342**: 163-191.

Dollinger, G. and J. D. Blacic (1975). Deformation mechanisms in experimentally and naturally deformed amphiboles. Earth And Planetary Science Letters **26**: 409-416.

Dorner, D. and B. Stöckhert (2004). Plastic Flow Strength of jadeite and diopside investigated by microindentation hardness tests. Tectonophysics **379**: 227-238.

Droop, G. (1987). A general equation for estimating Fe3+ concentrations in ferromagnesian silicates and oxides from microprobe analyses, using stoichiometric criteria. Mineralogical Magazine **51**: 431-435.

Duchêne, S., J. Blichert-Toft, B. Luais, P. Telouk, J. M. Lardeaux and F. Albarede (1997). The Lu-Hf dating of garnets and the ages of the Alpine high-pressure metamorphism. Nature **387**: 586-589.

Ellis, D. J. and D. H. Green (1979). Experimental-Study Of The Effect Of Ca Upon Garnet-Clinopyroxene Fe-Mg Exchange Equilibria. Contributions To Mineralogy And Petrology **71**(1): 13-22.

Erambert, M. and H. Austrheim (1993). The effect of fluid and deformation on zoning and inclusion patterns in poly-metamorphic garnets. Contributions To Mineralogy And Petrology **115**: 204-214.

Escher, A., J. Hunziker, M. Marthaler, H. Masson, M. Sartori and A. Steck (1997). Geologic framework and structural evolution of the western Swiss-Italian Alps. Deep Structure of the Swiss Alps, Results of NRP 20. O. Pfiffner, P. Lehner, P. Heitzmann, M. St. and S. A. Basel, Birkhäuser**:** 205-221.

Escher, A. and J. Watterson (1974). Stretching fabrics, folds and crustal shortening. Tectonophysics **22**: 223-231.

Essene, E. J. and W. S. Fyfe (1967). Omphacite in Californian metamorphic rocks. Contributions To Mineralogy And Petrology **15**: 1-23.

Foreman, R. (2004). The structural, microstructural and metamorphic evolution of the Drøsdal eclogite body, western Norway. Department of Earth and Ocean Science. Liverpool, University of Liverpool. **Thesis**.

Freed, R. L. and D. R. Peacor (1967). Refinement of the crystal structure of johannsenite. American Mineralogist **52**: 709-720.

Freer, R. (1979). An experimental measurement of cation diffusion in almandine garnet. Nature **280**: 220-222.

Freer, R. and A. Edwards (1999). An experimental study of Ca-(Fe,Mg) interdiffusion in silicate garnets. Contributions To Mineralogy And Petrology **134**(4): 370-379.

Frey, M. and J. Hunziker (1976). Equilibrium-Disequilibrium Relations in the Monte Rosa Granite, Western Alps: Petrological, Rb-Sr and Stable Isotope Data. Contributions To Mineralogy And Petrology **55**: 147-179.

Froitzheim, N. (2001). Origin of the Monte Rosa nappe in the Pennine Alps - A new working hypothesis. Geological Society of America Bulletin **113**: 604-614.

Fry, N. and A. Barnicoat, C. (1987). The tectonic implications of high-pressure metamorphism in the western Alps. Journal of the Geological Society, London **144**: 653-659.

Fynn, G. W. and W. J. A. Powell (1979). The cutting and polishing of electro-optic materials. London, Adams Hilger.

Gapais, D. and J.-P. Brun (1981). A comparison of mineral grain fabrics and finite strain in amphibolites from eastern Finland. Canadian Journal of Earth Sciences **18**: 995-1003.

Gibson, R. L. (1992). Sequential, syndeformational porphyroblast growth during Hercynian low-pressure/high-temperature metamorphism in the Canigou Massif, Pyrenees. Journal Of Metamorphic Geology **10**: 637-650.

Godard, G. (1988). Petrology of some eclogites in the Hercynides: The eclogites from the southern American Massif, France. Eclogites and Eclogite Facies Rocks. E. D. Smith, Elsevier, Amsterdam: 451-519.

Godard, G. (2001). Eclogites and their geodynamic interpretation: a history. Journal Of Geodynamics **32**: 165-203.

Godard, G. and van Roermund, H. L. M. (1995). Deformation-Induced Clinopyroxene Fabrics From Eclogites. Journal Of Structural Geology **17**(10): 1425-1443.

Gosso, G., G. Dal Piaz, V. Piovano and R. Polino (1979). High pressure emplacement of early-Alpine nappes, postnappe deformations and structural levels. Memorie dell'Instituto di Geologia e Mineralogia Padova **32**: 1-15.

Gotoh, Y. and I. Arai (1986). Calculation of interfacial energy of the fcc-bcc interface and its epitaxial orientation relationship. Japanese Journal of Applied Physics **25**: L583-L586.

Grujic, D. and N. Mancktelow (1995). Folds with axes parallel to the extension direction: an experimental study. Journal Of Structural Geology **17**: 279-291.

Hacker, B. R. and J. M. Christie (1990). Brittle/ductile and plastic/cataclastic transition in experimentally deformed and metamorphosed amphibolite. The Brittle-Ductile Transition in Rocks. A. G. Duba, W. B. Durham, J. W. Handin and H. F. Wang, AGU Geophysical Monograph. **56:** 127-148.

Han, Y., X. Wu, D. Meng and D. Li (2001). Microstructures (TEM) in omphacite and symplectitic plagioclase from UHP eclogite at Yingshan, Dabie Mountains, China. UHPM Workshop at Waseda University **3B04**: 95.

Haüy, R. J. (1822). Traité de Mineralogie, Bachelier, Paris Delance.

Helmstaedt, H., O. Anderson and A. Gavasci (1972). Petrofabric studies of eclogite, spinel-websterite and spinel-lherzolite xenoliths from kimberlite-bearing breccia pipes in Southeastern Utah and Northeastern Arizona. Journal Of Geophysical Research-Solid Earth **47**: 4350-4365.

Hirsch, D. M., D. J. Prior and W. D. Carlson (2003). An overgrowth model to explain multiple, dispersed high-Mn regions in the cores of garnet porphyroblasts. American Mineralogist **88**(1): 131-141.

Holland, T. and J. Blundy (1994). Non-ideal interactions in calcic amphiboles and their bearing on amphibole-plagioclase thermometry. Contributions To Mineralogy And Petrology **116**: 433-447.

Homam, S. M. (2003). Formation of atoll garnet in the Adara Aureole, NW Ireland. Journal of Science, Islamic Republic of Iran **14**: 247-258.

Hunziker, J. (1970). Polymetamorphism in the Monte Rosa, Western Alps. Eclogae geologicae Helvetiae **63**: 151-161.

Hunziker, J. (1974). Rb-Sr and K-Ar age determination and the alpine tectonic history of the Western Alps. Memorie dell'Instituto di Geologia e Mineralogia Padova **31**: 5-55.

Hunziker, J. and A. Zingg (1980). Lower Palaeozoic amphibolite to granulite facies metamorphism in the Ivrea Zone. Schweizerische Mineralogische und Petrographische Mitteilungen **60**: 181-213.

Inger, S., W. Ramsbotham, R. A. Cliff and D. Rex (1996). Metamorphic evolution of the Sesia-Lanzo Zone, Western Alps: time constraints from multi-system geochronology. Contributions To Mineralogy And Petrology **126**: 152-168.

Ji, S., Z.-M. Jin, J. Zhang and H. W. Green (2002). Eclogite rheology: Implications for subducted lithosphere: Comment and Reply. Geology **30**: 483-484.

Ji, S., K. Saruwatari, D. Mainprice, R. Wirth, Z. Xu and B. Xia (2003). Microstructures, petrofabrics and seismic properties of ultra high-pressure eclogites from Sulu region, China: implications for rheology of subducted continental crust and origin of mantle reflections. Tectonophysics **370**(1-4): 49.

Jiang, J. X. and A. C. Lasaga (1990). The Effect Of Postgrowth Thermal Events On Growth-Zoned Garnet - Implications For Metamorphic P-T History Calculations. Contributions To Mineralogy And Petrology **105**(4): 454-459.

Jin, Z.-M., J. Zhang, H. W. Green and S. Jin (2001). Eclogite rheology: Implications for subducted lithosphere. Geology **29**: 667-670.

Kamb, W. B. (1959). Theory of preferred orientation developed by crystallisation under stress. Journal of Geology **67**: 153-170.

Karato, S., Z. C. Wang, B. Liu and K. Fujino (1995). Plastic-Deformation Of Garnets - Systematics And Implications For The Rheology Of The Mantle Transition Zone. Earth And Planetary Science Letters **130**(1-4): 13-30.

Kern, H. and M. Fakhimi (1975). Effect of fabric anisotropy on compressional wave in various metamorphic rocks for the range 20-700°C at 2 kbars. Tectonophysics **28**: 227-244.

Koons, P. O. (1984). Implications To Garnet-Clinopyroxene Geothermometry Of Non-Ideal Solid-Solution In Jadeitic Pyroxenes. Contributions To Mineralogy And Petrology **88**(4): 340-347.

Koons, P. O. (1986). Relative geobarometry from high-pressure rocks of quartzofeldspathic composition from the Sesia Zone, Western Alps, Italy. Contributions To Mineralogy And Petrology **93**: 322-334.

Krabbendam, M. and J. Dewey (1998). Exhumation of UHP rocks by transtension in the Western Gneiss Region, Scandinavian Caledonides. Continental Transpressional and Transtensional Tectonics. R. Holdsworth, R. Strachan and J. Dewey. London, Geological Society of London. **135:** 159-181.

Kretz, R. (1974). Some models for the rate of crystallization of garnet in metamorphic rocks. Lithos **7**(3): 123.

Krogh, E. J. (1988). The Garnet-Clinopyroxene Fe-Mg Geothermometer - A Reinterpretation Of Existing Experimental-Data. Contributions To Mineralogy And Petrology **99**(1): 44-48.

Kurz, W. (2005). Constriction during exhumation: Evidence from eclogite microstructures. Geology **33**(1): 37-40.

Kurz, W., E. Jansen, R. Hundenborn, J. Pleuger, W. Schafer and W. Unzog (2003). Microstructures and crystallographic preferred orientations of omphacite in Alpine eclogites: implications for the exhumation of (ultra-) high-pressure units. Journal Of Geodynamics **37**(1): 1-55.

Lacassin, R. (1987). Kinematics of ductile shearing from outcrop to crustal scale in the Monte Rosa Nappe. Western Alps. Tectonics **6**(1): 69-88.

Langdon, T.G. and Vastava, R.B. (1982) An evaluation of deformation models for grain boundary sliding. Mechanical Testing for Deformation Model Development, Rohde, R.W. and Swearengen, J.C., 435-451, American Society for Testing materials, Philadelphia.

Lange, S., L. Nasdala, U. Poller, L. Baumgartner and W. Todt (2000). Crystallisation age and metamorphism of the Monte Rosa granite, Western Alps. 17th Swiss Tectonic Studies Group Meeting. Zurich.

Lapen, T., C. Johnson, L. Baumgartner, N. Mahlen, B. Beard and J. Amato (2003). Burial rates during prograde metamorphism of an ultra-high-pressure terrane: an example from Lago di Cignana, western Alps, Italy. Earth And Planetary Science Letters **215**: 57-72.

Lardeaux, J. M., J. M. Caron, P. Nisio, G. Pequignot and M. Boudeulle (1986). Microstructural criteria for reliable thermometry in low-temperature eclogites. Lithos **19**: 187-203.

Lardeaux, J. M. and M. I. Spalla (1991). From granulites to eclogites in the Sesia Zone (Italian Western Alps): a record of the opening and closure of the Piedmont ocean. Journal Of Metamorphic Geology **9**: 35-59.

Lawrence, R. J., F. Azough, R. Freer and C. A. Leach (2004). Grain boundary diffusion of Mg and Ca in synthetic diopside aggregates. Geochimica Et Cosmochimica Acta **68**(11): A96-A96.

Leake, B. E. (1978). Nomenclature of Amphiboles. American Mineralogist **63**: 1023-1052.

Litvin, Y. A. and T. Gasparik (1993). Melting of jadeite to 16.5 GPa and melting relations on the enstatite-jadeite join. Geochimica Et Cosmochimica Acta **57**: 2033-2040.

Llyod, G. E. (1987). Atomic number and crystallographic contrast images with the SEM: a review of backscattered electron techniques. Mineralogical Magazine **51**: 3-19.

Loomis, T. P., J. Ganguly and S. C. Elphick (1985). Experimental determination of cation diffusivities in aluminosilicate garnets. II. Multicomponents simulation and tracer diffusion coefficients. Contributions To Mineralogy And Petrology **90**: 45-51.

Lotgering, F. K. (1959). Topotactical reactions with ferrimagnetic oxides having hexagonal crystal structures. Journal of Inorganic and Nuclear Chemistry **9**: 113-123.

Mainprice, D., J. Bascou, P. Cordier and A. Tommasi (2004). Crystal preferred orientations of garnet: comparison between numerical simulations and electron back-scattered diffraction (EBSD) measurements in naturally deformed eclogites. Journal Of Structural Geology **26**(11): 2089-2102.

Mainprice, D. and A. Nicolas (1989). Development of shape and lattice preferred orientations: application to the seismic anisotropy of the lower crust. Journal Of Structural Geology **11**: 175.

Matthews, M., B. Harte and D. Prior (1992). Mantle Garnets - A Cracking Yarn. Geochimica Et Cosmochimica Acta **56**(7): 2633-2642.

Mauler, A. (2001). Texture and microstructures in eclogites. Electron backscatter diffraction applied on samples from nature and experiment. Zurich, Eidgenössische Technische Hochschule. **Thesis**.

Mauler, A., M. Bystricky, K. Kunze and S. Mackwell (2000). Microstructures and lattice preferred orientations in experimentally deformed clinopyroxene aggregates. Journal Of Structural Geology **22**(11-12): 1633-1648.

Mauler, A., G. Godard and K. Kunze (2001). Crystallographic fabrics of omphacite, rutile and quartz in Vendeé eclogites (Armorican Massif, France). Consequences for deformation mechanisms and regimes. Tectonophysics **342**(1-2): 81-112.

Mauler, A., K. Kunze, J. P. Burg and P. Philippot (1998). Identification of electron backscatter diffraction patterns in a monoclinic solid-state solution series: Example of omphacite. Materials Science Forum **273 - 275**: 705 - 710.

Milnes, A., M. Greller and R. Müller (1981). Sequence and style of major post-nappe structures, Simplon-Pennine Alps. Journal Of Structural Geology **3**: 411-420.

Morimoto, N., J. Fabries, A. K. Ferguson, I. V. Ginzburg, M. Ross, F. A. Seifert, J. Zussman, K. Aoki and G. Gottardi (1988). Nomenclature Of Pyroxenes. American Mineralogist **73**(9-10): 1123-1133.

Müller, W. F., F. E. Brenker, E. Barnert and G. Franz (2004). Chain multiplicity faults in deformed omphacite from eclogite. European Journal Of Mineralogy **16**: 37-48.

Müller, W. F., N. Walte, N. Miyajimi, D. J. Frost and R. Klemd (2007). Deformation experiments on natural omphacite: A TEM study. Geochimica Et Cosmochimica Acta **71**: Suppl. 1, A695.

Mülller, W. F. and G. Franz (2008). TEM-microstructures in omphacite and other minerals from eclogite near to a thrust zone; the Eclogite Zone Venediger nappe area, Tauern Window, Austria. Neues Jahrbuch fur Mineralogie - Abhandlungen **184**: 285.

Oberhänsli, R., J. Hunziker, G. Martinotti and W. Stern (1985). Geochemistry, geochronology and petrology of Monte Mucrone: An example of Eo-Alpine eclogitization of Permian granitoids in the Sesia-Lanzo Zone, Western Alps, Italy. Chemical Geology **52**: 165-184.

Orzol, J., B. Stöckhert, C. A. Trepmann and F. Rummel (2006). Experimental deformation of synthetic wet jadeite aggregates. Journal Of Geophysical Research-Solid Earth **111**(B6).

Paquette, J.-L., C. Chopin and J.-J. Peucat (1989). U-Pb zircon, Rb-Sr and Sm-Nd geochronology of high- to very-high-pressure meta-acidic rocks from the western Alps. Contributions To Mineralogy And Petrology **101**: 280-289.

Passchier, C., J. Urai, J. Van Loon and P. Williams (1981). Structural geology of the central Sesia Lanzo Zone. Geologie en Mijnbouw **60**: 497-597.

Passchier, C. W. and R. A. J. Trouw (1998). Microtectonics, Springer-Verlag, Berlin.

Perchuk, A. L., V. Y. Gerasimov and P. Philippot (1996). Theoretical modelling of eclogite uplift. Petrology **4**(5): 480-492.

Petreus, I. (1978). The divided structure of crystals I. Lineage and sectoral structure in pyrite and beryl. American Mineralogist **63**: 725-731.

Phakey, P. P. and S. Ghose (1973). Direct observation of anti-phase domain structure in omphacite. Contributions To Mineralogy And Petrology **39**(3): 239-245.

Philippot, P. (1987). 'Crack seal' vein geometry in eclogite rocks. Formation de veines par fracturation incrémentale et remplissage progressif dans le conditions du métamorphisme éclogitique. Geodaminica Acta **1**: 171-181.

Philippot, P. and H. L. M. Van Roermund (1992). Deformation Processes In Eclogitic Rocks - Evidence For The Rheological Delamination Of The Oceanic-Crust In Deeper Levels Of Subduction Zones. Journal Of Structural Geology **14**(8-9): 1059-1077.

Pickles, C., S. Kelley, S. Reddy and J. Wheeler (1997). Determination of high spatial resolution argon isotope variations in metamorphic biotites. Geochimica Et Cosmochimica Acta **61**: 3809-3833.

Piepenbreier, D. and B. Stöckhert (2001). Plastic flow of omphacite in eclogites at temperatures below 500 degrees C - implications for interplate coupling in subduction zones. International Journal Of Earth Sciences **90**(1): 197-210.

Platt, J. (1986). Dynamics of orogenic wedges and the uplift of high-pressure metamorphic rocks. Geological Society of America Bulletin **97**: 1037-1053.

Pleuger, J., N. Froitzheim and E. Jansen (2005). Folded continental and oceanic nappes on the southern side of Monte Rosa (western Alps, Italy): Anatomy of a double collision suture. Tectonics **24**: 1-22.

Pognante, U., R. Compagnoni and G. Gosso (1980). Micro-mesostructural relationships in the continental eclogitic rocks of the Sesia-Lanzo Zone (Italian Western Alps): A record of a subduction cycle. Rendiconti della Società Italiana di Mineralogia e Petrologia **36**: 169-186.

Poirier, J. P. and M. Guillopé (1979). Deformation induced recrystallisation of minerals. Bulletin de Mineralogie **102**: 67-74.

Prior, D., A. P. Boyle, F. E. Brenker, M. C. Cheadle, A. Day, G. Lopez, L. Peruzzo, G. J. Potts, S. Reddy, R. Spiess, N. E. Timms, P. W. Trimby, J. Wheeler and L. Zetterstrom (1999). The application of electron backscatter diffraction and orientation contrast imaging in the SEM to textural problems in rocks. American Mineralogist **84**: 1741-1759.

Prior, D., E. Mariani and J. Wheeler (2009). EBSD in the earth sciences: applications, common practise and challenges. Electron Backscatter Diffraction in Materials Science. A. J. Schwartz, M. Kumar, B. L. Adams and D. P. Field, Springer.

Prior, D., P. W. Trimby, U. D. Weber and D. J. Dingley (1996). Orientation contrast imaging of microstructures in rocks using forescatter detectors in the scanning electron microscope. Mineralogical Magazine **60**: 859-869.

Prior, D. J. (1993). Subcritical Fracture And Associated Retrogression Of Garnet During Mylonitic Deformation. Contributions To Mineralogy And Petrology **113**(4): 545-556.

Prior, D. J., R. J. Knipe, M. P. Bates, N. T. Grant, R. D. Law, G. E. Llyod, A. Welbon, S. M. Agar, K. H. Brodie, R. H. Maddock, E. H. Rutter, S. H. White, T. H. Bell, C. C. Ferguson and J. Wheeler (1987). Orientation of Specimens: Essential data for all fields of geology. Geology **15**: 829 - 831.

Prior, D. J., J. Wheeler, F. E. Brenker, B. Harte and M. Matthews (2000). Crystal plasticity of natural garnet: New microstructural evidence. Geology **28**(11): 1003-1006.

Prior, D. J., J. Wheeler, L. Peruzzo, R. Spiess and C. Storey (2002). Some garnet micro structures: an illustration of the potential of orientation maps and misorientation analysis in microstructural studies. Journal Of Structural Geology **24**(6-7): 999-1011.

Ramsbotham, W., S. Inger, R. Cliff, D. Rex and A. C. Barnicoat (1994). Time constraints on the metamorphic and structural evolution of the southern Sesia-Lanzo Zone, western Italian Alps. Mineralogical Magazine **58**: 758-759.

Rast, N. (1965). Nucleation and growth of metamorphic minerals. Controls of Metamorphism. W. S. a. F. Pitcher, G. W., Oliver and Boyd**:** 73-102.

Raterron, P., N. Doukhan, O. Jaoul and J. C. Doukhan (1994). High-Temperature Deformation Of Diopside .4. - Predominance Of (110) Glide Above 1000-Degrees-C. Physics Of The Earth And Planetary Interiors **82**(3-4): 209-222.

Ravna, E. J. K. and M. P. Terry (2004). Geothermobarometry of UHP and HP eclogites and schists - an evaluation of equilibria among garnet-clinopyroxene-kyanite-phengite-coesite/quartz. Journal Of Metamorphic Geology **22**(6): 579-592.

Rebay, G. and M. I. Spalla (2001). Emplacement at granulite facies conditions of the Sesia-Lanzo metagabbros: an early record of Permian rifting? Lithos **58**: 85-104.

Reddy, S., S. Kelley and J. Wheeler (1996). A $^{40}Ar/^{39}Ar$ laser probe study of micas from the Sesia-Lanzo Zone, Italian Alps: implications for metamorphic and deformation histories. Journal Of Metamorphic Geology **14**: 493-508.

Reddy, S. M., J. Wheeler, R. W. H. Butler, R. A. Cliff, S. Freeman, S. Inger, C. Pickles and S. P. Kelley (2003). Kinematic reworking and exhumation within the convergent Alpine Orogen. Tectonophysics **365**: 77-102.

Reddy, S. m., J. Wheeler and R. A. Cliff (1999). The geometry and timing of orogenic extension: an example from the Western Italian Alps. Journal Of Metamorphic Geology **17**: 573-589.

Reinecke, T. (1998). Prograde high- to ultrahigh-pressure metamorphism and exhumation of oceanic sediments at Lago di Cignana, Zermatt-Saas Zone, western Alps. Lithos **42**: 147-189.

Reinsch, D. (1979). Glaucophanites and eclogites from Val Chiusella, Sesia-Lanzo Zone (Italian Alps). Contributions To Mineralogy And Petrology **70**: 257-266.

Ridley, J. (1989). Structural and metamorphic history of a segment of the Sesia-Lanzo zone, and its bearings on the kinematics of Alpine deformation in the Western Alps. Alpine Tectonics. M. P. Coward, D. Dietrich and R. G. Park, Geological Society of London Special Publication. **45:** 189-201.

Ring, U. and O. Merle (1992). Forethrusting, backfolding, and lateral gravitational escape in the northern part of the Western Alps (Monte Rosa region). Geological Society of America Bulletin **104**: 901-914.

Robin, P.-Y. F. (1979). Theory of metamorphic segregation and related processes. Geochimica Et Cosmochimica Acta **43**: 1587-1600.

Rooney, T. P., R. E. Rieker and A. T. Gavasci (1975). Hornblende deformation features. Geology **4**: 364-366.

Rousell, D. H. (1981). Fabric and origin of gneissic layers in anorthositic rocks of the St. Charles sill, Ontario. Canadian Journal of Earth Sciences **18**: 1681-1693.

Rubatto, D., D. Gebauer and R. Compagnoni (1999). Dating of eclogite facies zircons: the age of Alpine metamorphism in the Sesia-Lanzo Zone (Western Alps). Earth And Planetary Science Letters **167**: 141-158.

Rubatto, D., D. Gebauer and M. Fanning (1998). Jurassic formation and Eocene subduction of the Zermatt-Saas-Fee ophiolites: implications for the geodynamic evolution of the Central Western Alps. Contributions To Mineralogy And Petrology **132**: 269-287.

Rubie, D. and R. Danthine (1982). Excursion E: Sesia-Lanzo Zone, Western Alps. International conference on planar and linear fabrics of deformed rocks. Zurich.

Sâbâu, G., E. Negulescu and H.-J. Massone (2006). Chemical zonation and relative timing of growth sections in garnets from eclogites of the Leaota Massif, South Carpathians. Mineralogical Magazine **70**: 655-667.

Sanderson, D. J. (1972). The development of fold axes oblique to the regional trend. Tectonophysics **16**: 55-70.

Schaller, W. T. (1938). Johannsenite, a new manganese pyroxene. American Mineralogist **23**: 575-582

Schwandt, C. S., R. T. Cygan and H. R. Westrich (1995). Mg Self-Diffusion In Pyrope Garnet. American Mineralogist **80**(5-6): 483-490.

Schwandt, C. S., R. T. Cygan and H. R. Westrich (1996). Ca self-diffusion in grossular garnet. American Mineralogist **81**(3-4): 448-451.

Schwerdtner, W. M. (1964). Preferred orientation of hornblende in a banded hornblende-gneiss. American Journal of Science **262**: 1212-1229.

Seward, G. G. E., D. J. Prior, J. Wheeler, S. Celotto, D. J. M. Halliday, R. S. Paden and M. R. Tye (2002). High-temperature electron backscatter diffraction and scanning electron microscopy imaging techniques: In-situ investigations of dynamic processes. Scanning **24**: 232-240.

Shannon, R. D. and R. C. Rossi (1964). Definition of topotaxy. Nature **202**: 1000-1001.

Shelley, D. (1983). Igneous and Metamorphic Rocks under the Microscope. Classification, textures, microstructures and mineral preferred orientations, Chapman and Hall, London.

Siegesmund, S., K. Helming and R. Kruse (1994). Complete texture analysis of a deformed amphibolite: comparison between neutron diffraction and U-stage data. Journal Of Structural Geology **16**: 131-142.

Skjernaa, L. (1980). Rotation and deformation of randomly oriented planar and linear structures in progressive simple shear. Journal Of Structural Geology **2**: 101-109.

Skrotzki, W. (1992). Defect structures and deformation mechanisms in naturally deformed hornblende. Physica Status Solidi **131**: 605-624.

Spiess, R., L. Peruzzo, D. J. Prior and J. Wheeler (2001). Development of garnet porphyroblasts by multiple nucleation, coalescence and boundary misorientation-driven rotations. Journal Of Metamorphic Geology **19**(3): 269-290.

Stampfli, G., J. Mosar, D. Marquer, R. Marchant, T. Baudin and G. Borel (1998). Subduction and obduction processes in the Swiss Alps. Tectonophysics **296**: 159-204.

Stöckhert, B. and J. Renner (1998). Rheology of crustal rocks at ultra-high pressure. When continents collide: Geodynamics and geochemistry of ultra-high pressure rocks. B. R. Hacker and J. G. Liou, Kluwer Academic Publishers: 57-95.

Storey, C. D. and D. J. Prior (2005). Plastic deformation and recrystallisation of garnet: A mechanism to facilitate diffusion creep. Journal Of Petrology **46**(12): 2593-2613.

Stünitz, H. (1989). Partitioning of metamorphism and deformation in the boundary region of the 'Seconda Zona Diorito-Kinzigitica', Sesia-Lanzo Zone, Western Alps. Zürich. **Thesis**.

Tatham, D. J., G. E. Llyod, R. W. H. Butler and M. Casey (2007). Amphibole and lower crustal seismic properties. Earth And Planetary Science Letters.

Terry, M. P. and F. Heidelbach (2004). Superplasticity in garnet from eclogite facies shear zones in the Haram Gabbro, Haramsoya, Norway. Geology **32**(4): 281-284.

Terry, M. P. and P. Robinson (2004). Geometry of eclogite-facies structural features: Implications for production and exhumation of ultrahigh-pressure and high-pressure rocks, Western Gneiss Region, Norway. Tectonics **23**(2).

Trepmann, C. and B. Stöckhert (2001). Mechanical twinning of jadeite - an indication of synseismic loading beneath the brittle-plastic transition. International Journal Of Earth Sciences **90**(1): 4-13

Trepmann, C. A. and B. Stöckhert (2002). Cataclastic deformation of garnet: a record of synseismic loading and postseismic creep. Journal Of Structural Geology **24**(11): 1845-1856.

Trimby, P. W. and D. J. Prior (1999). Microstructural imaging techniques: a comparison between light and scanning electron microscopy. Tectonophysics **303**: 71-81.

Tropper, P., E. J. Essene, Z. D. Sharp and J. C. Hunziker (1999). Application of K-feldspar-jadeite-quartz barometry to eclogite facies metagranites and metapelites in the Sesia Lanzo Zone (Western Alps, Italy). Journal Of Metamorphic Geology **17**: 195-209.

Twiss, R. J. and E. M. Moores (1992). Structural Geology, W.H. Freeman and Company, New York.

Ulrich, S. and D. Mainprice (2005). Does cation ordering in omphacite influence development of lattice-preferred orientation? Journal Of Structural Geology **27**(3): 419-431.

van der Klauw, S., T. Reinecke and B. Stöckhert (1997). Exhumation of ultrahigh-pressure metamorphic oceanic crust from Lago di Cignana, Piemontese zone, western Alps: the structural record in metabasites. Lithos **41**: 79-102.

van Panhuis-Sigler, M. and P. Hartman (1981). Morphologie théorique de certains pyroxenes déduite de la structure cristalline. Bulletin de Mineralogie **104**: 95-106.

van Roermund, H. L. M. (1983). Petrofabrics and microstructures of omphacites in a high temperature eclogite from the Swedish Caledonides. Bulletin de Mineralogie **106**: 709-713.

van Roermund, H. L. M. (1984). Omphacite Microstructures from a Spanish eclogite. Textures and Microstructures **6**: 105-116.

van Roermund, H. L. M. and J. N. Boland (1981). The dislocation substructures of naturally deformed omphacites. Tectonophysics **78**(1-4): 403-418

Vance, D. and R. K. O' Nions (1990). Isotopic Chronometry Of Zoned Garnets - Growth-Kinetics And Metamorphic Histories. Earth And Planetary Science Letters **97**(3-4): 227-240.

Venables, J. A. and R. Bin-jaya (1977). Accurate microcrystallography using electron back-scattering patterns. Philosophical Magazine **35**: 1317-1332.

Venables, J. A. and C. J. Harland (1973). Electron back-scattering patterns - A new technique for obtaining crystallographic information in the scanning electron microscope. Philosophical Magazine **27**: 1193-1200.

Voegelé, V., J. I. Ando, P. Cordier and R. C. Liebermann (1998). Plastic deformation of silicate garnets I. High-pressure experiments. Physics Of The Earth And Planetary Interiors **108**(4): 305-318.

Voegelé, V., P. Cordier, V. Sautter, T. G. Sharp, J. M. Lardeaux and F. O. Marques (1998). Plastic deformation of silicate garnets II. Deformation microstructures in natural samples. Physics Of The Earth And Planetary Interiors **108**(4): 319-338.

Vollmer, F. W. (1990). An application of eigenvalue methods to structural domain analysis. Geological Society of America Bulletin **102**: 786-791.

Von Mises, R. (1928). Mechanik der plastichen Formanderung von kristallen. Journal of Applied Mathematics and Mechanics **8**: 161-185.

Vuichard, J. P. and M. Ballèvre (1988). Garnet-chloritoid equilibria in eclogitic pelitic rocks from the Sesia Zone (Western Alps): their bearing on phase relations in high pressure metapelites. Journal Of Metamorphic Geology **6**: 135-157.

Wang, Z. and S. Ji (2000). Diffusion creep of fine-grained garnetite: implications for the flow strength of subducting slabs. Geophysical Research Letters **27**(15): 2333.

Wenk, H. R. and J. M. Christie (1991). Comments on the interpretation of deformation textures in rocks. Journal Of Structural Geology **13**: 1091-1110.

Wheeler, J. and R. W. H. Butler (1993). Evidence for extension in the western Alpine orogen: the contact between the oceanic Piemonte and overlying continental Sesia units. Earth And Planetary Science Letters **117**: 457-474.

Wheeler, J., D. J. Prior, Z. Jiang, R. Spiess and P. W. Trimby (2001). The petrological significance of misorientations between grains. Contributions To Mineralogy And Petrology **141**(1): 109-124.

Whitney, D. L. (1996). Garnets as open systems during regional metamorphism. Geology **24**(2): 147-150.

Williams, D. W. and G. C. Kennedy (1970). The melting point of Jadeite to 60 kilobars. American Journal of Science **269**: 481-488.

Williams, P. and R. Compagnoni (1983). Deformation and metamorphism in the Bard area of the Sesia-Lanzo Zone, Western Alps during subduction and uplift. Journal Of Metamorphic Geology **1**: 117-140.

Yoder, H. S. (1952). Change of melting point of diopside with pressure. Journal of Geology **60**: 364-374.

Zhang, J. and H. W. Green (2007). Experimental Investigation of Eclogite Rheology and Its Fabrics at High Temperature and Pressure. Journal Of Metamorphic Geology **25**(2): 97-115

Zhang, J. F., H. W. Green and K. N. Bozhilov (2006). Rheology of omphacite at high temperature and pressure and significance of its lattice preferred orientations. Earth And Planetary Science Letters **246**(3-4): 432-443.

Sample	Approx. Location	Grid Ref	Lithology	Mineralogy
5.1	Punta Telcio	0409705/5080840	Amphibolite	Amph, Grt, Qtz, Zoi, Plag, WM, Rut
5.2	Punta Telcio	0409729/5080406	Eclogite	Omph, Grt, Glauc, Qtz, Zoi, Rut, WM, Amph
5.3	Punta Telcio	0409053/5080591	Amphibolite	Amph, Grt, Qtz, Zoi, Plag, WM, Rut
5.4	Punta Telcio	0408840/5080435	Serpentinite	Serp, Bru, Mag
5.5	Punta Telcio	0410289/5080641	Amphibolite	Amph, Grt, Qtz, Zoi, Plag, WM, Rut
5.6	Punta Telcio	0410214/5080792	Eclogite	Omph, Grt, Glauc, Qtz, Zoi, Rut, WM, Amph
5.7	Punta Telcio	0409998/5080449	Metasediment	Qtz, Grt, WM
5.8	Colle della Barme d'Oropa	0416463/5055256	Streaked Eclogite	WM, Rut, Omph, Grt, Qtz, Zoi, Amph
5.9	Colle della Barme d'Oropa	0416505/5055236	Streaked Eclogite	WM, Rut, Omph, Grt, Qtz, Zoi, Amph
6.1	North of Stollemberg	0412032/5081951	Monte Rosa Paragneiss	Qtz, Grt, WM, Bio
6.2	West side of Stollemberg	0412016/5081610	Eclogite	Omph, Grt, Glauc, Qtz, Zoi, Rut, WM, Amph
6.3	Punta Telcio (Patch 1)	0410118/5080630	Eclogite	Omph, Grt, Glauc, Qtz, Zoi, Rut, WM, Amph
6.4	Punta Telcio (Patch 1)	0410118/5080630	Eclogite	Omph, Grt, Glauc, Qtz, Zoi, Rut, WM, Amph
6.5	Punta Telcio (Patch 1)	0410118/5080630	Eclogite	Omph, Grt, Glauc, Qtz, Zoi, Rut, WM, Amph
6.6	Punta Telcio (Patch 1)	0410118/5080630	Amphibolite	Amph, Grt, Qtz, Zoi, Plag, WM, Rut
6.7	Punta Telcio (Patch 3)	0410283/5080532	Eclogite	Omph, Grt, Glauc, Qtz, Zoi, Rut, WM, Amph
6.8	Punta Telcio (Patch 3)	0410253/5080531	Eclogite	Omph, Grt, Glauc, Qtz, Zoi, Rut, WM, Amph
6.9	Gressoney River Section	0411048/5065255	Garnet Glaucophane Schist	Grt, Glauc, Qtz, Plag
6.10	Gressoney River Section	0411051/5065250	Garnet Glaucophane Schist	Grt, Glauc, Qtz, Plag
6.11	Gressoney River Section	0411051/5065250	Garnet Glaucophane Schist	Grt, Glauc, Qtz, Plag
6.12	Punta Telcio (Patch 2)	0410169/5080527	Eclogite	Omph, Grt, Glauc, Qtz, Zoi, Rut, WM, Amph
6.13	Punta Telcio (Patch 2)	0410453/5080531	Eclogite	Omph, Grt, Glauc, Qtz, Zoi, Rut, WM, Amph
6.14	Punta Telcio (Patch 2)	0410158/5080529	Eclogite	Omph, Grt, Glauc, Qtz, Zoi, Rut, WM, Amph
6.15	Punta Telcio (Patch 2)	0410169/5080532	Amphibolite	Amph, Grt, Qtz, Zoi, Plag, WM, Rut
6.16	Punta Telcio (Patch 3)	0410194/5055525	Eclogite	Omph, Grt, Glauc, Qtz, Zoi, Rut, WM, Amph
6.17	Punta Telcio (Patch 3)	0410200/5080519	Amphibolite	Amph, Grt, Qtz, Zoi, Plag, WM, Rut
6.18	Punta Telcio (Patch 4)	0410182/5080472	Eclogite	Omph, Grt, Glauc, Qtz, Zoi, Rut, WM, Amph
6.19	Punta Telcio (Patch 4)	0410225/5080463	Eclogite	Omph, Grt, Glauc, Qtz, Zoi, Rut, WM, Amph
6.20	Punta Telcio	0410168/5080430	Metasediment	Qtz, Grt, WM

6.21	Punta Telcio	0410204/5080428	Metasediment	Qtz, Grt, WM
6.22	Punta Telcio (Patch 4)	0410233/5080420	Eclogite	Omph, Grt, Glauc, Qtz, Zoi, Rut, WM, Amph
6.23	Punta Telcio (Patch 4)	0410358/5080461	Eclogite	Omph, Grt, Glauc, Qtz, Zoi, Rut, WM, Amph
6.24	West Side of Stollemberg	0412035/5081558	Monte Rosa Paragneis	Qtz, Grt, WM, Bio, Chl
6.25	Plateau South of Stollemberg	0412212/5081237	Monte Rosa Paragneiss	Qtz, Grt, WM, Bio, Chl
6.26	Colle de Lazoney	0415878/5065390	Aplite	Qtz, WM, Omph, Grt
6.27	Colle de Lazoney	0415878/5065390	Metagranite	Qtz, WM, Omph, Grt
6.28	Colle de Lazoney	0415870/5065349	Aplite	Qtz, WM, Omph, Grt
6.29	Colle de Lazoney	0415870/5065349	Metagranite	Qtz, WM, Omph, Grt
6.30	Colle de Lazoney	0415712/5065338	Aplite	Qtz, WM, Omph, Grt
6.31	Colle de Lazoney	0415712/5065338	Metagranite	Qtz, WM, Omph, Grt
6.32	Colle Della Barme d'Oropa	0416515/5055328	Eclogite Micaschist (EMC)	Omph, Grt, Qtz, WM, Zoi, Rut
6.33	Colle Della Barme d'Oropa	0416515/5055328	Eclogite Micaschist (EMC)	Omph, Grt, Qtz, WM, Zoi, Rut
6.34	Colle Della Barme d'Oropa	0416623/5055280	Eclogite Micaschist (EMC)	Omph, Grt, Qtz, WM, Zoi, Rut
6.35	Colle Della Barme d'Oropa	0416627/5055282	Eclogite Micaschist (EMC)	Omph, Grt, Qtz, WM, Zoi, Rut
6.36	Colle Della Barme d'Oropa	0416919/5055109	Eclogite Micaschist (EMC)	Omph, Grt, Qtz, WM, Zoi, Rut
6.37	Colle Della Barme d'Oropa	0416923/5055093	Eclogite Micaschist (EMC)	Omph, Grt, Qtz, WM, Zoi, Rut
6.38	Colle Della Barme d'Oropa	0416741/5054883	Aplite	Qtz, WM, Omph, Grt
6.39	Colle Della Barme d'Oropa	0416742/5054894	Metagranite	Qtz, WM, Omph, Grt
6.40	Colle Della Barme d'Oropa	0416571/5054966	Eclogite Micaschist (EMC)	Omph, Grt, Qtz, WM, Zoi, Rut
6.41	Colle Della Barme d'Oropa	0416534/5055054	Eclogite Micaschist (EMC)	Omph, Grt, Qtz, WM, Zoi, Rut
6.42	Colle Della Barme d'Oropa	0416522/5055286	Streaked Eclogite	WM, Rut, Omph, Grt, Qtz, Zoi, Amph
6.43	Colle Della Barme d'Oropa	0416505/5055236	Streaked Eclogite	WM, Rut, Omph, Grt, Qtz, Zoi, Amph
7.1	Colle della Barme d'Oropa	0416544/5055304	Eclogite Pod	Omph, Grt
7.2	Colle de Lazoney	0416006/5065342	Metagranite	Qtz, WM, Omph, Grt
7.3	Colle de Lazoney	0416006/5065342	Metagranite	Qtz, WM, Omph, Grt
7.4	Colle de Lazoney	0415990/5065369	Metagranite	Qtz, WM, Omph, Grt
7.5	Colle della Barme d'Oropa	0416918/5055293	Eclogite Micaschist (EMC)	Omph, Grt, Qtz, WM, Zoi, Rut
7.6	Colle della Barme d'Oropa	0416918/5055294	Eclogite Micaschist (EMC)	Omph, Grt, Qtz, WM, Zoi, Rut
7.7	Colle della Barme d'Oropa	0416505/5055292	Streaked Eclogite	WM, Rut, Omph, Grt, Qtz, Zoi, Amph

7.8	Colle della Barme d'Oropa	0416505/5055292	Streaked Eclogite	WM, Rut, Omph, Grt, Qtz, Zoi, Amph
7.9	Colle della Barme d'Oropa	0416546/5055110	Aplite	Qtz, WM, Omph, Grt
7.10	Colle della Barme d'Oropa	0416546/5055110	Aplite	Qtz, WM, Omph, Grt
7.11	Colle della Barme d'Oropa	0416546/5055110	Eclogite Micaschist (EMC)	Omph, Grt, Qtz, WM, Zoi, Rut
7.12	Colle della Barme d'Oropa	0416553/5055114	Eclogite Micaschist (EMC)	Omph, Grt, Qtz, WM, Zoi, Rut
7.13	Colle della Barme d'Oropa	0416553/5055114	Eclogite Micaschist (EMC)	Omph, Grt, Qtz, WM, Zoi, Rut
7.14	Colle della Barme d'Oropa	0416547/5055064	Aplite	Qtz, WM, Omph, Grt
7.15	Colle della Barme d'Oropa	0416547/5055064	Eclogite Micaschist (EMC)	Omph, Grt, Qtz, WM, Zoi, Rut

Table A1. List of samples collected from investigated field areas associated with this study, their location lithology and mineraology